CANADIAN THESES ON MICROFICHE

THÈSES CANADIENNES SUR MICROFICHE

National Library of Canada
Collections Development Branch

Canadian Theses on
Microfiche Service

Ottawa, Canada
K1A 0N4

Bibliothèque nationale du Canada
Direction du développement des collections

Service des thèses canadiennes
sur microfiche

NOTICE

The quality of this microfiche is heavily dependent upon the quality of the original thesis submitted for microfilming. Every effort has been made to ensure the highest quality of reproduction possible.

If pages are missing, contact the university which granted the degree.

Some pages may have indistinct print especially if the original pages were typed with a poor typewriter ribbon or if the university sent us an inferior photocopy.

Previously copyrighted materials (journal articles, published tests, etc.) are not filmed.

Reproduction in full or in part of this film is governed by the Canadian Copyright Act, R.S.C. 1970, c. C-30. Please read the authorization forms which accompany this thesis.

AVIS

La qualité de cette microfiche dépend grandement de la qualité de la thèse soumise au microfilmage. Nous avons tout fait pour assurer une qualité supérieure de reproduction.

S'il manque des pages, veuillez communiquer avec l'université qui a conféré le grade.

La qualité d'impression de certaines pages peut laisser à désirer, surtout si les pages originales ont été dactylographiées à l'aide d'un ruban usé ou si l'université nous a fait parvenir une photocopie de qualité inférieure.

Les documents qui font déjà l'objet d'un droit d'auteur (articles de revue, examens publiés, etc.) ne sont pas microfilmés.

La reproduction, même partielle, de ce microfilm est soumise à la Loi canadienne sur le droit d'auteur, SRC 1970, c. C-30. Veuillez prendre connaissance des formules d'autorisation qui accompagnent cette thèse.

THIS DISSERTATION
HAS BEEN MICROFILMED
EXACTLY AS RECEIVED

LA THÈSE A ÉTÉ
MICROFILMÉE TELLE QUE
NOUS L'AVONS REÇUE

Canada

NL 339 (r. 85/09)

UNIVERSITÉ D'OTTAWA
UNIVERSITY OF OTTAWA

To My Parents and Nimal

Preface

There has been substantial interest in recent years in the electrochemical behaviour and properties of the Zn electrode. Part of this interest has been motivated by the use of the Zn electrode as an anode material in Zn/air, Zn/MnO_2 or Zn/NiO_2 batteries and also as a sacrificial anode for cathodic protection of steel or iron. Although considerable technological progress has been made, a number of specific limitations await satisfactory resolution. In the case of Zn batteries, knowledge of the nature of the passivation process during discharging, the Zn deposition process during charging and the change of the electrode shape in the course of these processes is required to optimize the performance of zinc batteries. For cathodic protection systems, a knowledge of the dissolution and passivation behaviour of Zn in the presence of certain ions is required, since in some cases the potential may become more noble than steel and the Zn then will no longer protect the steel from corrosion.

The work described in this thesis addresses some fundamental aspects of these interests. An experimental study was made of the electrochemical behaviour of Zn with respect to the electrolytic oxidation and reduction processes that occur in aqueous solutions containing CO_3^{2-}, HCO_3^-, Cl^- and SO_4^{2-} solutions for which only little or no work has been reported previously. Under these conditions, the nature of the film and the extent of solubility of Zn as zincate ions can be varied. Studies were also made of the morphology of electrodeposits of

zinc from acidic aqueous solutions containing zinc ions in various states of complexation as a complement to the anodic oxidation studies.

The work in this thesis will be published as indicated below:

(a) Thin Film Behaviour in the Oxidation of Zinc in Aqueous Carbonate Solutions.

J. Electroanal. Chem. - in course of publication.

(b) Mechanism of Passivation of Zinc Anodes as a Function of pH and Presence of Carbonate Ion.

J. Electrochem. Soc. - in course of publication.

Acknowledgements

I wish to express my sincere gratitude to my research director, Professor B.E. Conway, for his guidance and invaluable discussions throughout this study. His assistance during the preparation of this thesis is gratefully acknowledged.

I would like to thank all my colleagues and others who provided discussions, suggestions as well as contributing to a friendly atmosphere which made my stay in Ottawa very enjoyable. Special thanks are due to Drs. M.A. Sattar and David Harrington, who provided much encouragement, and were always willing to help and give their valuable advice, whenever needed.

The assistance of Mr. Egon Kristof for construction of glassware, Mr. G. Ben for preparing the photographed pages in this thesis and other members of the support staff is gratefully acknowledged.

I much appreciate the contribution of Mr. Rob Meyers who introduced me to the SEM and helped me whenever problems arose.

My thanks are also due to the University of Ottawa for the use of its research facilities.

Finally I would like to thank my friend Yamuna and my husband Nimal, for their assistance in preparing this thesis. Above all I want to express my deepest thanks to my dear parents, sisters and Nimal for their encouragement, understanding, help and love during my studies.

TABLE OF CONTENTS

LIST OF TABLES

LIST OF FIGURES

LIST OF PRINCIPAL SYMBOLS AND ABBREVIATIONS

A	electrode surface area, cm^2
a	(= zFs/RT) for reversible charge transfer process
am	amorphous
aq	aqueous
b	(= αzFs/RT) for irreversible charge transfer process
b	Tafel slope dE/d log i
C	Capacitance
C_{dl}	double layer capacitance
C, C_x	concentration (of species x)
C_0	bulk concentration of reactant
C_{crit}	critical concentration of precipitation
CV	cyclic-voltammetry
D	diffusion coefficient
E	electrode potential experimentally measured with respect to some reversible reference electrode
E_H	potential measured with respect to that of a H_2/H^+ electrode in the same solution
E_0	Standard reversible potential
E_p	potential of voltammetry peak maximum
$E_{p/2}$	potential of the half-peak current
E_r	equilibrium (reversible) potential
E_i	lower limit of potential in cyclic voltammetry
E_s	potential difference due to solution resistance
E_t	potential of limit in cyclic voltammetry
e	electron charge, $1.6 \times 10^{-19} C$

F	Faraday constant, 96487 C mol^{-1}
I	current
I	ionic strength
I_p	current at the peak maximum
i	current density, relative to apparent areas
i_d	current density due to diffusion-controlled reaction
i_e	diffusion excluded convective current density
i_l	limiting current density
i_s	current density due to surface reaction
"IR-drop"	potential drop near working electrode due to passage of current across local resistance R of solution
K	absolute temperature
k	proportionality constants
k_1, k_{-1}	forward and reverse rate constants for step 1
k_s	specific rate constant
K_1	equilibrium constant for step 1 = k_1/k_{-1}
l	the distance between the tip of the Luggin capillary and the electrode
M	molar concentration
NHE	normal (standard) hydrogen electrode
n	number of monolayers formed
Q	charge
Q_m	theoretical monolayer charge
q	charge density
q_a, q_c	anodic and cathodic charge densities

q_f	charge density to be passed to give complete coverage of a species
R	gas constant
R	resistance
R_s	the resistance of the path travelled by the current in the solution
RDE	rotating disc electrode
r	radius of the electrode
s	sweep-rate in cyclic-voltammetry dE/dt
s	second
(s)	solid phase
SEM	scanning electron microscopy
T	absolute temperature
t	time
z	number of electrons
z_a	number of electrons involved in the rate determining step
α	one of the crystalline forms of $Zn(OH)_2$
α	the charge-transfer coefficient for the electrochemical activation controlled reaction
γ	roughness factor
γ	one of the crystalline forms of $Zn(OH)_2$
β_1, β_2	crystalline forms of $Zn(OH)_2$
ε	one of the crystalline forms of $Zn(OH)_2$
δ	one of the crystalline forms of $Zn(OH)_2$
θ	fractional coverage of an adsorbed species
κ	specific conductivity

τ	passivation time
ν	kinematic viscosity
ϕ	coverage or activity of an intermediate
ω	rotation rate
η	activation overpotential

Abstract

This thesis describes a study of electrochemical passive film formation, dissolution and breakdown on Zn in aqueous solutions containing bicarbonate, carbonate, sulphate and chloride ions over the pH range 8 to 14, using cyclic-voltammetry, galvanostatic transient experiments and steady-state polarization measurements. Special attention was given to the comparative study of Zn oxidation in solutions of $NaHCO_3$ and Na_2CO_3 where the pH could be lowered to ca. 8. Under these conditions, a passivating film of hydroxy-carbonate can be formed while the dissolution of Zn as ZnO_2^{2-} is much diminished.

In cyclic-voltammetry, one, two or three current peaks were observed in both the cathodic and anodic sweeps, depending on the nature of the electrode surface and pH.

The thickness of the film in the first anodic peak, (designated A_1) is found to be dependent on the pH of the electrolyte and the potential sweep-rate. It was found at higher pH's (ca. 14), from the dependence of i_p on sweep-rate ($i_p \propto s^{1/2}$) and from rotating disc electrode (RDE) experiments ($i_p \propto \omega^{1/2}$), that the A_1 reaction is purely diffusion-controlled but as the pH decreases (ca. 11.5), RDE experiments on the A_1 peak yield $i_p = A + B\,\omega^{1/2}$, indicating both a diffusional and non-diffusional component. The sweep-rate dependence at pH's around 11.5 also shows mixed surface and diffusion control, according to the relation $i_p = k_1 s + k_2 s^{1/2}$. Plots of $i_p s^{-1/2}$ vs $s^{1/2}$ or $i_p s^{-1}$ vs $s^{-1/2}$ show two distinct straight lines.

Much attention was given to the preparation of electrode surfaces because of the surface sensitivity of the initial stages of Zn oxidation and reduction. By correlating the shapes of the peaks and peak potentials, the electrochemical behaviour associated with the A_1 process was understood.

Two processes take place at lower pH's (ca. 11.5): diffusion-controlled dissolution of Zn at the A_{1a} peak and direct passive film formation at the A_{1b} peak. The diffusion component for reaction at the A_1 peak in CO_3^{2-} solutions was first-order w.r.t CO_3^{2-} ions in the pH range 11.5-12 and first-order with respect to OH^- ions in the range 12.0-13.5.

Peak A_2, observed only in CO_3^{2-} solution, was found to be due to residual current passing through the film that had been already formed in the A_1 process, indicating that the anodic films formed in CO_3^{2-} media are probably more porous than the anodic films formed in Cl^- or SO_4^{2-} solutions at the same pH.

Breakdown of the passive film occurs at potentials positive to the A_1 peak in Cl^- or SO_4^{2-} solutions but not in CO_3^{2-} solution. This was explained in terms of the different structure of ZnO formed during oxidation in these solutions.

Galvanostatic experiments provided additional evidence for the mixed-control process observed in cyclic-voltammetry.

Tafel slopes for Zn oxidation were measured in the pH range of 8 to 13.5. At pH 8, a Tafel slope of 40 mV decade^{-1} was found and explained in terms of two consecutive one-electron transfer steps. Formation of less-soluble species at higher pH led to lower Tafel slopes (30-33 mV decade^{-1}).

A model of the various, rather complex processes involved in these studies, is suggested.

Morphological studies of Zn electrodeposition were also carried out from Zn(II) ion solutions containing various anions in acidic media under galvanostatic conditions. The technique of scanning electron microscopy was used to characterize the morphology of the Zn surfaces.

CHAPTER 1

INTRODUCTION

The zinc electrode has been intensively studied in recent years not only because of fundamental problems of interest in its electrochemistry but also because of its significance either in various manufactured electrochemical energy storage systems or in special applications, e.g. where zinc is employed as a sacrificial anode for cathodic protection of iron and steel, and where zinc is used as the anode material in zinc/air, zinc/manganese dioxide or zinc/nickel oxide batteries. The advantages of zinc as a battery electrode material compared to other metals are its favourable properties, both technologically and economically: low cost, low equivalent weight and relatively reversible behaviour in deposition and dissolution. Its attractiveness is diminished, however, by some limitations such as poor morphology of the plated metal resulting when zinc is electrodeposited and the susceptibility of zinc to facile corrosion. Many attempts have been made to improve those characteristics of the zinc electrode that are desirable and research in this subject is reflected in the extensive literature that has been published.

In the technological use of zinc electrodes, e.g. in Zn/Cl_2, Zn/Br_2, Zn/MnO_2 and Zn/air batteries, three principal fundamental electrochemical aspects of the behaviour of the Zn electrode are of interest: a) the mechanism and phenomenology of dissolution and passivation of Zn in alkaline solutions to form zincate (ZnO_2^{2-})

ions and ZnO films; b) the redeposition of Zn from ZnO_2^{2-} ions or from ZnO films; c) the deposition from chloro- or bromo-zinc complex anions in solution and d) the morphology of electrolytically deposited Zn and its distribution on the cathode (upon recharge) in large-area battery anode configurations. Aspect a) involves basic problems in dissolution and passivation of metals while aspects b), c) and d) involve microscopic and macroscopic mechanisms of electrocrystallization.

Although zinc is one of the oldest metals known and has been used in electrochemical research and technology for almost two hundred years, some of the chemistry and much of the electrochemistry of zinc has remained uncertain until recently.

This chapter will review the chemistry and some of the previous work on the electrochemistry of zinc that is related to the present research project; also the aims of the present work will be outlined in relation to the previously published work relevant to the subject of this thesis.

1.1 Chemistry of Zinc and Its Compounds

There are a number of source books for the chemistry of zinc and its compounds [1-3].

Zinc has two 4s-orbital electrons in its outer shell and it forms compounds in which the state of oxidation is +2 . There is some evidence for the existence of the +1 state as a transient intermediate in certain reaction mechanisms but it is not stable in aqueous solution [4]. The $3d^{10}$ levels are not active in the chemistry of Zn so no oxidation states above +2 exist.

Metallic zinc has an hexagonal close-packed structure (c =

0.4937nm, a = 0.2660nm) [5]. Since the axial ratio (c/a = 1.633) for the hexagonal close-packing of spheres is substantially smaller than that for zinc (c/a = 1.856), its structure deviates from that for perfect hexagonal close-packing by elongation along the six-fold axis but there is close-packing in the basal plane.

Six of the twelve nearest neighbours are at a distance of 0.2660 nm, while the other six are at 0.2907 nm, and the average metallic radius is 0.139 nm [6]. Bonds within the hexagonal layers of zinc atoms are stronger than those between the layers. Therefore a fresh (0001) basal plane can be obtained by cleaving a single-crystal of zinc e.g. in liquid nitrogen.

Zinc oxide has the hexagonal structure of the mineral Wurtzite and it is partially covalent; thus, the crystals are not purely ionic. Normally ZnO is white in colour but other colours of ZnO have been reported [7]. This behaviour has been explained in terms of various types of lattice defects. Many oxides have an intrinsic non-stoichiometric composition. Zinc atoms may be lodged in interstitial sites, giving rise to nonstoichiometry, which leads to appreciable conductivity of oxide films on Zn. ZnO should more accurately be written $Zn_{>1}O$. It is therefore an n-type semiconductor. Excess of zinc within the structure of zinc oxide makes films of oxide dark in colour [8,9].

There are several forms of zinc hydroxides: an amorphous form and six other crystalline forms, designated α, β_1, β_2, γ, δ and ε [10]. These zinc hydroxides have various degrees of stability, the most stable form being ε-$Zn(OH)_2$.

Zinc hydroxide dissolves in alkali to give anionic hydroxo-

complexes and there is good evidence for the existence of $Zn(OH)_4^{2-}$ [11-13] complex anions (which are commonly referred to as zincate, ZnO_2^{2-}) reflecting the amphoteric properties of ZnO or $Zn(OH)_2$. Fig. 1.1a[14] shows the distribution diagram for zinc hydroxide complexes as a function of log $[OH^-]$.

Raman studies of the chloride, bromide and iodide solutions demonstrate, amongst other species, the presence of ZnX_4^{2-} ions in concentrated zinc halide solutions[15-18]. Figs. 1.1b[14] and 1.1c[14] show the distribution diagrams for the complex ions that arise in zinc chloride and zinc bromide solutions. It can be seen from the above figures that the stability constants for zinc chloride complexes are much higher than those for corresponding zinc bromide complexes.

In the presence of dissolved carbonate ions, zinc forms many basic carbonates in addition to zinc carbonate. These species are of interest in the present work where zinc oxidation in CO_3^{2-} and HCO_3^- media was investigated. $Zn_5(OH)_6(CO_3)_2$ is well characterised among other basic carbonates. Also it naturally occurs as Hydrozincite which consists of zinc in coordination numbers [6] and [4] in the ratio of 2:3. Table 1.1[20] shows the crystallographic data and morphologies for various compounds formed in the $H_2O/Zn/CO_3^{2-}$ system.

1.1.1 Solubility Diagrams for Zn/H_2O and $Zn/H_2O/CO_3^{2-}$ Systems

For systems closed to the atmosphere, a solubility diagram (log $[Zn^{2+}]$ vs pH, for fixed dissolved carbonate concentration) can conveniently illustrate the conditions under which a particular solid phase predominates.

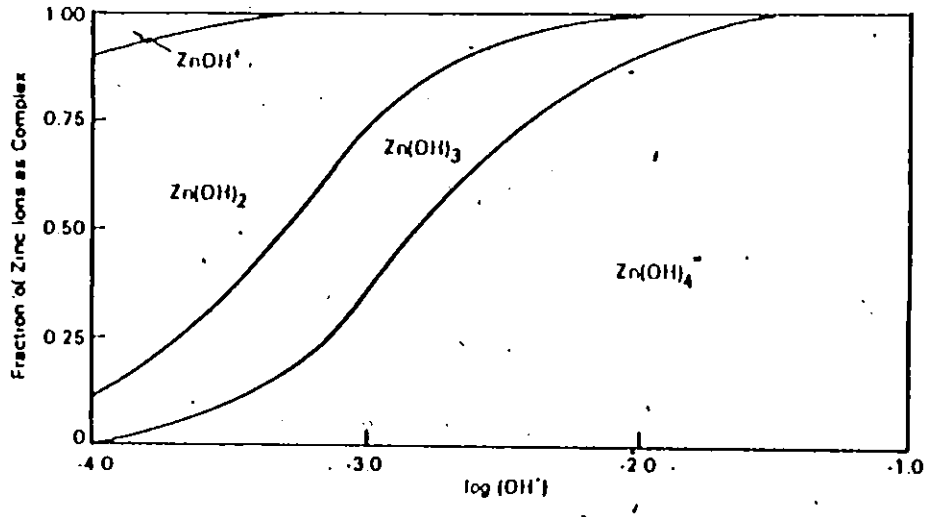

(a)

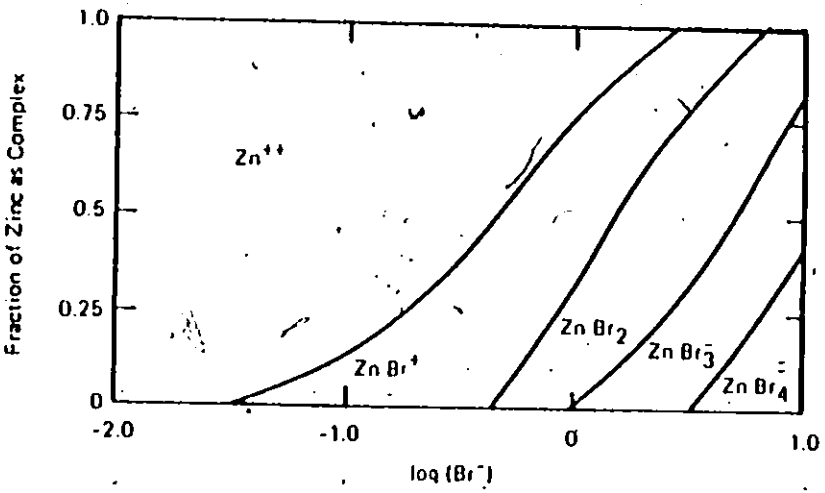

(c)

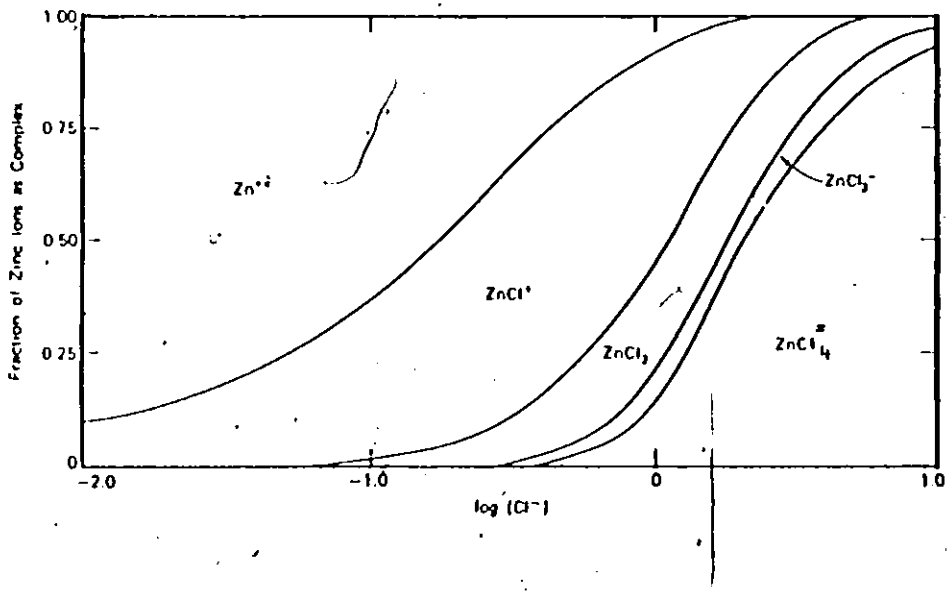

(b)

Fig. 1.1 Distribution diagram for

(a) Zinc/hydroxide system.

(b) Zinc/chloride system.

(c) Zinc/bromide system.

(Ref. 14)

Table 1.1 Solid Compounds in the System Zn^{2+} / H_2O / CO_2 (Ref. 20)

Compound	Crystallographic Data	Formation	Proven as a corrosion product	Remarks
Am. $Zn(OH)_2$	—	Film, Skin	+	Primary corrosion product.
α - $Zn(OH)_2$	—	—	+	Only known as highly basic salt.
β_1- and β_2 $Zn(OH)_2$	orthorhombic, a = 13.17 b = 6.42, c = 24,1 Å	Plates, needles	+	—
γ- $Zn(OH)_2$	orthorhombic, a = 7,96 b = 22.96, c = 3.29 Å	Flat rods	-	—
δ- $Zn(OH)_2$	orthorhombic, a = 13.24 b = 6.42, c = 34.0 Å	Plates	-	A hemihydrate, structurally similar to β-$Zn(OH)_2$.
ϵ- $Zn(OH)_2$	orthorhombic, a = 8.54 b = 5.17, c = 4.93 Å	Bipyramid as corr. prod. at room temp.	+	—
ZnO	hex., a = 3.243 c = 5.195 Å	As corr. prod. at room temp.	+	As corrosion product at room temp., only as active ZnO.
$ZnCO_3$	rhombohedral, a=5.62 Å $\alpha = 48^{0}2'$	Rhombohedral crystals	+	—
$Zn_4(OH)_2(CO_3)_3$	hexagonal, a = 13.32 c = 7.54 Å	Needles	-	—
$Zn_2(OH)_2CO_3 \cdot H_2O$	orthorhombic, a = 9.37 b = 3.13, c = 6.07 Å	Rectangular plates	+	Not clearly illustrable.
$Zn_5(OH)_6(CO_3)_2 \cdot H_2O$ (Hydrozincite)	monoclinic a = 13.62 b = 6.30, c = 5.42 $\beta = 95^{0}50'$	Plate like to fibrous	+	Highly unstable composition and variable lattice parameter. As corrosion product always misordered with OH^- - excess.

Fig. 1.2 shows the pH/solubility diagram for ε-$Zn(OH)_2$ and amorphous $Zn(OH)_2$ which are, respectively, the least and the most soluble of the seven kinds of hydroxide studied by Feitknecht [21].

As mentioned above, in the presence of carbonate, alkalinity arising both from zinc hydroxide, zinc hydroxy-carbonate and zinc carbonate species may be manifested. Fig. 1.3 shows the effect of carbonate on zinc solubility for 10^{-2}-10^{-4} mole litre^{-1} carbonate concentrations [20].

1.1.2 Potential-pH Diagrams

Potential-pH diagrams represent, from a thermodynamic point of view, the electrochemical and corrosion behaviour of any metal in aqueous solutions. They have the advantage of showing at a glance specific conditions of potential and pH under which the metal should be expected thermodynamically either not to react or to react to form some specific oxide or complex ion. Since corrosion or dissolution is often controlled kinetically, pH-potential diagrams do not give information on the latter aspect of stability of the species involved.

Since the effect of carbonate on anodic dissolution and passivation of zinc has been studied in the present work, potential-pH equilibrium diagrams for the $Zn/H_2O/CO_3^{2-}$ ternary system and the Zn/H_2O system are presented here.

The calculations necessary for the construction of the latter diagram are based on general formulae developed by Pourbaix and collaborators. All standard free energies (Table 1.2) were obtained from references 20 and 22. On the basis of the relationships in Table 1.3, the potential-pH diagram (Fig. 1.4)

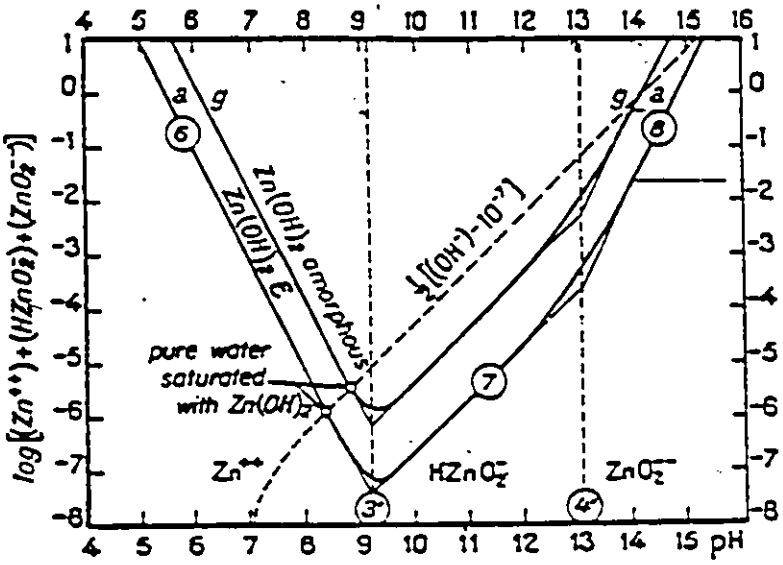

Fig. 1.2 Influence of pH on the solubility of the zinc hydroxides at 298 K. (Ref. 21)

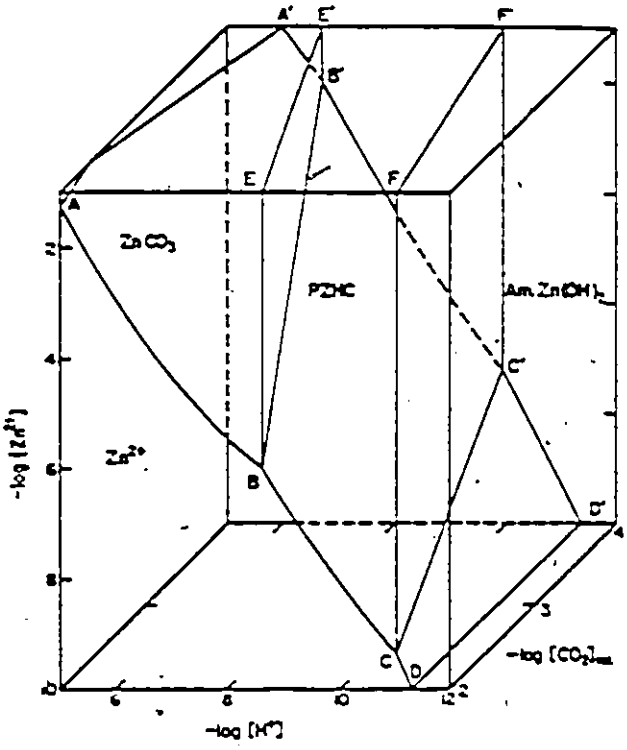

Fig. 1.3 Three-dimensional corrosion diagram for Zn^{2+}/ H_2O/CO_2 system. (Ref. 20)

was constructed. From this diagram, information about the thermodynamic conditions under which, e.g., an oxide (barrier) film may form on a zinc electrode surface may be obtained.

Passivation, in addition to being caused by oxidation with formation of an oxide film, may evidently arise also because of formation of an insoluble zinc carbonate layer which would not arise in the Zn/H_2O system. Again it should be stressed that this diagram gives no consideration of the kinetic phenomena that may be involved since the data used are based only upon thermodynamic information.

1.2 Previous Work on the Electrochemistry of Zinc

There are several reviews on the electrochemistry of the zinc electrode[19,23,24].

A large volume of both fundamental and applied research has been carried out on the zinc electrode in various solutions and can be conveniently discussed under three headings:

(a) Measurements near the equilibrium potential of the zinc electrode.

(b) Anodic dissolution and formation of passivating layers.

(c) Electrodeposition of Zn and morphology of electrolytic Zn deposits.

1.2.1 Exchange Reaction Measurements Near the Equilibrium Potentials

One of the ways of studing the overall reaction mechanism is to determine the reaction order for the species involved in the reaction. Gerischer[25] determined the discharge mechanism involved

Table 1.2

Equilibrium Constant Data for Several Important Reactions in the Zn / Carbonate / Water system

	Reaction equation	log K at 298 K (Ionic strength = 0)
1	$Zn\ (s) = Zn^{2+} + 2e$	25.82
2	$Zn^{2+} + OH^- = ZnOH^+$	5.04
3	$Zn^{2+} + 3\,OH^- = Zn(OH)_3^-$	13.9
4	$Zn^{2+} + 4\,OH^- = Zn(OH)_4^{2-}$	15.1
5	$ZnO\ (s) + 2H^+ = Zn^{2+} + H_2O$	11.18
6	$Zn(OH)_2(\varepsilon) + 2H^+ = Zn^{2+} + 2H_2O$	11.53
7	$Zn(OH)_2\ (am.) + 2H^+ = Zn^{2+} + 2H_2O$	12.45
8	$ZnCO_3\ (s) + 2H^+ = Zn^{2+} + H_2CO_3$	6.49
9	$Zn(OH)_{1.2}(CO_3)_{0.4}(s) + 2H^+ = Zn^{2+} + 1.2\,H_2O + 0.4\,H_2CO_3$	9.21
10.	$H_2O\ (l) = H^+ + OH^-$	-14

Table 1.3

Equilibrium Reactions for the Zn/Carbonate/Water System at 298 K

Potentials are given in volts based on equilibrium constant data from Table 1.2.

1. $Zn\ (s) = Zn^{2+} + 2e$

   $E = -0.762 + 0.030 \log Zn^{2+}$

2. $ZnO\ (s) + 2H^{+} = Zn^{2+} + H_2O$

   $pH = -0.5 \log[Zn^{2+}] + 5.59$

3. $ZnO\ (s) + H^{+} = ZnOH^{+}$

   $pH = 2.2 - \log[ZnOH^{+}]$

4. $ZnO\ (s) + 2H_2O = Zn(OH)_3^{-} + H^{+}$

   $pH = 16.9 + \log[Zn(OH)_3^{-}]$

5. $ZnO\ (s) + 3H_2O = Zn(OH)_4^{2-} + 2H^{+}$

   $pH = 14.85 + 0.5 \log[Zn(OH)_4^{2-}]$

6. $Zn\ (s) + H_2O = ZnO\ (s) + 2H^{+} + 2e$

   $E = -0.432 - 0.059\ pH$

7. $Zn\ (s) + H_2O + H^{+} = Zn(OH)^{+} + 2H^{+} + 2e$

   $E = -0.497 + 0.030 \log[ZnOH^{+}] - 0.03\ pH$

8. $Zn(s) + 3H_2O = Zn(OH)_3^{-} + 3H^{+} + 2e$

   $E = 0.066 - 0.087\ pH + 0.03 \log[Zn(OH)_3^{-}]$

9. $Zn(s) + 4H_2O = Zn(OH)_4^{2-} + 4H^{+} + 2e$

   $E = 0.444 + 0.03 \log[Zn(OH)_4^{2-}] - 0.118\ pH$

10. $Zn(OH)_{1.2}(CO_3)_{0.4}\ (s) + 2H^{+} = Zn^{2+} + 0.4\ H_2CO_3^{*} + 1.2\ H_2O$

    $pH = 4.60 - 0.5 \log Zn^{2+} - 0.4 \log (H_2CO_3^{*})$

11. $ZnCO_3\ (s) + 2H^{+} = Zn^{2+} + H_2CO_3^{*}$

    $pH = 3.25 - 0.5 \log Zn^{2+} - 0.5 \log (H_2CO_3^{*})$

12. $ZnCO_3\ (s) + 2e + 2H^+ = Zn\ (s) + H_2CO_3^*$

$E = -0.570 - 0.059\ pH - 0.03\ \log[H_2CO_3^*]$

13. $ZnCO_3\ (s) + H^+ + 2e = Zn + HCO_3^-$

$E = -0.759 - 0.03\ pH - 0.03\ \log[HCO_3^-]$

14. $Zn(OH)_{1.2}(CO_3)_{0.4}\ (s) + 1.6H^+ = Zn^{2+} + 0.4HCO_3^- + 1.2\ H_2O$

$pH = 4.18 - 0.635\ \log\ Zn^{2+} - 0.25\ \log[HCO_3^-]$

15. $Zn(OH)_{1.2}(CO_3)_{0.4}\ (s) + 1.6H^+ + 2e = Zn\ (s) + 0.4\ HCO_3^- + 1.2\ H_2O$

$E = -0.564 - 0.012\ \log[HCO_3^-] - 0.047\ pH$

16. $Zn(OH)_{1.2}(CO_3)_{0.4}(s) + 2H^+ = Zn\ (s) + 0.4\ H_2CO_3^* + 1.2\ H_2O + 2e$

$E = -0.49 - 0.012\ \log[H_2CO_3^*] - 0.059\ pH$

17. $Zn(OH)_{1.2}(CO_3)_{0.4}\ (s) + 2.8\ H_2O = 0.4\ HCO_3^- + Zn(OH)_4^{2-} + 2.4\ H^+$

$pH = 17.58 + 0.166\ \log[HCO_3^-] + 0.416\ \log[Zn(OH)_4^{2-}]$

18. $Zn(OH)_{1.2}(CO_3)_{0.4}\ (s) = 0.4\ H^+ + 0.4\ HCO_3^- + 0.2\ H_2O + ZnO\ (s)$

$pH = 11.2 + \log[HCO_3^-]$

19. $Zn(OH)_{1.2}(CO_3)_{0.4}\ (s) = 0.8H^+ + ZnO\ (s) + 0.2\ H_2O + 0.4\ CO_3^{2-}$

$pH = 10.76 + 0.5\ \log(CO_3^{2-})$

20. $ZnCO_3\ (s) + H_2O + H^+ = H_2CO_3^* + ZnOH^+$

$pH = -2.51 - \log[H_2CO_3^*] - \log[ZnOH^+]$

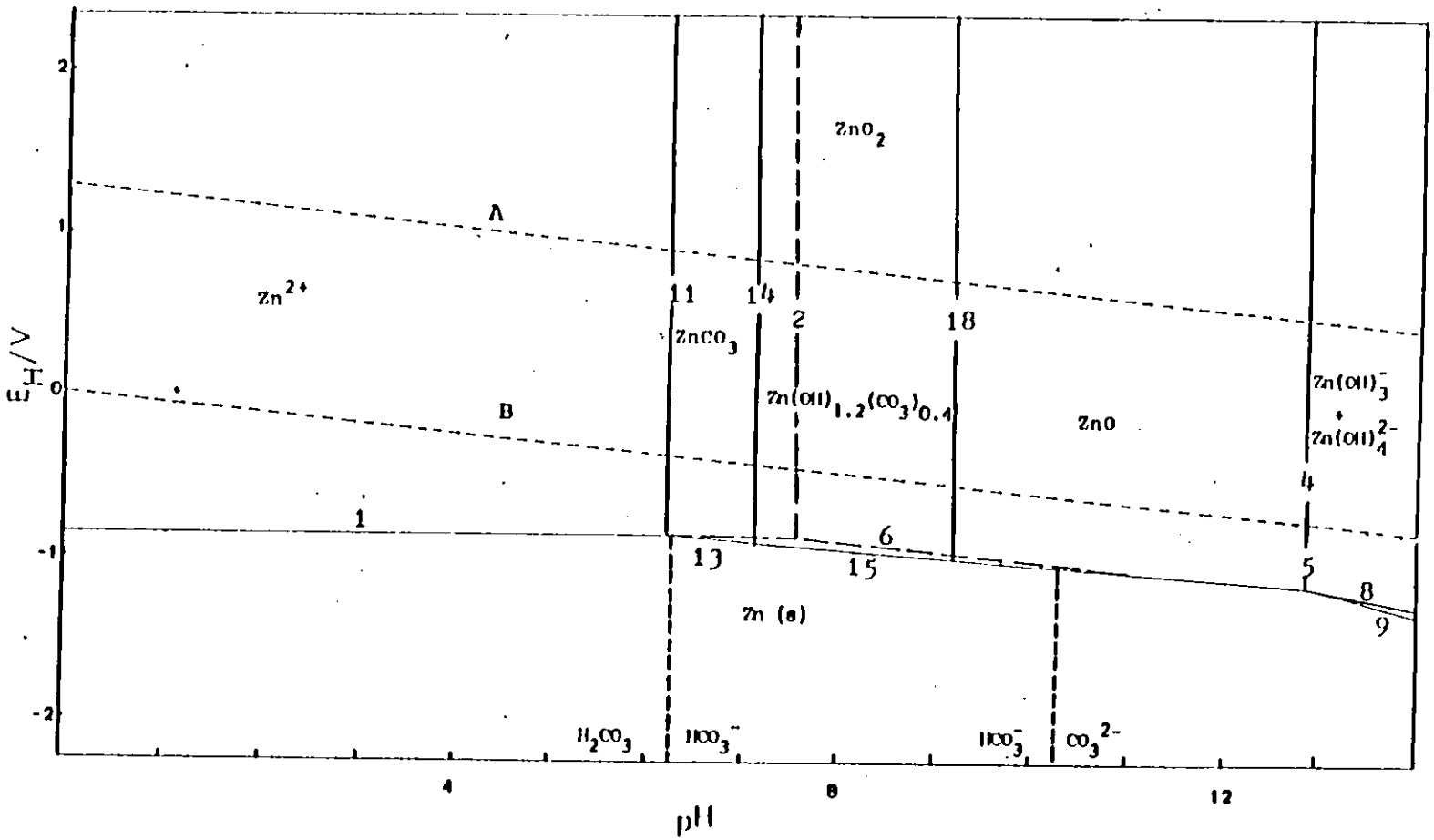

Fig. 1.4 Potential - pH diagram for the zinc/carbonate/water system at 298 K.

$a_{Zn} = 10^{-4}$ mol dm^{-3} (solution zinc species);

$a_C = 10^{-2}$ mol dm^{-3} (solution carbonate species)

Equilibrium lines numbered as in Table 1.3

A : $O_2 + 4H^+ + 4e \rightleftharpoons 2H_2O$

B : $2H^+ + 2e \rightleftharpoons H_2$

in the zinc electrode reaction for the first time by using impedance measurements; this was carried out using a zinc amalgam electrode by examination of the effect of concentration of electroactive species on the exchange current in 5M KCl containing various concentrations of hydroxyl ions at a total concentration of zinc ions equal to 0.1 M.

He proposed a mechanism where step (1) below is considered to be rate-determining in the overall reaction:

$$Zn(Hg) + 2OH^- \xrightarrow{r.d.s.} Zn(OH)_2 + 2e \quad (1)$$

$$Zn(OH)_2 + 2OH^- \rightleftharpoons [Zn(OH)_4]^{2-} \quad (2)$$

Study of the electrochemical Zn cation / Zn metal exchange process at a solid electrode is more complicated than at a Zn-amalgam electrode because of lattice structure effects. However, Farr and Hampson[26-29] studied Zn ion exchange at single-crystal ((0001) face), polycrystalline and heavily cold-worked zinc electrodes in various alkaline solutions by means of impedance measurements and the galvanostatic double-pulse technique. It was found that the exchange current was independent of the zincate ion concentration. Farr et al. suggested, that this reaction proceeds through adsorption of an intermediate Zn^+ species at the electrode. Surface-diffusion rather than charge-transfer as the rate-controlling step was proposed by Farr and Hampson[26] and the zinc electrode reaction was written in terms of the following steps:

$$Zn_{kink} + OH^- \xrightarrow{r.d.s} (Zn_{ad}OH)^- \quad (3)$$

$$(Zn_{ad}OH)^- \rightleftharpoons Zn(OH) + e \quad (4)$$

$$Zn(OH) + OH^- \rightleftharpoons Zn(OH)_2 + e \quad (5)$$

$$Zn(OH)_2 + 2OH^- \rightleftharpoons [Zn(OH)_4]^{2-} \quad (6)$$

Galvanostatic and potentiostatic transient techniques were used by Bockris et al.[30], to study the Zn ion /Zn metal behaviour in 0.1M - 3.0M KOH over the zincate concentration range 10^{-4}M to 0.5M. They suggested the most probable reaction path to be as follows:

$$Zn + OH^- \rightleftharpoons ZnOH + e \quad (7)$$

$$ZnOH + OH^- \rightleftharpoons Zn(OH)_2^- \quad (8)$$

$$Zn(OH)_2^- + OH^- \xrightarrow{r.d.s.} Zn(OH)_3^- + e \quad (9)$$

$$Zn(OH)_3^- + OH^- \rightleftharpoons Zn(OH)_4^{2-} \quad (10)$$

The third step (9) was considered to be rate-determining. Bockris et al. suggested that the conclusion derived from the results obtained by Hampson and co workers[26-29] could have arisen from the fact that no attempt was made in their work to correct for ohmic resistance effects in the solution. This is important when considering a highly reversible reaction such as the Zn/Zn^{2+}.

Dirkse[31] has considered the importance of controlling the ionic strength in studying electrode reactions and suggested that the results obtained by Bockris et al.[30] were due to lack of control of the total ionic strength. He measured the exchange-current by means of the galvanostatic method using concentrations of KOH up to 6M, keeping the ionic strength constant with KF. The reaction order was then found to be <u>one</u> with respect to hydroxide and <u>zero</u> with respect to zincate ions. This suggested that the anodic rate-determining step is related to the removal of zinc

atoms from the metal lattice which may involve a surface-diffusion step before the metal atom is oxidised; the mechanism can be written as follows, excluding possible surface-diffusion steps prior to process (11):

$$Zn(\text{lattice}) + OH^- \xrightarrow{\text{r.d.s.}} ZnOH^- \qquad (11)$$

$$ZnOH^- \rightleftharpoons ZnOH + e \qquad (12)$$

$$ZnOH + OH^- \rightleftharpoons Zn(OH)_2^- \qquad (13)$$

$$Zn(OH)_2^- \rightleftharpoons Zn(OH)_2 + e \qquad (14)$$

$$Zn(OH)_2 + 2OH^- \rightleftharpoons Zn(OH)_4^{2-} \qquad (15)$$

From the above, it will be seen that the reaction mechanism has not yet been definitely established. It may well depend on conditions, e.g. concentration of zinc ion and pH. The reaction orders measured are only valid near the equilibrium potentials and not at higher overvoltages where appreciable currents pass. As the reaction potential is forced to increase from the equilibrium value, the importance of the surface-diffusion step diminishes and the charge-transfer process tends to become the rate-controlling step.

1.2.2 Anodic Dissolution and Passivation

1.2.2.1 Dissolution

A simple active dissolution process occurs when a cation is dissolved and readily moves away from the metal/solution interface. One of the experimental approaches for the study of reaction kinetics at higher overvoltages is to determine the Tafel slope associated with a series of steady-state measurements in the

absence of any other effects such as diffusion.

The reaction products formed in the anodic dissolution may, however, be either soluble or insoluble; in the latter case, they can lead to the formation of a passive layer. Mechanisms of anodic film formation are usually quite specific for the metal and conditions involved, and their elucidation is, in many cases, still in progress. There have been several monographs published on this topic [32-37], e.g. "Anodic Oxide Films" by L.Young[34], "The Anodic Behaviour of Metals" by T.P.Hoar[32], "Anodic Films" by Vermilyea[35] and "Electrochemistry of Metals and Semiconductors" by A.K.Vijh[37].

Generally speaking, there are three possible mechanisms for the formation of passive layers: (a) passivation can arise by direct formation of an adsorbed oxygen film or of a compact oxide film. This is called the direct film formation mechanism. (b) Secondly, precipitation of dissolved metal ions to form an oxide or hydroxide film on the metal surface may occur; this is called the "dissolution-precipitation" mechanism. Sometimes this occurs as a necessary step prior to development of a compact oxide film that is the real passivating agent (see page 21). (c) The third process is direct anodic deposition, where an oxide film is electrolytically formed as a 2-d surface process, e.g. as at Pt or Au. This mechanism does not apply to the oxidation of Zn.

Zinc in oxidation state II has amphoteric characteristics. Zn reacts readily with non-oxidizing acids, releasing hydrogen and giving the divalent cation Zn^{2+}. In alkaline media it forms soluble zincate ions.

Fig. 1.5[38] shows the overall corrosion rate in short-time

tests in aqueous environments at room temperature. The lowest corrosion rate arises within the pH range 7 to 12. This is due to the formation of sparingly soluble oxide or hydroxide films on the surface which restricts the corrosion rate. At higher pH's , the film becomes soluble, allowing again free dissolution, this time to form ZnO_2^{2-} ions and again H_2. The corrosion of zinc in acid or alkali, with production of " nascent hydrogen" and H_2, is utilized in the Jones Reductor for reductive preparation of other inorganic salts in solution and for reduction of some organic compounds.

Zembura and Burzyuska[39] studied the corrosion of zinc in deaerated 0.1N NaCl in the pH range 1.6 to 13.3 using a rotating-disc electrode technique. Fig. 1.6 shows the logarithm of current-density as a function of pH of the solution. Current-density was determined by analysing the zinc concentration in solution as a function of corrosion time.

In acidic solutions, up to pH 3.5, the overall process is controlled chemically whereas, in the pH range 3.5 to 4.5, intermediate mixed kinetics involving hydrogen ion transport arise. This is understandable because of the significant decrease of the hydrogen ion concentration with increase of pH of the solution. In the pH range 4.5 - 8.5, the dissolution rate corresponds to the sum of two reaction rates: one of them is controlled "chemically" and the other diffusionally. The chemical reaction* was assumed[39] to be that involving direct reaction

---

* Actually this so-called "chemical" reaction is almost certainly a mixed anodic/cathodic electrochemical corrosion process.

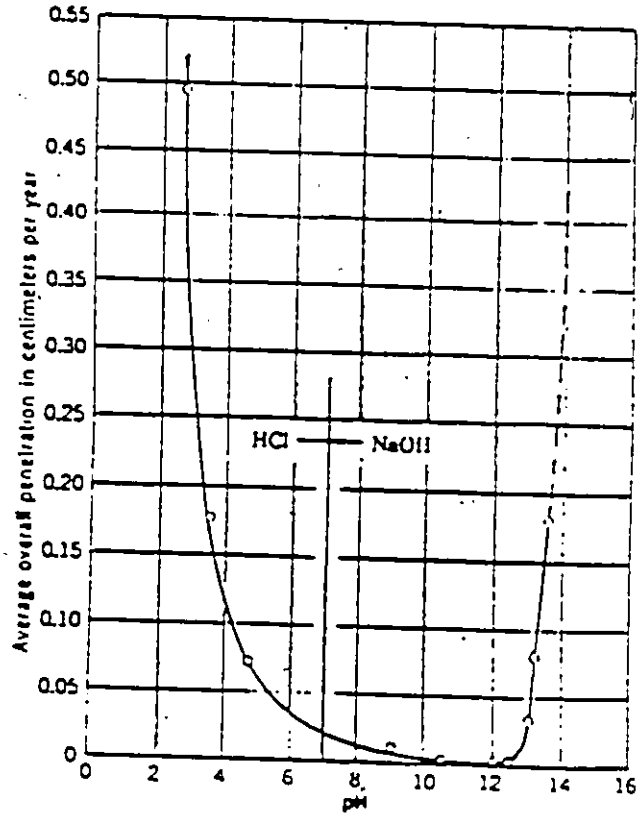

Fig. 1.5 Effect of pH on corrosion of zinc in aerated solutions at 303K. (Ref. 38)

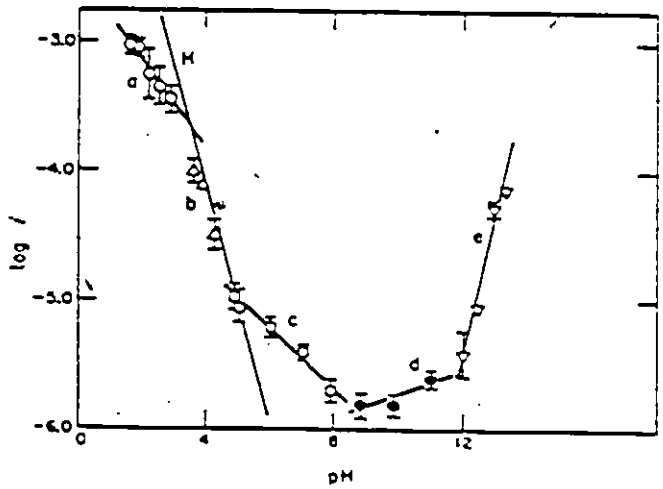

The logarithm of c.d. as the function of pH of the solution. Line H—dependence of $\log i_{H^+, lim}/\sqrt{m}$ on pH determined by Kolny.[23] Lines a, d—the reaction control, b—intermediate control, c—two simultaneous reactions, e—diffusional control regime.

Fig. 1.6 The corrosion of zinc in de-aerated 0.1M NaCl in the pH range 1.6 to 13.3 at 298K. (Ref. 39)

between zinc and water. In the pH range 8.5 to 11.0, the dissolution rate of a zinc disc electrode does not depend on the rotation rate, so that mass-transfer effects are not involved. Thus, mainly a chemical reaction is rate-controlling whereas, at pH values above 11, diffusion is important. It is thus found that the mechanisms for dissolution and passivation of zinc depend very much on pH.

Active dissolution of zinc in $3x10^{-2}$M - 2M NaOH made up to a constant ionic strength of 3M with NaCl was studied by Armstrong et al.[40] using a rotating-disc electrode. An anodic Tafel slope of 42 ± 5 mV/decade and a cathodic slope of 105 ± 10 mV/decade were found in the absence of diffusion effects. These results are in agreement with those of Bockris et al.[30], where the Tafel slopes observed were 49 mV/decade and 113 mV/decade for cathodic and anodic regions, respectively.

A Tafel slope of approximately 40 mV/decade is consistent with two consecutive one-electron transfer reactions with the monovalent zinc ion, Zn^+ as an intermediate with the second electron transfer step being rate-determining (see reactions shown on page 15).

The effects of anions on the active dissolution of zinc was studied by Baugh[41,42] in 1M aqueous $NaClO_4$, NaCl and Na_2SO_4 solutions in the pH range 3.8-5.8 . The anodic Tafel slopes were 40 mV/decade for aqueous $NaClO_4$ and Na_2SO_4, and 30 mV/decade for aqueous 1M NaCl. These results were confirmed by means of studies using a rotating disc electrode. In the 1M NaCl solution, the rate-controlling process is actually diffusion, i.e. slow diffusion of a zinc chloro-complex from the electrode into the

bulk.

Ashton and Hepworth[43] studied the effect of crystal orientation on the anodic dissolution of zinc single-crystals in NaOH solution using steady-state measurements. The reaction overvoltage for hexagonal close-packed metals increases in the order (0001) > (1010) > (1120) and their polycrystalline electrode showed behaviour similar to that for the (1010) plane.

Many experiments have been carried out in order to study the mechanism of passivation of zinc[44-79]. It is often suggested that passivation of zinc occurs through a dissolution-precipitation mechanism, i.e. zincate ions build up near the electrode until a critical concentration is reached where $Zn(OH)_2$ or ZnO precipitates and decreases the rate of dissolution of zinc further. However, Powers and Breiter[48] have identified a dense passivating layer beneath a porous precipitate (type I) layer by means of photomicroscopy. Two mechanisms were proposed for the formation of this dense passivating layer (type II), although no reliable experiment has been carried out to distinguish between these mechanisms. The two mechanisms are based on the "adsorption model" (by Kabanov[47]) and the "two-dimensional nucleation model" (by Armstrong and Bulman[40]). According to the adsorption model, a monolayer of $Zn(OH)_2$ is adsorbed (deposited) on the zinc electrode surface, which becomes converted to a passive film of zinc oxide with release of protons. In the two-dimensional nucleation model it is considered that passivation occurs when full coverage of the ZnO monolayer is attained on the electrode surface followed direct nucleation of zinc oxide.

Buchholz[77], using photocurrent spectra, has observed the formation of passive films which he attributed to an initial adsorbed phase proceeding to a multilayer of ZnO in 0.01M sodium borate solution at pH 9.2. The spectra obtained for the initial states of electrochemical oxidation of zinc were different from those arising in "vacuum oxidation" in so far as the appearance of an extra peak was observed, so that it was concluded that the initial monolayer is probably adsorbed oxygen, an hydroxide species or $Zn(OH)_2$ itself, i.e. a state more complicated than simply an oxygen species. Observation of an entirely new peak beyond that for the $Zn(OH)_2$ region indicates that a completely different layer grows in addition to the initial layer, rather than changing the initial layer itself. This was found to be ZnO which is believed to be the real passive film.

Huber[78] studied the anodically generated coating that can be formed on Zn in Na_2CO_3, NaOH and Na_2SO_4 solutions, using X-ray, electron-diffraction and electron-microscopy. $Zn(OH)_2$ deposition was found to occur at grain-boundaries as a loose, white layer if local saturation occurs in the dissolution region, but passivation required an inner film of zinc oxide (cf. ref. 48). Formation of zinc oxide was found to be independent of the nature of the electrolyte. This film exhibits different colours, due to various amounts of zinc in the ZnO structure. Excess zinc increases conductivity and helps to facilitate oxygen evolution. In Na_2CO_3, a white film was formed which has a very low concentration of excess zinc. Huber also showed that films formed in 0.2N NaOH + 0.8N Na_2SO_4 solutions are not homogeneous - they have an inner yellow layer beneath a white layer.

Results obtained by Nikitina[52] seemed to be in good agreement with those from the work of Huber. She studied Zn oxidation in 3M - 10M aqueous KOH solution at 253 K to 293 K using microscopy and X-ray diffraction techniques, and identified prismatic γ-$Zn(OH)_2$, rhombic ε-$Zn(OH)_2$ and ZnO, depending on the KOH concentration and temperature. The ε-zinc hydroxide was found at higher temperature and higher concentrations of KOH, whereas, at lower temperature and lower alkali concentrations, the γ-zinc hydroxide was found.

1.2.2.2 Passivation Mechanisms

Many workers have studied the mechanism of passivation by means of constant-current techniques[50,51,57-60,72,79]. The current-density, i, and passivation time, τ, have been typically correlated by the equation

$$\tau_p = ki^{-m} \qquad (16)$$

where k is a proportionality constant and m is an exponent that can take values between 1 and 2. It was found that m = 1 for a surface process and m = 2 for a diffusion-controlled process. Fig. 1.7 shows some results obtained by Frank[74] for several systems. He explained the passivation behaviour observed for the case where m = 1.5 in terms of formation of a sparingly soluble salt layer the nuclei of which could grow either laterally, or in depth, over the surface. Also the thickness of the nuclei tend to decrease at higher current-densities due to increasing supersaturation.

Many mechanisms have been proposed to explain Zn passivation; hence there are differences between the various treatments of passivation data in the literature.

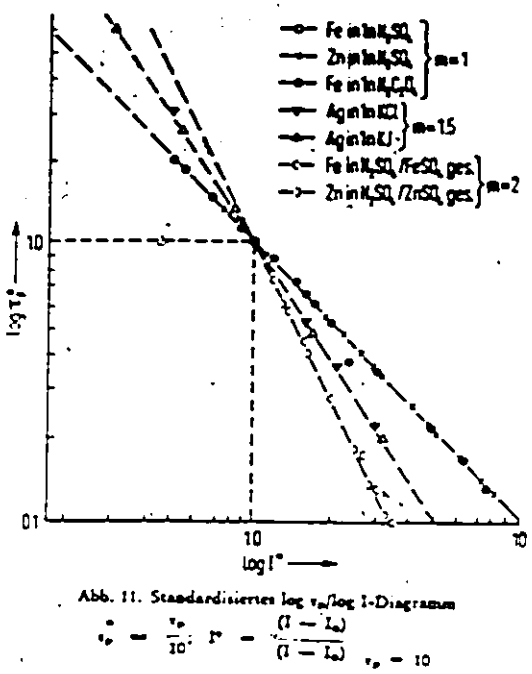

Abb. 11. Standardisiertes log τ_p/log I-Diagramm

$$i^* = \frac{\tau_p}{10}; \quad I^* = \frac{(I - I_d)}{(I - I_d)_{\tau_p = 10}}$$

Fig. 1.7 Log τ vs log i plots for some systems by Frank[74].

Dirkse and Hampson[59] believed that passivation occurs when a "critical" concentration of zincate is reached at the electrode. They modified eqn. (16) above and used the following eqn. (17) to explain their results:

$$i(\tau_p)^{1/2} = (C_{crit} - C_b)zF(\pi D/4)^{1/2} \qquad (17)$$

where C_b is the bulk concentration of zincate and C_{crit} is the critical concentration of zincate for the precipitation of ZnO, D the diffusion coefficient of zincate, z the valency change in the electrode reaction and F is the Faraday. This equation is valid provided diffusion is the only mode of mass-transfer.

Eisenberg et al.[60] introduced a free convection term into eqn. (16), writing

$$(i - i_e)\tau_p^{1/2} = k \qquad (18)$$

where i_e corresponds to the diffusion-excluded convective current

density. Diffusional and convective mass-transfer of zincate was considered to be the rate-determining step in passivation.

Elder[79] regarded the anodic reaction of passivation as a kinetically-controlled process involving either "chemical" dissolution of zinc or complex formation of dissolved zinc species preceding diffusion of zincate, so that

$$i\tau_p^{1/2} = k_o - k_i i \qquad (19)$$

Yamashita et al.[75] used the chronoellipsometric method to study passivation of Zn and found that two types of film are formed: a "type (I)" film at time t_1 and a "type (II)" film at time t_2.

Liu et al.[72] proposed a three-step mechanism for the process of anodic passivation of Zn in alkaline solution, as illustrated in Fig. 1.8. Step 1 corresponds to the dissolution of Zn and formation of zincate ions which accumulate near the Zn electrode surface. When the critical concentration of zincate is reached, the formation of a primary film of ZnO is initiated (cf. ref. 48). Then the rate of mass-transfer of hydroxide ions at the electrode is diminished due to the presence of this porous ZnO layer. Finally, when the electrode potential reaches a value close to the Zn/ZnO standard potential, a compact layer of ZnO is formed which is responsible for the passivation of the electrode. Restricted rate of transfer of OH^- ion through a porous oxide film or formation of a compact film of ZnO have been proposed as the basis of passivation mechanisms for low and high current-densities, respectively.

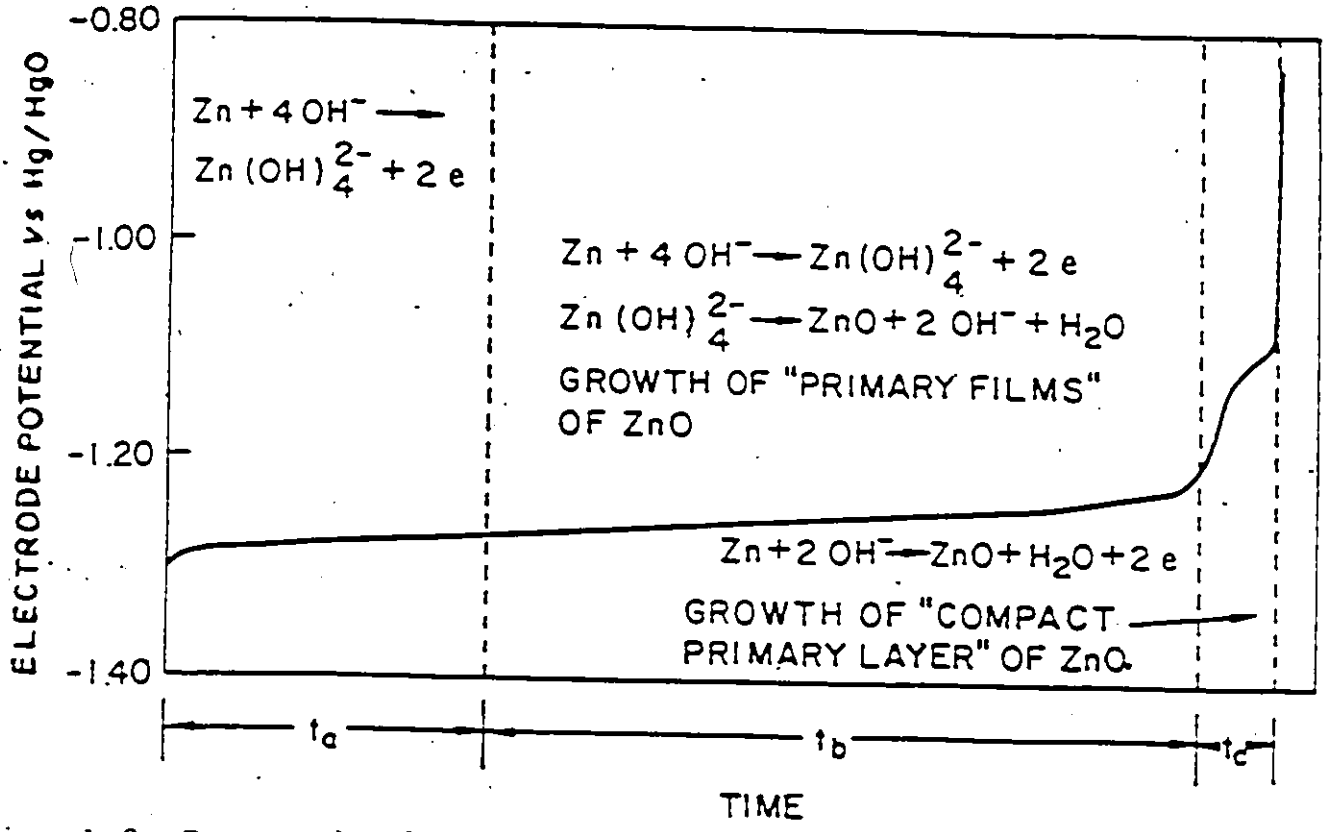

Fig. 1.8 Proposed scheme for the processes associated with the anodic passivation of zinc in alkaline solutions. (Ref. 72)

We see that many studies have been carried out on the anodic behaviour of Zn in alkaline (OH^-) electrolyte; however, only a few papers have been published on the effect of carbonate ions on the Zn electrode reaction.

Kaesche[73] has presented results obtained in galvanostiatic experiments in 1M Na_2CO_3, 0.1M $NaHCO_3$ and 0.01M $NaHCO_3$ solutions. Passivation was fast in 1M Na_2CO_3 due to formation of a monolayer of oxide, compared to the behaviour in $NaHCO_3$ solution where thick oxide layers were formed. Also log τ_p vs log i plots obtained in 1M Na_2CO_3 solution had a slope of -1.6 ± 0.1. He suggested that the behaviour of Zn in 1M Na_2CO_3 is different from that in more alkaline solutions and the passivation time is governed by diffusion associated with supersaturation of the adherent

boundary layer of solution at the Zn interface.

The effect of carbonate ions on passivation of Zn in more alkaline solutions 1M - 8M KOH was studied by Sato et al.[76]. They found that the reaction was diffusion-controlled with respect to zincate but carbonate ions reduced the passivation time to a certain extent. It was proposed that this effect arose because of increase in viscosity of the solution.

1.2.3 Electrodeposition of Zn

There have been several publications on the kinetics of Zn deposition and on morphology of deposits from $ZnCl_2$ and hydroxide solutions[80-109] and afew on electrodeposition of Zn from $ZnBr_2$ electrolytes[110-113].

A substantial variety of morphologies arise in Zn deposition. Increase in current-density in the process of electrodeposition of Zn leads to progressively spongy, compact and then dendritic deposits. One major problem in the development of a secondary battery involving the Zn electrode has been the formation of dendritic deposits on recharging. Diggle et al.[82,83] advanced a model for zinc dendrite growth in alkaline media on the basis of the theory developed by Barton and Bockris[102] on dendritic electrocrystallization of silver. According to this model, initation of a dendrite is treated in terms of growth of a pyramid on the substrate surface. It is assumed that as the pyramid grows through the diffusion layer, the effective radius of curvature of the tip decreases until it reaches a critical radius, which is the condition for the initiation of a dendrite. However, Mansfeld and Gilman[84] showed that pyramids and dendrites grow independently and

from different sites so that their results do not support the above model.

Epelboin et al.[85,86] proposed a complex model in which the electrode reaction kinetics were correlated with morphology of the electrodeposits. The mechanism of deposition of zinc was represented as follows (Zn^* represents Zn atoms at kink sites on the lattice surface):

$$H^+ + e \longrightarrow H_{ads} \quad (20)$$

$$H_{ads} + H^+ + e \longrightarrow H_2 \quad (21)$$

$$Zn^{2+} + e \longrightarrow Zn^+_{ads} \quad (22)$$

$$Zn^{2+} + Zn^+_{ads} + e \longrightarrow 2Zn^+_{ads} \quad (23)$$

$$Zn^+_{ads} + e \longrightarrow Zn \quad (24)$$

$$Zn^+_{ads} + e \longrightarrow Zn^* \quad (25)$$

$$Zn^{2+} + Zn^* + 2e \longrightarrow Zn + Zn^* \quad (26)$$

$$Zn^* \longrightarrow Zn \quad (27)$$

$$Zn^+_{ads} + Zn^* + e \longrightarrow Zn^* + Zn \quad (28)$$

$$Zn^+_{ads} + H_{ads} \longrightarrow H^+ + Zn \quad (29)$$

$$Zn^+_{ads} + H_{ads} \longrightarrow Zn^* + H^+ \quad (30)$$

In alkaline solutions, because of the low concentration of H^+ ions, reactions (20), (21), (29) and (30) are not important. Step (23) is autocatalytic. This step was believed to play an important role in determining the morphology of deposits. At high current densities, production of Zn^* (kink sites) increases due to formation of high concentrations of Zn^+_{ads} (step 25) and these kink sites can lead to formation of dendrites. Growth of spongy deposits at low current densities was explained in terms of

coupling between the autocatalytic step and surface diffusion which leads to uneven current distribution.

Many workers have reported the effect of additives on the morphology of electrodeposited Zn[87-94,97-101]. The use of organic additives in Zn electroplating has been reviewed by Boto[101]. Mansfeld et al.[84, 89-91] found that addition of inorganic additives such as lead and tetra-ethylammonium ions prevents the heterogeneous growth of Zn deposits. Kardas[97] has explained this phenomenon in terms of faster adsorption of these inhibitors at the tips of the dendrites because of the thinner diffusion layer at the tips. According to Wairt[86], additives modify the kinetics thus altering the rates of the elementary intermediate steps taking place at the interface and seem to decrease the importance of the supposed autocatalytic step in the reaction mechanism.

McBreen et al.[98-100] have studied the effect of additives more noble than Zn such as metal oxides of Pb, Sn, Hg, Tl and In. These will be removed from the solution partially by reduction to metals prior to the deposition of Zn and this leads effectively to a substrate effect because continuing Zn deposition then takes place on areas of the other metal, M, produced by the reduction of its oxide. Two kinds of substrate effects were found.

One for interatomic distances of M, greater by 15% or more than that of Zn, results in formation of Zn deposits that are oriented perpendicular to the basal plane and are compact deposits. Their morphologies are reproducible in anodic/cathodic cycling. The other effect arises when the interatomic distance is close to that of Zn and leads to formation of Zn deposits in

crystallographic orientations parallel to the basal plane; these deposits are not compact.

Many workers have reported the application of a periodically changing current in the process of industrial electroplating to improve the quality of deposits[115-118]. Three types of time-dependent currents have been used: (a) periodic reversal of the current, (b) square-wave pulsation of the current and (c) superimposition of a (a.c.) current on a direct cathodic deposition current. The beneficial effects of these modulation regimes have been discussed quantitatively. It seems that periodically changing current helps to minimize dendrite formation and to improve the uniformity of Zn deposits during the charging of the Zn electrode, an effect that is believed to arise from the changed time-dependence of mass-transfer and discharge processes.

1.3 Aims of The Work

The general aims of the present work have been to elucidate the electrochemical kinetics and thermodynamic behaviour of the zinc electrode in alkaline solution, especially the mechanism of its oxidation to solution-soluble species such as zincate (ZnO_2^{2-}) and to solid oxide or oxyhydroxide films at the metal's surface. While results of a number of works on the general topic of zinc oxidation and redeposition have been recorded in the literature (part of which has been reviewed in section 1.2), in the present work extensions of previous research, which was mainly conducted in strongly alkaline NaOH solutions, have been made in new directions by selective experiments in various carbonate, bicarbonate, chloride and sulphate electrolytes over a range of

pH's from 8 to 13. Previously, little or no work has been done under the latter conditions where the nature of the film and the extent of solubility of zinc as ZnO_2^{2-} ion can be varied.

Also, by means of a combination of electrochemical techniques such as cyclic-voltammetry and galvanostatic transient measurements, coupled with use of a rotating zinc electrode to modify mass transfer in a controlled way, attempts have been made to distinguish quantitatively the rates of the surface film formation and solution diffusion processes in the oxidation and redeposition of Zn under various conditions, including cases where the above two processes are coupled. These electrochemical procedures have been supplemented by use of scanning electron microscopy (SEM) to characterize morphology of the oxide film, redeposited Zn, and ageing and etching effects.

The electrochemical kinetic part of the work has been carried out in order to provide some elucidation of the mechanism of anodic Zn oxidation and cathodic reduction under systematically varied conditions. These mechanistic studies have the following particular aims:

(a) establishment of the role of diffusion-control, if any, dependent on reaction conditions;

(b) establishment of the role of film formation or dissolution in relation to reaction conditions and diffusion.

(c) evaluation of the kinetics of Zn oxidation in hydroxide and carbonate solutions in relation to their pH and composition, and the solubility of the zinc species under these conditions;

and

(d) evaluation of the thickness of oxide or carbonate films formed under various conditions.

Morphological studies on Zn electrodeposits from Zn ion solutions containing various anions in the acidic media have been carried out under galvanostatic conditions and SEM was used to characterize the morphology of Zn deposits. This aspect of work in the reduction of Zn from Zn(II) state in the cathodic direction is complementary to that conducted in the oxidation of Zn in the anodic direction.

CHAPTER 2

EXPERIMENTAL

2.1 Introduction

This chapter gives the details of the experimental arrangements and techniques used for the study of anodic dissolution and oxide film formation (passivation) at zinc electrodes in solutions having a wide range of pH's and containing various anions. The experimental procedures used in the work on electrodeposition of zinc will be described in chapter 6.

In general, several methods must be used in a complementary fashion in order to understand any electrochemical reaction in a reasonably complete manner. In the present work, cyclic-voltammetry, steady-state polarization, galvanostatic and rotating-disc electrode techniques were used. Scanning electron microscopy was also employed to characterize the morphologies of the zinc surfaces in addition to use of the above electrochemical methods for examining the reaction processes.

Poor reproducibility and difficulty in some aspects of interpretation of results obtained by different techniques is a well known and recognized problem in investigation of electrochemical behaviour of some metals. The results of the present study are no exception. There is ample evidence that the behaviour of an electrode is sensitive to many factors such as: pretreatment of the electrode, i.e its surface, preparation of solutions, degree of purity of solutions and various other experimental conditions. This is because electrode reactions are

essentially surface processes that are dependent on the state of the electrode metal interface and susceptible to any changes in it, e.g. due to adsorption, modification of its morphology, etc. Therefore special care has to be taken in preparing electrodes, solutions, etc; also repeated experiments must be carried out, as far as possible, under identical conditions, an obvious requirement.

The details of the cell, procedure for preparation of solutions and electrodes, and other general techniques used are given below. Experimental conditions for the various methods employed will be described in the relevant results sections.

2.2 Experimental Methods

The methods used in this work will now be briefly described.

2.2.1 Steady-State Polarization Experiments

Steady-state current vs potential relations were obtained potentiostatically at a Zn electrode. A Wenking potentiostat (ST 72 model) was used to vary in a controlled way the potential of the experimental Zn electrode and thus the cell voltage and corresponding current passing. Both current and potential were read from Racal-Dana digital multimeters (type 4002).

The potential was first adjusted to a value 10 mV cathodic to the equilibrium potential and after equilibrium was attained (4-5 minutes) the potential was increased progressively in the anodic direction. Current vs potential polarization data were obtained by monitoring the current at various potentials and measuring the current 1 min. after each adjustment of potential. Measurements were made in both ascending and descending directions

of potential change along the polarization curve.

2.2.2. Cyclic-Voltammetry

A very important development of the " potentiostatic" method involves the dynamical examination of a current vs potential curve in which the potential, instead of being adjusted point-by-point manually, is changed with time in the form of a triangular wave: it is increased at a constant rate up to a limit and then the direction of sweep is reversed. This is achieved by feeding into the potentiostat a program of potential linearly varing with time, set by an electronic function generator. A Tacussel GSATP function generator was used by means of which various sequential linear changes of potential with time could be applied.

The basic electrical circuit used in the work is well known and is shown in Fig. 2.1. The non-steady state currents passed between the working-electrode and the counter-electrode were measured by means of the potential ΔE generated across a decade resistance box (Leeds and Northrup Co.) in series with the counter-electrode circuit when a current I was being passed ($\Delta E = IR$). Experimental current (I) vs electrode potential (E) profiles were recorded by means of a Houston (type 2000) X-Y recorder in slow sweeps or were monitored on a Nicolet digital oscilloscope (206 Model) when the sweeps were made at higher rates ($s > 300$ $mV\ s^{-1}$). Continuous read-out of the working electrode potential was available on a digital multimeter (Racal-Dana type 4002) appropriately wired in the circuit.

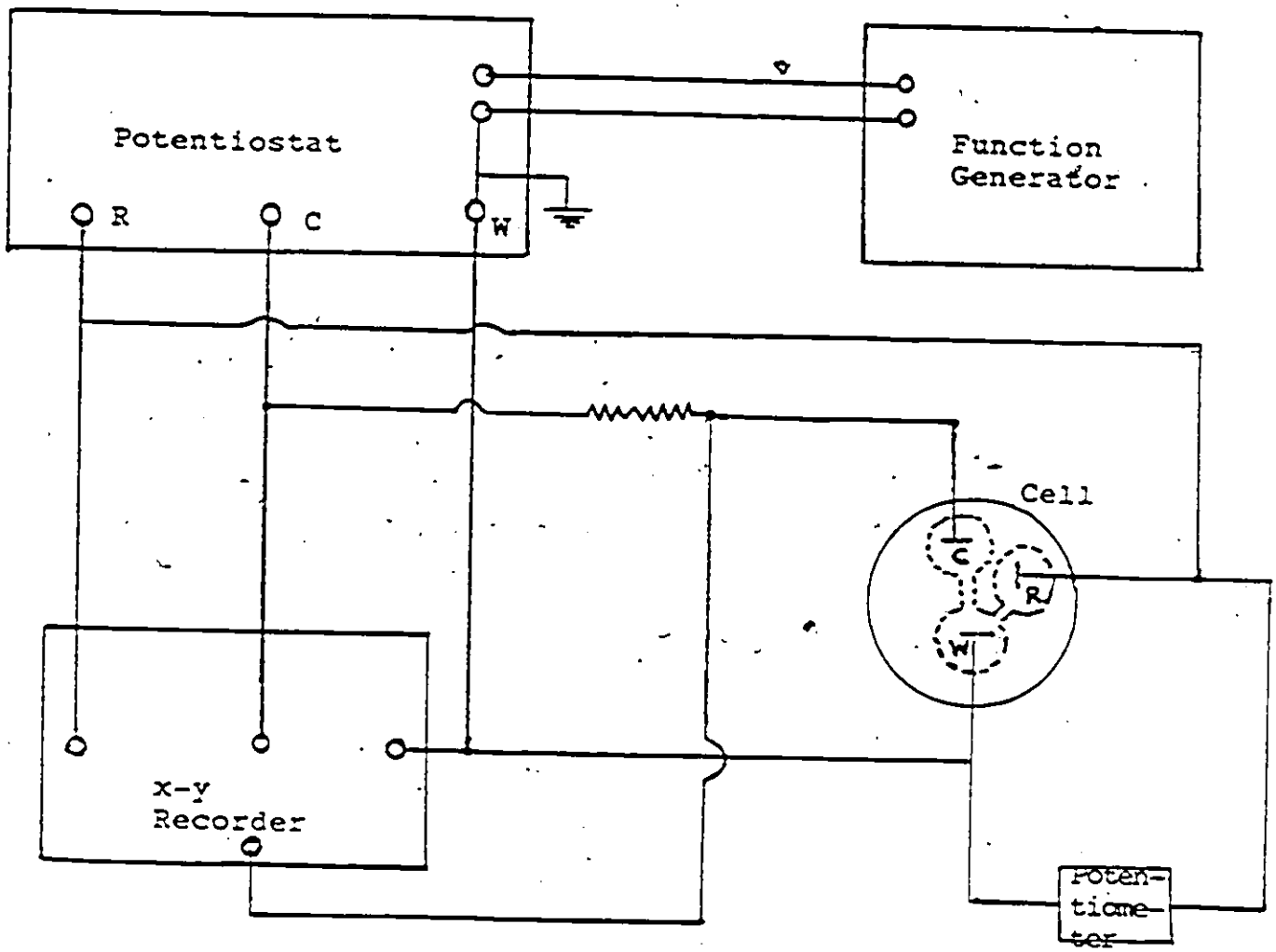

Fig 2.1 Electrical circuitry employed in potentiodynamic sweep studies.

2.2.3 Rotating-Disc Electrode (RDE) Experiments

The simplest type of electrochemical reaction involves only mass-transfer of a reactant to the electrode by diffusion and heterogeneous electron transfer involving non-adsorbed species with the mass-transfer step being the slowest one in a reaction, i.e. the process is diffusion controlled. However, the diffusion limitation may be eliminated by sufficiently fast movement of the electrode past the solution or vice-versa, so that the extent of limitation of the rate due to the effect of mass-transport relative to the otherwise possible rate of electron-transfer is diminished or made almost negligible.

In the present work, a rotating-disc electrode was used. This electrode is rather simple to construct and consists of a disc of the electrode material embedded in a rod of an insulating material. The surface of the disc electrode is a smooth flat metal face exposed to the solution but with a well defined and insulated circumference. The electrode can be rotated about its center at various angular velocities, over a wide range up to ca. 10^4 r.p.m , Fig. 2.3 shows the surface of the In rotating-disc electrode used in these experiments. The shaft was screwed into the rotor head of an ASR2 rotator device made by Pine Instrument Company (Grove City, Pa.).

This electrode was also used to establish whether solution-soluble species are involved in the electrode processes characterized by the anodic I vs E profiles in addition to quantitative investigations of mass-transfer effects in the kinetics of the various electrode reactions involved.

2.2.4 Galvanostatic Experiments

The galvanostatic E vs t behaviour of Zn electrodes was studied using a Princeton Applied Research (model 173) Potentiostat/Galvanostat. The polarization circuit could be switched very fast from the cathodic to the anodic direction of current or back to the cathodic direction with the aid of a rapidly acting push-button switch on the galvanostat. The resulting potential-time curves at constant current thus obtained were monitored on a Nicolet digital oscilloscope (model 206). These instruments were also used to evaluate the roughness factor of Zn electrodes by measuring the double-layer capacitance.

2.2.5 Solution Resistance and IR-drop

An electrolyte through which a current is passing will contribute to the overpotential observed at an electrode by the factor $I \times R_S = \eta_S$, where I is the current and R_S is the series resistance of the path travelled by the current in the solution and/or through any contact resistance. This uncompensated resistance can be calculated using eqn. (31), which is derived from the work of Newman[119]

$$R_S = (1/2\kappa r)\tan^{-1}(\ell/r) \qquad (31)$$

In this equation r is the radius of the electrode, κ the specific conductance of the medium and ℓ is the distance between the tip of the Luggin capillary and the electrode. Using r = 0.15 cm, κ = 0.17 Ω^{-1} cm^{-1} for 1 M NaOH aqueous solution with ℓ taken as 0.5 cm, yields R_S = 7.9 Ω.

The actual solution resistance was measured by the current

interruption technique, where the electrode was first polarized galvanostatically and then put on open-circuit by means of a fast microswitch. The ensuing voltage decay was monitored on an oscilloscope. The solution resistance thus measured was found to be 8.2 Ω in quite good agreement with the value calculated from eqn. (31).

IR-drop leads to a distortion of steady-state polarization and cyclic-voltammetry curves rather than to just a constant shift in the potential scale as in galvanostatic results, where I, and hence IR, are constant.

The maximum currents observed in steady-state polarization experiments in 1M Na_2SO_4, NaCl and NaOH aqueous solutions (pH > 11.5) were of the order of 0.1 mA, which gives rise to an IR-drop of 0.9 mV. In Na_2SO_4 and NaCl solutions at pH ca. 8.2, the maximum currents were ca. 1.5 mA. In these solutions, polarization studies were carried out with an electrode having a smaller surface area. Fig. 2.3 shows an illustration of the electrode used; it had a radius of ca. 0.05 cm. The maximum currents obtained were < 0.2 mA and the calculated IR-drops were less than 6.2 mV.

In cyclic-voltammetry experiments, the currents normally increase with increasing sweep-rate. The maximum currents observed were less than 0.6 mA for solutions used in this work so that IR-drops were less than 5 mV. Appreciable IR drops lead to distortion of cyclic-voltammetry profiles since the I value is continuously varying.

We see that the effect of uncompensated resistance can be

neglected in most aspects of the present results.

2.2.6 Scanning Electron Microscopy (SEM)

A substantial variety of morphologies arise in Zn electrodeposition and dissolution studies. Therefore SEM is a very useful tool for directly observing the state of an electrode surface before and after electrochemical experiments. A Semco Nanolab (model 10) SEM was used, where the magnification could be varied from 10x to 100,000x.

The very large depth of focus and high resolution are the major advantages of SEM. The low-energy secondary electrons that are emitted from the surface are collected and focussed for image formation. Therefore a point-by-point image of the specimen surface is built-up on the viewing screen. This gives rise to a remarkable "three-dimensional" effect. Also magnification can be varied continuously, without refocusing being necessary.

However, unlike in-situ electrochemical methods used, this is necessarily an ex-situ technique which requires transfer of the electrode from the solution to a high vacuum environment in the instrument. Removal of an electrode from solution eliminates the potential control required to generate a definite state of the surface. Also it is possible that removal of solvent could result in the collapse of porous film structures with a consequent change in composition and state of oxide films due to the removal of hydrate water. These are some disadvantages in the use of SEM in electrochemical studies but they are rather trivial in comparison with the great advantage of direct "visibility" of the surface

morphology, provided the above points are kept in mind in interpreting SEM micrographs.

2.3 Cell and Solutions

The all-glass cell used in the electrochemical studies of passivation of Zn is shown in Fig. 2.2. It was of the conventional three-compartment design, with electrolytic contact between the working-electrode compartment and the reference electrode being maintained via a Luggin probe. The counter-electrode was placed in a compartment connected to the cell by means of a glass stop-cock. The same cell was used for experiments using rotating-disc electrodes but the cell top was replaced with a lid as shown in Fig. 2.2.

Glassware used for the first time was washed by soaking overnight in fresh chromic-sulphuric acid mixture. It was then rinsed several times and soaked in doubly-distilled water. After it had stood overnight in water, it was then soaked in concentrated H_2SO_4 for the same length of time, followed by washing and standing again in doubly-distilled water.

All solutions were prepared from "AnalaR" grade chemicals in doubly-distilled water. Since oxygen is chemically reactive with many substances and can be reduced electrochemically, solutions were freed from oxygen by bubbling nitrogen gas through the solution in the cell prior to, and during, the electrochemical measurements.

Nitrogen gas was purified by passage through a conventional gas train[120], which consisted of dehydrating agents, molecular sieve (4A type) and magnesium perchlorate-calcium chloride mixture

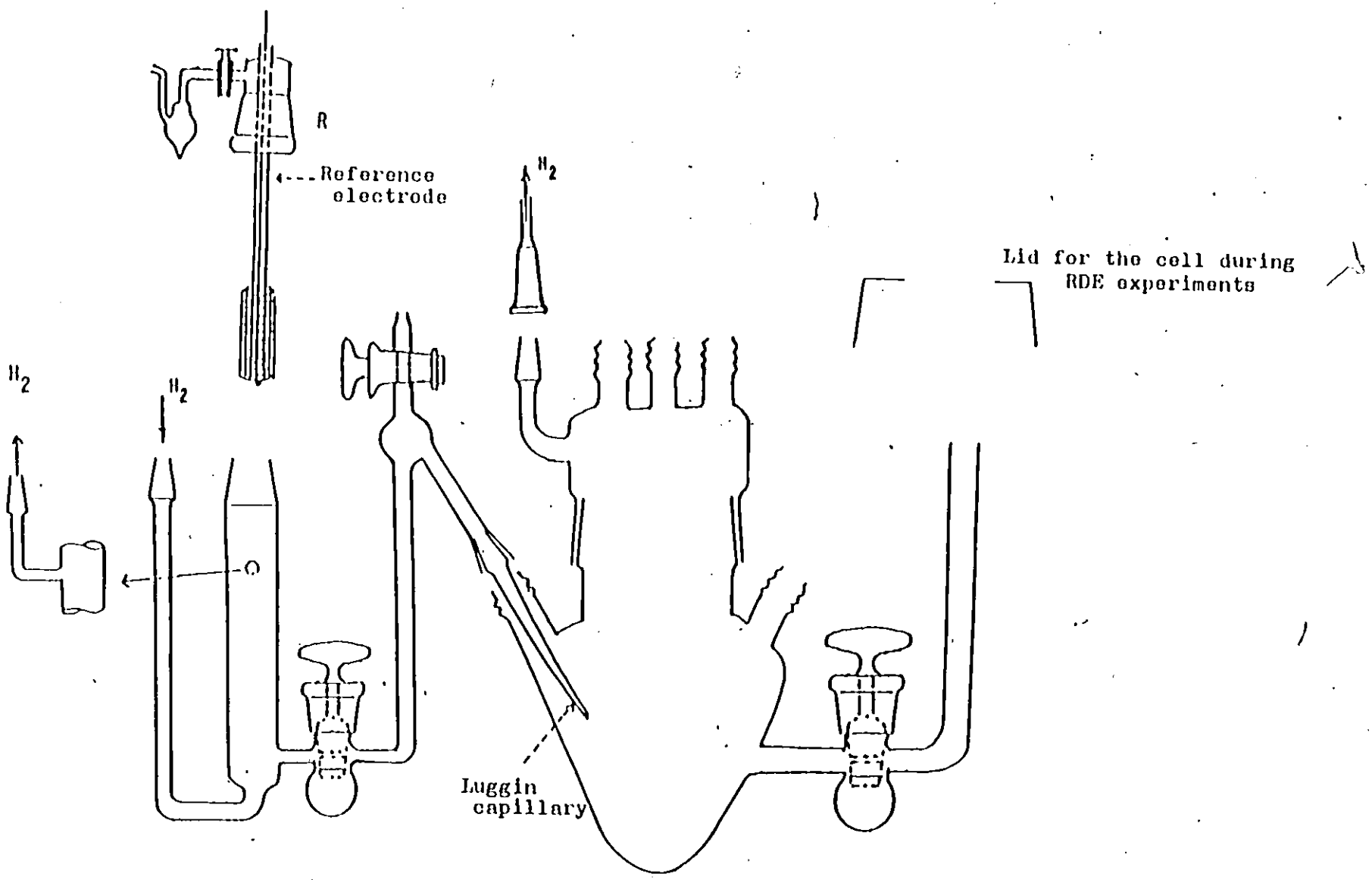

Fig. 2.2 Three-compartment cell used in dissolution and passivation studies of Zn.

for drying and then through copper turnings at 625 K for removal of oxygen. The copper surface was periodically regenerated by heating the copper turnings in H_2 gas. The last traces of impurities were removed by passage of the gas through activated charcoal traps cooled in liquid nitrogen.

All the electrochemical experiments on Zn were carried out at room temperature, 298 K. The pH's of the solutions were measured with a Fisher Accumet pH meter (model 620) equipped with a glass electrode.

2.4 Electrodes

2.4.1 Reference Electrode

All potentials were referred to a platinized Pt/H_2 reversible electrode in the same solution. This consisted of a platinum gauze electrode which was platinized according to the method recommended by Feltham and Spiro [121]. Hydrogen gas was bubbled near the electrode to set up the $H_2/H^+(H_2O)$ equilibrium at the electrode. The hydrogen gas used was also purified the same way as for nitrogen but was catalytically deoxygenated by passage through a furnace containing palladized asbestos at 725 K instead of copper turnings at 625 K.

2.4.2 Counter Electrode

A platinum gauze having a large surface area was used as the counter electrode.

Platinum gauze electrodes used as counter and reference electrodes were prepared as follows: about 3 cm of Pt wire and a piece of Pt gauze were "degreased" overnight in refluxing acetone and then spot welded to a much longer Ag wire. A thin capillary

of soft glass was first fused on to the Pt wire, the glass bead that was formed on the wire was then sealed into a drawn-down soft-glass tube which had been previously cleaned, leaving about 1.5 cm Pt wire protruding beyond the glass seal. Finally the Pt gauze was spot-welded on to the Pt wire. Reliable seals cannot be made in Pyrex glass tubes.

2.4.3 Working Electrode

It has been shown by many workers that soft metals must be treated with care to avoid changing their surface structure during electrode preparation. A low-speed Buchler Isomet diamond saw was used for cutting electrode samples from longer Zn rods. Mechanical polishing of Zn was avoided in the present work since polishing material can become embedded in the Zn surface; also distortions produced by mechanical polishing can be propagated to a depth of 20-100 times that of a deepest scratch. Therefore more Zn metal must be removed from the surface after a mechanical polishing step. One way of doing this is to etch heavily in acids. The effect of mechanical polishing on zinc surfaces will be discussed in more detail under the topic of electrodeposition of Zn in chapter 6.

Several different electrode preparations were studied in the course of the work.

2.4.3.1 Polycrystalline Electrodes

Polycrystalline Zn wire, obtained from Metco Canada Ltd., (diameter 0.3 cm, purity 99%), was set in a glass tube with epoxy adhesive (2216 B/A type-3M company) as shown in Fig. 2.3 . The

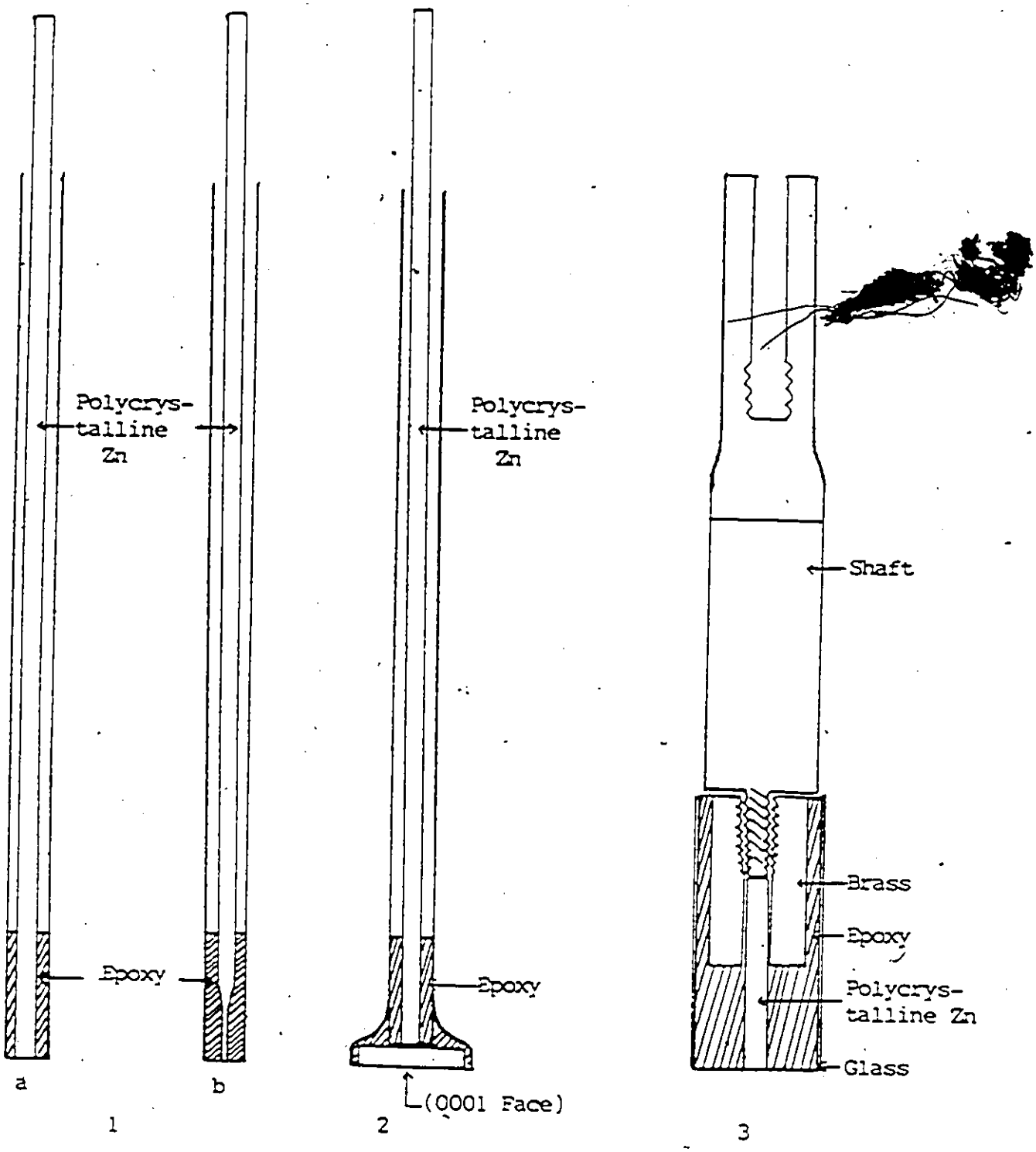

1 Polycrystalline Zn electrode
2 Single-crystal Zn electrode
3 Rotating-disc Zn electrode

a) used in most experiments
b) used in certain steady-state polarization experiments

Fig. 2.3 Working electrodes used in dissolution and passivation studies on Zn.

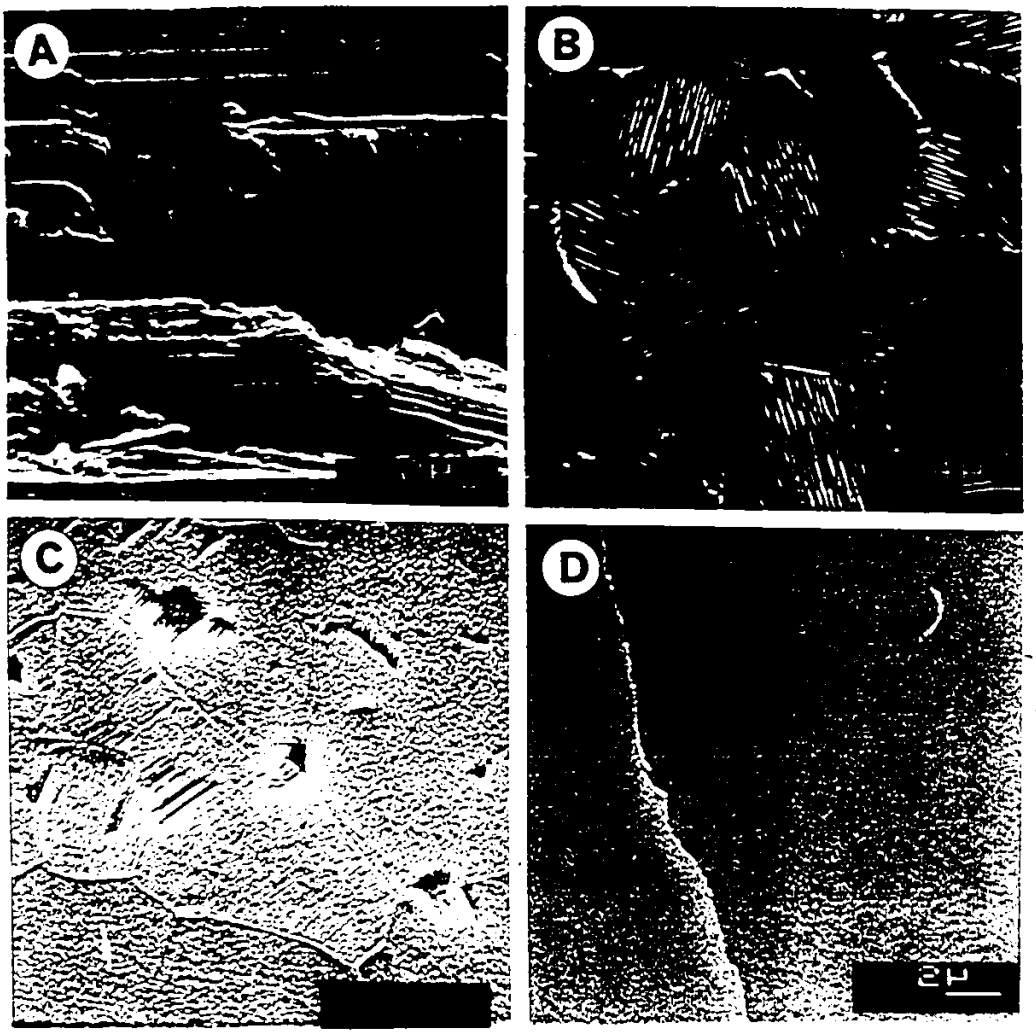

Fig. 2.4 SEM pictures of the state of all Zn electrode surfaces used.

(A) After cutting by the diamond saw.

(B) After etching in 48% HBr acid for 8 s.

(C) After electropolishing in H_3PO_4 and EtOH (1:1).

(D) Single-crystal - (0001 face) cleaved surface.

(E) Annealed surface at 423 K.

(F) Polycrystalline electrode after standing in water for 3 h.

(E) and (F) - see following page.

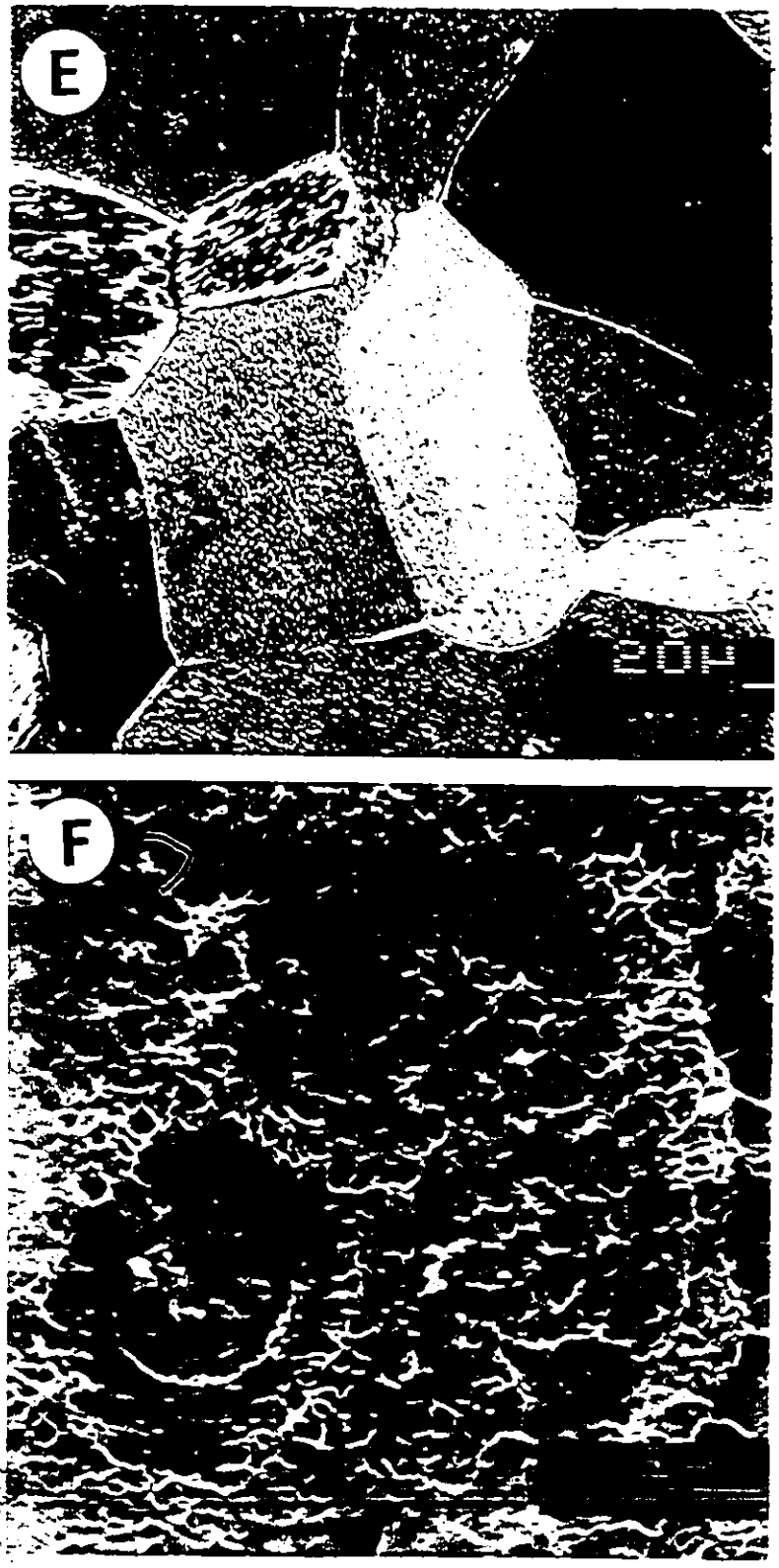
E
20μ
F

sealed electrodes were then cut using the diamond saw and either etched in acid or polished electrochemically in a 1:1 mixture of H_3PO_4 and EtOH in order to obtain a clean mirror-like surface as described by Jacquet [122].

Most of the experiments were carried out with polycrystalline electrodes etched in 48% aq. HBr for 8 s followed by thorough rinsing with doubly-distilled water. In Fig. 2.4 are shown some SEM pictures of polycrystalline zinc electrode surfaces: after cutting, being etched in aq. HBr and being electropolished. More details of the morphologies of etched surfaces in different acids will be discussed in chapter 3.

2.4.3.2 Single-Crystal (0001 face) Electrode

Single-crystals of Zn, 1.3 cm in diameter, were obtained from Atomergic Chemicals Corp., N.Y. . Surfaces with orientation parallel to the basal plane were obtained by cooling the crystal to liquid nitrogen temperature and mechanically cleaving it to expose a (0001) plane. The resulting ca. 2 mm thick wafers were then mounted on polycrystalline electrodes prepared described as in section (3.4.3.1). Electrical connections were made using conductive epoxy (Acme E-solder No: 3022). Fig. 2.3 shows the single-crystal electrode used and an SEM picture of a cleaved surface is given in Fig. 2.4D.

2.4.3.3 Rotating-Disc Electrode

The structure of the rotating-disc electrode is shown in Fig. 2.3. A piece of Zn, 0.3 cm in diameter, obtained from Metco Canada Ltd. was pressed into the brass holder and then allowed to set in epoxy (Araldite) for 48 hours in a glass tube. The sealed

electrode was then cut with a diamond saw to give a flat surface which was then etched in acid.

2.3.3.4 Annealed Electrodes

A polycrystalline Zn rod, 1.3 cm in diameter, obtained from Atomergic Chemicals Corp., was sliced with a slow-speed diamond saw. The resulting 2 mm thick wafers were electropolished in 1:1 H_3PO_4 and EtOH mixture and annealed at 423 K and 673 K temperatures in an H_2 atmosphere for 2 hours, followed by slow cooling to room temperature. Finally, these Zn samples were mounted on to the polycrystalline rod electrode in the same way as described above for the single-crystals.

All electrodes were rinsed with doubly distilled water before being transferred into the experimental electrolyte. Rinsing of the Zn electrodes with water should be done rapidly because their surfaces could become covered with zinc oxide or hydroxide if they are allowed to stand in water for a period of time. Fig. 2.4F shows the surface of the electrode after standing in water for 3 h.

Surfaces which were to be examined under SEM were cut with the diamond saw and specimens were first washed thoroughly with distilled water, then by ethanol and prepared for examination in the SEM instrument.

2.5 Surface Roughness Factor

In order to make quantitative studies of growth of very thin films, it is of importance to know the true initial area of the

metal surface. The true area often appreciably exceeds the corresponding apparent geometrical surface area because of a certain degree of "roughness". There are a number of methods for determination of the roughness factor, i.e. the ratio of the true to the apparent surface area. One method that has been used in electrochemical studies is the measurement of extent of adsorption of some reference substance, an organic dye of known molecular size for example. On the other hand, the real surface area of a Pt electrode can be accurately obtained by integration of the current-time curve for the H-adsorption peaks in a cyclic-voltammogram obtained e.g. in 0.5M aq. H_2SO_4 solution over the potential range +0.4V to +0.05 V vs a hydrogen electrode, assuming that a monolayer of adsorbed H requires a charge of about 210 μC cm^{-2} of real surface area for its deposition or ionization. However, this method cannot be used for the determination of the true area of Zn electrode surfaces.

Bowden and Rideal[123] calculated the roughness factor of electrodes by assuming that the double-layer capacitance for a very carefully polished surface is approximately equal to that of mercury on the cathodic side of the potential of its zero charge because the roughness factor is very close to one.

In the present work, the double-layer capacitance was measured for polycrystalline etched surfaces and the single-crystal (0001 face) cleaved surface by the galvanostatic transient technique. When current is reversed from a constant cathodic value to a constant anodic one, the overpotential first rises rapidly due to charging of the double-layer. Fig. 2.5 shows the potential-time curve obtained for the single-crystal surface.

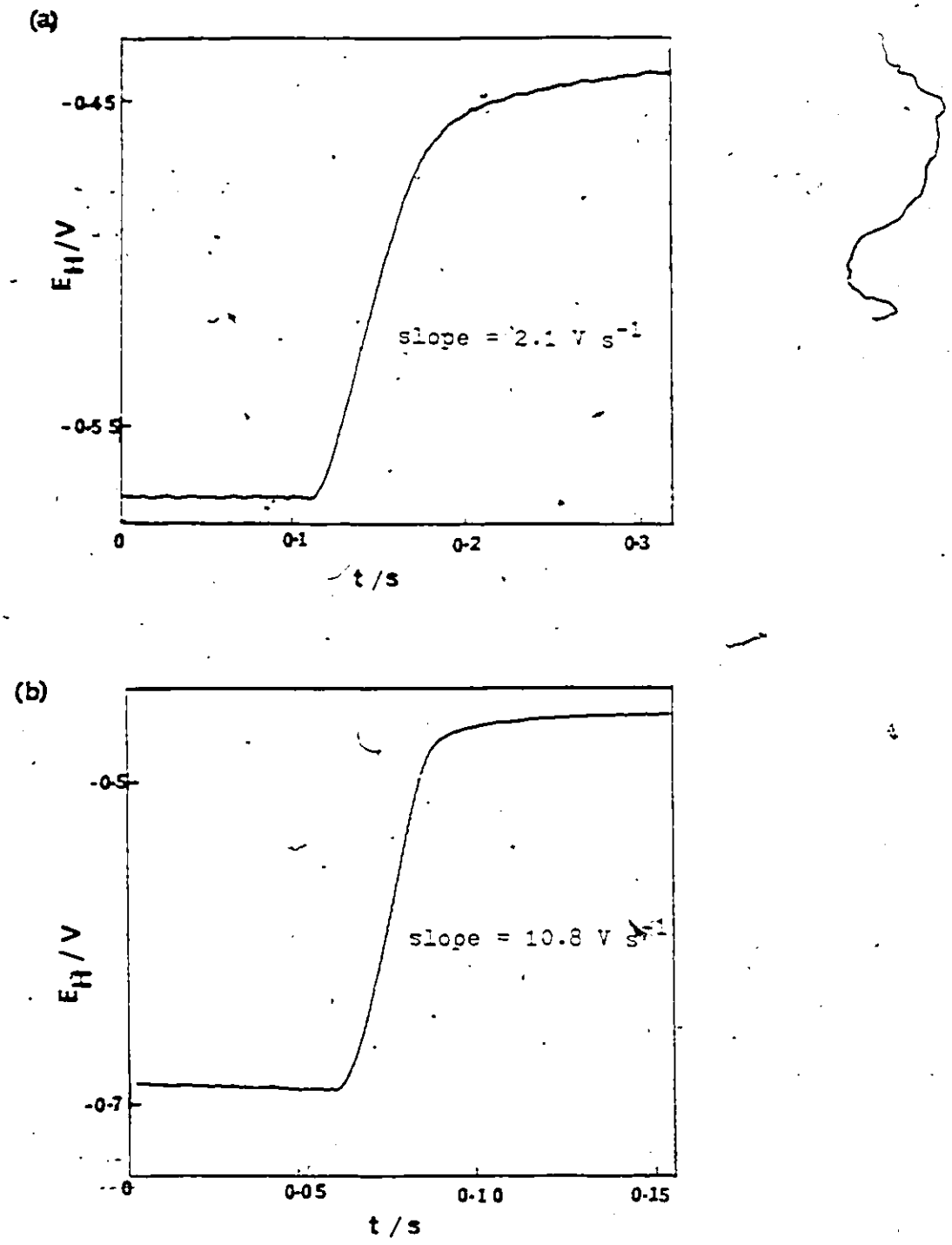

Fig. 2.5 Galvanostatic polarisation E-t curves for measurements of double-layer capacitance for Zn in 1M Na_2SO_4 solution at pH 11.5 at 50 μA current (298 K).
(a) Single-crystal(cleaved) surface of area 1.13 cm^{-2}.
(b) Unetched polycrystalline surface of area 0.07 cm^{-2}.

Double-layer capacitances calculated from these experimental results are given in Table 2.1 . It can be seen that the values of double-layer capacitance obtained for the cleaved Zn electrode surface (22 $\mu F\ cm^{-2}$) are in good agreement with that for a mercury electrode[124] on the cathodic side of the potential of zero charge, in the absence of specific adsorption of ions; viz. 20 $\mu F\ cm^{-2}$. The roughness factor of an etched Zn surface was calculated assuming that the roughness factor of the cleaved Zn surface was close to one. It was found that it is difficult to obtain etched Zn surfaces having exactly identical roughness from one specimen to another. The roughness factor varied between 2 and 4 for a Zn polycrystalline electrode etched in 48% aq. HBr for 8 s, the condition used for preparation of most of the Zn surfaces employed in much of the experimental work in this programme of research.

2.6 Current Densities and Densities of Charge per cm^{-2} for Oxide Film Formation and Reduction

In cyclic-voltammetry experiments, the voltage in the sweep is itself varing linearly with time. An i vs E curve can therefore be regarded as i vs t curve for formation and reduction of the oxide films which develop on Zn over an appropriate potential range. The charge for the oxide film formation or reduction process can be obtained by estimating the area under the oxidation and reduction i vs E curves*. This is one way of measuring, quite accurately, the amount of charge required to form electrochemically a monolayer or more of oxide on metals.

---

* A small correction is made for the charge (C. Δ E) required to change the charge held in the double-layer capacitance over the voltage range, ΔE, of the cyclic-voltammetry experiment. For thick film formation, as here with Zn, this correction is quite small, ca. 1%.

Table 2.1

Roughness-Factor of Zn Electrodes

Current I / μA	Unetched surface			Etched surface		
	C_{dl} / μF cm^{-2} Polycrystalline	C_{dl} / μF cm^{-2} Single-crystal	Roughness factor	C_{dl} / μF cm^{-2} Polycrystalline	C_{dl} / μF cm^{-2} single-cryst.	Roughness factor
5	76.0	—	—	—	—	—
10	69.3	20	3.5	39.6	—	—
20	—	—	—	46.7	16	2.9
25	86.3	—	—	—	—	—
50	76.4	21	3.6	65	22	3.0
75	80.6	22	3.7	—	—	—

Notes

1. All measurements were carried out in 1M Na_2SO_4 solution at pH 11.5.
2. Area of the single-crystal is 1.13 cm^2 and 0.07 cm^2 for the polycrystalline electrodes.

In this work, the areas under i vs E curves were measured by using a planimeter. Charge densities (C cm^{-2}) for film formation were calculated using the true surface area of the electrode, taking the roughness factor for certain of the Zn electrodes as 3 (see above section 2.5).

Current-densities quoted in the present work are defined as current divided by the geometrical area in cm^2, since the real to apparent surface area ratios could not always be easily or reliably determined.

CHAPTER 3

Cyclic-Voltammetry Experiments with the Zinc Electrode

3.1 Introduction

This chapter presents results obtained by the cyclic-voltammetry method (see section 2.2.2.) applied to the investigation of the processes of formation, dissolution and breakdown of passive films formed on zinc from aqueous solutions containing bicarbonate, carbonate, sulphate and chloride over the pH range 7.5 to 14.

Since cyclic-voltammetry has been employed extensively in this work, a brief account is given below about the type of results that are expected from the use of this method.

3.2 Sweep-rate Dependence of Current and Potential

3.2.1 General

The characteristic current response behaviour in cyclic-voltammograms has been evaluated in the literature for various types of reactions. Two principal conditions may arise, as with any electrode process:

(1) The electrode reaction behaves kinetically in a reversible or an irreversible way and a transition between these kinds of behaviour may take place depending on reaction conditions (e.g. potential, sweep-rate, temperature).

(2) the rate (or current) of the electrode reaction is

either activation (i.e. reaction kinetic) or diffusion-controlled.

In the first case (1) reaction kinetic control may involve a) direct dissolution of the metal into solution or deposition from ionic species in solution or b) formation or reduction of a surface film, e.g. of an oxide of the metal. We shall refer to the latter type of reaction as a "surface film" process or briefly as a "surface" process.

3.2.2 Diffusion-Control

A simple charge transfer process, $O + ze \rightleftharpoons R$, may behave reversibly or irreversibly. In the reversible case both backward and forward reaction rates are identical or at least comparable. The rate of electron transfer is sufficiently rapid at the electrode surface, that the potential can then be related to the concentrations (activities) of oxidized [O] and reduced [R] species of the redox couple by the Nernst equation:

$$E_t = E_o + \frac{RT}{zF} \ln [O]/[R] \qquad (32)$$

where E_o is the standard reversible potential.

The fundamental equations for linear potential sweep and cyclic-voltammetry experimental conditions, where diffusion plays a role in the observed kinetics, have been developed by Nicholson and Shain[125] and by Delahay [126] and others[127,128]. For a diffusion-controlled reaction, the current I is linear in the square-root of the sweep-rate (s) according to the equation

$$I = zFAC_o(\pi Da)^{1/2}.\chi(at) \qquad (33)$$

where C_o is the bulk concentration of reactants, A is the area of the electrode, D is the diffusion constant and $\chi(at) = zFst/RT = (zF/RT)(E_t - E_i)$ is a generalized function. The function $\pi^{1/2}\chi(at)$ and hence the current, depends on potential and gives rise to a maximum. At 298 K

$$\pi^{1/2}\chi_p(at) = 0.4463 \qquad (34)$$

for A in cm^2, D in $cm^2 s^{-1}$, C_o in mol cm^{-3} and s in V s^{-1}. Then

$$I_p = (2.69 \times 10^5) z^{3/2} D^{1/2} s^{1/2} C_o A \qquad (35)$$

and

$$E_p - E_{p/2} = (-56.5)/z \text{ mV} \qquad (36)$$

where E_p and $E_{p/2}$ are the potentials at the peak current (I_p) and half-peak current ($0.5 I_p$), respectively. Thus, for the reversible case, E_p is independent of scan-rate and I_p is proportional to $s^{1/2}$.

For the irreversible case, potential is determined by a Tafel type relation involving α the charge-transfer coefficient for the electrochemical activation-controlled interfacial reaction. The current is then given by:

$$I = zFAC_o(\pi Db)^{1/2} \chi(bt) \qquad (37)$$

where b is analogous to $\underline{a}$, but applies to irreversible charge transfer according to $bt = \alpha zFst/RT$. Again the I vs E profile has the form of a curve exhibiting a maximum (peak) current, I_p, given by:

$$I_p = (2.99 \times 10^5)(\alpha z_a)^{1/2} zAC_o D^{1/2} s^{1/2} \qquad (38)$$

where z_a is the number of electrons involved in the rate-determining step and α is charge transfer coefficient. The units are the same as for I_p as specified above eqn. (35) and the peak potential is given under these conditions by:

$$E_p = E_{1/2} - 2.3RT/\alpha z_a F \left[0.52 - 1/2 \log (2.3RT2/\alpha z_o FD) - \log k_s + 1/2 \log s\right] \quad (39)$$

where $E_{1/2}$ is the half-wave potential and k_s is the specific rate constant at the standard potential. It is seen from eqn. (39) that the variation of E_p with log (sweep-rate) is an indication kinetically of the departure of the system from equilibrium. Therefore reversible and irreversible I vs E profiles differ somewhat in shape[126], corresponding to differences in shapes of polarographic curves for reversible and irreversible conditions.

3.2.3 Surface Reaction Control

Here a simple surface process $X^- + M \rightleftharpoons MX + e$ is considered where X^- is a solution species with activity a_x and MX is an adsorbed electrodeposited species. The activity of MX is taken as equal to its fractional coverage, θ_x, for Langmuir adsorption behaviour. The fraction of free metal sites is equal to $(1-\theta_x)$. Note, the film at coverage θ_x may not be distributed randomly but in islands; then the Langmuir treatment does not apply.

The ad-species is deposited at the electrode at a rate proportional to the free surface site fraction, $1-\theta_x$, and the backward reaction takes place at a rate proportional to θ_x; also

the reaction is taken to be potential-dependent with the usual Butler-Volmer factor exp ($\alpha n F/RT$), i.e. the Tafel exponent.

In the reversible case, the current I can be written

$$I = Q_m[\ k_1 C_x(1-\theta_x)\exp \alpha n F/RT - k_{-1} C_x \theta_x \exp -(1-\alpha) n F/RT\ ] \quad (40)$$

where Q_m is the charge required for formation or desorption of a monolayer, k_1 and k_{-1} are standard rate constants for the reversible potential and n is the overpotential. The second term is negligible in the irreversible case, since $k_1 >> k_{-1}$ or $\alpha n F/RT >> 1$.

The equations for dependence of current and potential on sweep-rate for cyclic-voltammograms of a simple surface process were derived by Srinivasan and Gileadi [29].

For a highly reversible adsorption process, expressing the rate in terms of current density i, the peak value of i, i_p is given by:

$$i_p = (Q_m F/4RT)\ s \quad (41)$$

with

$$E_p = -RT/F \ln k_1 \quad (42)$$

and also the pseudocapacitance $C_\phi = Q\ d\theta_x/dn$ is given by i/s.

For a highly irreversible reaction, where the net rate of the process is nearly equal to its forward rate,

$$i_p = 1/e\ (Q_m \alpha F/RT)\ s \quad (43)$$

and

$$E_p = (RT/\alpha F) \ln s + (RT/\alpha F) \ln (Q_m \alpha F/k_1 RT) \quad (44)$$

The peak potential, E_p, varies with log s (as is also the case

for diffusion control, eqn. (39)) rather than being independent of s as in the case for a reversible process. Also i_p for an irreversible process is lower than for a corresponding reversible one and the i vs E profiles differ somewhat in shape for reversible and irreversible conditions (for the former, the i vs E curves are symmetrical).

A result that is important for the present work is that I_p for a surface process is linear in sweep-rate but is square-root in s for a diffusion-controlled process. Sometimes mixed-control is observed as in some cases encountered in the present work. Also multilayer oxide film formation is found to arise under most conditions but if the quantity of oxide involved in a series of measurements at various sweep-rates is constant, the same result that I_p is linear in s is found. This type of behaviour will be referred to as that of a "surface process".

3.2.4 Complications due to Pre-and Post-Electrochemical Reactions

The overall reaction for Zn dissolution/passivation must be more complicated than the simple irreversible/reversible electrochmical adsorption reaction, based on the Langmuir adsorption isotherm, shown above. The overall process can be composed of several stages: chemical or electron-transfer steps, and also product species may be either adsorbed (deposited) or transferred directly-into the solution phase without adsorption (deposition). Also multilayer film formation takes place under some conditions, as will be shown later.

More complicated models involving other isotherms have been

proposed by Kozlowska, Conway and Klinger[130] and by Laviron[131] in the case of 2-dimensional surface processes. Delahay[132] has considered various cases for the regime of diffusion control in different kinds of treatment of film processes; Calander et al.[133] proposed a "pore resistance" model for passivation, i.e. resistance of the solution in the pores becomes the factor that limits the current and eventually this gives rise to the characteristic sudden drop in current as the film is being formed. Under potentiodynamic conditions, this situation was shown[133] to give rise to currents that are also proportional to $s^{1/2}$, as with diffusion-control.

While monolayer deposition of ZnO was encountered under some conditions in the present work, in a number of experiments the quantity of oxide generated per cm^2 in a potential-sweep is often greater than that corresponding to a monolayer and the material can evidently (see SEM pictures) be deposited in 3-dimensional structures on the metal surface. Then the current-potential profile cannot be treated simply in terms of a 2-dimensional adsorption process according to eqn. (40) with terms θ_x or $1-\theta_x$ in fractional coverage by a monolayer.

However, multilayer film formation and reduction also usually gives rise to a current peak whose height (in current) is often proportional to sweep-rate, as was mentioned on page 58 but the slope of such a relation is different from that for the peak for a monolayer process. The ascending current profile for an anodic film process follows a Tafel law (modified sometimes by the resistance of the oxide film) involving the free surface fraction of the metal that at any amount is determined by the extent and

geometry of the film growth. Eventually, when the free metal surface fraction approaches zero, the current is rapidly diminished to almost zero (passivation). Hence a peak current vs potential (time) relation also results. Some anodic film growth processes may start with formation of a monolayer which then becomes extended to a multilayer film.

Similarly, for reactions of a multilayer film, the current initially increases exponentially in the (cathodic) sweep but finally declines to zero as reducible material of the film runs out.

3.3 Experimental Results

Typical cyclic-voltammograms for dissolution, formation and reduction of the anodic film formed on zinc in 1M Na_2CO_3 and 3M NaCl solutions at pH 11.5, and the notation used for designating the peaks, are shown in Fig. 3.1 . Depending on the nature of the electrode surface, electrolyte and pH, between one, two or three current peaks are observed in both the cathodic and anodic sweeps.

The difference between the cyclic-voltammograms for zinc in 1M Na_2CO_3 (Fig. 3.1a) and 3M NaCl (Fig. 3.1b) at the same pH is obvious: in 1M Na_2CO_3 solution, two anodic peaks (A_1 and A_2) and a plateau region which includes the third, flatter peak (A_3) was observed, whereas in 3M NaCl solution a sudden rise in current is seen at about -0.15 V more positive than the first anodic peak A_1 which usually appears around -0.38 V E_H for both solutions. The A_2 and A_3 peaks appear around -0.07 V and +1.7 V,

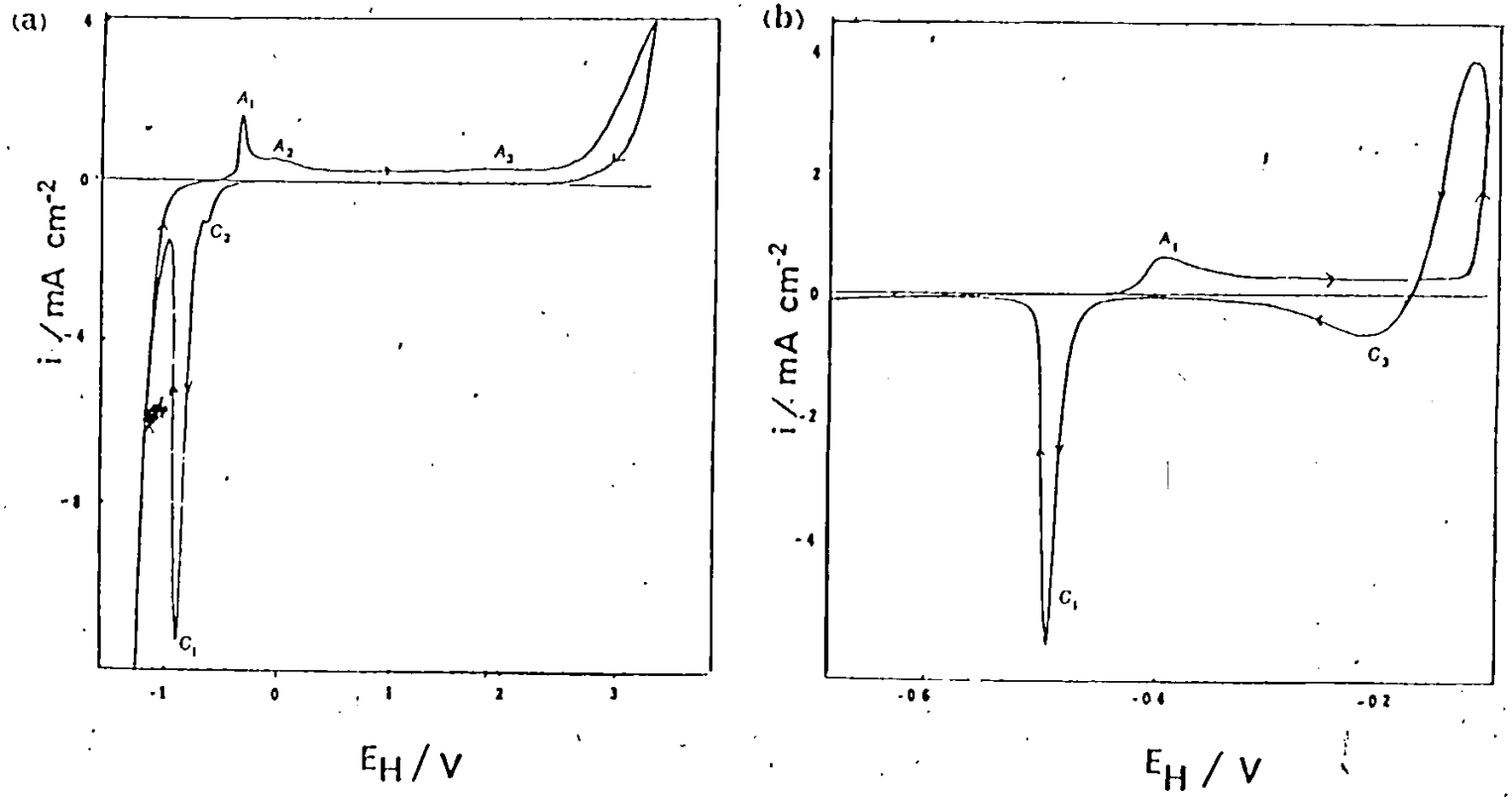

Fig. 3.1 Typical cyclic-voltammograms of polycrystalline Zn in (a) 1M Na_2CO_3 (b) 3M NaCl solution at pH 11.5.
s = 50 mV s^{-1}, electrode - polycrystalline, of apparent area 0.07 cm^2, etched in HCl.

respectively.

In order to study the relationship between distinguishable anodic and the corresponding cathodic processes over various ranges of potential in the sweep, the upper limit of potential at which the anodic sweep was reversed was varied in successive sweeps (the so-called "cutting" experiment where the range of a sweep was successively cut or increased). Examples are shown in the next section.

3.3.1 Sweep Reversal Studies

Fig. 3.2a shows the cyclic-voltammograms obtained for Zn in 3M K_2CO_3 and Fig. 3.2b those for Zn in 3M NaCl solution with a progressively increasing potential limit in the anodic sweep. Reversal of the anodic sweep at potentials more positive than the peak potentials A_1 and A_2 gives rise to the reduction peak C_1. When the anodic sweep was reversed in region A_3, the cathodic peak C_2 was observed. In the case of 3M NaCl solution at pH 11.5, peak C_3 became evident if the forward (anodic) sweep was reversed just after the sudden rise in current. Sometimes in carbonate solution a small reduction peak appeared before the C_2 peak. The behaviour of the current peaks C_3 and C_2 will be discussed in more detail in section (3.5).

3.3.2 Current Peaks A_1 and C_1

A more detailed study of the current peaks A_1 and C_1 (Fig. 3.1a) is helpful for understanding the early stages in the passivation of Zn in alkaline solution.

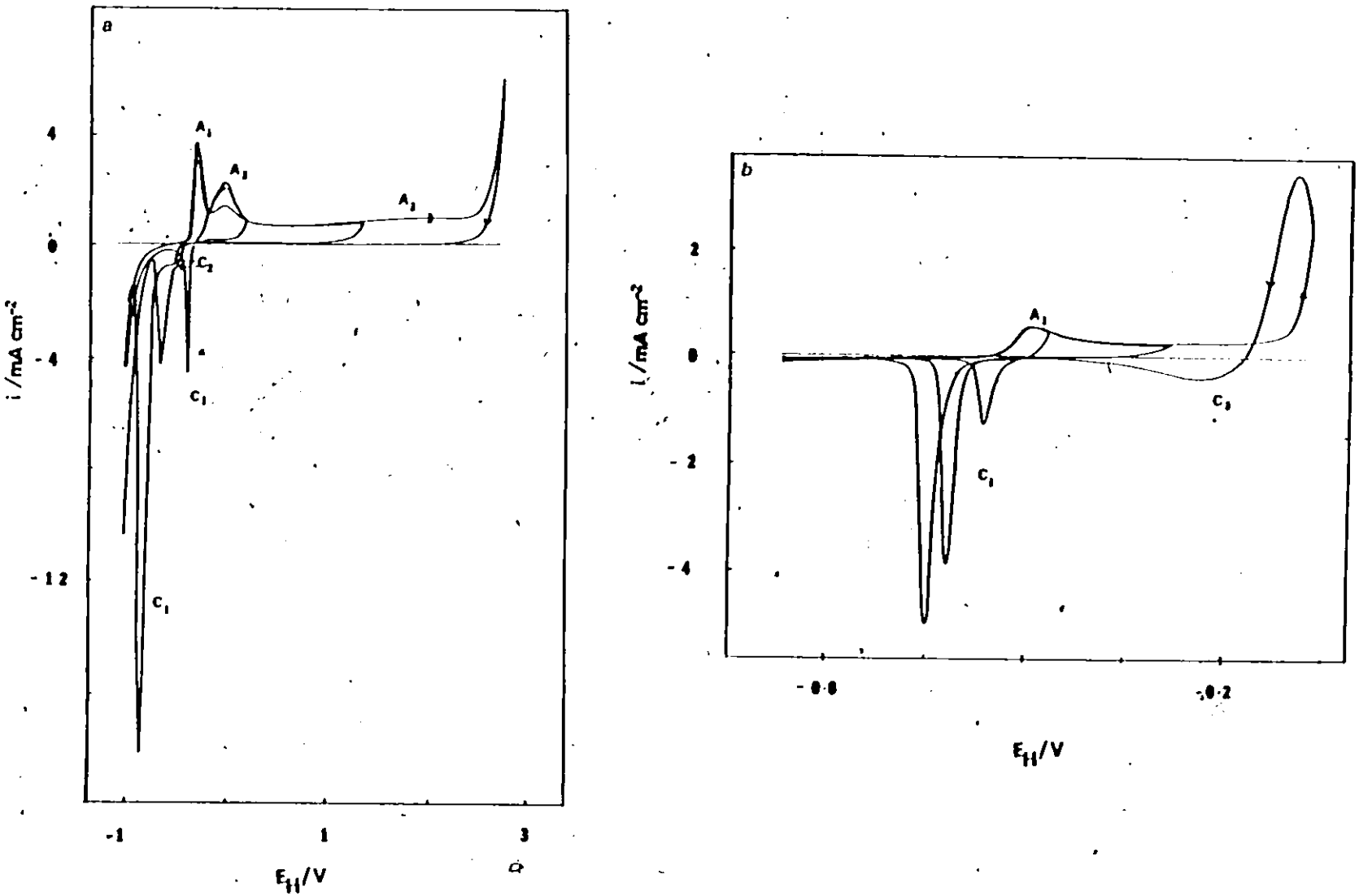

Fig. 3.2 Series of cyclic-voltammograms obtained for an etched Zn electrode with progressively increasing potential limit in the anodic sweep.

(a) 3M K_2CO_3 at pH 13.3, s = 100 mV s^{-1}

(b) 3M NaCl at pH 11.5, s = 50 mV s^{-1}

This diagram designates the principal processes for which peak currents arise in anodic and cathodic sweeps.

Current vs potential profiles for Zn in the range -0.6 V to -0.2 V with different solutions and at various sweep-rates were generated. Table 3.1 lists the potentials of the current maxima for the A_1 and C_1 peaks (Fig. 3.1a) at a sweep-rate of 100 mV s^{-1} in various solutions. Fig. 3.3 shows a typical cyclic-voltammograms obtained over this short potential range at various sweep-rates. It can be seen from Table 3.1 that the peak potentials do not depend appreciably on the electrolyte when the pH is between 11.5 and 13.3.

The peak A_1 could be due to formation of an hydroxide or oxide of Zn. Several forms of hydroxides and oxides have been identified and aspects of the chemistry of these compounds were discussed already in chapter 1 (section 1.1.1. and 1.1.2).

While it is recognized that some inherent danger exists in comparing cyclic-voltammetric peak potentials with thermodynamic equilibrium potentials, it is nevertheless a useful procedure which provides a check on the viability of a proposed oxidation/reduction mechanism. We now consider some data, on this basis, below.

The reversible potentials for amorphous $Zn(OH)_2$ (the most unstable form and, for that reason, the most soluble), for ε-$Zn(OH)_2$ (the least soluble and the most stable hydroxide) and for inactive ZnO, were calculated, using the equilbrium constants given in Table 1.2.

The reaction equations and corresponding Nernst relations are as follows:

$$Zn\ (s) + H_2O = ZnO\ (s) + 2H^+ + 2e \qquad (45)$$

Table 3.1

Peak Potentials of the A_1 and C_1 Peaks for Various Solutions

Solution	pH	Potential range/V ($s = 100\ mV\ s^{-1}$)	E_p/V (A_1 peak)	E_p/V (C_1 peak)
3M K_2CO_3	13.3	(-0.530)-(-0.254)	-0.362	-0.432
1M K_2CO_3	13.0	(-0.615)-(-0.232)	-0.371	-0.460
0.1M NaOH	13.0	(-0.657)-(-0.232)	-0.350	-0.450
1M Na_2CO_3	11.5	(-0.618)-(-0.218)	-0.350	-0.454
1.0M Na_2CO_3 + 2.0M NaCl	11.5	(-0.648)-(-0.192)	-0.353	-0.548
0.1M Na_2CO_3 + 0.5M Na_2SO_4	11.5	(-0.625)-(-0.219)	-0.349	-0.475
1M Na_2SO_4	11.5	(-0.634)-(-0.230)	-0.348	-0.481
3M NaCl	11.5	(-0.643)-(-0.243)	-0.353	-0.488
1M $NaHCO_3$	7.9	(-0.592)-(-0.291)	-0.397	-0.470

Notes

1. Peak potentials given above are for A_1 and C_1 peaks (see Fig. 3.1a) in CV's at a sweep-rate of $100\ mV\ s^{-1}$.
2. Peak potentials at a constant pH, e.g. 11.5 are independent of the anions present in the solution.

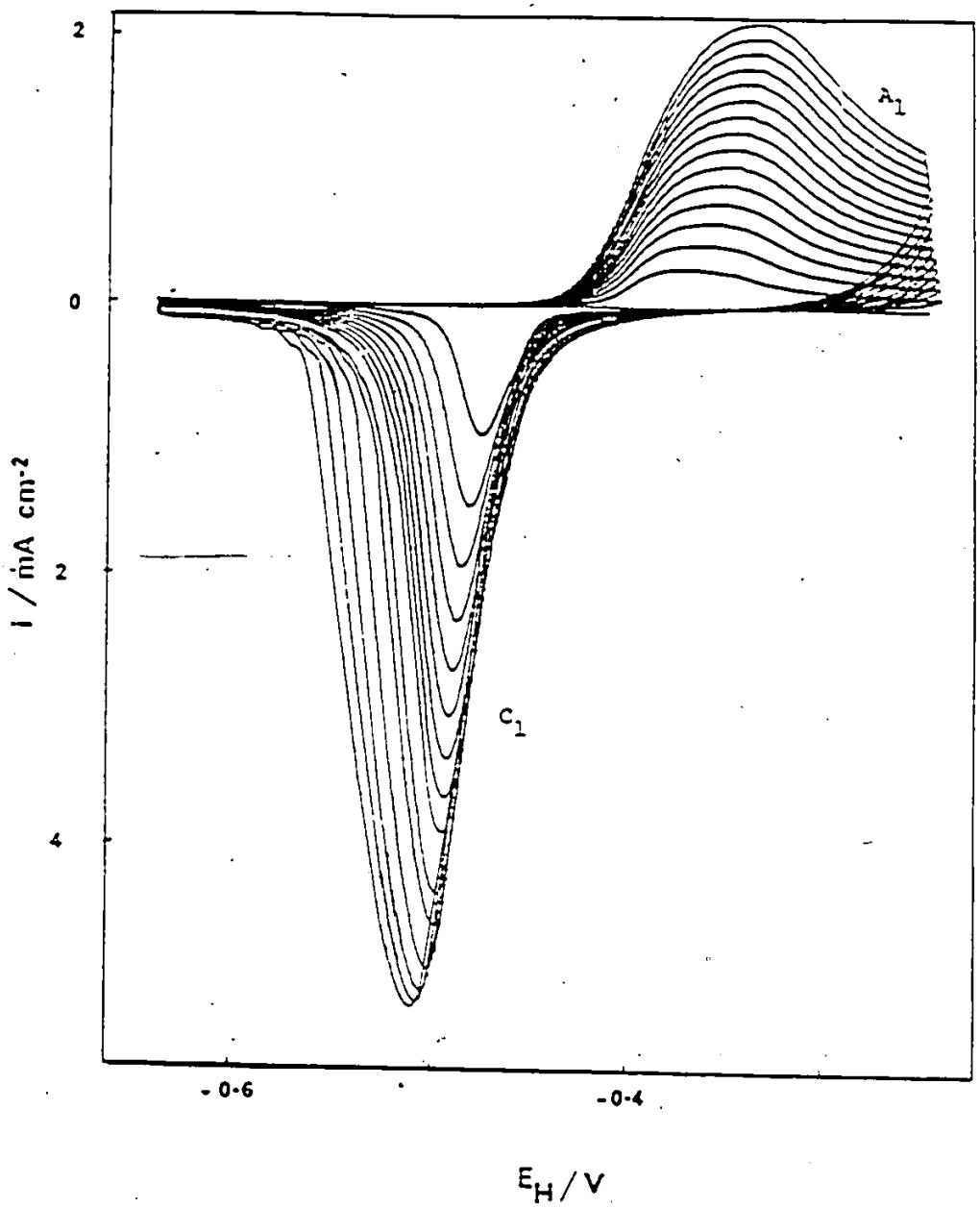

Fig. 3.3 Cyclic-voltammtry i vs E profiles for a polycrystalline Zn electrode in 3M NaCl solution at pH 11.5 with variable sweep-rate.

Sweep-rate varies from 300 mV s^{-1} to 20 mV s^{-1}, with successive 20 mV s^{-1} decrease of s.

$$E_R = (-0.429 - 0.059\ pH)\ V$$

$$Zn\ (s) + 2H_2O = Zn(OH)_{2\ am.} + 2H^+ + 2e \quad (46)$$

$$E_R = (-0.394 - 0.059\ pH)\ V$$

$$Zn\ (s) + 2H_2O = \epsilon\text{-}Zn(OH)_2 + 2H^+ + 2e \quad (47)$$

$$E_R = (-0.422 - 0.059\ pH)\ V$$

In the present work, potentials E are referred to the reversible potential, E_H, of a Pt/H_2 reference electrode in the same solution. Therefore the reversible potentials thus derived for ZnO, $Zn(OH)_{2\ am.}$ and ϵ-$Zn(OH)_2$ are -0.429 V , -0.394V and -0.422V, respectively.

On account of their amphoteric character, ZnO and $Zn(OH)_2$ dissolve in alkali to form zincate. The data given above are valid only for conditions (ionic strength I = 0) for which the respective compounds in the solid form are at equilibrium with species in solution. Even though the solid phase that is formed at the electrode is unstable in the alkaline media and tends to dissolve as soluble zincate, a passive layer is always maintained in a steady-state on the surface of the polarized electrode (depending on pH) since a finite oxidation rate is imposed by the net current passing. In such cases, the potential of the electrode is determined by this surface film in relation to the anodic current passing.

Oxidation of Zn and reduction of ZnO commences at -0.468 V and -0.343 V, respectively, in 3M NaCl solution at pH 11.5 (Fig. 3.3). The E_R values given above lie between the potentials at

the feet of the A_1 and C_1 peaks. Therefore it is likely that the peaks A_1 and C_1 correspond to the formation and reduction of ZnO or $Zn(OH)_2$.

3.3.2.1 Role of Film or Solution Processes?

It is of interest to know whether the formation of ZnO, $Zn(OH)_2$, or both, at peak A_1 involves direct formation of a solid film of either or both of these species, or if the film is generated subsequently from zinc dissolved anodically as zincate, i.e. a dissolution/precipitation process occurs.

Cyclic-voltammograms for both processes will be somewhat similar in the sense that current peaks are generated; however, the dissolution/precipitation type of process will give rotation-dependent charges under the peaks and anodic/cathodic charge-ratios will be > 1. The effect of both rotation and sweep-rate on charge under the anodic and cathodic peaks thus provides useful information for answering this question.

In a process involving film formation or reduction, since the consumable reactant quantity is fixed (determined by the film coverage and/or thickness, assuming 100% current efficiency) the charge under a cyclic-voltammogram peak, Q, is given by $Q = \int I dt = \int (I/s) dE$ and the anodic/cathodic charge ratio, Q_a/Q_c, i.e. the ratio of the charge passed in the anodic peak, Q_a, to that in the cathodic peak, Q_c, is close to unity and will be independent, ideally, of s.

However, in a process involving initial dissolution followed by precipitation of the solid oxide or hydroxide phase, the

charge ratio, Q_a/Q_c, may vary with sweep-rate, but thus Q_a/Q_c is found to be close to unity at higher sweep-rates and greater than one at lower sweep-rates. This arises because, at lower sweep-rates, any soluble product(s) of oxidation of Zn have time to remain dissolved in the electrolyte and diffuse into the bulk solution. Therefore only a fraction of the oxidation product will be available for reduction at the electrode in a following cathodic sweep at low sweep-rates. These effects will be modified by mass-transfer, as at a rotating disc electrode - a situation that was experimentally investigated and will be discussed later.

Another common case where the required charge under a CV peak can depend on sweep-rate should be noted: it is when mass-transfer of reactant(s) to the electrode determines the current; then reactant material is consumed from the diffusion layer, eventually depleting the solution completely at the electrode interface. The charge under the I vs E(t) profile then increases with decrease in s because there is more time for reactants to diffuse to the electrode surface at the lower sweep-rates.

The charges passed for the formation of zinc oxide or hydroxide, and its subsequent reduction, were calculated from the $\int i\,dt$, areas under the respective peaks for various sweep-rates. Results are summarized in Table 3.2 for the series of different sweep-rates used. In strongly alkaline electrolytes, the charge ratio, Q_a/Q_c, was close to unity only at higher sweep-rates (> 200 mV s^{-1}); however, as the pH is decreased, dissolution of the film only becomes important at slower sweep-rates (< 20 mV s^{-1}), i.e. when there is more time during the sweep for dissolution to

occur.

Two distinguishable mechanisms of film formation coupled with diffusion can be: i) a regular dissolution/precipitation mechanism where dissolution of the metal as soluble ions occurs with diffusion of these ions into solution and, after some transition time corresponding to formation of a boundary layer, precipitation of oxide or hydroxide occurs; ii) formation of an oxide film at the metal/solution interface by direct electrodeposition of OH^- ions with growth by field-assisted diffusion of ions in the film (Mott-Cabrera mechanism) coupled with dissolution of the oxide at its external surface by reaction with OH^- (at high pH) to give soluble zincate ions which diffuse away. A steady-state oxidation rate can eventually be set up when the rates of the two processes become equal. Both the types of processes (i) and (ii) will be pH dependent owing to the influence of pH on solubility of Zn species.

From the above results it can be concluded that the reactions taking place at peaks A_1 and C_1 correspond more to a film reaction involving solution diffusion processes than to direct formation of a film by electrodeposition of OH.

3.3.2.2 Thickness of the Anodically Formed Films at Zn Electrodes

From the evaluated charge under the peak A_1, it can be decided whether the thickness of the oxidation product, zinc oxide, corresponds to a monolayer or multilayer, assuming that the product formed does not dissolve and then diffuse into bulk

Table 3.2

Effect of pH and Sweep-Rate on Charge per cm^2 Arising in Peaks A_1 and C_1

	Solution	pH	s = 4 mV s^{-1}			s = 20 mV s^{-1}			s = 60 mV s^{-1}		
			q_a $\mu C\ cm^{-2}$	q_c $\mu C\ cm^{-2}$	q_a/q_c	q_a $\mu C\ cm^{-2}$	q_c $\mu C\ cm^{-2}$	q_a/q_c	q_a $\mu C\ cm^{-2}$	q_c $\mu C\ cm^{-2}$	q_a/q_c
A	1.0M KOH	14.0	697×10^3	7.5×10^3	92.5	160×10^3	32×10^3	4.9	71×10^3	28×10^3	2.5
B	0.2M NaOH+0.03M Na_2CO_3	13.3	51×10^3	3.7×10^3	13.8	10.5×10^3	5.9×10^3	1.8	7.9×10^3	3.8×10^3	2.1
C	0.1M NaOH	13.0	24×10^3	0.5×10^3	48.0	5.3×10^3	532	9.9	2.3×10^3	640	3.6
D	0.1M NaOH+0.96M Na_2SO_4	13.0	15×10^3	0.87×10^3	17.2	4.5×10^3	589	7.6	1889	523	3.6
E	0.05M NaOH+0.98M Na_2SO_4	12.7	5.3×10^3	1.6×10^3	3.3	2058	1206	1.7	1357	805	1.7
F	0.03M NaOH+0.99M Na_2SO_4	12.5	3100	644	4.8	989	471	2.1	725	480	1.5
G	0.03M NaOH+0.99M Na_2CO_3	12.5	5096	994	5.1	1516	659	2.3	961	598	1.6
H	0.025M NaOH	12.4	3759	320	11.7	787	286	2.8	857	471	1.8
I	1M Na_2SO_4	11.5	1126	829	1.4	787	758	1.0	593	589	1
J	1M Na_2CO_3	11.5	1964	1064	1.9	1178	820	1.4	838	701	1.2
K	3M NaCl	11.5	1156	835	1.4	789	656	1.2	600	546	1.1
L	0.5M Na_2CO_3	11.4	1559	537	2.9	876	631	1.4	579	476	1.2
M	0.1M Na_2CO_3+0.5M Na_2SO_4	11.2	1253	933	1.4	848	688	1.2	629	556	1.1
N	0.1M Na_2CO_3	11.2	1083	768	1.4	664	692	1	537	495	1.1
O	1M $NaHCO_3$	8.5	—	—	—	3627	1168	3.1	1912	876	2.2

Notes

1. This table summarizes the charges passed for the formation of ZnO or $Zn(OH)_2$ in peak A_1 and its subsequent reduction in peak C_1 in various solutions for a series of different sweep-rates.
2. All experiments were made with a Zn electrode etched in 48% HBr and roughness factor was assumed as 3 for the charge density calculations.
3. All charges were calculated relative to the zero current baseline, since double-layer charging currents were relatively negligible.
4. In strongly alkaline electrolytes, the charge ratio, q_a/q_c was close to unity only at higher sweep-rates (>20 mV s^{-1}) but, as pH decreases, dissolution of the film becomes important only at lower sweep-rates (<20 mV s^{-1}).

Table 3.2 (continued)

	Solution	pH	s = 100 mV s^{-1}			s = 200 mV s^{-1}			s = 300 mV s^{-1}		
			q_a $\mu C\ cm^{-2}$	q_c $\mu C\ cm^{-2}$	q_a/q_c	q_a $\mu C\ cm^{-2}$	q_c $\mu C\ cm^{-2}$	q_a/q_c	q_a $\mu C\ cm^{-2}$	q_c $\mu C\ cm^{-2}$	q_a/q_c
A	1.0M KOH	14.0	—	—	—	—	—	—	—	—	—
B	0.2M NaOH+0.03M Na_2CO_3	13.3	5863	2967	2	3721	1998	1.9	2755	1568	1.8
C	0.1M NaOH	13.0	1804	895	2	1324	763	1.7	1126	707	1.6
D	0.1M NaOH+0.96M Na_2SO_4	13.0	1375	523	2.6	1027	678	1.5	871	688	1.3
E	0.1M NaOH+0.98M Na_2SO_4	12.7	1149	711	1.6	900	688	1.3	810	532	1.5
F	0.05M NaOH+0.98M Na_2SO_4	12.5	626	462	1.4	523	480	1.1	485	377	1.3
G	0.03M NaOH+0.99M Na_2CO_3	12.5	829	575	1.4	655	617	1.1	608	546	1.1
H	0.025M NaOH	12.4	721	485	1.5	579	509	1.2	523	452	1.2
I	1M Na_2SO_4	11.5	556	480	1.2	490	551	0.9	443	462	1
J	1M Na_2CO_3	11.5	768	631	1.2	608	772	0.8	556	485	1.2
K	3M NaCl	11.5	565	471	1.2	500	714	0.7	448	458	1
L	0.5M Na_2CO_3	11.4	593	523	1.1	490	622	0.8	452	452	1
M	0.1M Na_2CO_3+0.5M Na_2SO_4	11.2	584	509	1.1	490	475	1	504	490	1
N	0.1M Na_2CO_3	11.2	476	438	1.1	400	556	0.7	410	532	0.8
O	1M $NaHCO_3$	8.5	1507	692	2.2	1003	542	1.9	—	—	—

solution* and that the structure of the product is known, i.e. its density is available as an experimental datum.

The thickness of the layer corresponding to peak A_1 was calculated assuming that the product formed was ZnO. There is extensive literature on the structure of ZnO. Finch and Quarell [134] state that ZnO is "pseudomorphic", i.e. the basal plane of ZnO is identical with that of Zn metal, both structures being hexagonal, but other workers [135] have not found evidence for a pseudomorphic structure. It has been observed that the ratio of the volume per ZnO "molecule" to volume per Zn atom is, in fact, 1.55. Fig. 3.4 shows the Zn [5] and ZnO [136,137] structures relevant to this calculation.

The area of the base of the unit-cell of an hexagonally close-packed structure is a^2 Sin 60^o, where $\underline{a}$ is the distance between the atoms or ions along the a-axis. Therefore the charge density in a monolayer, q_m, is given by:

$$q_m = 2e/a^2 \sin 60^o \qquad (48)$$

The values of $\underline{a}$ for metallic Zn and ZnO are 0.2660 nm and 0.325 nm, respectively. The calculated oxidation charge density per cm^2 for a monolayer of Zn is therefore 522 $\mu C\ cm^{-2}$ and 350 $\mu C\ cm^{-2}$ for formation of ZnO.

Table 3.3 gives the number of layers of ZnO formed at the first anodic peak (A_1) in various solutions and for a range of sweep-rates. These calculations were made on the basis that the roughness factor of the electrode was 3, as shown in chapter 2, section 2.5, and the charge required per cm^2 for a monolayer of

* This question is settled by recourse to the electrode rotation experiments.

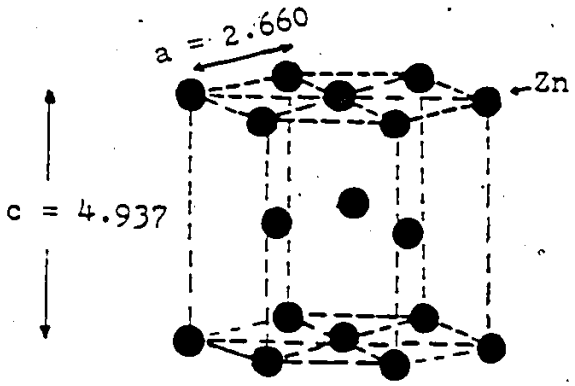

Fig. 3.4a Hexagonal close-packed unit cell of Zn.

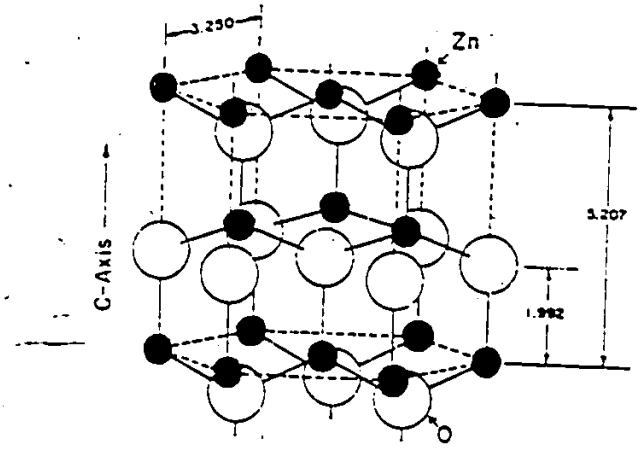

Fig. 3.4b Wurtzite unit cell of ZnO. (Ref. 136,137)

Note - Dimensions are given in Angstrom units. Sizes of the atoms in ZnO and Zn are not drawn to scale.

ZnO formed or reduced was 350 $\mu C\ cm^{-2}$, as derived above.

We see from Table 3.3 that the apparent thickness of the ZnO film generated depends very much on pH of the electrolyte and also on the sweep-rate. The relationship to the former is connected with solubility (amphoteric behaviour of ZnO) and to the latter through the time scale (order of $\Delta E/s$) over which the oxide film growth and dissolution process can take place. It is interesting that at high sweep-rates and/or with electrolytes (sodium carbonate or dilute NaOH) in which Zn is less soluble, only 1 or 2 equivalent molecular layers of ZnO are formed. This is a significant conclusion.

3.3.2.3 Sweep-rate Dependence of Peak Currents

A number of experiments were carried out with variation of sweep-rate between 300 mV s^{-1} and 2 mV s^{-1} to determine the i_p vs s relationships. Peak currents i_p were plotted as function both of s and $s^{1/2}$; also plots of log i_p vs log s were made (Figs. 3.5 and 3.6). Table 3.4 shows the slopes of the resulting log i_p vs log s plots obtained with solutions having a wide range of pH's. Some of these values were not as expected, especially the linear dependence of i_p on $s^{0.75}$ for alkaline solutions around pH 11.5. This behaviour is significantly different from either of the limiting i_p vs s or i_p vs $s^{1/2}$ relations expected on the basis of the usual kinetic models outlined above. It should be stressed, however, that the unusual values of the exponent that are found are based on excellent linearity of the log-log plots over a wide

Table 3.3

The Effect of pH and Sweep-Rate on the Thickness of Anodic Film at peak A_1

	Solution	pH	Charge in Peak A_1 calculated as number of layers (or equivalent layers*) at various sweep rates/mV s^{-1}					
			4	20	60	100	200	300
A	1.0M KOH	14.0	2000	450	200			
B	0.2M NaOH+0.03M Na_2CO_3	13.3	146	30	22	17	11	8
C	0.1M NaOH	13.0	69	15	7	5	4	3
D	0.1M NaOH+0.96M Na_2SO_4	13.0	43	13	5	4	3	2
E	0.05M NaOH+0.98M Na_2SO_4	12.7	15	6	4	3	2	2
F	0.03M NaOH+0.99M Na_2SO_4	12.5	9	3	2	2	1	1
G	0.03M NaOH+0.99M Na_2CO_3	12.5	14	4	3	2	2	2
H	0.025M NaOH	12.4	11	3	2	2	2	1
I	1M Na_2SO_4	11.5	3	2	2	2	1	1
J	1M Na_2CO_3	11.5	5	3	2	2	1	1
K	3M NaCl	11.5	3	2	2	2	1	1
L	0.5M Na_2CO_3	11.4	4	3	2	2	1	1
M	0.1M Na_2CO_3+0.5M Na_2SO_4	11.2	4	2	2	2	1	1
N	0.1M Na_2CO_3	11.2	3	2	2	1	1	1
O	1M $NaHCO_3$	8.5		11	5	5	3	

Notes

1. * Calculated on the hypothetical basis that ZnO/$Zn(OH)_2$ formed during oxidation does not go into solution.
2. All measurements are for Zn electrodes etched in 48% HBr; roughness factor of the electrode is taken as 3 and C_a values from Table 3.2.
3. All calculations were carried out assuming ZnO_2 is formed and charge required per monolayer is 350 $\mu C\ cm^{-2}$.
4. Thickness of the film is smallest around pH 11.5. The film is thicker in the presence of CO_3^{2-} than in presence of Cl^- or SO_4^{2-} ions.

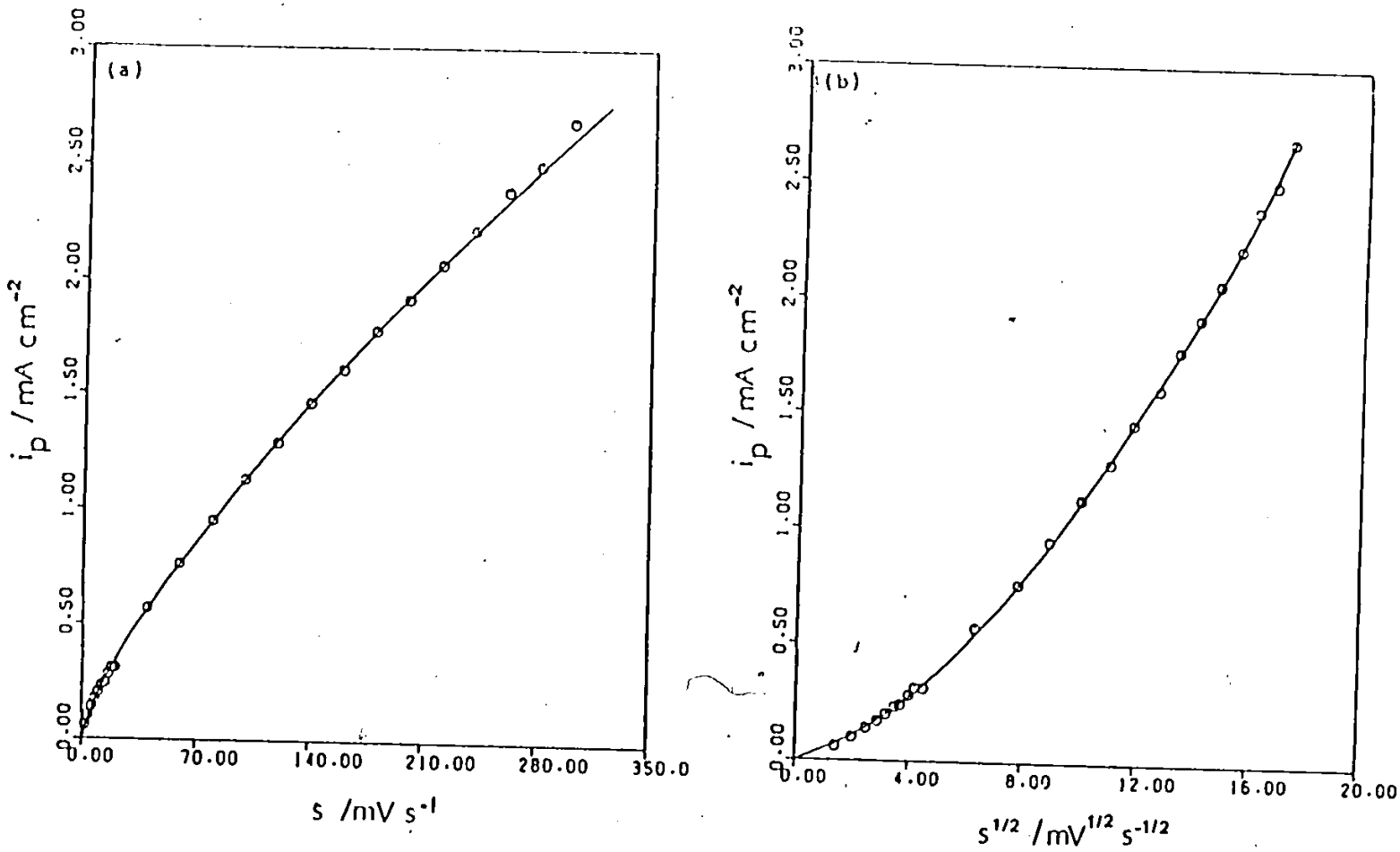

Fig. 3.5 Dependence of the peak current density as a function of (a) s and (b) $s^{\frac{1}{2}}$ for the A_1 peak in 0.1M Na_2CO_3 + 0.5M Na_2SO_4 at pH 11.2
s - 300 ---> 2 mV s^{-1} Electrode - polycrystalline of apparent area 0.07 cm^2 and etched in HBr.

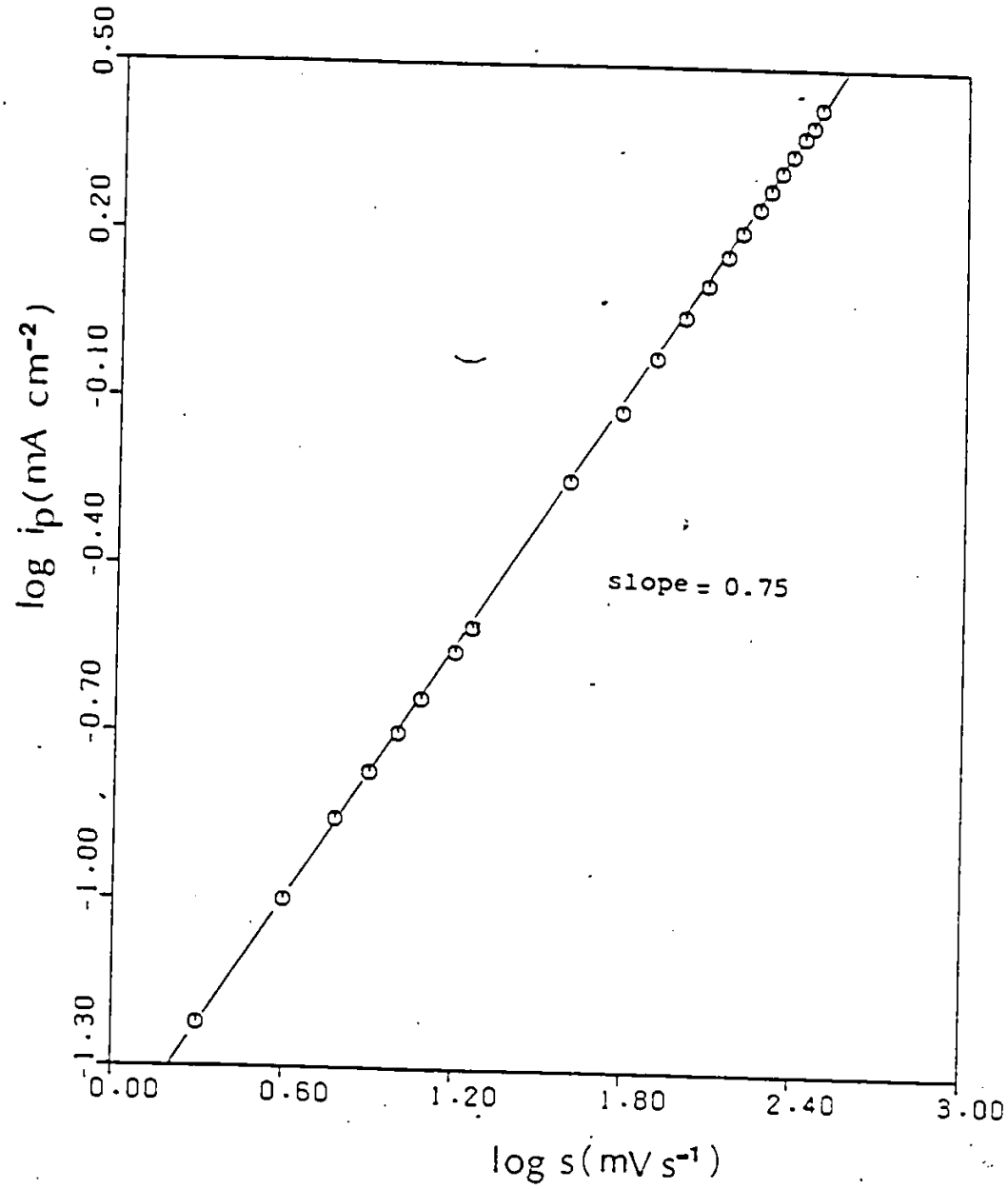

Fig. 3.6 Log i_p vs log s relationship for peak A_1 in 0.1M Na_2CO_3 + 0.5M Na_2SO_4 at pH 11.2 for polycrystalline Zn electrode, of apparent area 0.07 cm^2, etched in HBr.

Table 3.4

The Effect of pH on the Slopes of log i_p versus log s Plots

Solution	pH	Slope of log i_p vs log s plot
B 0.2M NaOH+0.03M Na_2CO_3	13.3	0.54
C 0.1M NaOH	13.0	0.46
D 0.1M NaOH+0.96M Na_2SO_4	13.0	0.56
E 0.05M NaOH+0.98M Na_2SO_4	12.7	0.53
F 0.03M NaOH+0.99M Na_2SO_4	12.5	0.64
G 0.03M NaOH+0.99M Na_2CO_3	12.5	0.60
H 0.025M NaOH	12.4	0.61
I 1M Na_2SO_4	11.5	0.78
J 3M NaCl	11.5	0.75
K 1M Na_2CO_3	11.5	0.72
L 0.5M Na_2CO_3	11.4	0.76
M 0.1M Na_2CO_3+0.5M Na_2SO_4	11.2	0.75
N 0.1M Na_2CO_3	11.2	0.78
O 1M $NaHCO_3$	8.5	0.51

Notes

1. Most of these runs were carried out in a sequence of increasing or decreasing sweep-rates over the range 2 mV s^{-1} to 300 mV s^{-1}.
2. Most of these slopes are the average data from 2-3 runs. Results are reproducible.

range of the two variables involved as seen in Fig. 3.6.

This unusual behaviour observed could arise for a number of reasons:

(a) Local change in pH near the electrode;

(b) Roughening of the electrode surface;

(c) IR-drop effect;

(d) Necessity for baseline correction, i.e. where the double-layer charging current is significant in relation to the i_p values observed at various s.

Several of these factors will now be considered:

(a) With all reactions that involve a pH change, the local pH near the electrode interface will alter as the reaction proceeds unless the solution is buffered. Fig. 3.7 shows that a linear log i_p vs log s plot is also obtained in Na_2HPO_4 and Na_2SO_4 buffered solution at pH 11.5 (ionic strength = 3 mol dm^{-3}). Therefore it is unlikely that the unusual dependence of i_p on sweep-rate [the $s^{0.75}$ relation (Fig. 3.6)] is due to change in pH near the electrode during the experiment since for the result in Fig. 3.7 the solution is effectively buffered.

(b) Continued cycling of the potential for a long period in the voltammetry experiment causes an increase in current. This is due to change in surface area, which arises on account of the difference in volumes of ZnO or $Zn(OH)_2$ species and Zn metal atoms, i.e. Zn occupies a 20% smaller volume than ZnO from which it is redeposited, causing a disorganization of the surface. It was found that there is more roughening of the electrode surface in long period CV experiments than over short times, as may be expected. Fig. 3.8 shows a series of cyclic-voltammograms

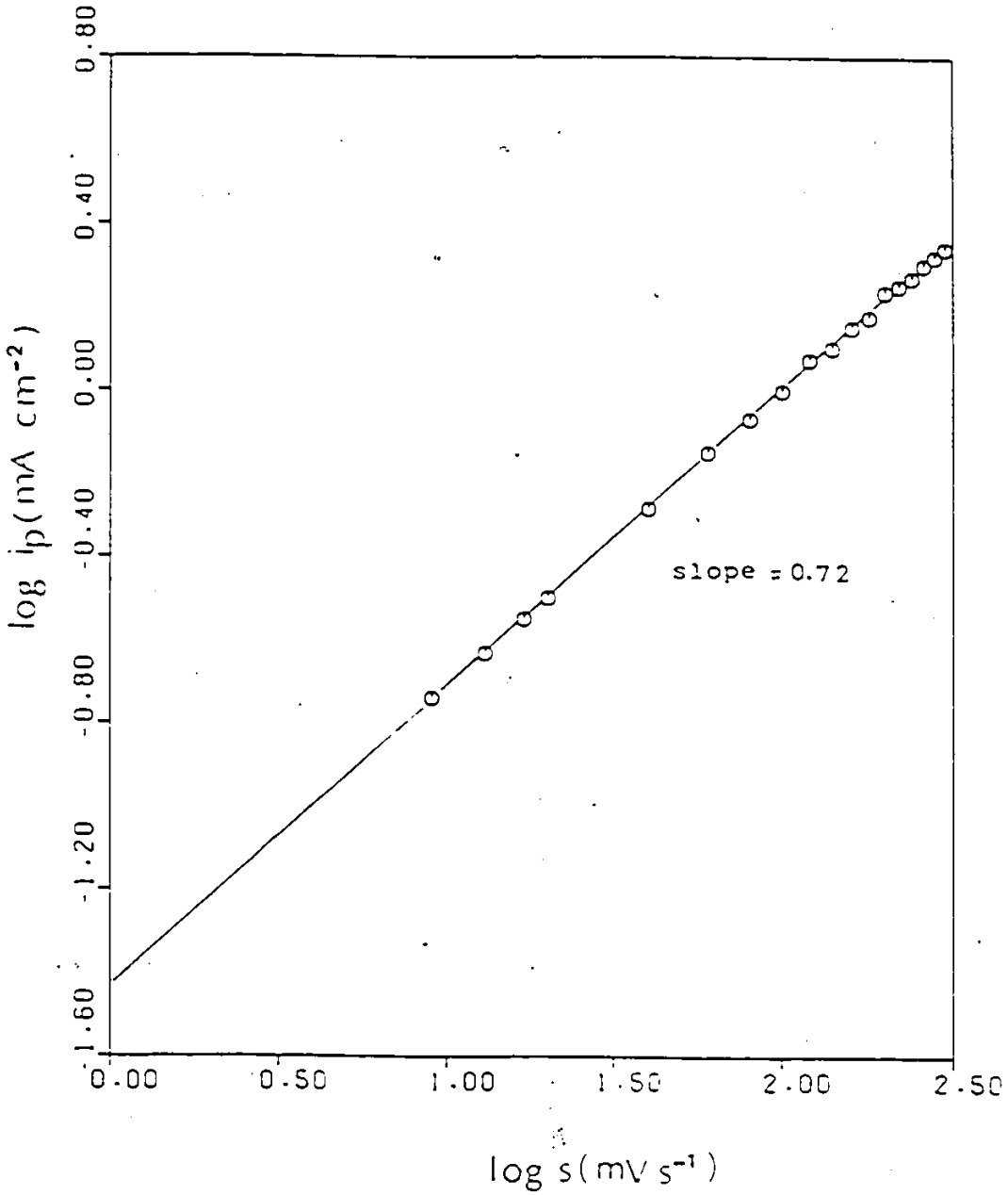

Fig. 3.7 Log i_p vs log s relationship for peak A_1 in 0.97M Na_2SO_4 + 0.03M Na_2HPO_4 at pH 11.5 for polycrystalline Zn electrode, of apparent area 0.07 cm^2, etched in HBr.

obtained with a random order in which the sweep-rate values were changed. Also there was no significant difference in the i vs s plots obtained at increasing and decreasing sweep-rates (Fig. 3.9).

(c) As discussed in section (2.2.5), the actual potential difference measured between the working and reference electrodes may not be the same as the applied potential difference if there is a significant solution resistance ("IR" drop) in the potential measuring circuit. Also, under such conditions, the actual sweep-rate applied at the electrode interface is not constant and changes with time during the sweep. In most of the experiments where i_p was found to be linearly dependent on $s^{0.75}$ (Table 3.4), the maximum i_p value was always less than 0.3 mA in the aqueous solutions used (area of the electrode was 0.071 cm^2 and ionic strength of the solutions was 3 mol dm^{-3}). Therefore the IR-drop effect could be neglected in such cases.

(d) Here i_p values were calculated taking the baseline as the zero-current line, since double-layer charging currents could be neglected, as mentioned earlier. It was of interest to establish the behaviour of the zinc electrode in weakly alkaline solution, pH ca. 11.5, at sweep-rates higher than 300 mV s^{-1}. Fig 3.10 shows the behaviour of i_p vs $s^{1/2}$ for the A_1 peak at sweep-rates in the range of 50 mV s^{-1} to 1800 mV s^{-1} (For the latter rates, the CV's were recorded on an oscilloscope). The behaviour at higher sweep-rates was found to be the same as at lower values, i.e. i_p was found to be linearly dependent on $s^{0.75}$.

It seems likely that the observed sweep-rate dependence o:

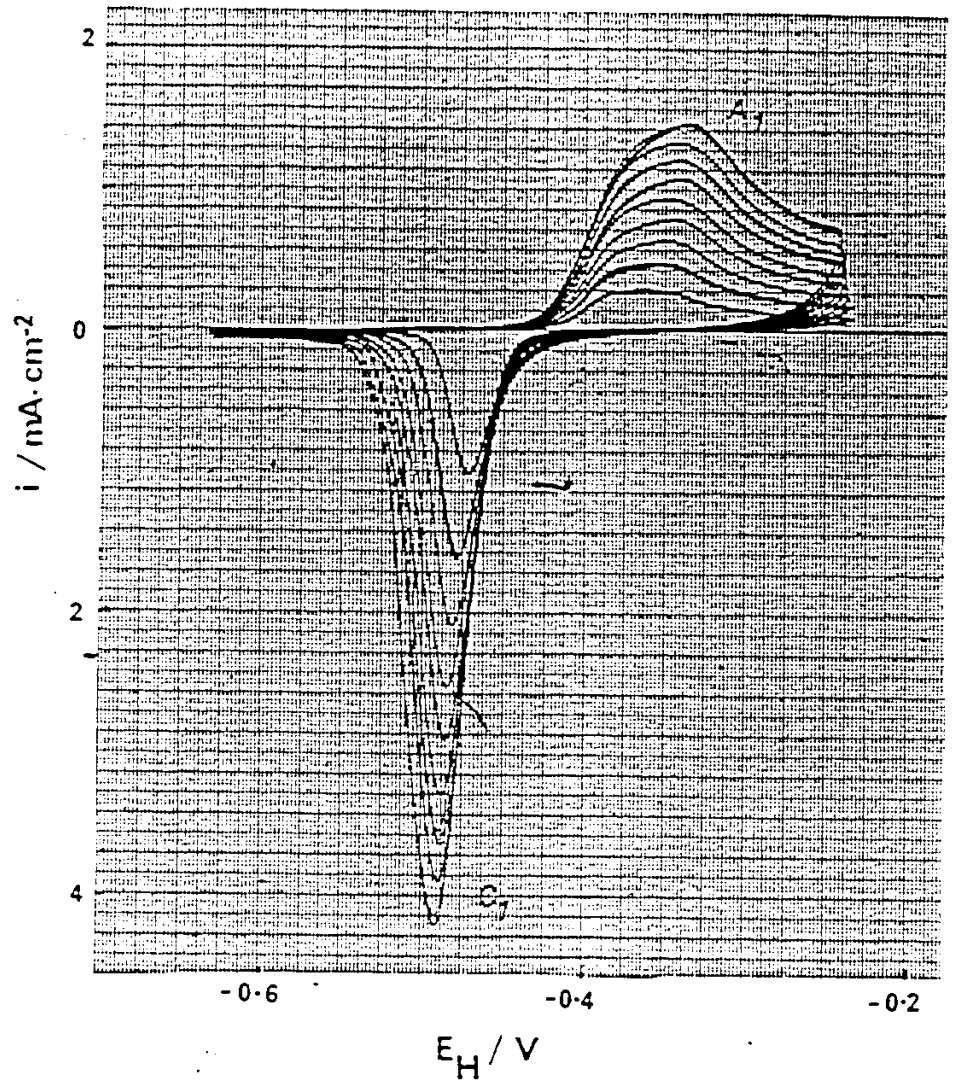

Fig. 3.6 Cyclic-voltammetry i vs E profiles for Zn polycrystalline electrode in 3M NaCl solution at pH 11.5 with sweep-rate changed in a random order in the 20 mV s^{-1} to 180 mV s^{-1} sweep-rate range.

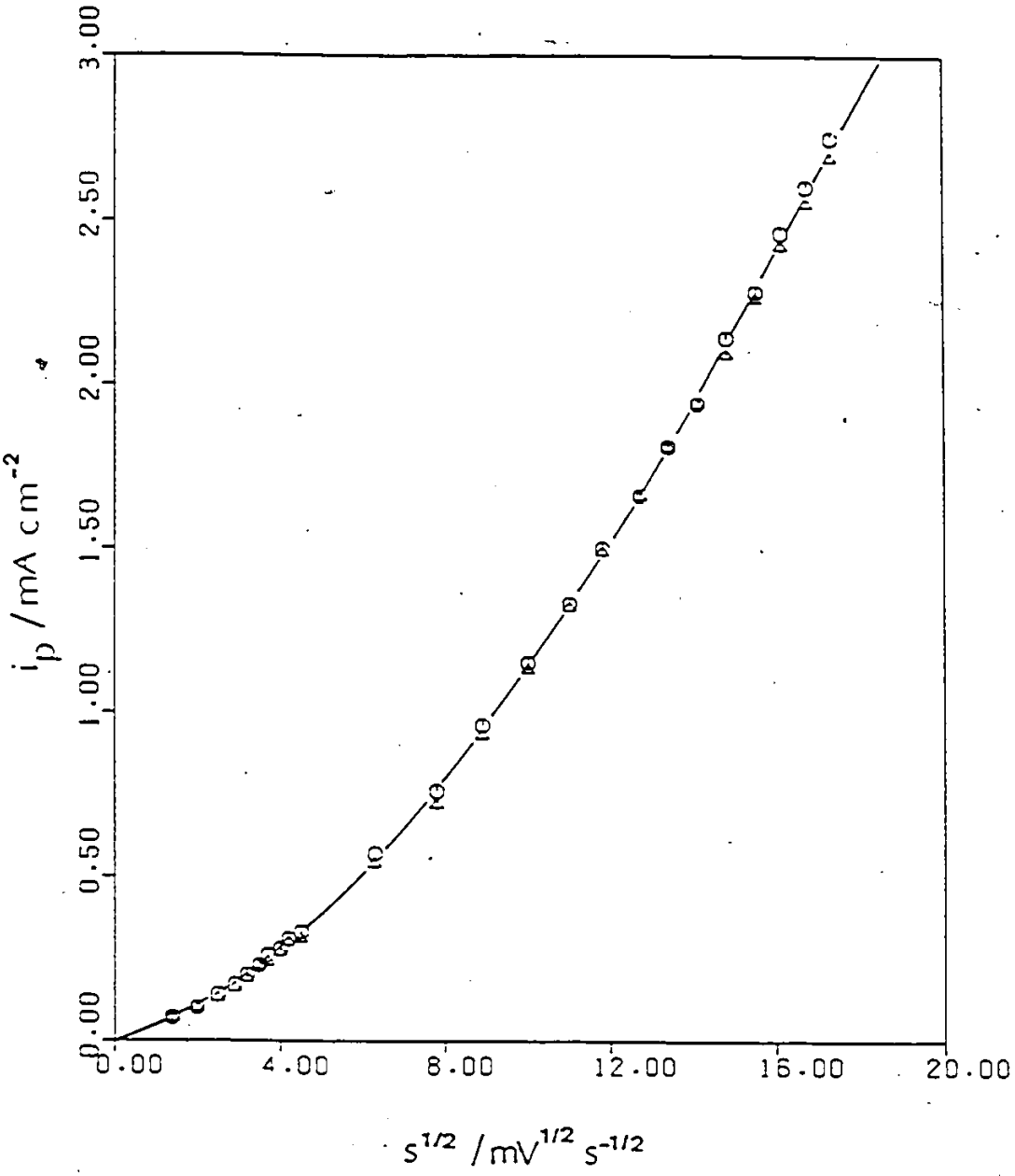

Fig. 3.9 The effect of direction of sweep-rate change on i_p vs $s^{\frac{1}{2}}$ dependence for polycrystalline Zn electrode in 0.5M Na_2CO_3 at pH 11.4 for peaks A_1.

s - (○) 300 mV s^{-1} ---→ 2 mV s^{-1}, (△) 2 mV s^{-1} ---→ 300 mV s^{-1}

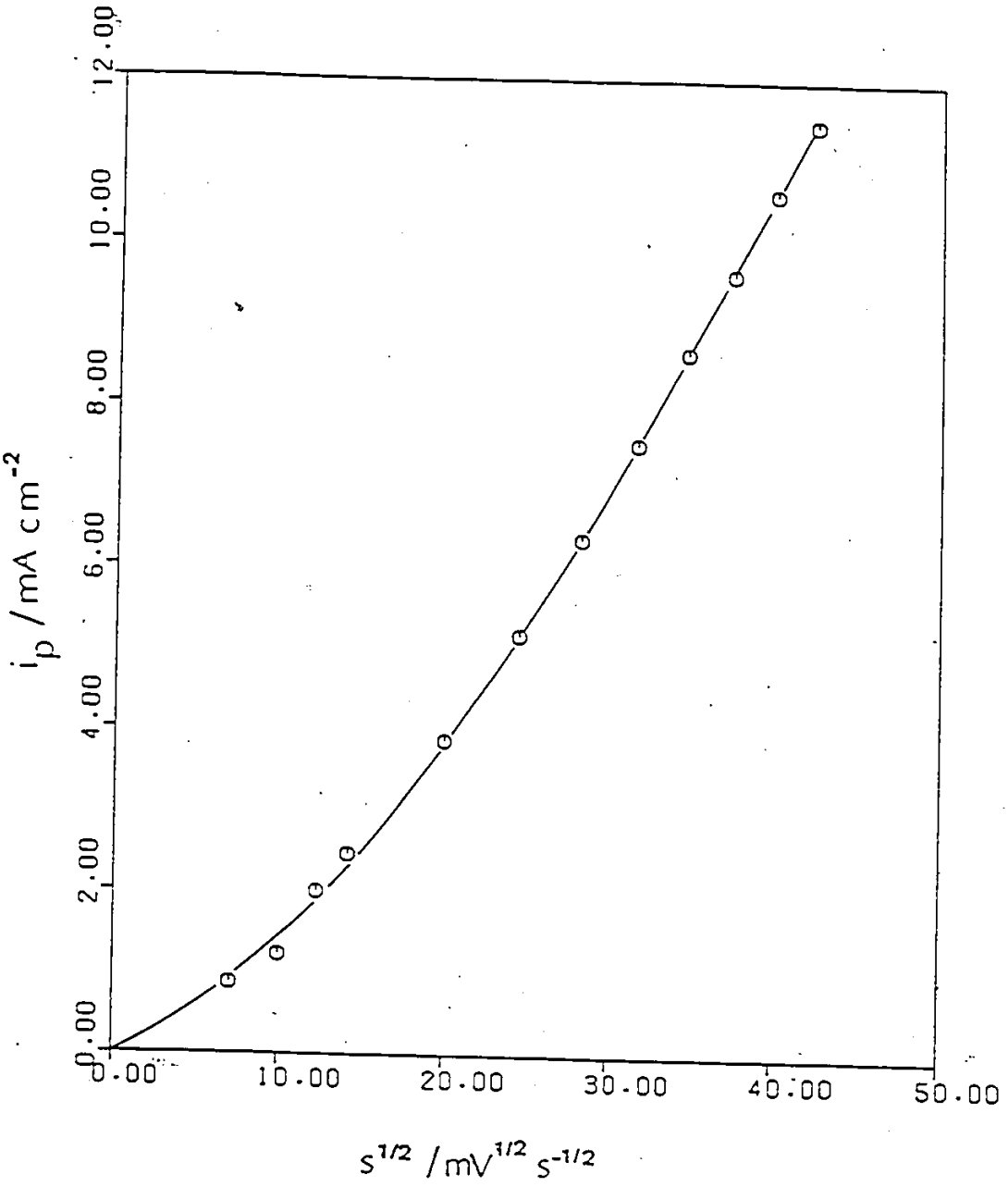

Fig. 3.10 i_p vs $s^{\frac{1}{2}}$ relationship for peak A_1 at higher sweep-rates for polycrystalline Zn electrode in 1M Na_2SO_4 solution at pH 11.5.

s = 1800 mV s^{-1} - 50 mV s^{-1}

the peak current around pH 11.5 is not due to experimental errors, as the $s^{0.75}$ relation is based on many points and arose in a number of independent experiments.

From Table 3.4 it is seen that, at higher pH (ca. 14) the zinc oxidation reaction is mainly diffusion-controlled, $i_p \propto s^{1/2}$ but as the pH is decreased the reaction is no longer simply diffusion-controlled. A useful way of studying and quantitatively controlling the diffusion effect is to employ a rotating disc electrode (RDE), as will be described below.

3.3.2.4 Electrode Rotation Effect

The rotating-disc electrode (RDE) has frequently been applied to investigations of the kinetics of electrode processes having rates dependent on diffusion of the reactant substances to the electrode interface. It is one of the few electrode systems for which the hydrodynamic and the convective-diffusion equations have been solved rigorously for steady-state conditions. The mathematical solution was derived by Levich[138]. The limiting current I_L is given by

$$I_L = 0.620nFAD_o^{2/3}\omega^{1/2}\nu^{-1/6}C_o \qquad (49)$$

where ω is the angular velocity of rotation and ν is the kinematic viscosity of the solution.

Therefore i_L should vary linearly with $\omega^{1/2}$ in a diffusion-controlled process. Fig. 3.11 shows the effect of rotation on the i vs E curve obtained in 1M Na_2CO_3 solution (pH ca. 11.5) at a very low sweep-rate (5 mV s^{-1}). The major difference of shape and charge of the anodic peaks compared with the cathodic ones at

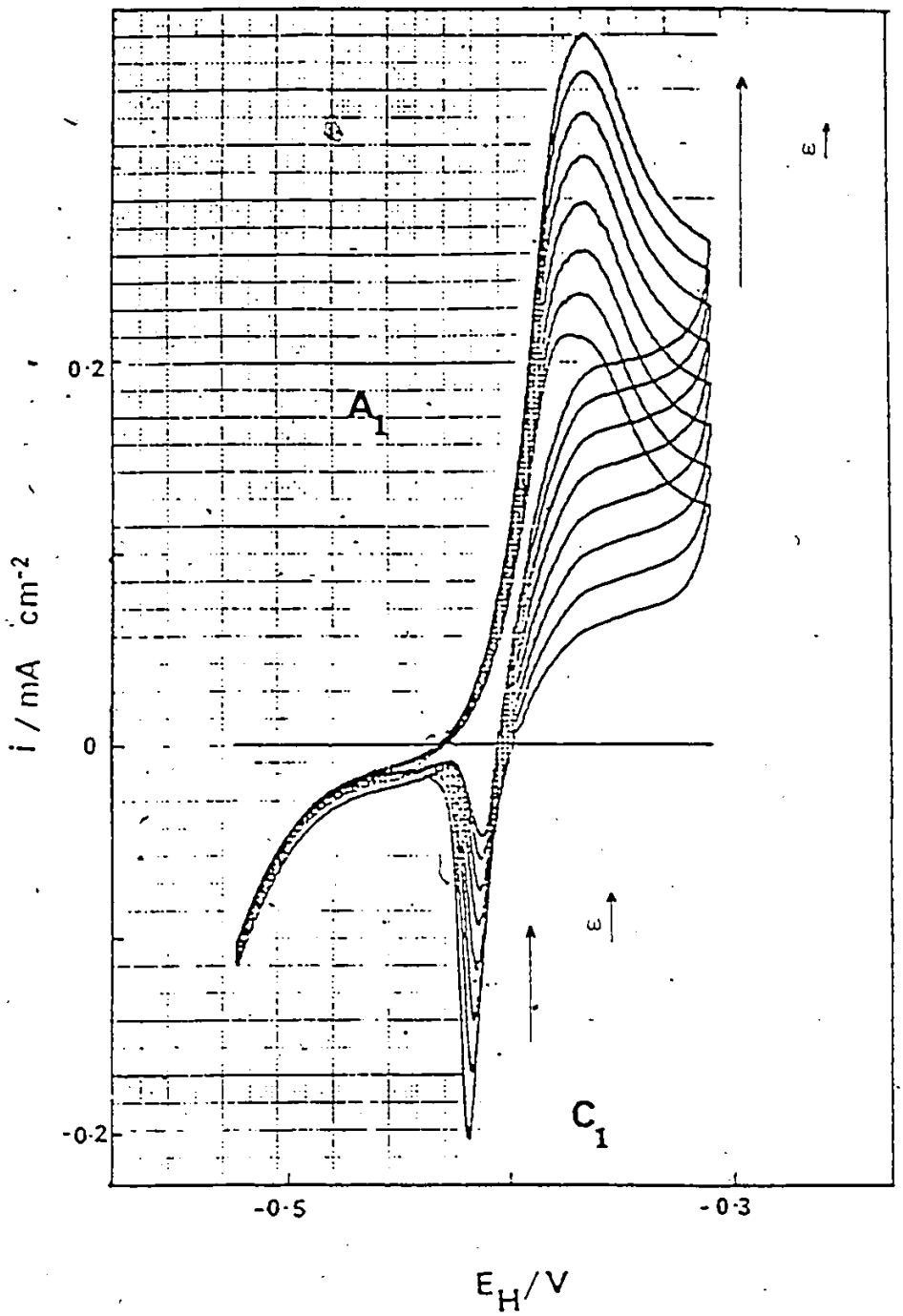

Fig. 3.11 Cyclic-voltammetry i vs E profiles for a polycrystalline Zn RDE in 1M Na_2CO_3 solution at pH 11.5 with variable rotation rate.

ω - 100,156,225,307,400,506,625 and 756 rpm.

s - 5 mV s^{-1}

various rotation rates in Fig. 3.11 arises because soluble oxidized Zn species are spun off into the solution and are not recovered in the conjugate cathodic sweep; thus Q_a/Q_c values are >>1.

For the process under investigation here it is important to know which species controls the rate of the reaction : is it the OH^- ion for example? This question is answered in the affirmative in the following section.

3.3.2.5 OH^- Ion Effect

The effect of rotation on the current vs potential profiles at 5 mV s^{-1} was evaluated in a series of solutions in 1M aqueous Na_2CO_3. Appropriate amounts of NaCl and NaOH were used to keep the ionic strength constant at 4 mol dm^{-3} while the pH was varied from 11.5 to 13.5. Table 3.5 gives the slopes of i_p vs $\omega^{1/2}$ plots obtained with the rotating electrode in various solutions while Fig. 3.12 shows a plot of i_p vs $\omega^{1/2}$. It is seen that for pH > 12, where $i_p \propto \omega^{1/2}$, diffusion of OH^- ions evidently determines the current at peak A_1. In Fig. 3.13, it can be seen that between pH 12 and 11.5, however, the effect of rotation, in terms of the values of the log of the slopes of $di_p/d\omega^{1/2}$ relations that are observed, is greater than could be due to the mass-transfer of OH^- ions, corresponding to the extension of the linear relation in Fig. 3.13 to pH's below 12 (dotted section of the line).

The question arises whether there is any effect from carbonate ions under the conditions 11.5 < pH < 12 and this will be discussed in more detail when the effect of carbonate on

Table 3.5

The Effect of pH on the Slope of i_p vs $\omega^{\frac{1}{2}}$ Relations

Solution	pH	Slope of i_p vs $\omega^{\frac{1}{2}}$ $\mu A\ cm^{-2} rpm^{-\frac{1}{2}}$
1M Na_2CO_3+1M NaCl+0 M NaOH	11.46	10.32
1M Na_2CO_3+1M NaCl+0 M NaOH	11.59	7.78
1M Na_2CO_3+1M NaCl+0.02M NaOH	11.92	9.33
1M Na_2CO_3+1M NaCl+0.025M NaOH	12.32	16.12
1M Na_2CO_3+1M NaCl+0.03 M NaOH	12.52	29.98
1M Na_2CO_3+1M NaCl+0.07 M NaOH	12.80	71.55
1M Na_2CO_3+0.85M NaCl+0.15M NaOH	13.15	229.78
1M Na_2CO_3+0.75 M NaCl+0.25M NaOH	13.38	377.68

Notes

1. pH of the solutions was varied keeping the ionic strength at 4 mol dm^{-3}.
2. All measured at 5.5 mV s^{-1}, for Zn RDE etched in 48% HBr.
3. Rotation rate was varied from 100 rpm to 2500 rpm.
4. Slopes of i_p vs $\omega^{\frac{1}{2}}$ relations given are average data from eight runs.
5. i_p vs $\omega^{\frac{1}{2}}$ slopes were independent of OH^- ion concentration in solutions pH <12.
6. For typical plot of i_p vs $\omega^{\frac{1}{2}}$, see Figure 3.12.
7. The logs of these slopes $di_p/d\omega^{\frac{1}{2}}$ are what is plotted in Fig. 3.13 as a function of pH.

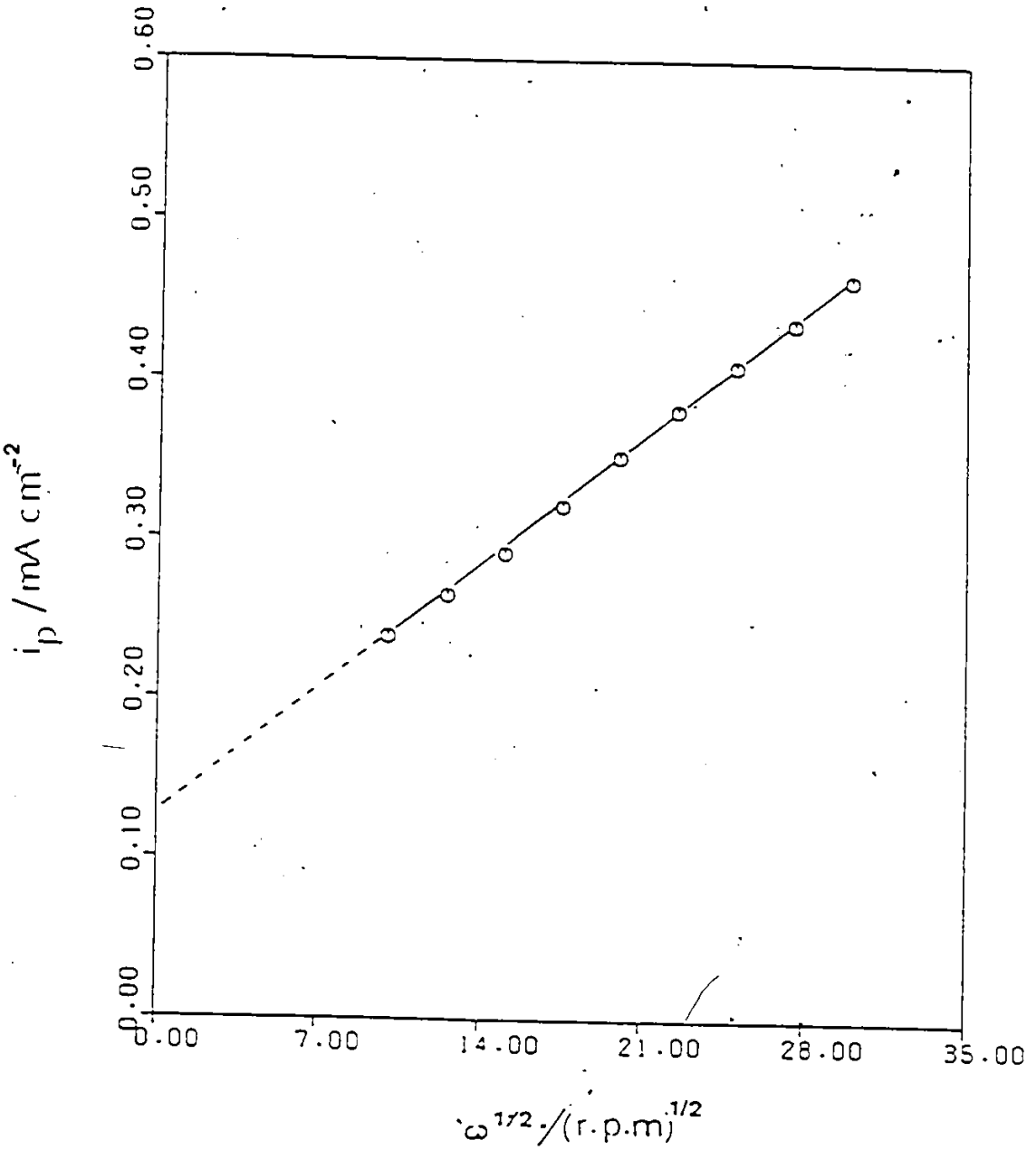

Fig. 3.12 Dependence of i_p for peak A_1 on $\omega^{\frac{1}{2}}$ for polycrystalline Zn RDE in 1M Na_2CO_3 + 1M NaCl solution at pH 11.5.

Electrode - RDE, polycrystalline, of apparent area 0.07 cm^2, etched in HBr (see page 94 for comment on significance of intercept $\omega^{\frac{1}{2}} \rightarrow 0$).

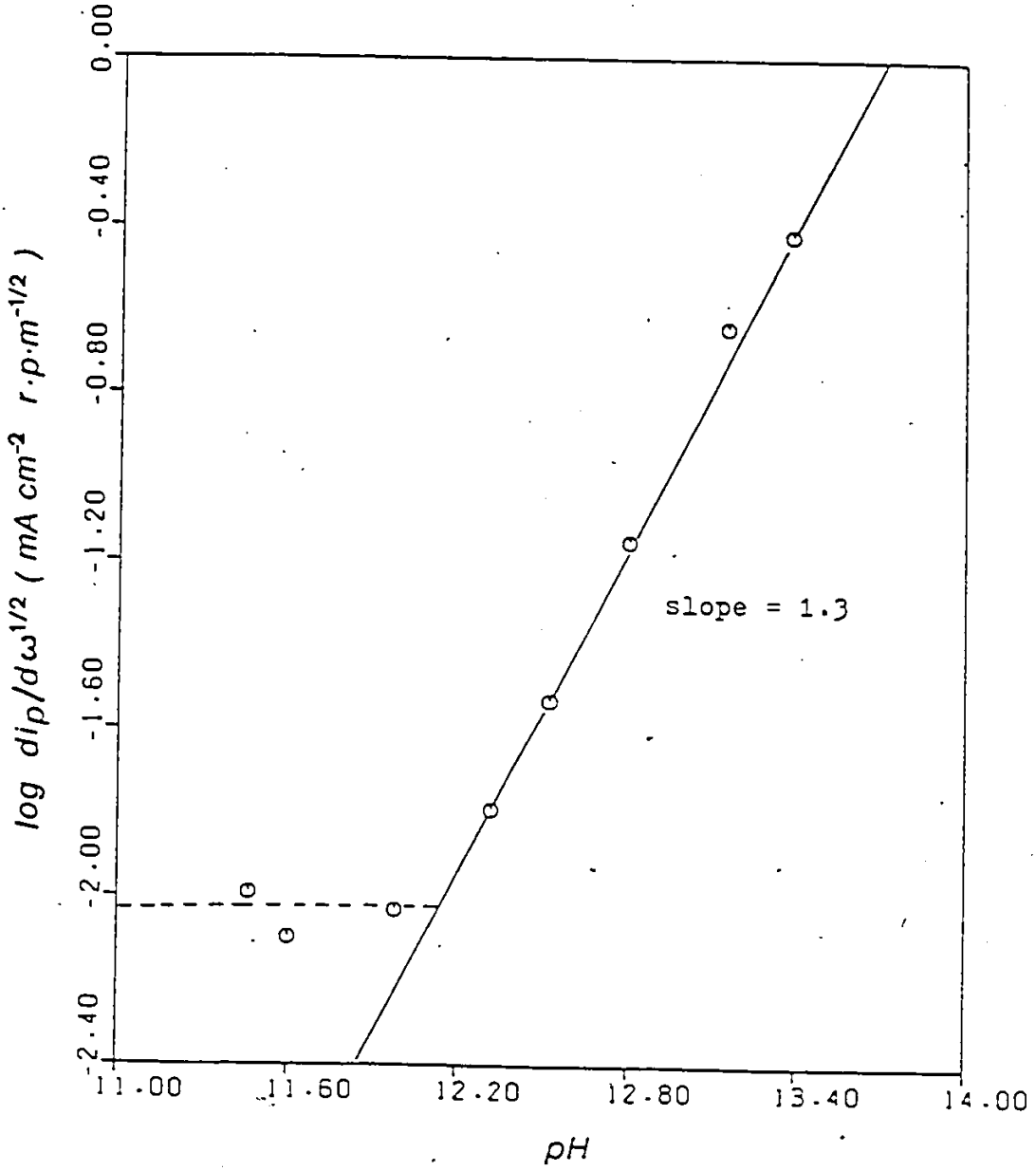

Fig. 3.13 Dependence of log $(di_p/d\omega^{\frac{1}{2}})$ for peak A_1 on pH for various solutions of 1M Na_2CO_3 + xM NaCl + yM NaOH with constant ionic strength.

Solutions - see Table 3.5, pH= 11.5-13.4

dissolution and passivation of zinc is examined in section (3.5).

From the experimental results obtained using the RDE, it is clear that the reaction at peak A_1 is diffusion-controlled in the pH range 11.5-13.5 . It can be seen that, for pH > 12 , the currents appear to be controlled by diffusion of OH^- ions. This could be because the dissolution of Zn and the consequent accumulation of zincate ions or insoluble ZnO or $Zn(OH)_2$ near the electrode surface diminishes the local OH^- ion concentration and its mass-transfer rate if a precipitated film is present at the electrode surface. However, it is also possible that rotation affects the transport rate of dissolved zinc ions away from the electrode. That the film thickness or concentration of electroactive zincate is increased with pH is indicated by the data in Table 3.3, e.g. for a given sweep-rate.

3.3.2.6 Reactions in Weakly Alkaline Solutions (pH ca. 11.5)

We see from Table 3.3 that, around pH 11.5, the extent of oxidation of Zn is quite small in the time scale of the sweep, probably due to passivation. This is also clear (Fig. 1.5) from the experimental results obtained by Roetheli et al.[38] which show that the rate of dissolution of zinc in acidic, neutral and alkaline media is represented as f(pH) by a U-shaped curve, with the slowest dissolution occurring around pH 11. Since both the q_a/q_c and q_a quantities vary with the sweep-rate, the reaction under these conditions appears to involve, at least in part, a solution process.

Unlike the behaviour expected for a pure diffusion process at

the rotating disc electrode, where in the i vs $\omega^{1/2}$ relation, i should pass through zero as $\omega^{1/2} \rightarrow 0$, Fig. 3.12 has the form $i_p = A + B\omega^{1/2}$ which represents the experimental behaviour in 1M Na_2CO_3 + 1M NaCl at pH 11.5. This kind of dependence indicates the simultaneous occurrence of two types of reactions: one of them being limited diffusionally ($i_p \propto \omega^{1/2}$) and the other chemically or heterogeneously, i.e. through a surface film process.

Zembura et al.[39] studied the corrosion of Zn in 0.1M NaCl in the pH range 1.6 to 13.3, using a RDE (Fig. 1.6). They found that in the pH range 8.5 to 11.0 the dissolution rate of Zn did not depend on the rotation rate but above pH 11 diffusion became important. Therefore it could be possible that the dissolution/passivation reactions around pH 11.5 are controlled both diffusionally and chemically because there should be a pH range where a transition from surface process kinetics to diffusion control takes place, as the ZnO film becomes more soluble.

The linear dependence of i_p on $s^{0.75}$ obtained from the cyclic-voltammograms for solutions around pH 11.5 is obviously different from the linear or square-root dependences of peak currents (i_p) on sweep-rate as expected limitingly for pure surface reaction (s^1) or diffusion-controlled ($s^{1/2}$) processes, respectively. However, these results are not without experimental precedents. For instance, Harrington[139] found that the growth of anodic films of Bi_2S_3 formed on a bismuth electrode in alkaline sulphide solution, through the reaction

$$2Bi\ (s) + 3HS^-(aq) \rightarrow Bi_2S_3\ (s) + 3H^+(aq) + 6e \quad (50)$$

also yields a linear i_p vs $s^{0.75}$ relationship (Fig. 3.14). In this case, however, it was found that the formation of a monolayer of Bi_2S_3 was only little effected by electrode rotation[139]. A number of mechanisms were suggested as explanations of the behaviour of the Bi_2S_3 current peak. To explain the i_p vs s exponent of 0.75, it was suggested that, at higher sweep-rates, surface-diffusion is involved and is partly rate-limiting, though this suggestion may not apply to the present results.

3.3.2.7 Processes Under "Mixed" Control

As discussed in section (3.3.9), the peak current I_p for a surface process is ideally linear in sweep-rate and, for a diffusion-controlled process, in square-root of sweep-rate. If the process is under "mixed" control, as suggested in the previous section. i.e. one of the reactions is limited diffusionally and the other, to which it is coupled*, is a surface process, then the simplest basis for treating such a situation is to assume that the peak current is the sum of peak currents for the surface and solution processes: i.e., as a function of s,

$$i_p = k_1 s + k_2 s^{1/2} \quad (51)$$

where the k's are some proportionality constants having the

---

* Coupling between the "surface" and the "solution" processes could arise if there is diffusion of OH^- or zinc ions through an anodically formed porous oxide film whose thickness depends on s.

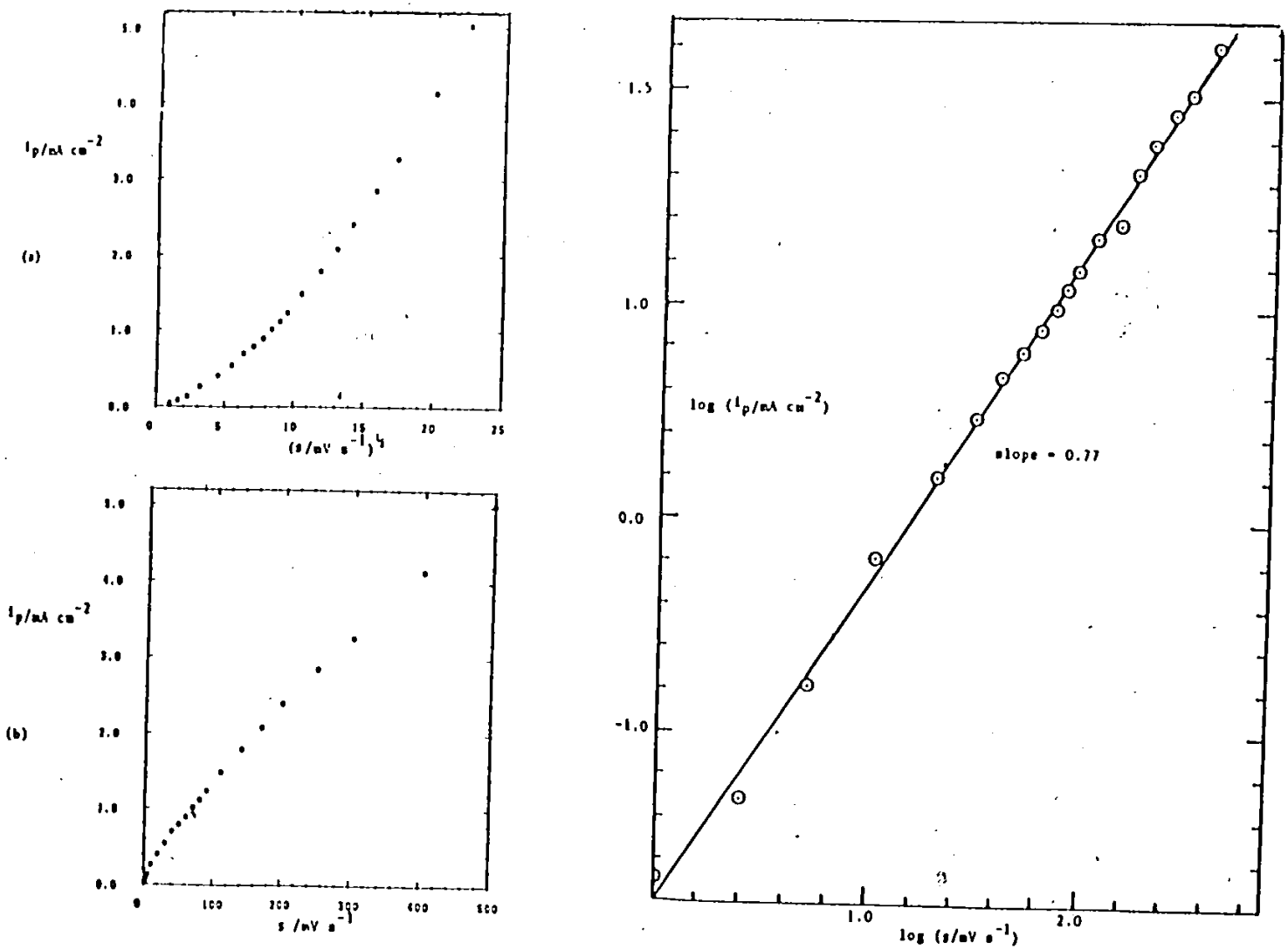

Fig. 3.14 Peak current vs sweep-rate relationships for anodic films of Bi_2S_3 formed on a bismuth electrode in alkaline sulphide solution (a) i_p vs $s^{\frac{1}{2}}$; (B) i_p vs s and (c) log i_p vs log s (slope = 0.77).

appropriate dimensions. Eqn. (51) implies a parallel mixture of surface ($k_1 s$) and diffusion ($k_2 s^{1/2}$) current components. This is a matter requiring further discussion, as will be given later.

For the purpose of making test plots of i_p data as a function of s, equation (51) can also be written either as

$$i_p s^{-1/2} = k_1 s^{1/2} + k_2 \qquad (52)$$

or

$$i_p s^{-1} = k_1 + k_2 s^{-1/2} \qquad (53)$$

It is interesting then to examine how $i_p s^{-1/2}$ varies with $s^{1/2}$ or $i_p s^{-1}$ varies with $s^{-1/2}$. Fig. 3.15 shows the behaviour of such plots for the A_1 peak for Zn oxidation in 1M Na_2SO_4 solutions at pH 11.4 : it can be seen that both plots consist of <u>two</u> straight lines rather than a single one (this is an unexpected result).

If the process is under mixed-control, as suggested, then i_p should vary with electrode rotation rate. A series of experiments were carried out with increasing and decreasing rotation-rate to study the effect of rotation on the $i_p s^{-1/2}$ <u>vs</u> $s^{1/2}$ plots. Fig. 3.16 shows the results obtained with 1M Na_2SO_4 solution at pH 11.5 at sweep-rates between 300 mV s^{-1} and 20 mV s^{-1}. The smallest sweep-rate, 20 mV s^{-1}, was used to avoid roughening of the electrode, since one electrode had to be used for each set of experiments over a range of increasing or decreasing rotation-rates. It was clearly shown by repeating the experiment at the rotation-rate of 500 r.p.m. (Fig. 3.16), that the observed dependence of peak current on rotation does not

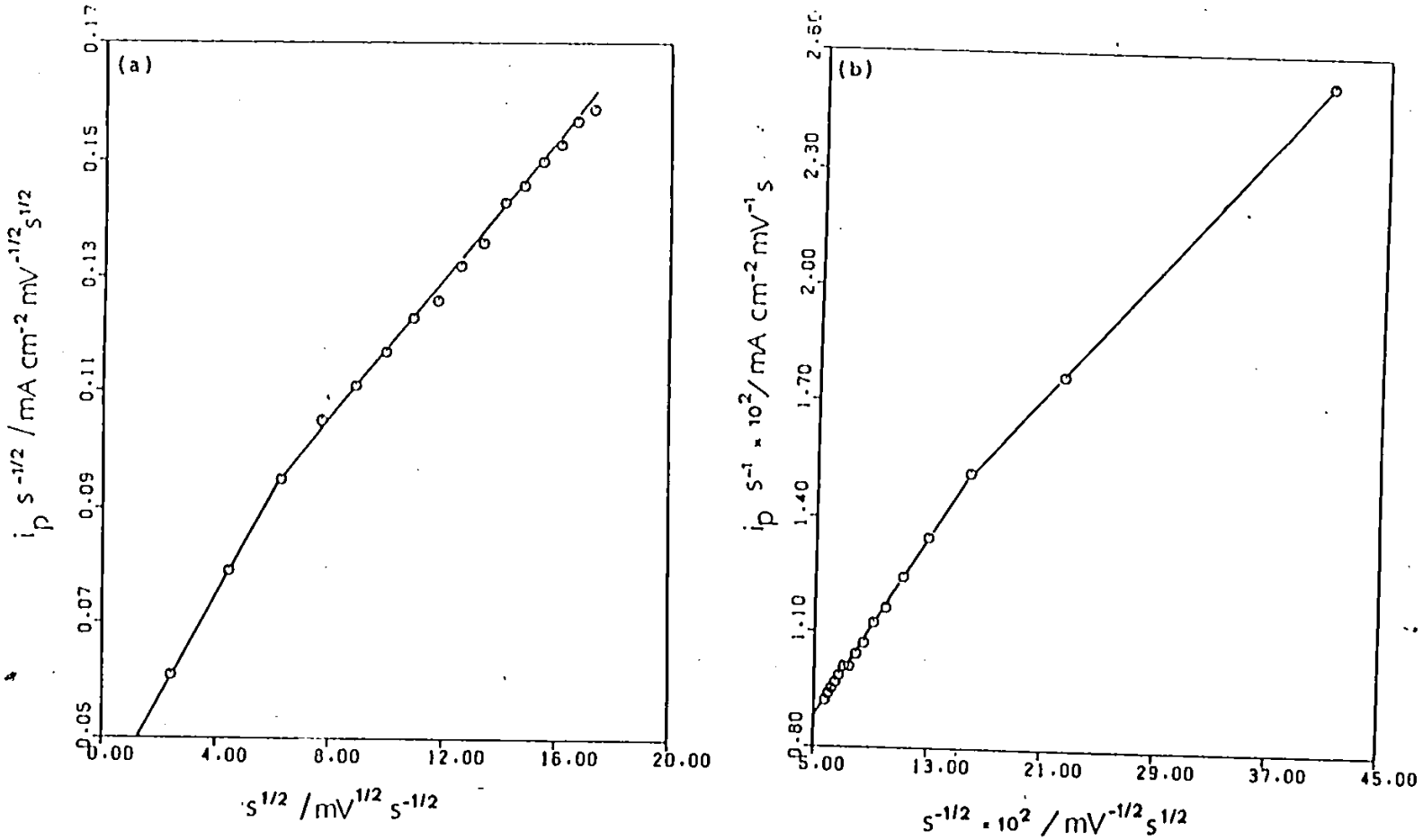

Fig. 3.15 Dependence of (a) $i_p s^{-\frac{1}{2}}$ on $s^{\frac{1}{2}}$ and (b) $i_p s^{-1}$ on $s^{-\frac{1}{2}}$ for peak A_1 in 1M Na_2SO_4 solution at pH 11.4 for polycrystalline Zn electrode.

s - 300 mV s^{-1} --- 6 mV s^{-1}

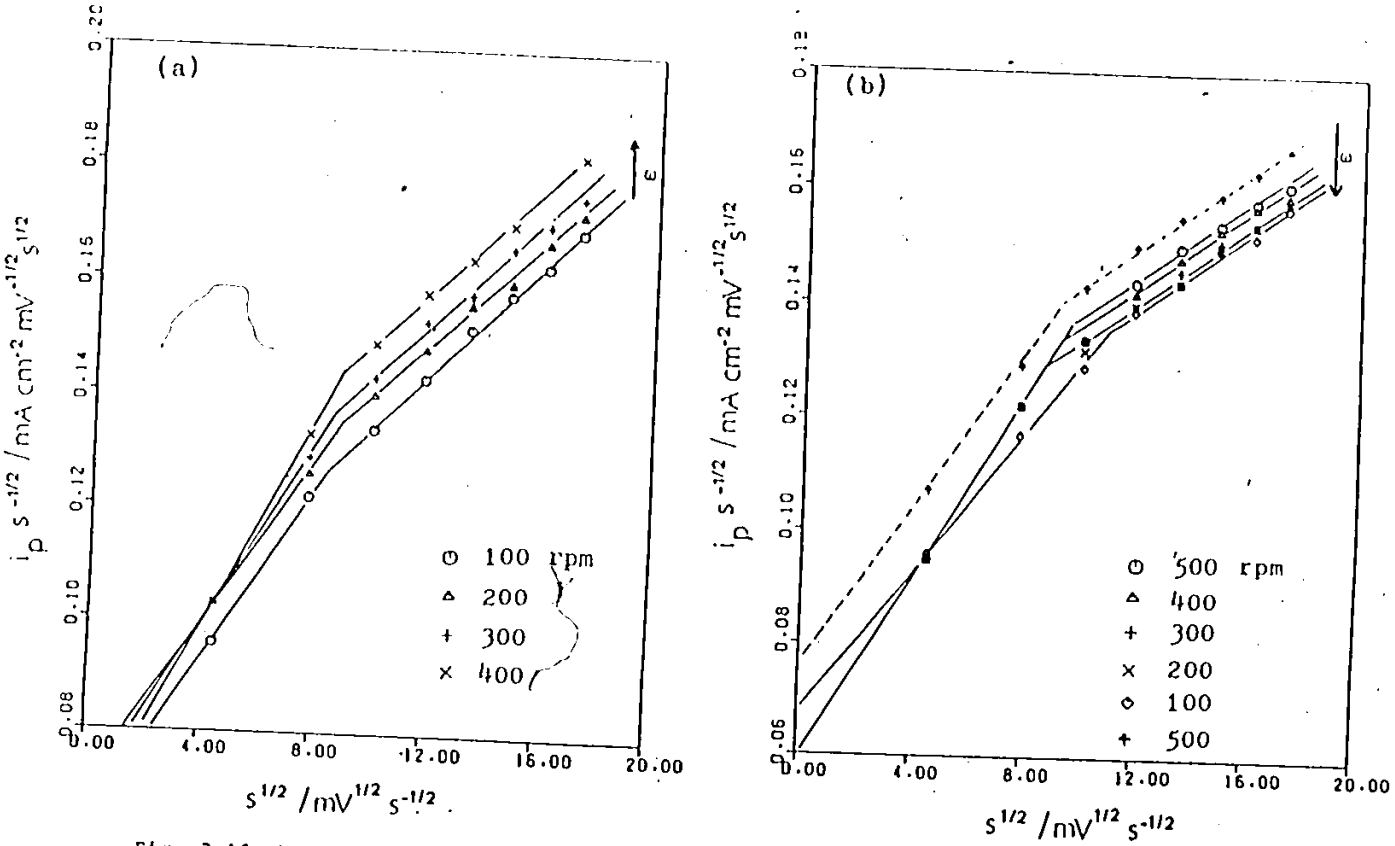

Fig. 3.16 The effect of (a) increasing and (b) decreasing rotation rates on $i_p s^{-\frac{1}{2}}$ vs $s^{\frac{1}{2}}$ dependence for A_1 peak in 1M Na_2SO_4 solution at pH 11.5 for polycrystalline Zn RDE.

ω - (a) 100, 100, 300, 400 rpm

(b) 500, 400, 300, 200, 100, 500, rpm

s - 300 mV s^{-1} ____ 20 mV s^{-1}

Electrode - RDE, polycrystalline, of apparent area 0.07 cm^2 and etched

arise because of a trivial effect of surface roughening during the experiment but was rather due to a contribution to the current from a process involving mass-transport through the solution to the electrode interface.

Now two questions arise:

(a) Why is log i_p linear in log s with a slope of 0.75 (e.g. as in Fig. 3.6)?

and

(b) Why do the $i_p s^{-1/2}$ vs $s^{1/2}$ plots consist of two straight lines instead of a single one?

(a) If i_p was determined by parallel surface and solution processes according to eqn. (51), then log i_p cannot for algebraic reasons, vary in an explicitly linear manner with log s. Fig. 3.17 shows however, that a plot of log i_p vs log s does give a linear relation with a slope of 0.78, where in this figure $i_{p\ calc.}$ are i_p values back calculated from the k_1 and k_2 values obtained from the experimental data of Fig. 3.15 for various sweep-rates, plotted according to eqns. (52) or (53). From these results, it is clear that log i_p vs log s plots cannot actually be truly linear, so that their apparently linear form is due to the large degree of "compression" of the range of i_p and s values that arises in a "log" vs "log" plot.

(b) It can be seen from Fig. 3.16 that the $i_p s^{-1/2}$ vs $s^{1/2}$ plots also consist of two straight lines even up to the highest rotation-rate (500 rpm), but this is not the case for the results in 1M Na_2CO_3 solution at pH 11.5. At higher rotation-rates (500 rpm) the $i_p s^{-1/2}$ vs $s^{1/2}$ plot consists of only one straight line (Fig. 3.18). The interesting question arises: what can be the

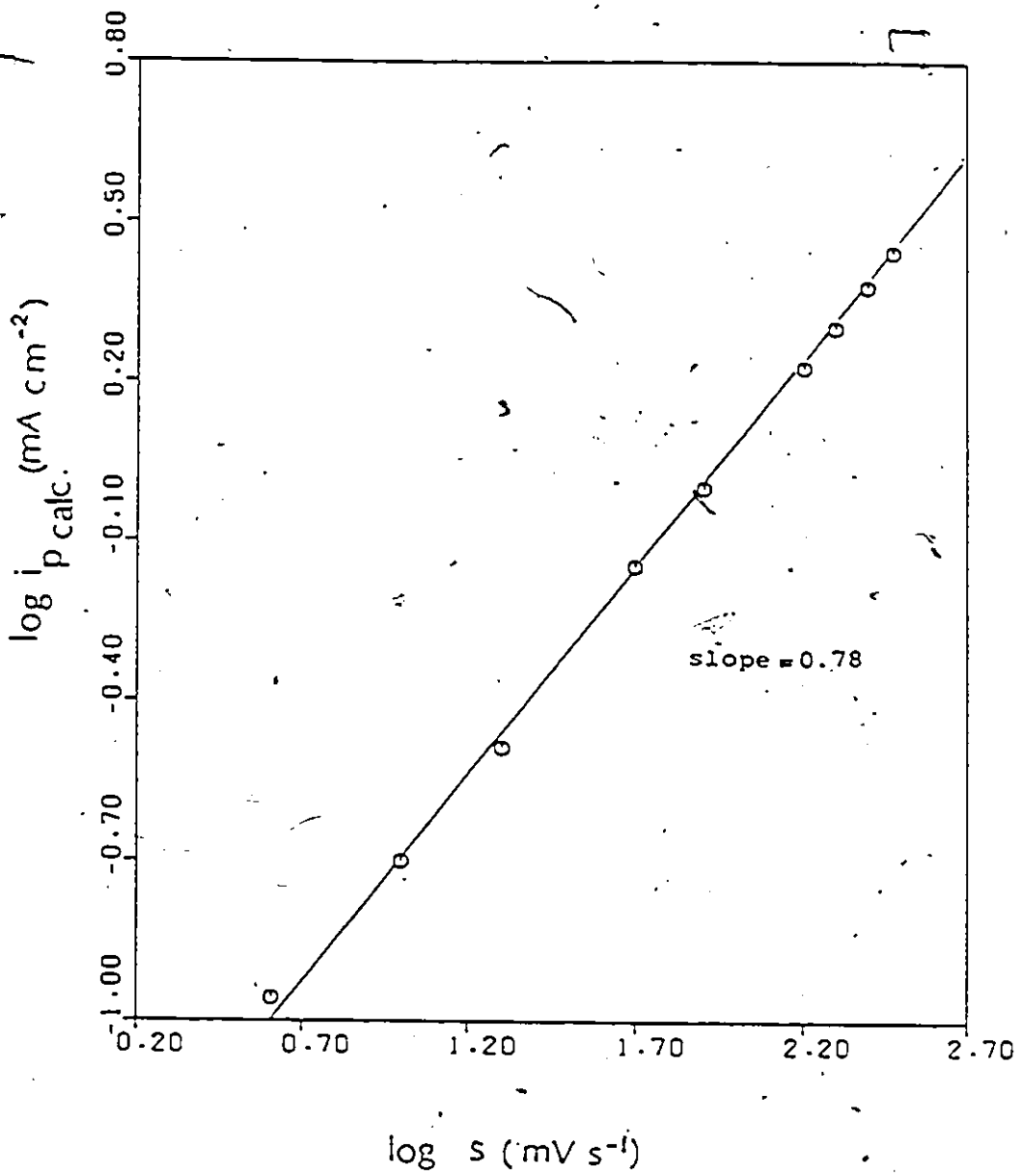

Fig. 3.17 Log $i_{P_{calc.}}$ vs log s relationship for peak A_1. Log $i_{P_{calc.}}$ values were calculated from the k_1 and k_2 values obtained from the experimental data of Fig. 3.15 for Zn in 1M Na_2SO_4 at pH 11.5 for various sweep-rates.

$k_1 = 0.74 \times 10^{-2}$ mA cm^{-2} $mV^{-1}s$ (at lower sweep-rate)

$k_2 = 4.0 \times 10^{-2}$ mA cm^{-2} $mV^{-\frac{1}{2}}s^{\frac{1}{2}}$

$k_1 = 0.58 \times 10^{-2}$ mA cm^{-2} $mV^{-1}s$

$k_2 = 6 \times 10^{-2}$ mA cm^{-2} $mV^{-\frac{1}{2}}s^{\frac{1}{2}}$ (at higher sweep-rate)

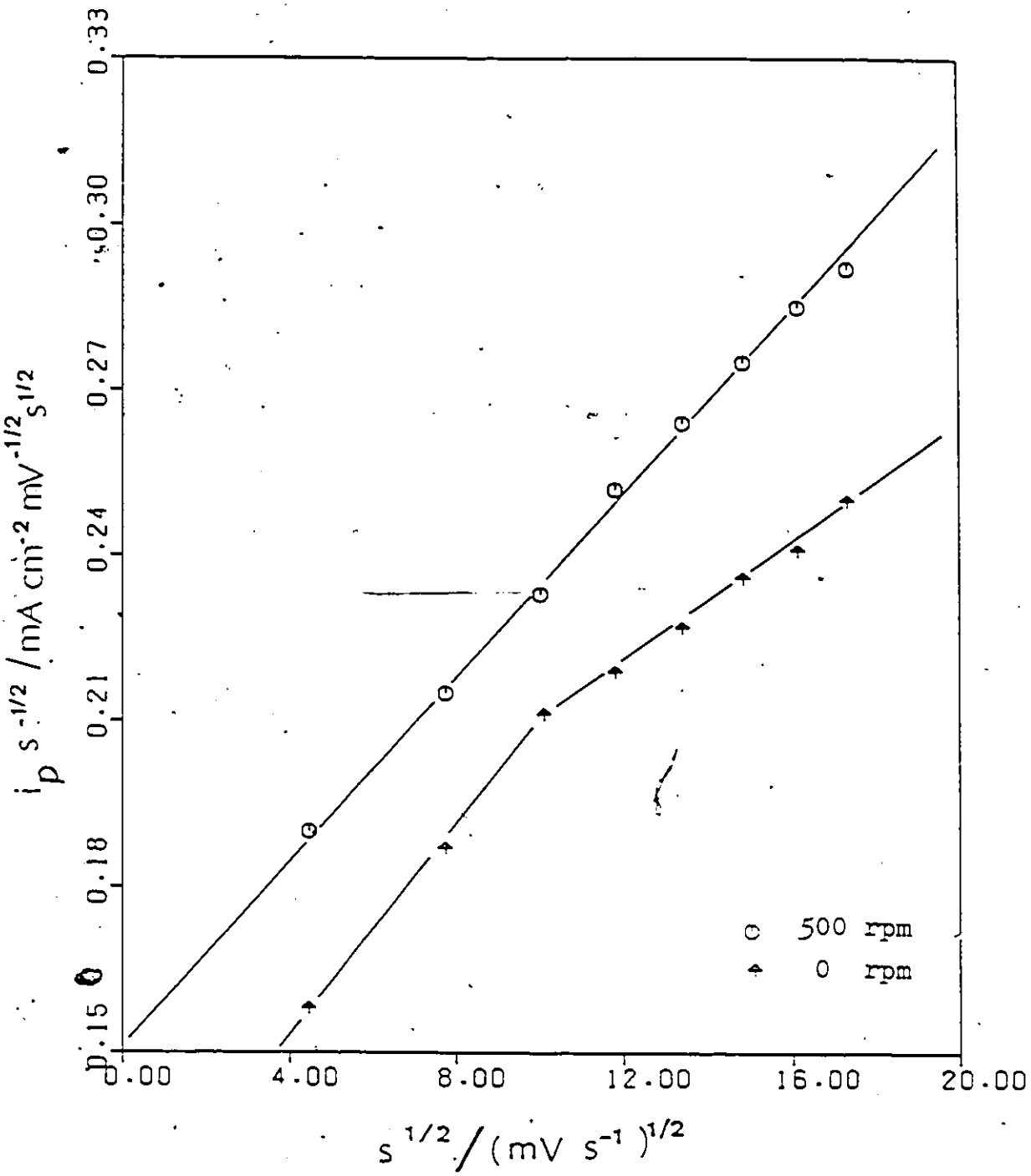

Fig. 3.18 Dependence of $i_p s^{-\frac{1}{2}}$ for peak A_1 on $s^{\frac{1}{2}}$ in 1M Na_2CO_3 solution at pH 11.5 for Zn RDE at 500 rpm and 0 rpm. s = 300 - 20 mV s^{-1}

Electrode - RDE, polycrystalline Zn of apparent area 0.07 cm^2 and etched in HBr.

reason for such behaviour?

Fig. 3.19 shows the cyclic-voltammograms obtained for Zn in 1M Na_2CO_3 and 1M Na_2SO_4 solutions at pH 11.5 for the corresponding $i_p s^{-1/2}$ vs $s^{1/2}$ plots. It is seen that shapes of the cyclic-voltammograms are quite different from each other even though the Zn electrodes were prepared in a similiar way, i.e. both were etched in concentrated HBr for 8 s. Table 3.6 summarizes the q_a, q_b and q_a/q_c values, and the peak potentials for the A_1 and C_1 peaks for cyclic-voltammograms obtained with Zn in 1M Na_2CO_3 and 1M Na_2SO_4 solutions at pH 11.5 at various sweep-rates at a rotation-rate of 500 rpm .

It can be seen from the q_a/q_c values that the reaction associated with the A_1 peak for the 1M Na_2CO_3 solution involves, to a greater extent, a solution transport process than does that for 1M Na_2SO_4 solution. Also it is clear from the difference of cathodic (C_1) and anodic (A_1) peak potentials, and the shift of peak potentials with sweep-rate, that the reaction at the A_1 peak is more irreversible in SO_4^{2-} solution than in CO_3^{2-} solution.

3.3.2.8 Behaviour of Zn Electrodes Having Various Types of Surface Preparation

3.3.2.8.1 Annealed Surfaces

It is interesting to compare the values of k_1 and k_2 obtained for different electrode surfaces when two lines arise in the plot according to eqn. (52) or (53). Fig. 3.20 shows the $i_p s^{-1/2}$ vs $s^{1/2}$ plots obtained with 1M Na_2SO_4 solution at pH 11.75 for Zn electrodes treated in different ways. It is seen that all the $i_p s^{-1/2}$ vs $s^{1/2}$ plots consist of two straight lines;

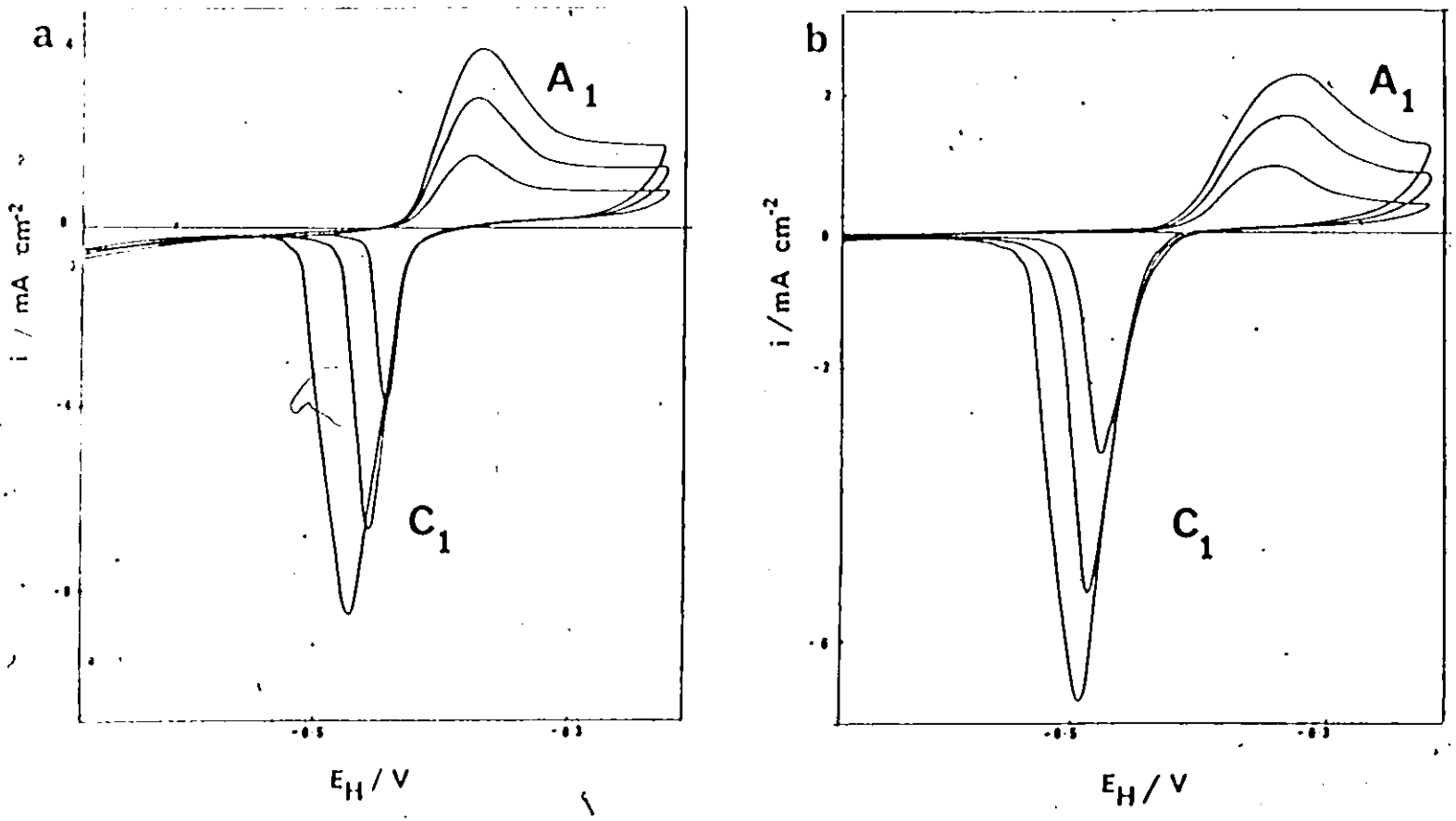

Fig. 3.19 Typical cyclic-voltammetry i vs E profiles for a polycrystalline Zn electrode in (a) 1M Na_2CO_3 and (b) 1M Na_2SO_4 solutions at pH 11.5 with varying sweep-rate.

$s = 60$, 140 and 220 mV s^{-1}

$\omega = 500$ rpm.

Table 3.6

Comparison of Charge per cm^2 and Peak Potentials for Anodic (A_1) and Cathodic (C_1) Peaks at Various Sweep-rates in Carbonate and Sulphate solutions

1) Solution: 1M Na_2CO_3, pH = 11.5

mV s^{-1}	q_a/μC cm^{-2}	q_c/μC cm^{-2}	q_a/q_c	E_p/V (A_1 peak)	E_p/V (C_1 peak)	ΔE_p/V
300	787	627	1.3	-0.359	-0.481	0.122
220	848	678	1.3	-0.366	-0.468	0.105
100	1069	537	2.0	-0.368	-0.448	0.080
20	2426	838	2.9	-0.376	-0.433	0.057

2) Solution: 1M Na_2SO_4, pH = 11.5

mV s^{-1}	q_a/μC cm^{-2}	q_c/μC cm^{-2}	q_a/q_c	E_p/V (A_1 peak)	E_p/V (C_1 peak)	ΔE_p/V
300	513	612	0.8	-0.322	-0.507	0.185
220	546	476	1.2	-0.327	-0.492	0.165
100	697	659	1.1	-0.337	-0.484	0.147
20	904	1078	0.8	-0.357	-0.472	0.115

Notes

1. All data obtained with a Zn electrode etched in 48% HBr with roughness factor assumed to be 3 for charge density calculations.
2. All charges are calculated relative to the zero current base-line.
3. q_a/q_c close to unity for 1M Na_2SO_4 solution and greater than one for 1M Na_2CO_3.
4. ΔE_p is greater for CO_3^{2-} solution than for SO_4^{2-}.

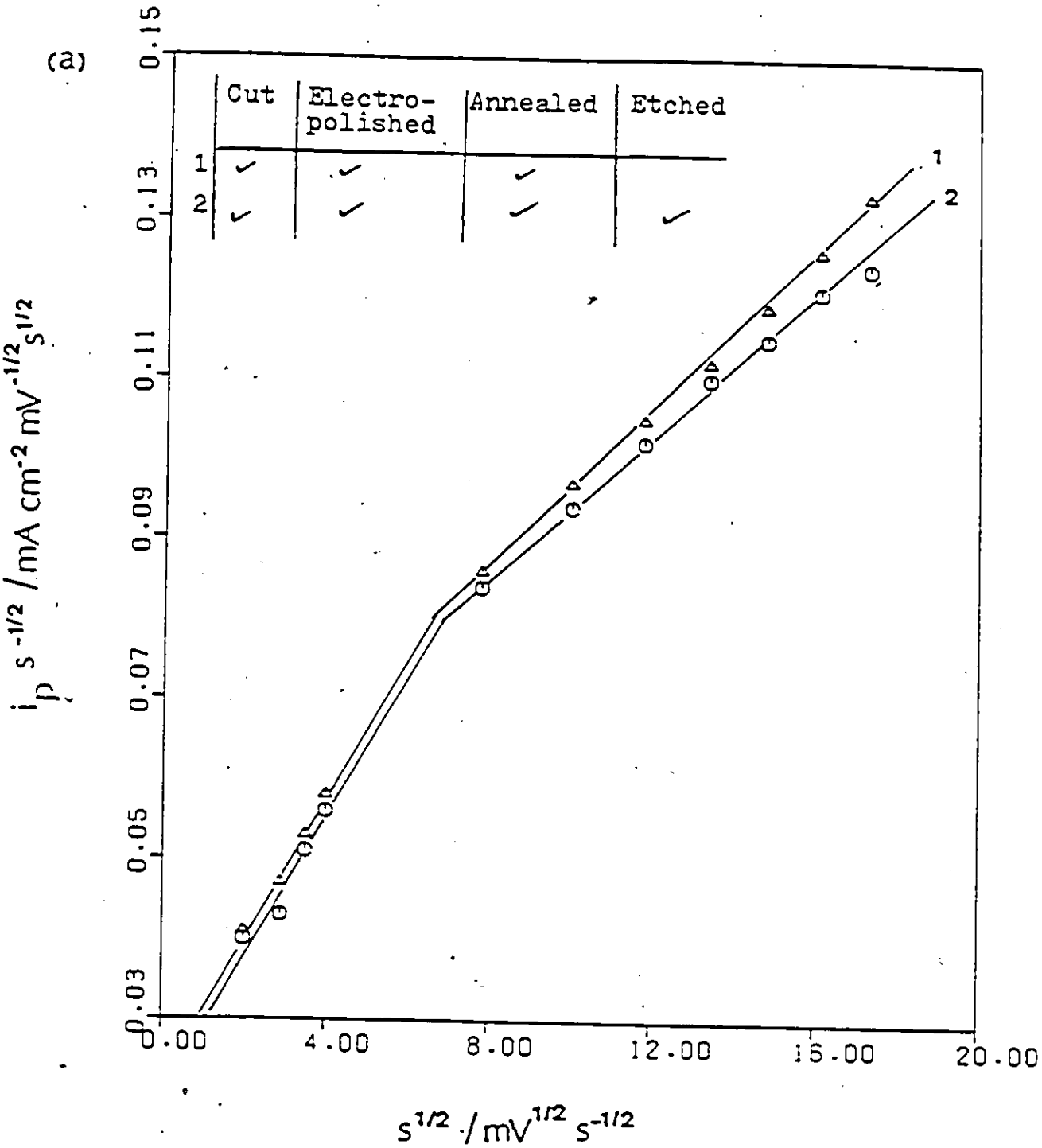

Fig. 3.20 Dependence of $i_p s^{-\frac{1}{2}}$ for peak A_1 on $s^{\frac{1}{2}}$ in 1M Na_2SO_4 at pH 11.75 for Zn polycrystalline annealed, electropolished and etched electrodes.
Electrode - polycrystalline, of apparent area 1.13 cm^2 and treated as described in Figs. 3.20 (a), (b) and (c)
s - 300 mV s^{-1} - 2 mV s^{-1}

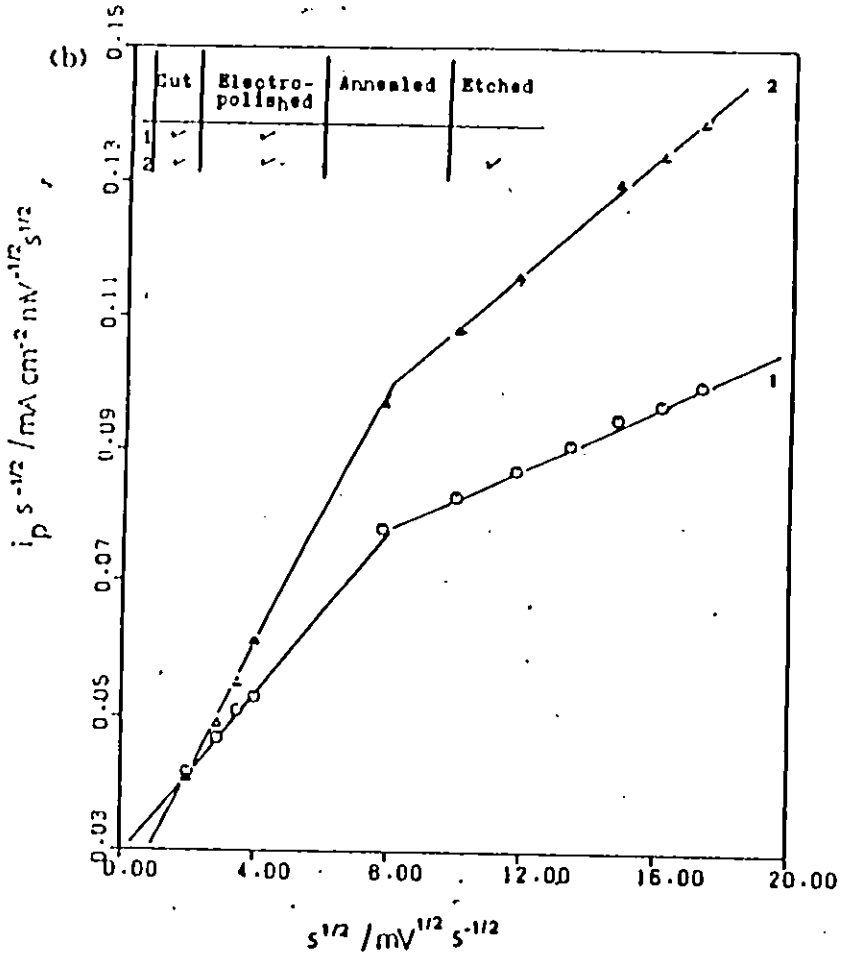

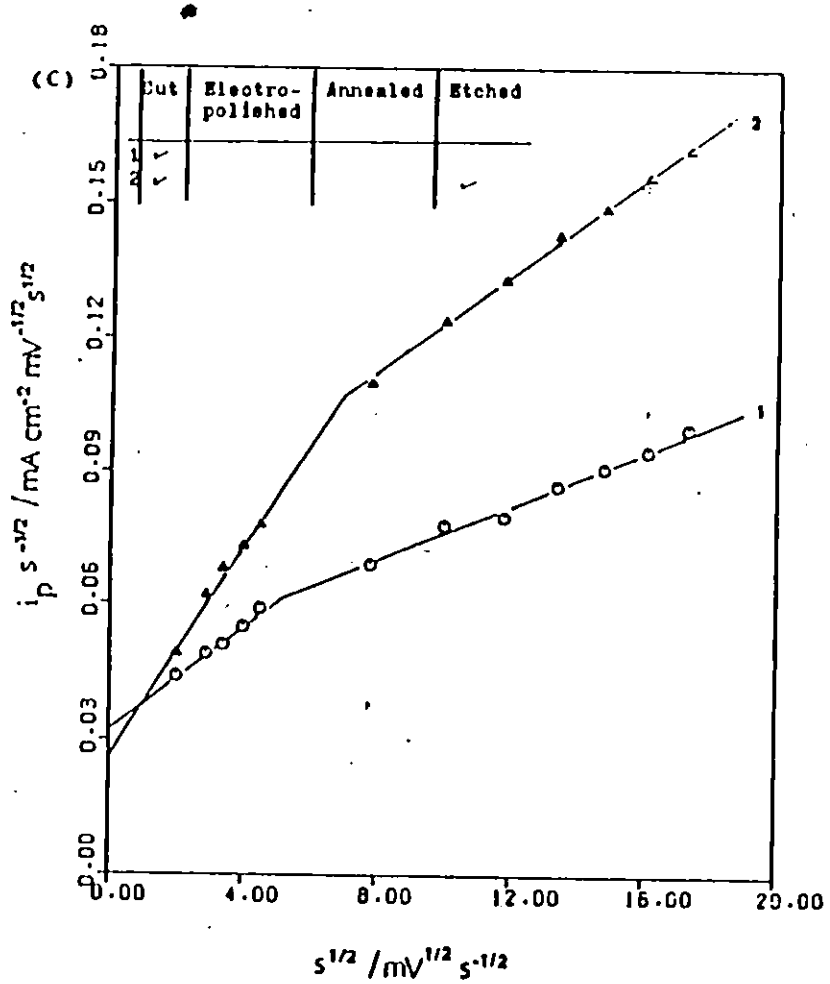

Figs. 3.20b and 3.20c .

the increase in current which arises after etching of the Zn surface is due to an increase of real surface area.

Table 3.7 summarizes the k_1 and k_2 values obtained; it is interesting that all etched surfaces (see following section 3.3.2.8.2) give the same k_1 value, ca. 0.98×10^{-2} mA cm^{-2} $mV^{-1}s$ except the annealed surface, where the real surface area is less than that of the electrode that had not been annealed, because of a smaller number of grain boundaries. Table 3.8 shows that similar results are obtained for etched surfaces in 1M Na_2SO_4 solution at pH 11.5 where k_1 is around 0.75×10^{-2} A cm^{-2} V^{-1} s. For a surface process i_p is proportional to sweep-rate and is given by $i_p = Cs$, where C is the Faradaic reaction capacitance[129] associated with the surface electrochemical reaction and for an irreversible surface process

$$i_p = (nQ_m\alpha F/eRT)\, s \qquad (43)$$

where Q_m is the charge required to form a monolayer, α is the transfer coefficient which, as shown in section (5.4), has a value of 3/2 for the zinc dissolution reaction in alkaline media (Tafel slope ca. 40 mV $decade^{-1}$), and the number of monolayers formed (n) can be calculated assuming that q_m = 350 μC cm^{-2} (page 74). The thickness of the layer due to the surface film process was found to be close to a monolayer at sweep-rates < ca. 20 mV s^{-1} . The k_1 value decreases discontinuously with increasing sweep-rate, i.e. when two lines in the plot are observed.

From these results, it seems that the observed behaviour involves the formation of a very thin film, the growth of which

Table 3.7

Comparison of k Values Obtained for Various Zn Surfaces in 1M Na_2SO_4 at pH 11.75 Solution

		Preparation of Electrode				$k_1 \times 10^2$	$k_2 \times 10^2$	$k'_1 \times 10^2$	$k'_2 \times 10^2$
		Cut	Electro-polished in H_3PO_4 EtOH 1:1 solution	Annealed at 423K for 2 h	Etched in 48% HBr	A $cm^{-2}V^{-1}s$	mA $cm^{-2}mV^{-\frac{1}{2}}s^{\frac{1}{2}}$	A $cm^{-2}V^{-1}s$	mA $cm^{-2}mV^{-\frac{1}{2}}s^{\frac{1}{2}}$
A	1	✓	✓	✓		0.79	2.68	0.27	5.94
		✓	✓	✓	✓	0.79	2.68	0.29	6.02
	2	✓	✓	✓		0.84	2.60	0.49	4.73
		✓	✓	✓	✓	0.84	2.43	0.48	4.93
	3	✓	✓	✓	✓	0.97	2.15	0.43	5.57
B	1	✓	✓			0.59	3.04	0.25	5.81
		✓	✓		✓	0.97	2.23	0.43	6.48
	2	✓	✓			0.53	1.96	0.31	3.67
C	1	✓				0.60	3.20	0.32	4.49
		✓			✓	1.01	3.27	0.54	6.96

Notes

1. All measurements were carried out in 1M Na_2SO_4 solution at pH 11.75 using polycrystalline electrodes of area 1.13 cm^2 (Automergic Chemical Corp.) treated as shown in above table.
2. Sweep-rate was varied from 2 mV s^{-1} to 300 mV s^{-1}.
3. All $i_p s^{-\frac{1}{2}}$ plots consist of two regions. k_1 and k_2 are the constants at lower sweep-rates and k'_1 and k'_2 at higher sweep-rates.
4. All etched electrodes gave the same k_1 (98×10^{-4} mA $cm^{-2}mV^{-1}s$) value except the annealed electrode which has a smaller number of grains, therefore smaller real surface area.

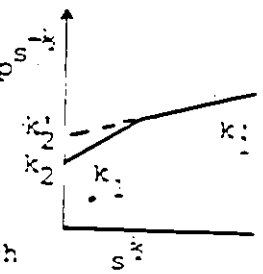

Table 3.8

Comparison of k Values Obtained in Na_2SO_4 Solution at pH 11.5

	Description of the Zn electrode		$k_1 \times 10^2$ $A\,cm^{-2}V^{-1}s$	$k_2 \times 10^2$ $mA\,cm^{-2}mV^{-\frac{1}{2}}s^{\frac{1}{2}}$	$k_1' \times 10^2$ $A\,cm^{-2}V^{-1}s$	$k_2' \times 10^2$ $mA\,cm^{-2}\,mV^{-\frac{1}{2}}s^{\frac{1}{2}}$
A	Polycrystalline, area = 1.13 cm^2	Etched in 48% HBr	0.77	1.17	0.28	3.36
		Unetched	0.81	1.45	0.45	3.63
B	Polycrystalline area = 0.071cm^2	Etched in 48% HBr	0.78	4.45	0.54	5.59
			0.75	6.79	0.48	8.85
			0.75	4.67	0.57	5.98
			0.74	6.36	0.74	6.32
			0.86	3.99	0.58	6.01
C	Cleaved surface Area = 1.13 cm^{-2}	Etched in 48% HBr	0.76	1.68	0.65	2.89
		Used	0.75	2.55	0.35	5.72
			0.95	3.29	0.35	5.72
		New	2.57	—	—	13.27

Notes

1. All measurements were carried out in 1M Na_2SO_4 solution at pH 11.5 using polycrystalline electrodes of geometrical area of 1.13 cm^2 and 0.071 cm^2, treated as shown above.
2. Sweep-rate is varied from 2 mV s^{-1} to 300 mV s^{-1}.
3. All $i_p s^{-\frac{1}{2}}$ plots consist of two regions except for the cleaved (0001) face (new) electrode; k_1 and k_2 are the constants at lower sweep-rates and k_1' and k_2' at higher sweep-rates. Behaviour of the (0001) face is given under section (3.3.10.1. C).

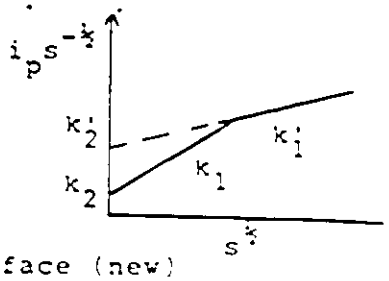

4. All etched electrodes gave the same k_1 (0.77×10^{-2} mA cm^{-2} $mV^{-1}s$) value, except (0001) face (new) where the k_1 value is 2.57×10^{-2} mA cm^{-2} $mV^{-1}s$.

may depend very much on the surface crystallographic orientation and conditions of preparation of the electrode. In the next section are presented the results obtained at various etched surfaces.

3.3.2.8.2 Etched Surfaces

The number of anodic and cathodic peaks, and also the shape of the peaks A_1 and C_1 depend very much on the surface preparation. The Zn electrodes were etched in various acids besides concentrated HBr (48%). Table 3.9 gives the concentration of these acid solutions used and also the etching times.

Table 3.9

Concentration of Acids Employed for Etching and the Etching Time

Acid	Concentration of Acid / M	Etching Time/s
HCl	12.4	5
HBr	9.0	8
HNO_3	7.7	8
$HClO_4$	11.6	6
TFMSA	11.3	300

Zn does not react with TFMSA (CF_3SO_3H) or $HClO_4$ in the same way as it does with concentrated HBr, HNO_3 or HCl. This is clear from Fig. 3.21 which shows the states of the Zn electrode surface etched in $HClO_4$ before and after electrochemical cycling at

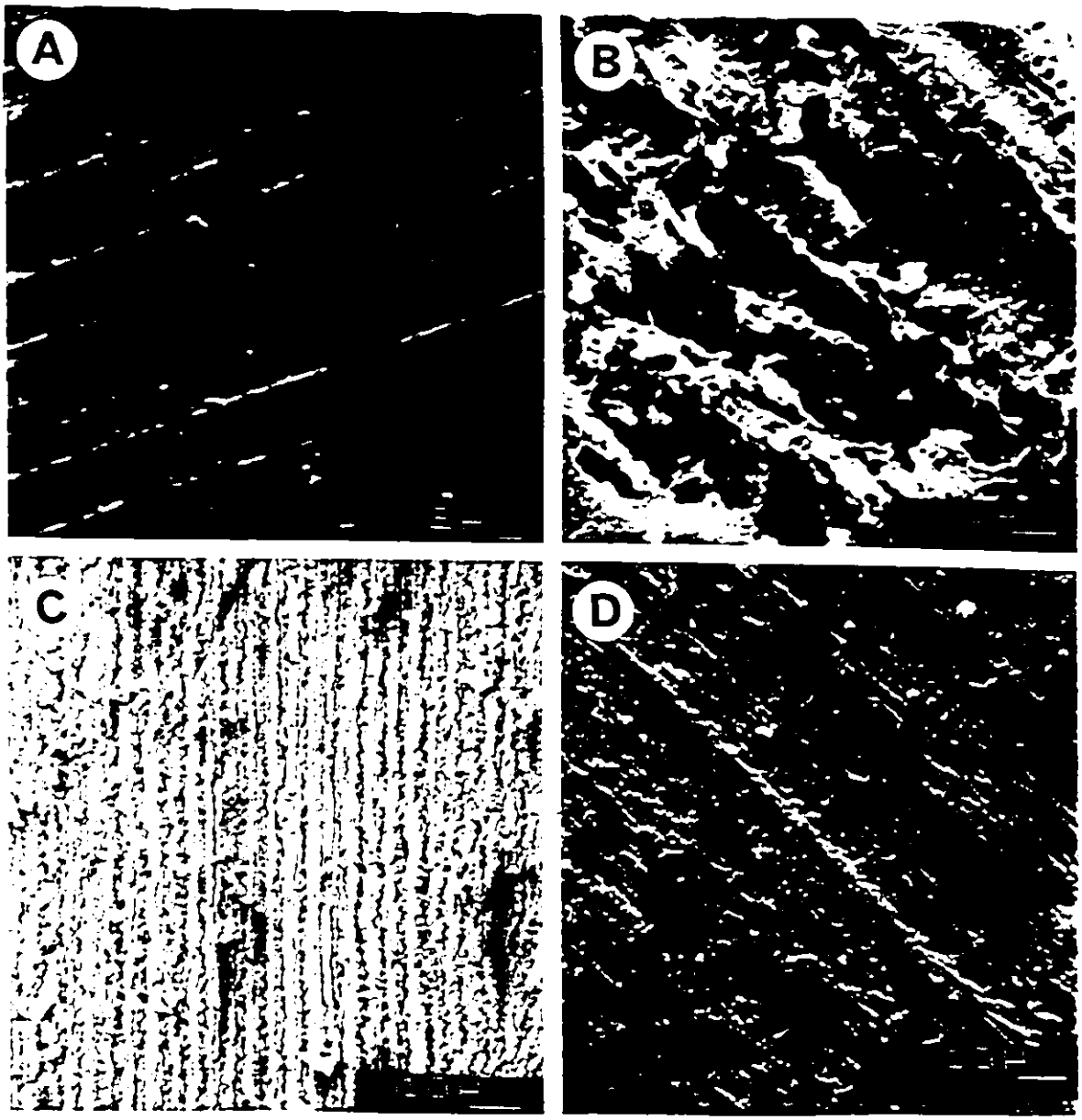

Fig. 6.5 The state of the Zn electrode surface etched in $HClO_4$ before and after electrochemical cycling in 1M Na_2CO_3 at pH 11.5.

(A) Before cycling

(B) and (D) After cycling in the (-0.706 V) - (-0.206V) potential range over 300 mV s^{-1} - 6 mV s^{-1} sweep-rate range.

(C) After cycling in the (-0.753 V) - (-0.126 V) potential range over 300 mV $^{-1}$ - 20 mV s^{-1} sweep-rate range.

sweep-rates in the range 300 mV s^{-1} to 20 mV s^{-1} in 1M Na_2CO_3 solution at pH 11.5. The scratches seen on the Zn surface arise from the initial cutting of the Zn rod by the diamond saw; it can be seen that some changes of surface morphology have taken place during the cycling. The cyclic-voltammograms obtained with a Zn surface that had been etched in $HClO_4$ are shown in Fig. 3.22 . It is clear that CV's obtained at very low sweep-rates exhibit two well defined anodic peaks A_{1a} and A_{1b} (Fig. 3.22) and a broad reduction region which is probably compounded from two overlapping cathodic peaks.

Similar results were obtained with a Zn surface etched in TFMSA . The $i_p s^{-1/2}$ vs $s^{1/2}$ plots for Zn etched in this acid are shown in Fig. 3.23a. It is clear from Fig. 3.23b which shows the $i_p s^{-1}$ vs $s^{-1/2}$ plot for the two anodic peaks (at lower sweep-rates), that the behaviour of these two peaks fits very well to eqn. (51). At higher sweep-rates it is difficult to separate the two anodic peaks.

It is of interest to see how the current for the cathodic peak (C_1) varies with sweep-rate. Fig. 3.24 shows the $i_p s^{-1/2}$ vs $s^{1/2}$ plots obtained for the cathodic peak current, from the cyclic-voltammograms recorded in 1M Na_2CO_3 solution at pH 11.5 (Fig 3.22). It is seen from Figs. 3.23a and 3.24 that the discontinuity in these plots arises at the same sweep-rates. This means that the broad cathodic peak may be composed of two peaks as is the case in the anodic A_1 peak region. It is interesting to see next how rotation of the electrode affects the cathodic C_1 and the anodic A_1 peaks.

Fig. 3.25 shows the effect of rotation on the currents

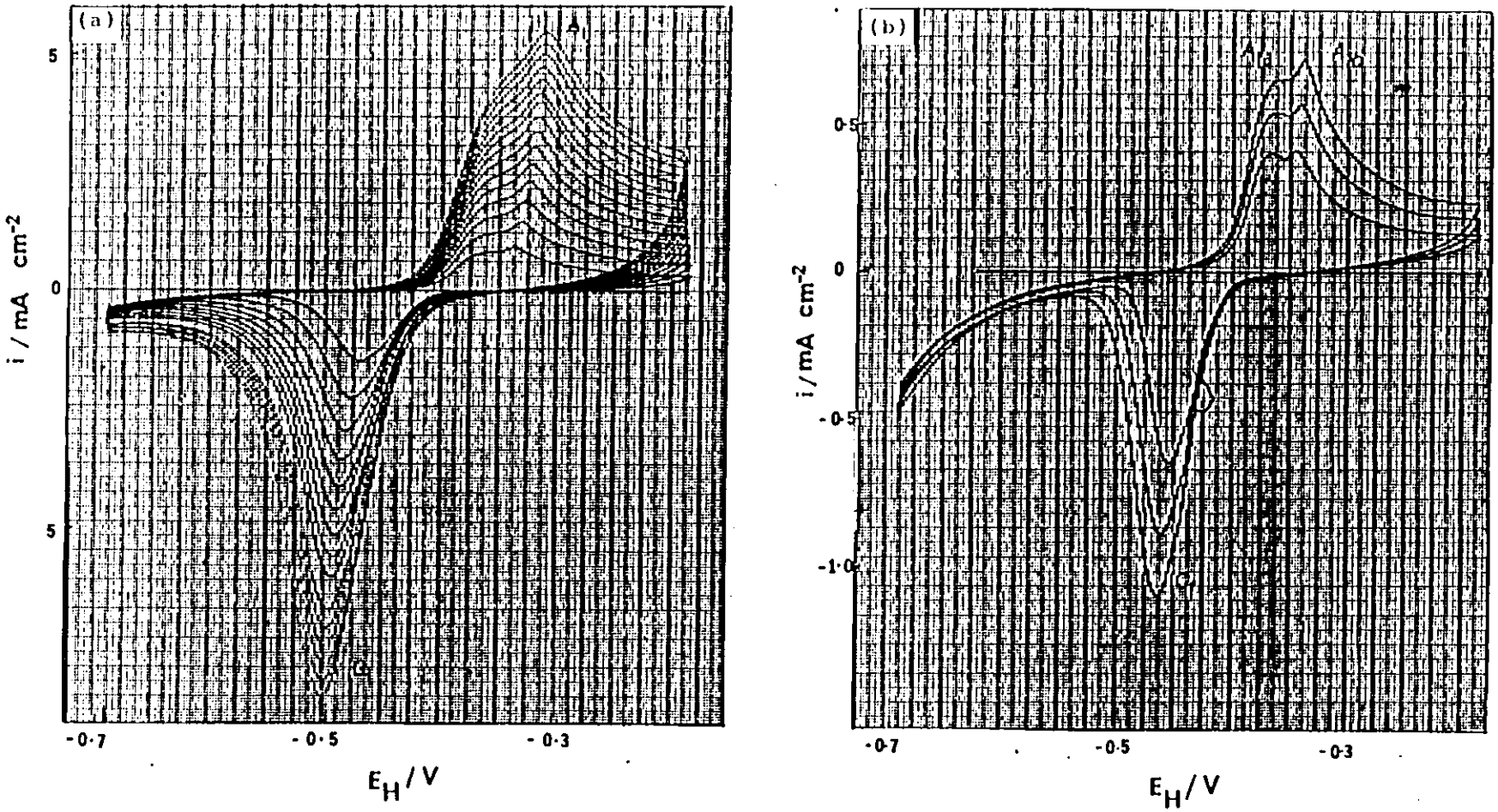

Fig. 3.22 Typical cyclic-voltammetry i vs E profiles for variable sweep-rates in 1M Na_2CO_3 solution at pH 11.5 for polycrystalline Zn electrode etched in $HClO_4$

s - (a) Sweep-rate varied from 300 mV s^{-1} to 20 mV s^{-1} with 20 mV s^{-1} sweep-rate decrease.

s - (b) 14, 10 and 6 mV s^{-1}.

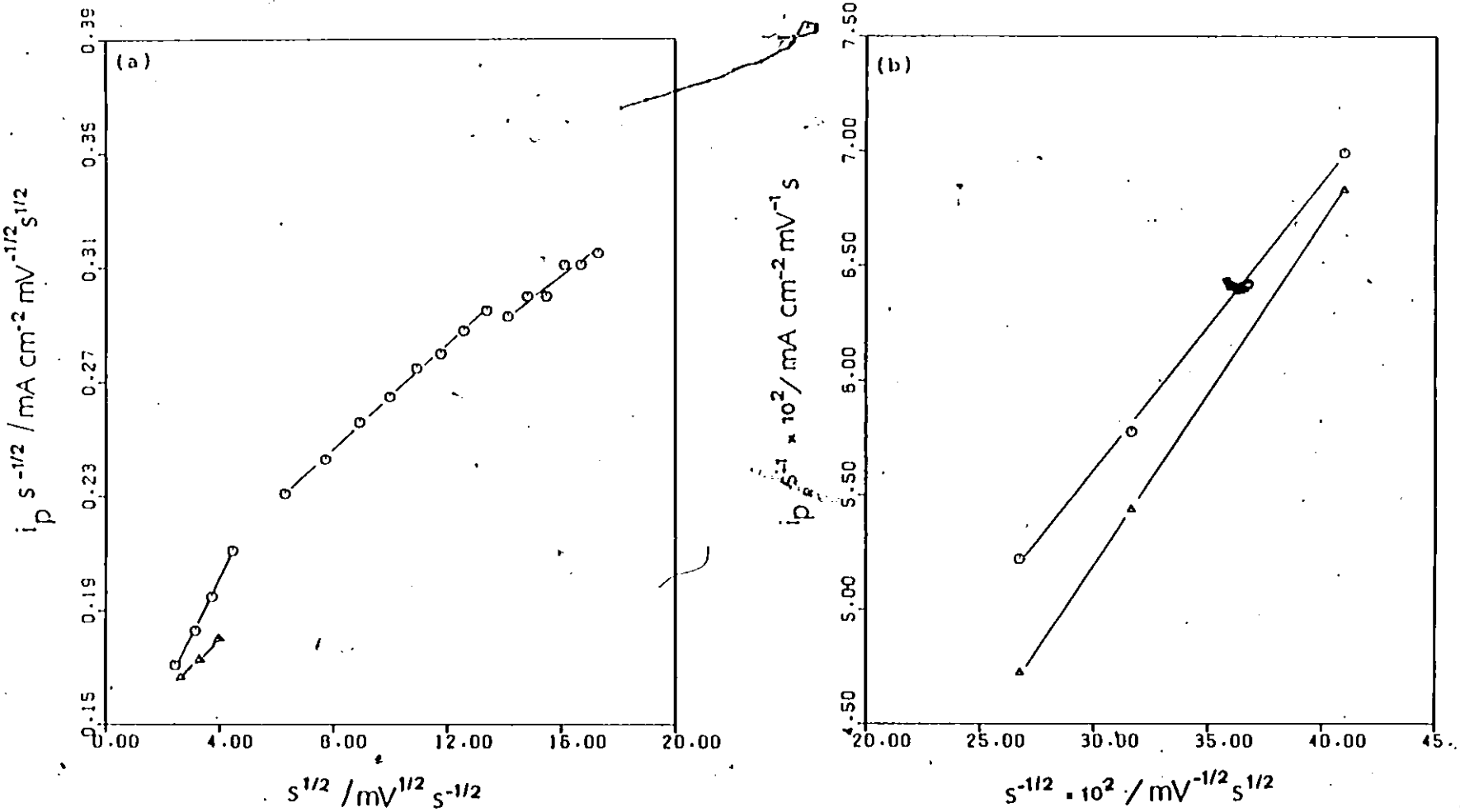

Fig. 3.23 (a) Dependence of $i_p s^{-\frac{1}{2}}$ for peak A_1 on $s^{\frac{1}{2}}$ plotted for data of Figs. 3.22(a) and 3.22(b).

(b) Dependence of $i_p s^{-1}$ for peaks A_{1a} and A_{1b} on $s^{-\frac{1}{2}}$ plotted for Fig. 3.22(b).

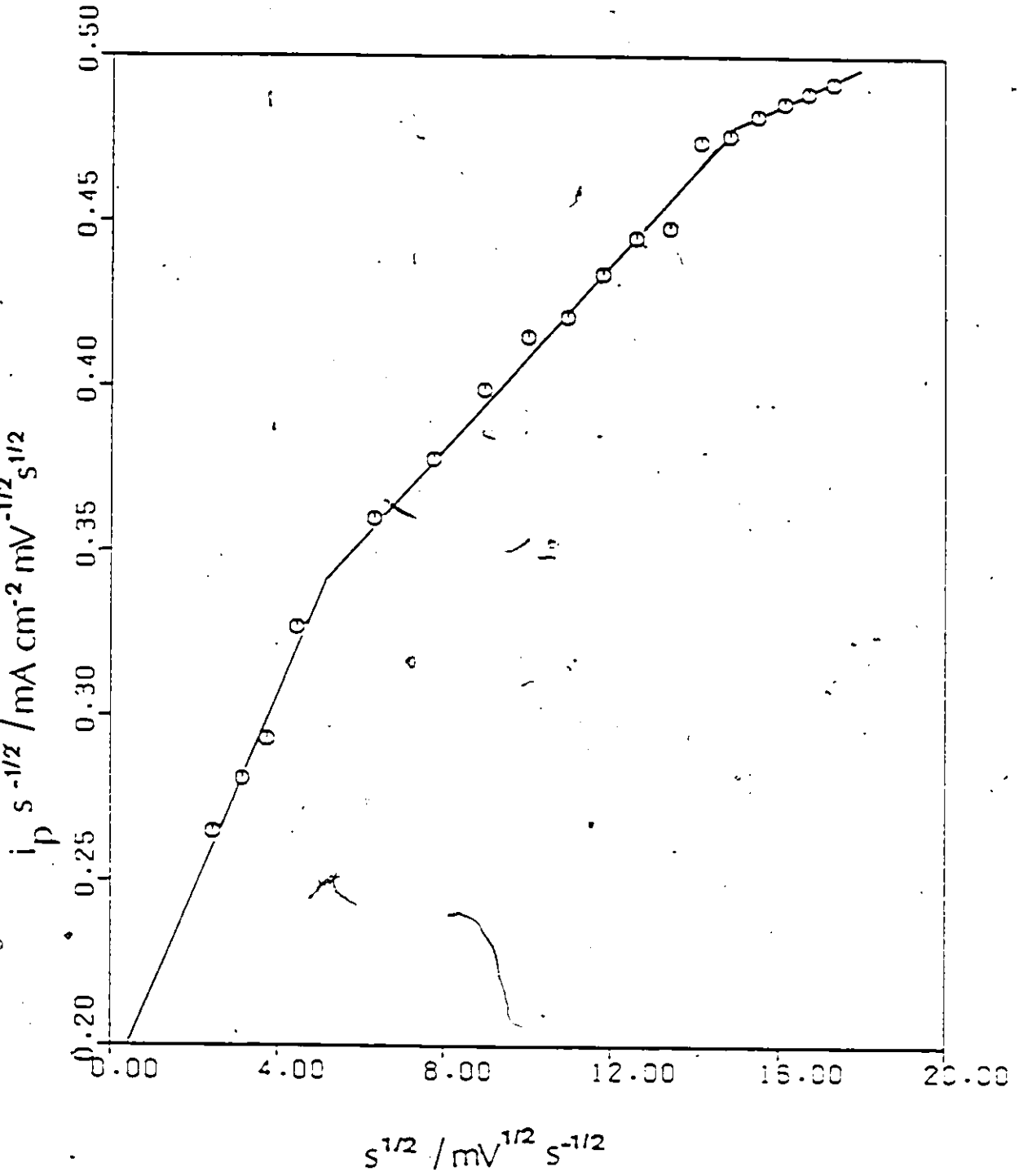

Fig. 3.24 Dependence of $i_p s^{-\frac{1}{2}}$ for C_1 peak on $s^{\frac{1}{2}}$ for data of Fig. 3.22a .

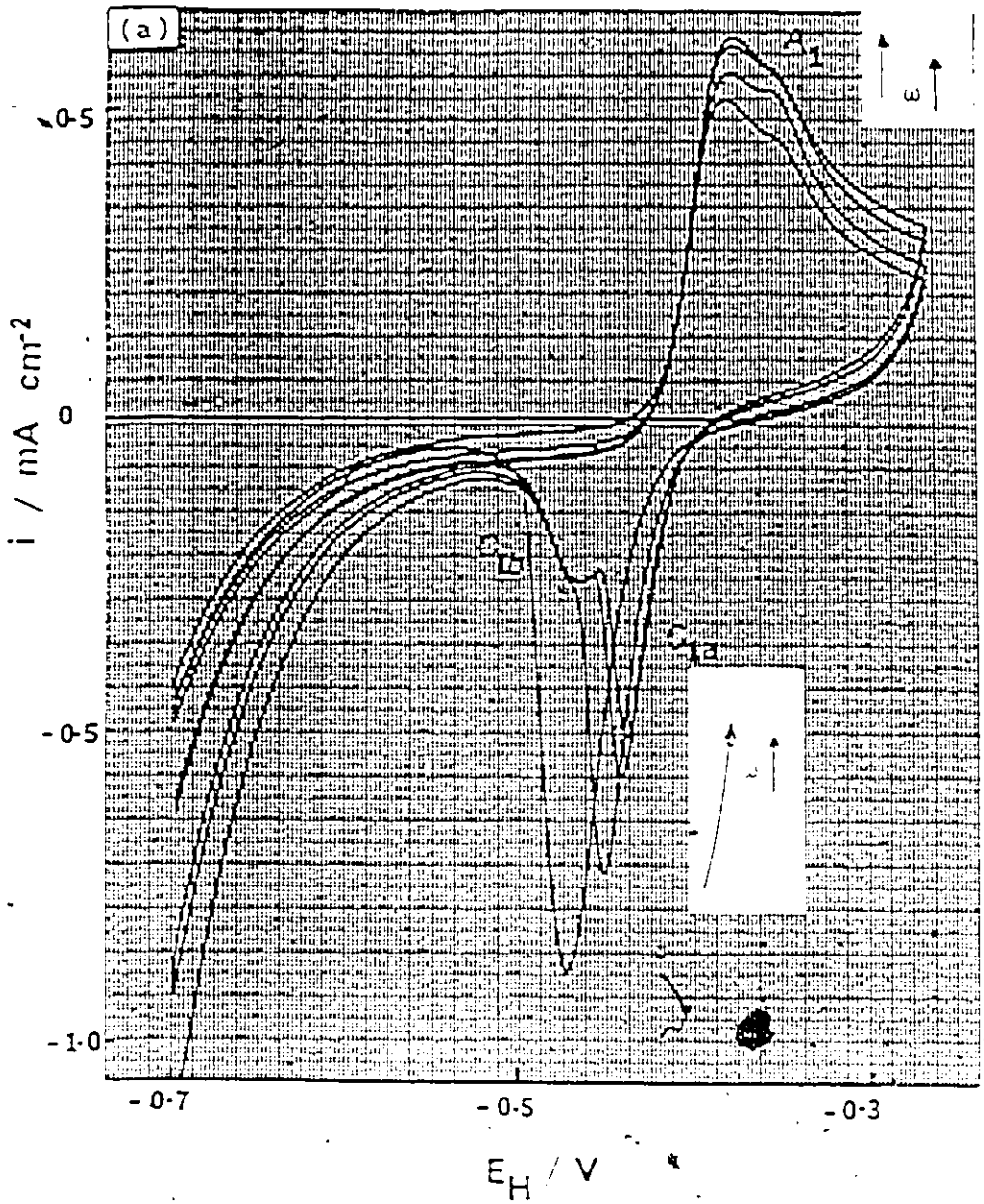

Fig. 21 The effect of rotation on the cathodic peak C1 for polycrystalline GaAs RDE in 0.2M Na_2SO_4 + 0.5M Na_2CO_3 solution at pH 11.5 for various anodic reversal potentials of the sweep.

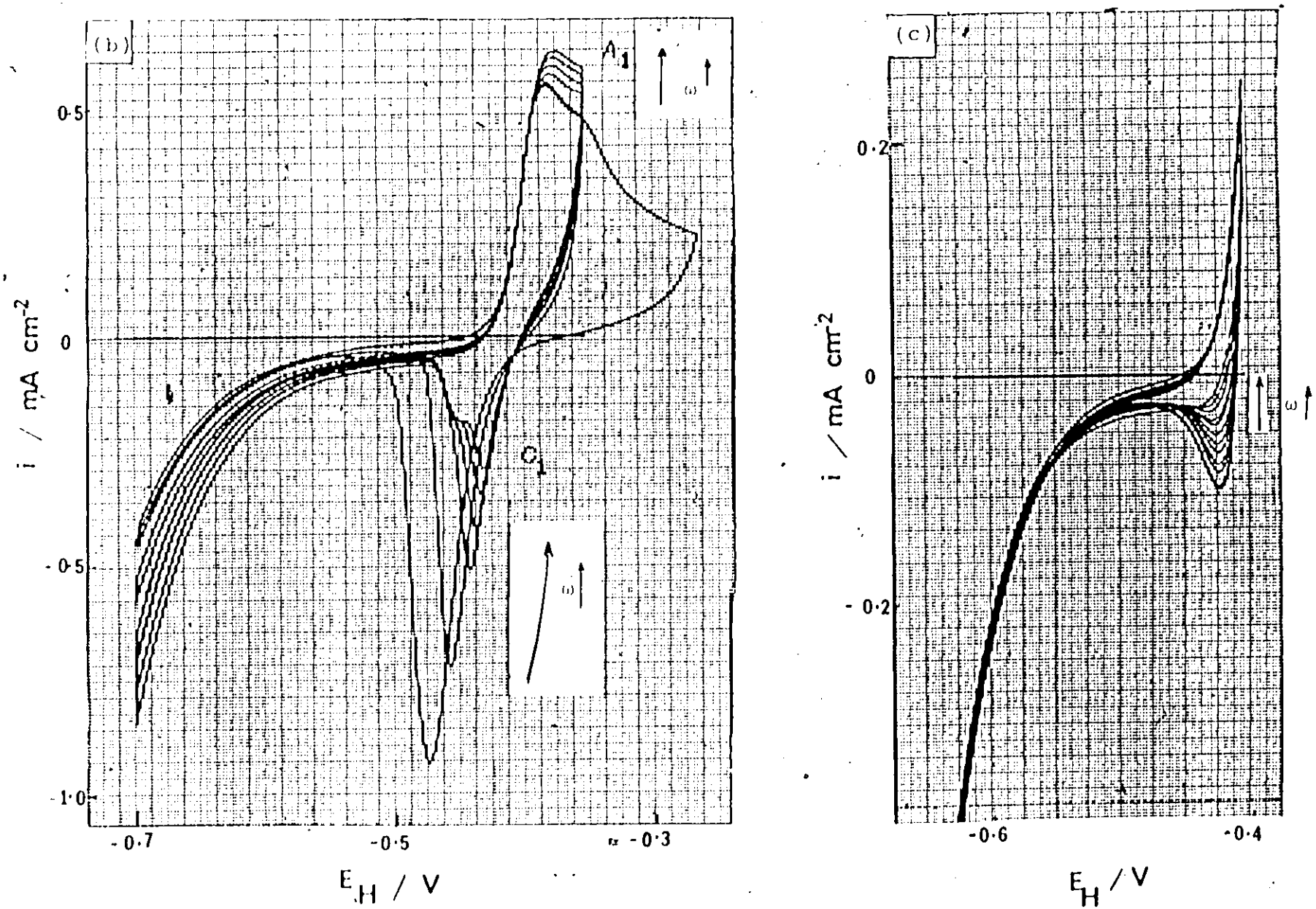

Figs. 3.25 (b) and (c).

associated with the cathodic peak C_1. It is clear from Fig. 3.25c that $ZnO/Zn(OH)_2$ formation at the beginning of Zn dissolution is completely determined by a solution transport process, because the dissolution current does not change at all with cycling or rotation, while the reduction current decreases with rotation because e.g. some anodically formed, soluble zinc species is spun away. As the anodic overpotential is increased, it is seen that the cathodic peak C_1 consists, in fact, of two resolved peaks. One peak depends on rotation-rate (C_{1a}) while the other (C_{1b}) does not (Fig. 3.25a-b). Presumably, therefore, the latter involves material bound to the surface to an extent of the order of a monolayer; this is confirmed by the observation of i_p for C_{1b} being linear in s (see section 3.3.3).

Table 3.10 gives the k_1 and k_2 values obtained for the two anodic peaks in the CV of Zn electrodes at lower sweep-rates, the Zn having been etched in TFMSA and $HClO_4$ solutions. It is clear that the currents of the second anodic peak (A_{1b}) are more surface-controlled than those in the first anodic peak; also the A_{1b} reaction process behaves more irreversibly than that of the first peak (A_{1a}).

Now it is interesting to compare the peak potentials of the two anodic (A_{1a} and A_{1b}) and the two cathodic peaks (C_{1a} and C_{1b}). Table 3.11 summarizes some of the results obtained from cyclic-voltammetry experiments in 1M Na_2CO_3 solution at pH 11.5 for various conditions of surface preparation. Columns 2,3,14 and 15 give the peak potentials for these four peaks at a sweep-rate of 20 mV s^{-1} ; also the predominant cathodic and anodic peak

Table 3.10

k_1 and k_2 Values for Peaks A_{1a} and A_{1b}

	Zn electrode etched in $HClO_4$		Zn Electrode etched in TFMSA	
	A_{1a}	A_{1b}	A_{1a}	A_{1b}
$k_1 \times 10^2$/mA cm^{-2} mV^{-1} s	0.75	1.77	0.59	0.98
$k_2 \times 10^2$/mA cm^{-2} mV$^{-\frac{1}{2}}$ s$^{\frac{1}{2}}$	14.85	12.73	10.75	10.61

Notes

1. k_1 and k_2 values obtained from $i\, s^{-\frac{1}{2}}$ vs $s^{\frac{1}{2}}$ plots at lower sweep rates (2-20 mV s^{-1}) in 1M Na_2CO_3 solution at pH 11.5 for Zn electrodes etched in $HClO_4$ (Fig. 3.28) and TFMSA.
2. k_1 value is smaller for peak A_{1a} than for peak A_{1b} for both electrodes.

for each CV at 20 mV s^{-1} is marked with a "*". It is also clear from these data that the second cathodic peak, C_{1b} corresponds to the second anodic peak (A_{1b}) and the first cathodic peak (C_{1a}) corresponds to the first anodic peak (A_{1a}). The difference between peak potentials of A_{1a} and C_{1a} is about 70 mV while between the peaks A_{1b} and C_{1b} it is about 130 mV, i.e. the oxidation/reduction process involved at the A_{1a}/C_{1a} peaks is more reversible than that at the A_{1b}/C_{1b} peaks.

It can be seen from Table 3.11 and Figs. 3.23a and 3.24 that various pairs of k_1 and k_2 are required to represent the i_p as f(s) results over several ranges of sweep-rate; in some cases there are four ranges, depending on the pH (Table 3.11). This complex behaviour arises probably because there are usually two component peaks in the CV and there is also a dependence on the state of the Zn surface determined by the etching conditions. Further, the behaviour observed depends on the thickness of the ZnO film that is developed and this depends itself on the pH and sweep-rate.

It is therefore rather very difficult to derive quantitative information from these results, especially in the case of carbonate solutions (section 3.5). Table 3.12 summarizes the sweep-rates at which a discontinuty in the $i_p s^{-1/2}$ vs $s^{1/2}$ plots arises for the cathodic and anodic peaks. It is clear that the discontinuity is observable almost at the same sweep-rate for the cathodic as for the anodic peaks in the lower sweep-rate regime. This means that two reactions take place within the potential range of the anodic peaks (A_{1a} and A_{1b}) and the conjugate cathodic peaks (C_{1a} and C_{1b}) must correspond to two parallel

Table 3.11

K values and peak potentials for A_1 and C_1 obtained at various surfaces (Data for the distinguished regions of the $i_p/s^{\frac{1}{2}}$ vs $s^{\frac{1}{2}}$ plots of Fig. 3.22 are given in this table (see schematic diagrams at feet of the two tables for anodic and cathodic peaks.)) .

ANODIC BEHAVIOUR

Surface Preparation	Peak Potential/V Sweep rate 20mV s^{-1}		Region 1		Region 2		Region 3		Region 4		Region 5	
	A_{1a}	A_{1b}	$k_1 \cdot 10^2$	$k_2 \cdot 10^2$	$k_1 \cdot 10^2$	$k_2 \cdot 10^2$	$k_1 \cdot 10^2$	$k_2 \cdot 10^2$	$k_1 \cdot 10^2$	$k_2 \cdot 10^2$	$k_1 \cdot 10^2$	$k_2 \cdot 10^2$
Etched in TFMSA	-0.384	-0.354*	0.75	11.5	—	—	0.74	12.15	0.98	10.66	0.59	10.74
Etched in $HClO_4$	-0.386	-0.356*	0.86	17.03	—	—	0.91	17.39	1.77	12.73	0.75	14.83
Etched in HCl	—	-0.363*	0.54	8.70	0.38	10.93	0.55	9.16	1.05	6.54	—	—
Etched in 1:4 H_3PO_4 and anodically polished in KOH	—	-0.352*	0.98	22.3	—	—	1.41	18.3	2.73	11.51	—	—
Electropolished in H_3PO_4, EtOH 1 min.	-0.386	-0.361*	0.68	8.20	0.51	10.70	0.69	8.78	6.93	8.78	—	—
Etched in HBr	-0.385*	-0.363	0.64	7.07	—	—	0.76	6.63	—	—	—	—
	-0.378*	—	—	—	—	—	0.91	8.44	—	—	1.02	7.52
Unetched	-0.394	-0.352*	0.64	8.68	0.48	10.87	0.65	8.62	1.06	6.43	—	—
	-0.387*	-0.368	0.65	12.85	—	—	0.41	16.12	—	—	—	—

Notes

1. This table shows k_1 and k_2 values obtained from $i/s^{\frac{1}{2}}$ vs $s^{\frac{1}{2}}$ plots for both A_1 and C_1 peaks for various electrodes as described above, in 1M Na_2CO_3 solution at pH 11.5.
2. There are five regions of the $i_p/s^{\frac{1}{2}}$ vs $s^{\frac{1}{2}}$ plots for the anodic peak and three such regions for the cathodic peak over the sweep-rate range 2 mV s^{-1} to 300 mV s^{-1} (the region 2 is not seen in the plots for the cathodic peak).
3. Peak potentials for A_{1a}, A_{1b}, C_{1a} and C_{1b} are given and the predominant peak is indicated with an '*'.
4. When peak A_{1b} is predominant in the anodic process, C_{1b} is predominant in the cathodic process. Similarly, when A_{1a} is more predominant in the anodic reaction, C_{1a} is in the cathodic reaction.

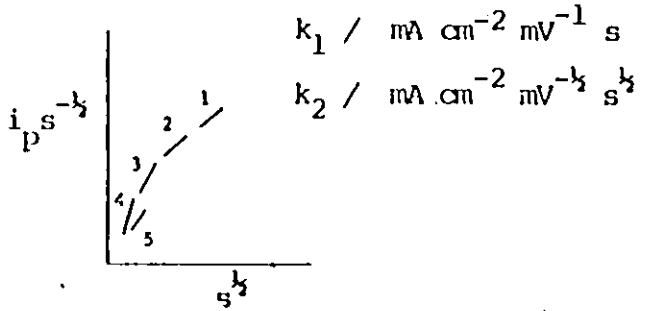

Table 3.11 (continued)

CATHODIC BEHAVIOUR

Surface Preparation	Peak Potential/V s = 20 mV s^{-1} C_{1a}	C_{1b}	Region 1 $k_1 \cdot 10^2$	$k_2 \cdot 10^2$	Region 2 $k_1 \cdot 10^2$	$k_2 \cdot 10^2$	Region 3 $k_1 \cdot 10^2$	$k_2 \cdot 10^2$	Region 4 $k_1 \cdot 10^2$	$k_2 \cdot 10^2$
Etched in THSA	-0.460	-0.480*	0.67	32.9	—	—	1.22	24.14	4.36	8.20
Etched in $HClO_4$	-0.466	-0.489*	0.59	39.0	—	—	1.33	27.05	3.21	18.28
Etched in HCl	—	-0.478*	0.13	24.32	—	—	0.65	17.02	2.63	7.21
Etched in 1:4 H_3PO_4 and anodically polished in KOH	-0.463	-0.480*	0.07	49.7	—	—	0.83	37.05	4.51	15.67
Electicpolished in H_3PO_4: EtOH 1 min.	-0.469	-0.480*	0.54	22.10	—	—	0.98	15.84	1.60	11.52
Etched in HBr	-0.457*	—	—	—	—	—	—	—	—	—
	-0.457*	—	—	—	—	—	0.61	17.25	3.17	5.20
unetched	—	-0.487*	1.05	10.08	—	—	0.85	11.91	0.99	10.89
	-0.440	—	—	—	—	—	—	—	5.43	7.95

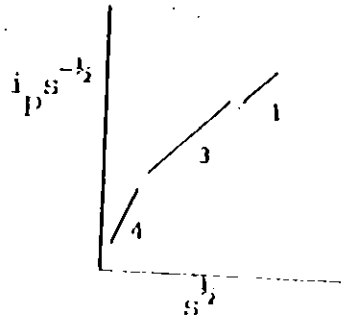

cathodic

k_1 / mA cm^{-2} mV^{-1} s

k_2 / mA cm^{-2} $mV^{-\frac{1}{2}}$ $s^{\frac{1}{2}}$

Table 3.12

Sweep-Rate at which the Discontinuity Occurs in Anodic and Cathodic $i_p s^{-\frac{1}{2}}$ vs $s^{\frac{1}{2}}$ plots for Peaks A_1 and C_1

(for designation of inflection points x, y, z, x' and z' see schematic diagram below)

Surface Preparation	Peak potential /V--Sweep rate 20 mV s^{-1} A_{1a}	A_{1b}	x $s^{\frac{1}{2}}$ / (mV s^{-1})$^{\frac{1}{2}}$	y $s^{\frac{1}{2}}$ / (mV s^{-1})$^{\frac{1}{2}}$	x' $s^{\frac{1}{2}}$ / (mV s^{-1})$^{\frac{1}{2}}$
Etched in THISA	-0.384	-0.354*			6.2
Etched in $HClO_4$	-0.386	-0.356*			5.4
Etched in HCl	—	-0.363*	14	10.4	5.5
Etched in 1:4 H_2SO_4 and anodically polished in EtOH	—	-0.352*			5.3
Electropolished in H_2SO_4: EtOH 1 min.	-0.386	-0.361*	14.7	10.5	
Etched in HBr	-0.385*	-0.363			
	-0.378*				
unetched	-0.394	-0.352*	14.1	10.8	6.3
	-0.387*	-0.369			

Peak Potential/V sweep rate 20mVs^{-1}: C_{1a}	C_{1b}	z' 1 $s^{\frac{1}{2}}$ / (mV s^{-1})$^{\frac{1}{2}}$	x' 3 $s^{\frac{1}{2}}$ / (mV s^{-1})$^{\frac{1}{2}}$ 4
-0.460	-0.480*	16	5.1
-0.466	-0.489*	15.1	4.8
—	-0.478*	13.9	5.0
-0.463	-0.480*	16.6	5.8
-0.469	-0.480*	14.3	6.9
-0.457*	—		
-0.459*	—		4.7
—	-0.487*		
-0.440*	—		7.2

Notes

1. This table shows the $s^{\frac{1}{2}}$ values at which the discontinuity occurs in the anodic and cathodic $i/s^{\frac{1}{2}}$ plots. x, y, z values in the anodic region and x' and z' values in the cathodic region. These experiments were carried out in 1M Na_2CO_3 solution at pH 11.5 for the various electrodes described above, in the 2 mV s^{-1} - 300 mV s^{-1} sweep-rate range. k_1 and k_2 values are compared in Table 3.10.
2. Defining diagrams: x and x' values for the anodic and cathodic peaks have the same values.

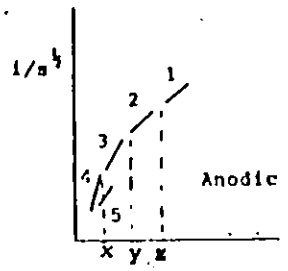

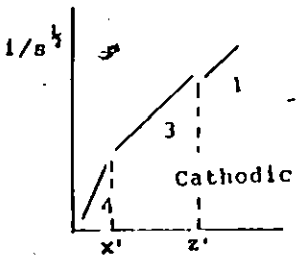

processes that occur independently from one another, e.g. on different crystal faces.

Table 3.13 summarizes similar results obtained with other solutions but the electrodes used were prepared by etching the Zn electrode in concentrated HBr for 8 s. It can be seen that at higher pH's, $i_p s^{-1/2}$ is <u>independent of s</u> for solutions at pH 12.5 and 11.5 i.e. the process is mainly diffusion-controlled. These plots consist of only two straight lines. An interesting question is whether this behaviour of Zn surfaces etched in concentrated HBr is something to do with the crystallographic surface structure that is left after etching in acid?

Figs. 3.19(a), (b) and 3.3 show the cyclic-voltammograms obtained with a Zn electrode etched in concentrated HBr and concentrated HCl. Such surfaces gave only <u>one</u> anodic peak (A_1) and <u>one</u> cathodic peak (C_1) which are, however, compounded of at least two peaks. Thus it could be that these etched electrodes exhibit randomly oriented crystal surfaces giving rise to an average behaviour characteristic of many surface orientations.

The difference in k_1 and k_2 values, and also the charges under the A_1 and C_1 peaks for Na_2CO_3 and Na_2SO_4 solutions in Fig. 3.19 and Table 3.6, is mainly due to the effect of CO_3^{2-}, a feature that will be discussed further in section (3.5). It is well known that crystallographic features of the metal lattice, which determine the geometry of crystal surface planes, control the mode of dissolution of the metal. Etched surfaces consist of facets that are relatively closely-packed planes together with grain boundaries. Effects on dissolution rate arise because the

Table 3.13

Comparison of k_1 and k_2 Values for the A_1 Peak for Zn Oxidation in Various solutions

(Region 1 to 5 compared to those defined in Table 3.11)

Solution	pH	Peak potential/V sweep-rate 20mV s^{-1}		Region 1		Region 2		Region 3		Region 4		Region 5	
		A_{1a}	A_{1b}	$k_1 \cdot 10^2$	$k_2 \cdot 10^2$	$k_1 \cdot 10^2$	$k_2 \cdot 10^2$	$k_1 \cdot 10^2$	$k_2 \cdot 10^2$	$k_1 \cdot 10^2$	$k_1 \cdot 10^2$	$k_1 \cdot 10^2$	$k_2 \cdot 10^2$
0.2M NaOH+0.03M Na_2CO_3	13.3	-0.364*	—	—	136.73	—	—	—	—	—	—	—	—
0.1M NaOH	13.0	-0.370*	—	0.18	45.11	—	—	—	—	—	—	—	—
0.03M NaOH+0.99M Na_2SO_4	12.5	-0.388*	—	0.39	140	—	—	—	—	—	—	0.72	10.56
0.03M NaOH+0.99M Na_2CO_3	12.5	-0.392*	-0.365	0.38	137.72	—	—	—	—	—	—	1.54	8.27
1M Na_2SO_4	11.5	-0.385*	—	0.57	5.98	—	—	—	—	—	—	0.75	4.71
1M Na_2CO_3	11.5	-0.385	-0.363	0.60	7.07	—	—	0.76	6.36	—	—	—	—
1M Na_2CO_3	11.5	-0.378	—	—	—	—	—	0.91	8.44	—	—	1.02	7.52
0.5M Na_2CO_3	11.4	-0.364	—	0.61	5.37	—	—	0.81	3.63	—	—	—	—
0.1M Na_2CO_3	11.2	-0.369	—	0.45	6.05	—	—	0.55	4.78	—	—	—	—
0.2M $NaHCO_3$+0.27M Na_2SO_4	8.4	-0.375	-0.355*	0.30	12.27	—	—	0.37	11.48	—	—	—	—
0.4M $NaHCO_3$+0.2M Na_2SO_4	8.4	-0.408	-0.350*	—	31.96	0.33	30.26	1.46	20.79	1.24	2163	—	—

Notes

1. This table compares k_1 and k_2 values obtained from $i/s^{\frac{1}{2}}$ vs $s^{\frac{1}{2}}$ plots in the 2 mV s^{-1} to 300 mV s^{-1} sweep-rate range using various solutions in the pH range 13.0-8.4 for a Zn electrode etched in 48% HBr.
2. At higher pH's only one region can be seen in the $i/s^{\frac{1}{2}}$ vs $s^{\frac{1}{2}}$ plots and $k_2 > k_1$. As the pH decreases, two regions are observed. k_1 and k_2 values are compatible.
3. At higher pH's the predominant peak is A_{1a} and as the pH decreases only one uniform peak can be seen. The predominant peak is marked with "*".

k_1 / mA cm^{-2} mV^{-1} s

k_2 / mA cm^{-2} $mV^{-\frac{1}{2}}$ $s^{\frac{1}{2}}$

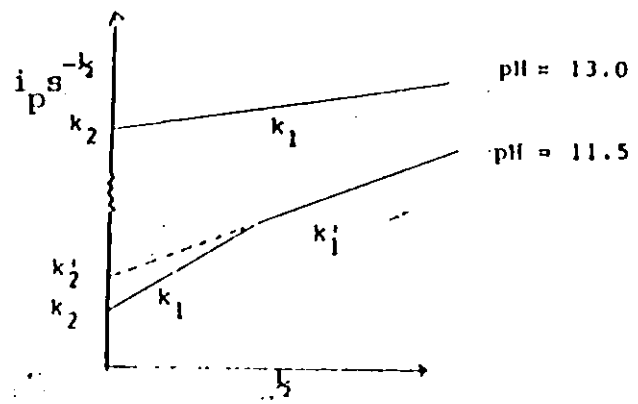

ends of incomplete rows, i.e. kink sites, have a much lower free energy of activation for dissolution and thus provide the actively dissolving sites at any instant. These kink positions are intermediate between a solution solvated ion and a lattice atom[151].

From the peak potentials listed in Table 3.11 it is clear that the first anodic peak (A_{1a}) corresponds to an oxidation reaction at a site where metal cations are more readily dissolved, e.g. at grain boundaries and irregularities, while the second anodic peak (A_{1b}) could correspond to less facile oxidation. It seems likely that the behaviour observed at Zn surfaces which have been etched in TFMSA and $HClO_4$ is due to small amount of active sites on the surface for dissolution or oxidation (see e.g. SEM photos in chapter 2, section 2.4) compared to the situation at Zn surfaces etched in concentrated HBr.

3.3.2.8.3. "Surface" and "Solution Transport" Currents

It is interesting to examine how the surface and solution processes contribute to the total anodic and cathodic currents and to enquire if there is any relation of these contributions to the shapes of the cathodic and anodic peaks.

Figs. 3.26a and 3.26b show the contributions of surface and solution currents to the total (surface and mass transfer components) anodic and cathodic currents, respectively, of peaks A_1 and C_1. These currents were back calculated using the k_1 and k_2 values obtained from the $i_p s^{-1/2}$ vs $s^{1/2}$ plots for the zinc surfaces etched in $HClO_4$ (Fig. 3.23a). It is surprising to find that the contribution from the process controlled by solution

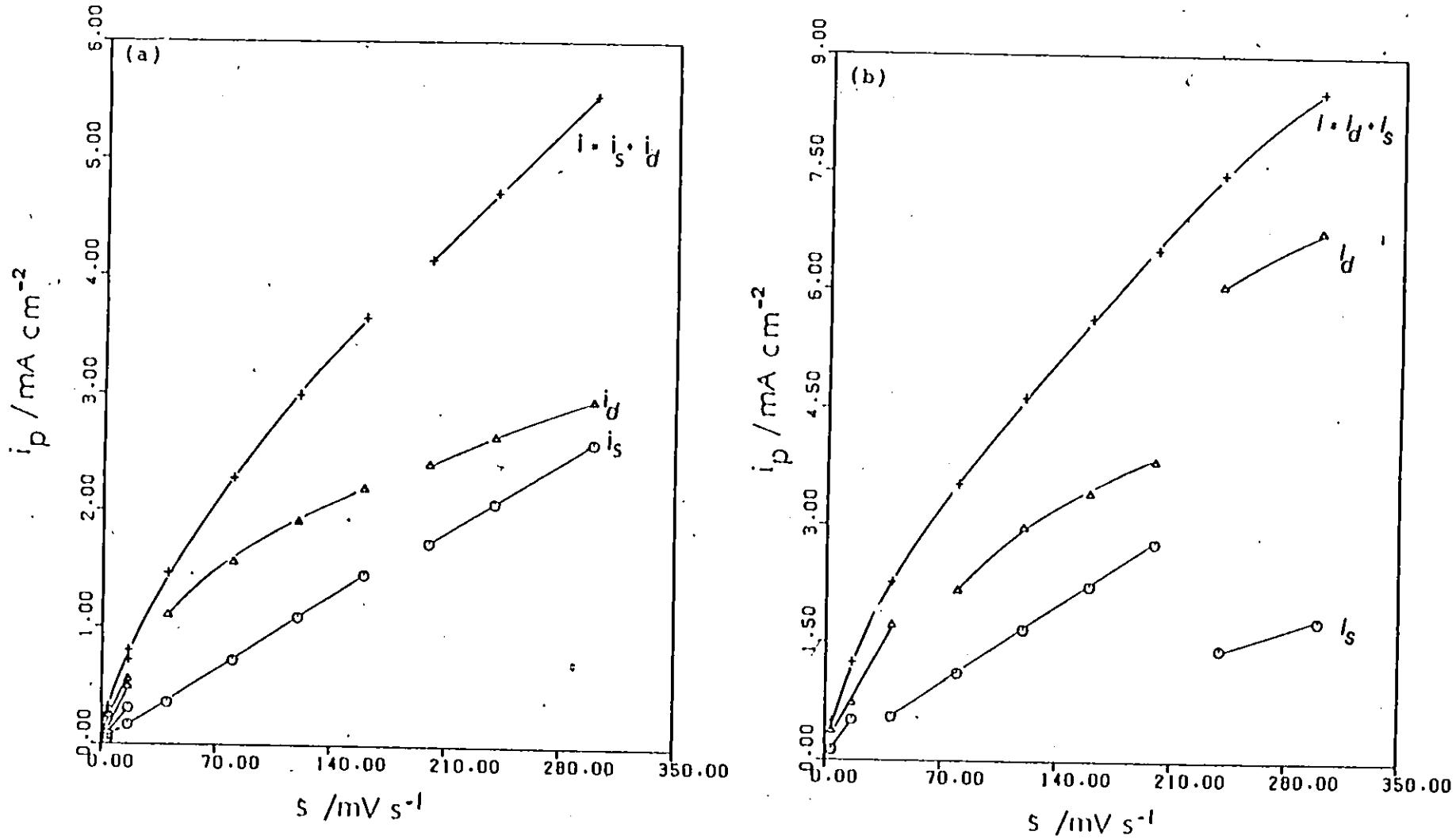

Fig. 3.26 Contribution of surface and solution currents to the total (a) anodic currents of peak A_1 and (b) cathodic currents of peak C_1. These currents were calculated from k_1 and k_2 values obtained from the experimental data of Figs. 3.23 a and 3.24 for Zn in 1M Na_2CO_3 at pH 11.5.

transport is higher than from the surface process, the two contributions being evaluated from the respective k_1 and k_2 values. One might have expected this result to be the other way around because, as seen in Fig. 3.22, the second anodic peak (A_{1b}) is predominant and q_a/q_c is almost unity (little transport of material into solution). Table 3.14 summarizes the q_a, q_c and q_a/q_c values from cyclic-voltammograms obtained for various preparations of the zinc surface.

Fig. 3.27a shows the contributions of surface and solution transport currents (derived from the k_1 and k_2 values evaluated for peak A_1) to the total anodic current for cast Zn electrodes etched in concentrated HBr. In this case, $I_{surface} > I_{solution}$, even though the q_a/q_c values are greater than one (Table 3.14). The k values obtained from the $i_p s^{-1/2}$ *vs* $s^{1/2}$ plot in this case do not depend very much on the sweep-rate range even though there is some discontinuty in this graph (Fig 3.27b).

In order to understand this unusual behaviour better it is desirable to use well-defined crystallographic planes. In the present work a Zn (0001) cleaved surface was studied. The results obtained in these experiments will be discussed in the next section.

(C) Behaviour of the Zn(0001) Single-Crystal Face

The Zn (0001) single-crystal electrode was prepared as described in section (2.4.3.2). Fig 3.28 shows the CV's obtained in 1M Na_2SO_4 solutions at pH 11.5. It is clear from these CV's that there are quite substantial differences between the

Table 3.14

Charges per cm^2 for Peaks A_1 and C_1 for Various Zn Electrodes in 1M Na_2CO_3 Solution at pH 11.5

Electrode preparation		Sweep-rate (s) / $mV\ s^{-1}$			
		6	20	100	300
Unetched	$q_a/\mu C\ cm^{-2}$	1678	1112	768	646
	$q_c/\mu C\ cm^{-2}$	839	746	589	509
	q_a/q_c	2.0	1.5	1.3	1.3
Etched in TFMSA	$q_a/\mu C\ cm^{-2}$	2357	1636	1028	863
	$q_c/\mu C\ cm^{-2}$	1372	1282	834	702
	q_a/q_c	1.7	1.3	1.2	1.3
Etched in $HClO_4$	$q_a/\mu C\ cm^{-2}$	3610	2592	1513	1127
	$q_c/\mu C\ cm^{-2}$	1782	1687	1602	853
	q_a/q_c	2.0	1.5	0.94	1.3
Etched in HBr; Cast Electrode	$q_a/\mu C\ cm^{-2}$	2370	1414	938	853
	$q_c/\mu C\ cm^{-2}$	556	617	599	603
	q_a/q_c	4.3	2.3	1.6	1.4
Etched in HBr	$q_a/\mu C\ cm^{-2}$	2100	1130	626	504
	$q_c/\mu C\ cm^{-2}$	725	457	532	556
	q_a/q_c	2.9	2.5	1.2	0.9

Notes:

1. All measurements were carried out in 1M Na_2CO_3 solution at pH 11.5 under identical conditions.
2. q_a/q_c values are higher for zinc electrodes etched in HBr 48% than in other acids.

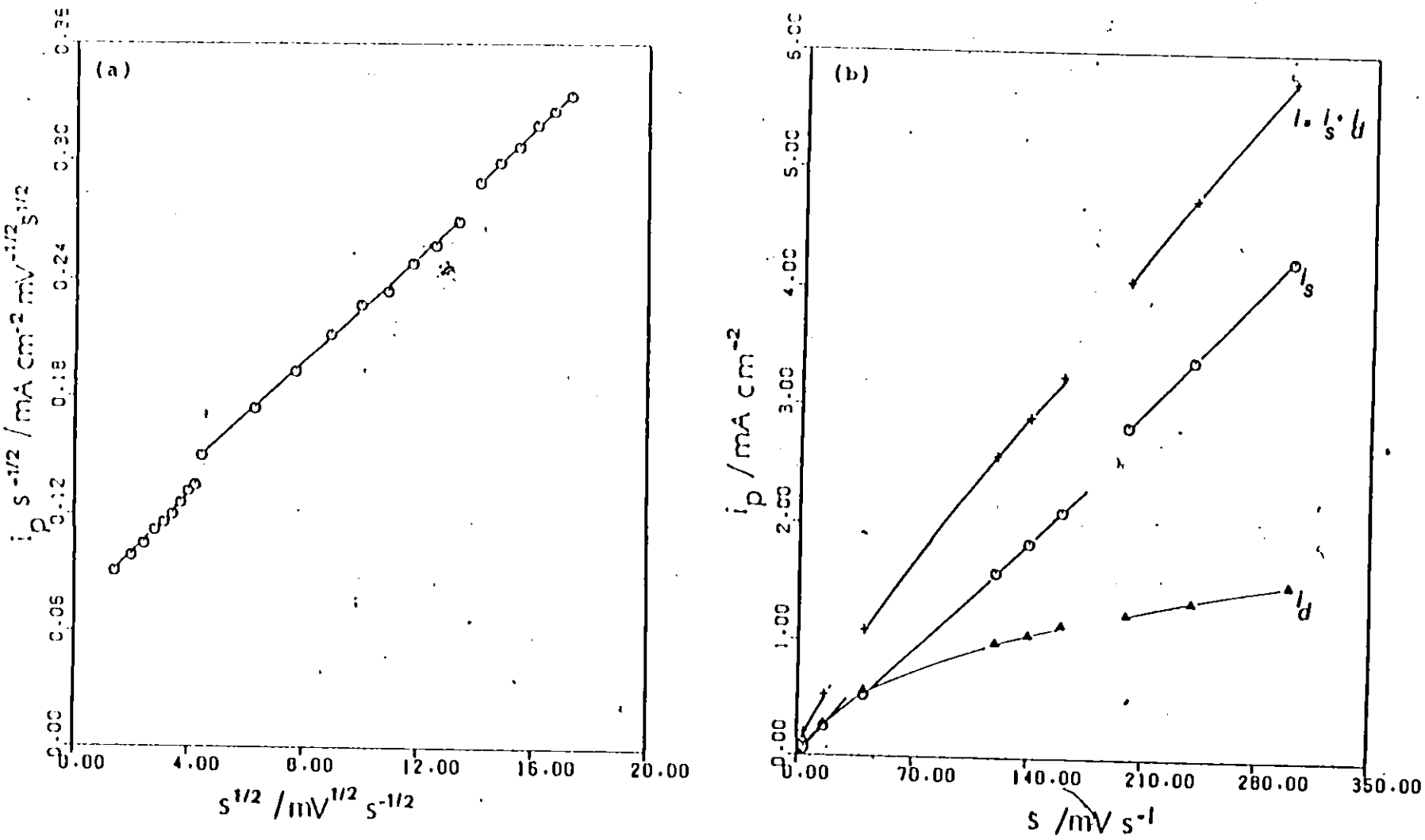

Fig. 3.27 (a) Dependence of $i_p s^{-\frac{1}{2}}$ for peak A_1 on $s^{\frac{1}{2}}$ (b) contribution of surface and solution currents to the total current calculated from k_1 and k_2 values obtained from Fig. 3.27 a in 1M Na_2CO_3 at pH 11.5 for cast Zn electrode etched in HBr.

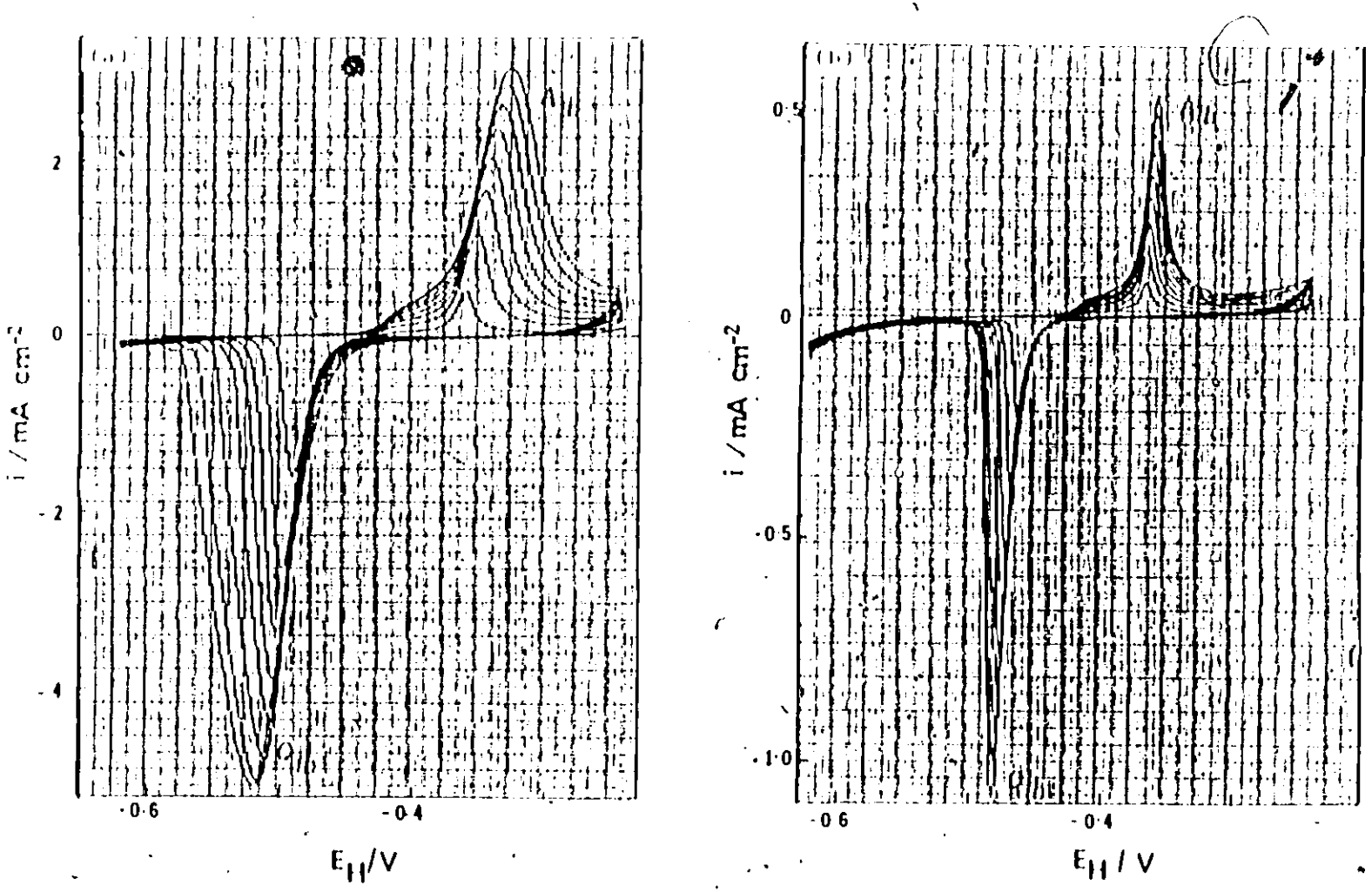

Fig. 3.28 Typical cyclic-voltammetry i vs E profiles for a freshly cleaved Zn (0001) face (no etching treatment) in 1M Na_2SO_4 solution at pH 11.5 with variable sweep-rates.

(a) s - 180 ——→ 20 mV s^{-1}

(b) s - 18 ——→ 2 mV s^{-1}

Electrode - (0001) face of area 1.13 cm^2.

behaviour of the polycrystalline (see Fig. 3.3) and this single-crystal Zn electrode. The CV does not consist of the usually observed (see e.g. Fig. 3.22) first anodic peak (A_{1a}), except as a minor shoulder. The peak potentials for the anodic A_1 peak and the cathodic C_1 peak for a sweep-rate of 20 mV s^{-1} arise at ca. -0.354 V and -0.485 V, respectively. This clearly shows that the second anodic peak, A_{1b}, observed at etched polycrystalline electrodes (Fig. 3.22) corresponds to the oxidation of less active sites.

Table 3.15 gives the q_a, q_b and q_a/q_b values for various sweep-rates. It would appear that these data correspond completely to a surface process because q_a/q_c values are close to 1, but (see below) contrary conclusions follow from the dependence of i_p on s. Fig. 3.29 shows a CV obtained with a Zn (0001) surface etched in concentrated HBr. It can be seen from this figure that etching in acid must have exposed other crystal planes. The anodic and cathodic peaks obtained with a Zn (0001) surface are substantially narrower than for either a reversible or an irreversible 2-d surface process, but evidently the process is not simply a 2-d one. Thus Figs. 3.30a and 3.30b show the log i_p *vs* log s and $i_p s^{-1/2}$ *vs* $s^{1/2}$ plots for the Zn (0001) surface and they indicate that only at very low sweep-rates does the log i_p *vs* log s plot have a slope of 1 with $i_p s^{-1/2}$ being linear $s^{1/2}$ (surface process behaviour) with the line passing through the origin (Fig. 3.30a); however, as the sweep-rate is increased, the slopes are changed in both plots and, at higher sweep-rate, i_p becomes linear in $s^{1/2}$ (diffusion behaviour).

It seems likely that this is the reason for the unusual

Table 3.15

Charges per cm^2 for Peaks A_1 and C_1 for Zn (0001) Face Electrode in 1M Na_2SO_4 Solution at pH 11.5

s/ mV s^{-1}	q_a/ $\mu C\ cm^{-2}$	q_c/ $\mu C\ cm^{-2}$	q_a/q_c	No. of layers
300	532	579	1.1	2
200	569	520	1.1	2
100	695	593	1.3	2
60	632	632	1.0	2
20	867	790	1.1	3
6	987	987	1.0	3

Notes

1. Roughness factor assumed to be 1 for charge density calculations.
2. All charges are calculated relative to the zero current base-line.
3. q_a/q_c close to unity for Zn (0001) face in the sweep-rate range studied. (s = 6 mV s^{-1} - 300 mV s^{-1}).

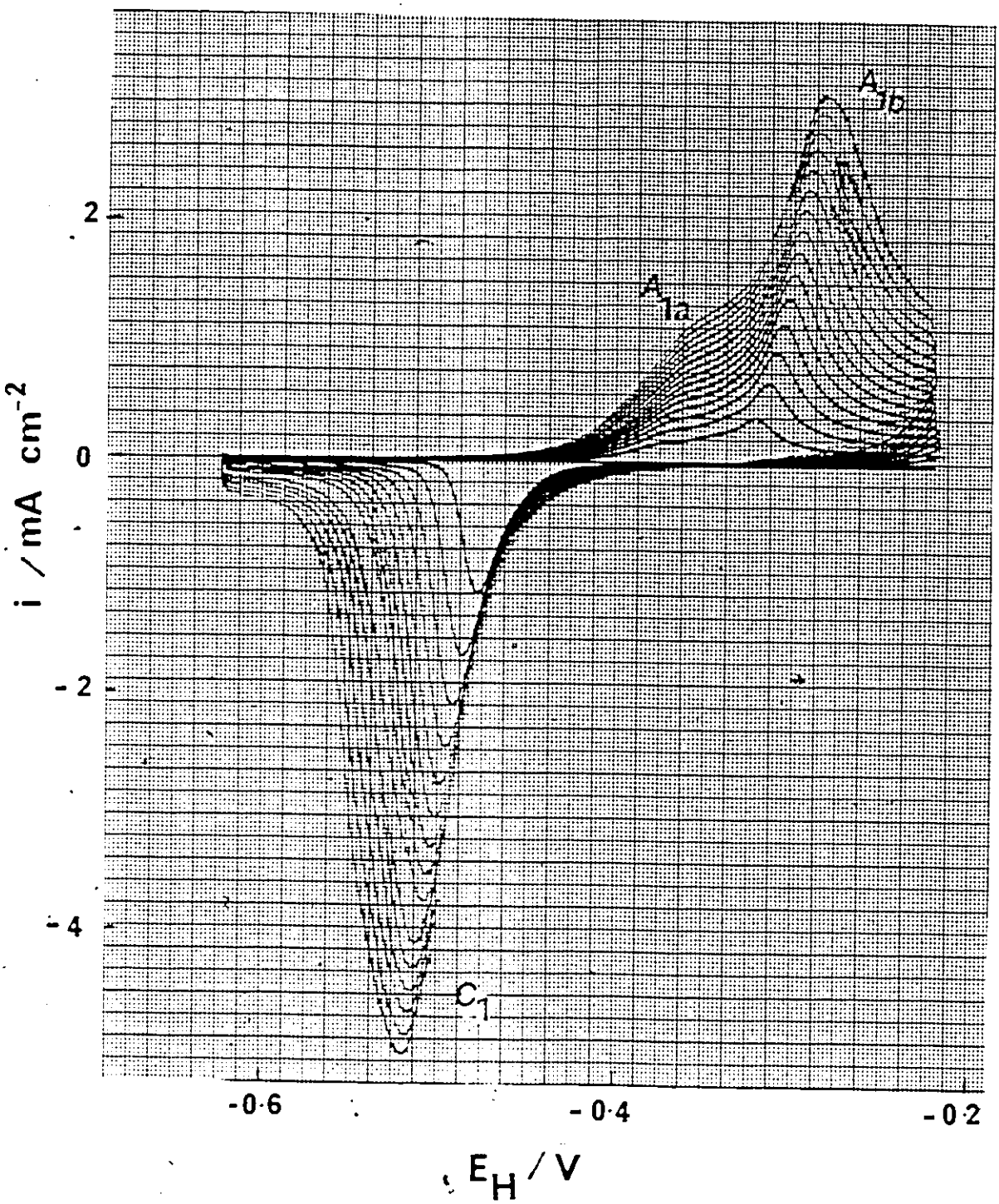

Fig. 3.29 Cyclic-voltammetry i vs E profiles at various sweep-rates from 1M Na_2SO_4 solution at pH 11.5 for an initially cleaved Sn electrode face but etched in HBr.

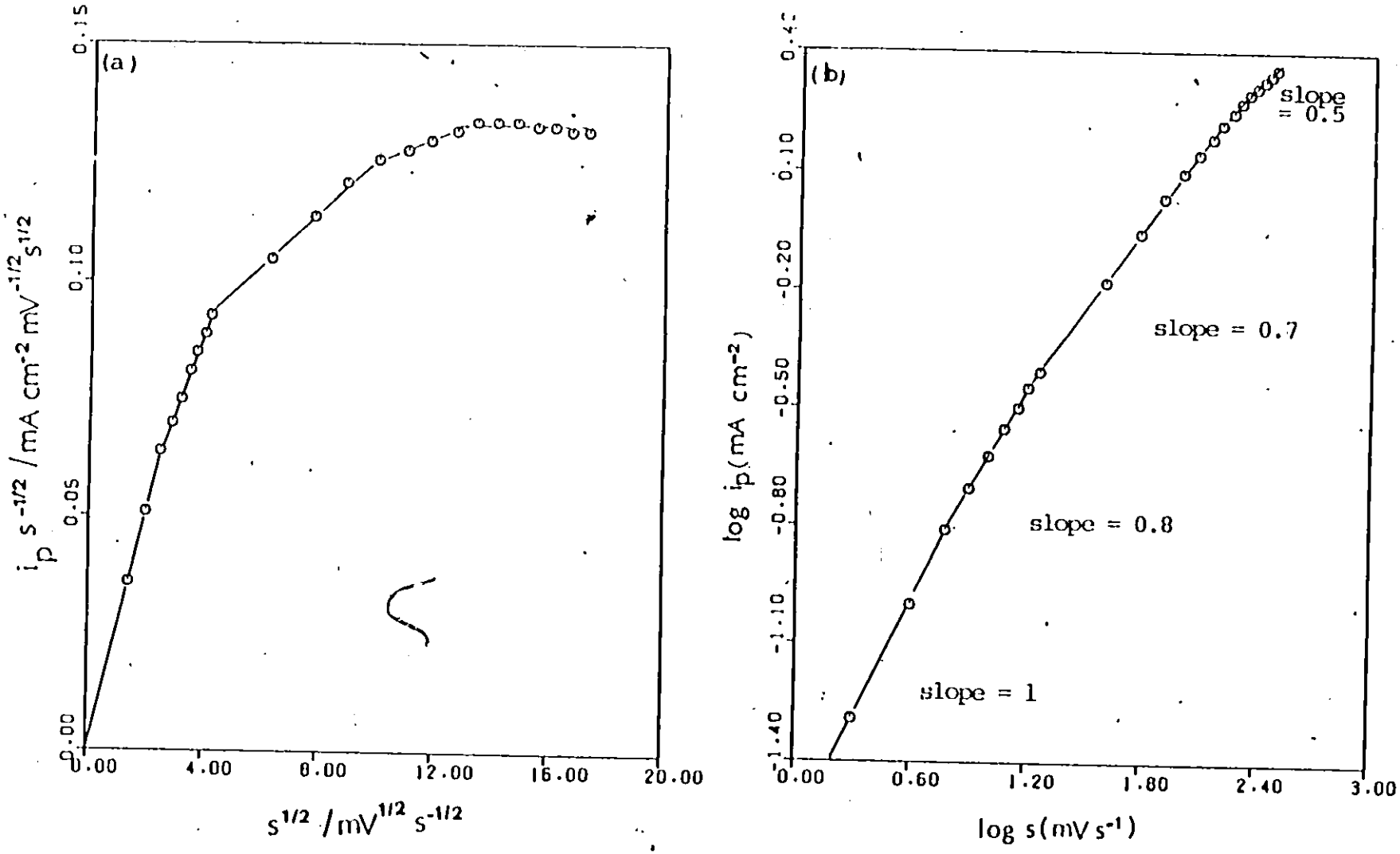

Fig. 3.30 Dependence of (a) $i_p s^{-½}$ on $s^{½}$ and (b) log i_p on log s for peak A_1 in Fig. 3.28 (freshly cleaved (0001) face).

behaviour of polycrystalline electrodes etched in $HClO_4$ and TFMSA, where the current contribution from the solution process is greater than that for the surface one, even though $q_a/q_b = 1$ at the higher sweep-rates.

This behaviour can be explained further since surfaces etched in TFMSA or $HClO_4$ appear to have less active sites (SEM Fig. 3.21) compared to a surface etched in concentrated HBr or HCl. Therefore, a significant fraction of the total peak current could be due to a surface process, so that the k_2 value increases with sweep-rate in several ranges as for the case of the (0001) face. In the case of zinc etched in concentrated HBr or HCl, as mentioned earlier, the surface consists of many active sites, e.g. grain boundaries, and then the current arising in the second anodic peak (A_{1b}) may be quite small. Therefore the $i_p s^{-1/2}$ vs $s^{1/2}$ plots do not exhibit much discontinuity, as found with other etched surfaces.

In 1 M Na_2CO_3 at pH 11.5 for polycrystalline electrodes etched in HBr, for sufficiently high rotation rates (>500 rpm), the $i_p s^{-1/2}$ vs $s^{1/2}$ plots show one straight line, rather than two distinct lines and it can be seen from q_a/q_c values that reaction associated with the A_1 peak involves to a greater extent, a solution process than does that for 1M Na_2SO_4 solution.

The charge measurements from k_1 values obtained from $i_p s^{-1/2}$ vs $s^{1/2}$ plots from 1M Na_2SO_4 at pH 11.5 for polycrystalline electrode etched in HBr showed that the thickness of the film corresponds closely to a monolayer at lower sweep-rate, ca. 20 mV s^{-1}. Comparing this behaviour with the results obtained from Zn

(0001) face in 1M Na_2SO_4 solutions at pH 11.5 it can be concluded that polycrystalline electrode in 1M Na_2SO_4 solution at pH 11.5 is completely covered by a monolayer of compact film even at higher sweep-rates and the unusual sweep-rate dependence on i_p of the A_{1b} process gives rise to the two regions in the $i_p s^{-1/2}$ vs $s^{1/2}$ plots for polycrystalline Zn electrode etched in HBr and the several regions for electrodes etched in other acids.

3.3.3 Further Studies on the Processes Associated with Peak C_1

From Fig. 3.25 it is clear that the cathodic region designated as C_1 consists of two resolvable peaks. We have seen that one peak does not depend on rotation-rate while the other does. If the peak which is independent of rotation-rate is due to a surface process, as indicated, then this peak current should be linear in sweep-rate. However, it is not very easy to evaluate the effect of sweep-rate on peak-current for a small peak. This difficulty was obviated by extending the potential range of the sweep to more positive values so that the cathodic peak became larger, as in Fig. 3.31. Figs. 3.31a and 3.31b show the CV's obtained over the potential range -0.727 V to +0.148 V at sweep-rates of 20 mV s^{-1} and 100 mV s^{-1} at various rotation rates.

It is seen from these CV's that the current of the cathodic peak C_1 depends on rotation rate, more at higher sweep-rates than at lower, but it becomes independent of rotation rate above 2500 rpm. If the peak current in C_1 (>2500 rpm) is completely due to the surface process then it should vary linearly with sweep-rate. Fig. 3.32a shows the CV obtained in an experiment designed to

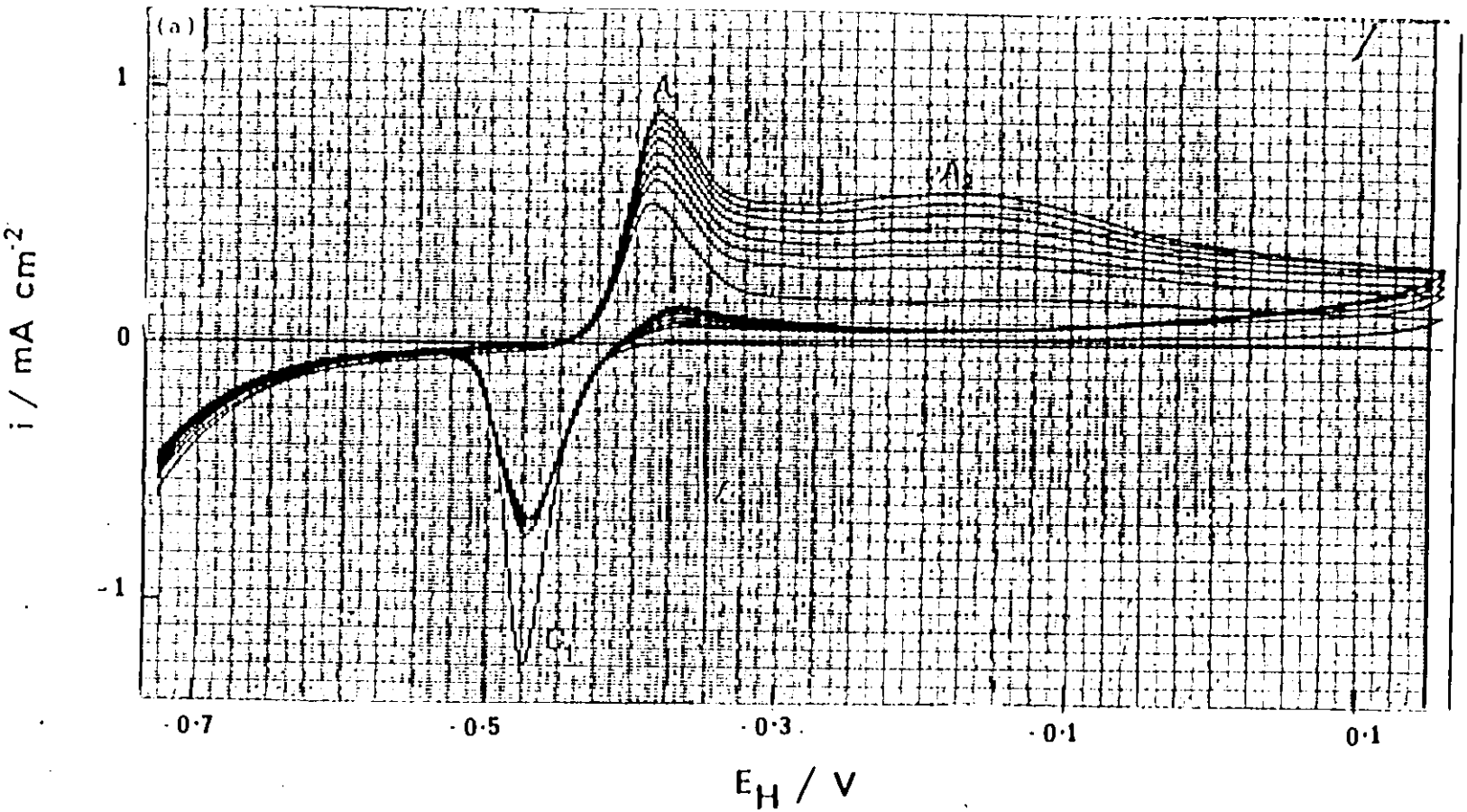

Fig. 3.31 The effect of rotation on I vs E profiles for polycrystalline Zn RDE in 1.0M Na_2CO_3 solution at pH 11.5, at sweep-rates of (a) 20 mV s^{-1} (b) 100 mV s^{-1}.

0, 400, 625, 900, 1225, 1600 and 2025 rpm for both (a) and (b) electrode RDE, of apparent area 0.073 cm^2 and etched in HBr. (See

following sheet.)

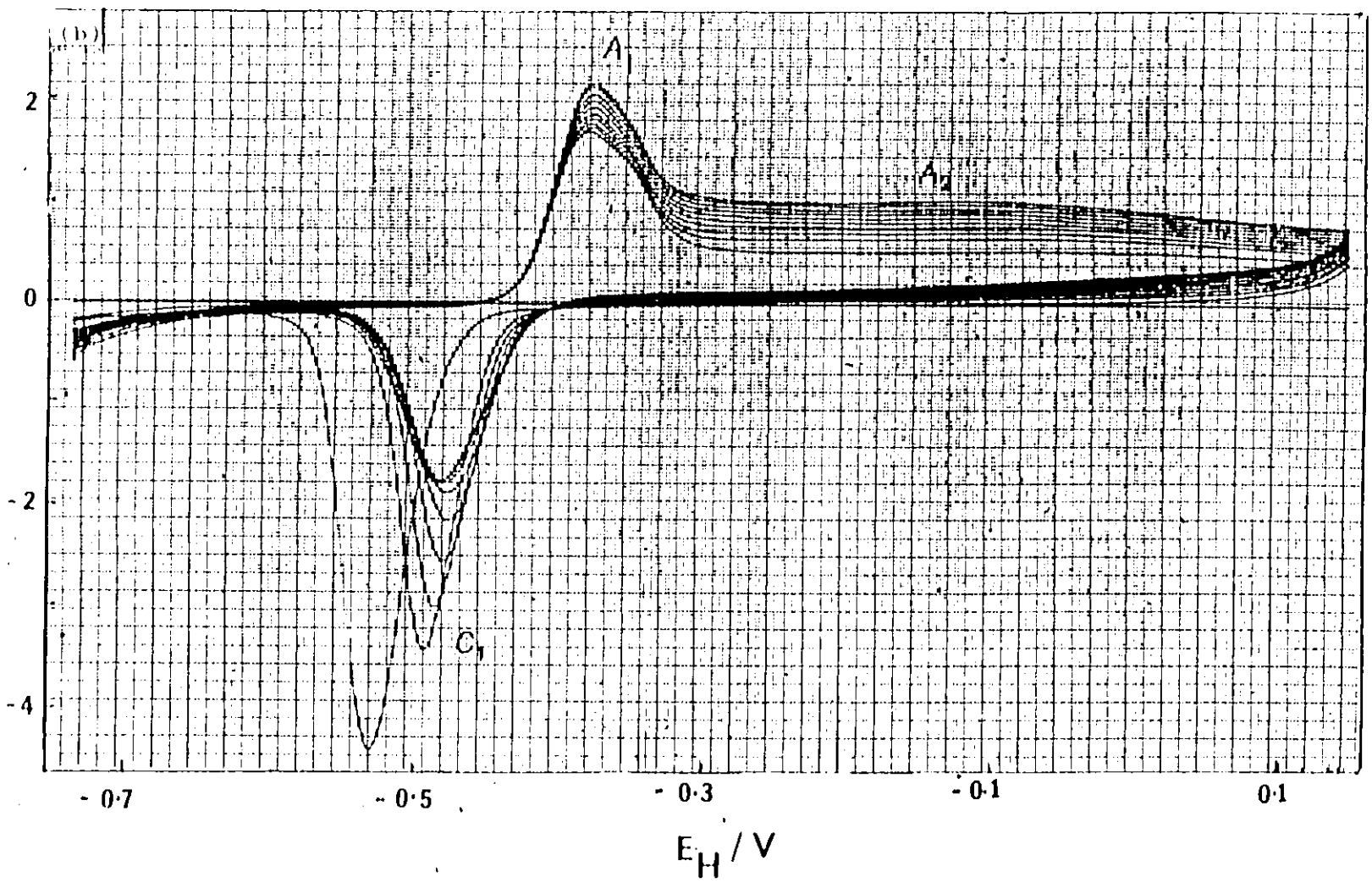

Fig. 3.31 (b)

study the effect of sweep-rate on the C_1 peak current keeping the anodic sweep-rate constant at 40 mV s^{-1} and changing the reverse sweep-rate from 40 mV s^{-1} to 4 mV s^{-1}. In this experiment, the electrode was rotated at a constant rate of 2500 rpm, the rate beyond which i_p, for C_1 ceases to decrease any more with rotation. As can be seen from Fig. 3.32b, the dependence of i_p for C_1 on s now clearly linear, i.e. the reduction peak C_1 appears to correspond completely to a surface process. The slope of the i_p vs s relation for C_1 is 2.4×10^{-2} mA s mV^{-1} cm^{-2}. The thickness of the bound zinc oxide/hydroxide film thus corresponds to 2-3 layers . This means that only 2-3 layers of $ZnO/Zn(OH)_2$ (constant amount) are detectable on reduction of the electrode surface film, so that most of the charge that was passed in the anodic sweep (equivalent to 8 or 9 monolayers of ZnO) is not recovered in the cathodic sweep in peak C_1 because most of the products of the oxidation in the anodic sweep (ZnO or dissolved ZnO_2^{2-}) are evidently dissolved and/or transported away into the solution due to rotation of the electrode before reduction can occur, leaving a residual oxide species bound to the surface. At small cathodic sweep-rates it is seen from Figs. 3.32a and 3.33 that an anodic current region designated as AC_1 arises on the cathodic sweep. This may be due to re-established oxidation of Zn after dissolution of some of the previously deposited oxide has taken place during the time of the cathodic sweep up to the AC_1 potential region (hence the effect increases with decreasing s).

In contrast to the rotation effect in Fig. 3.31a, it is seen

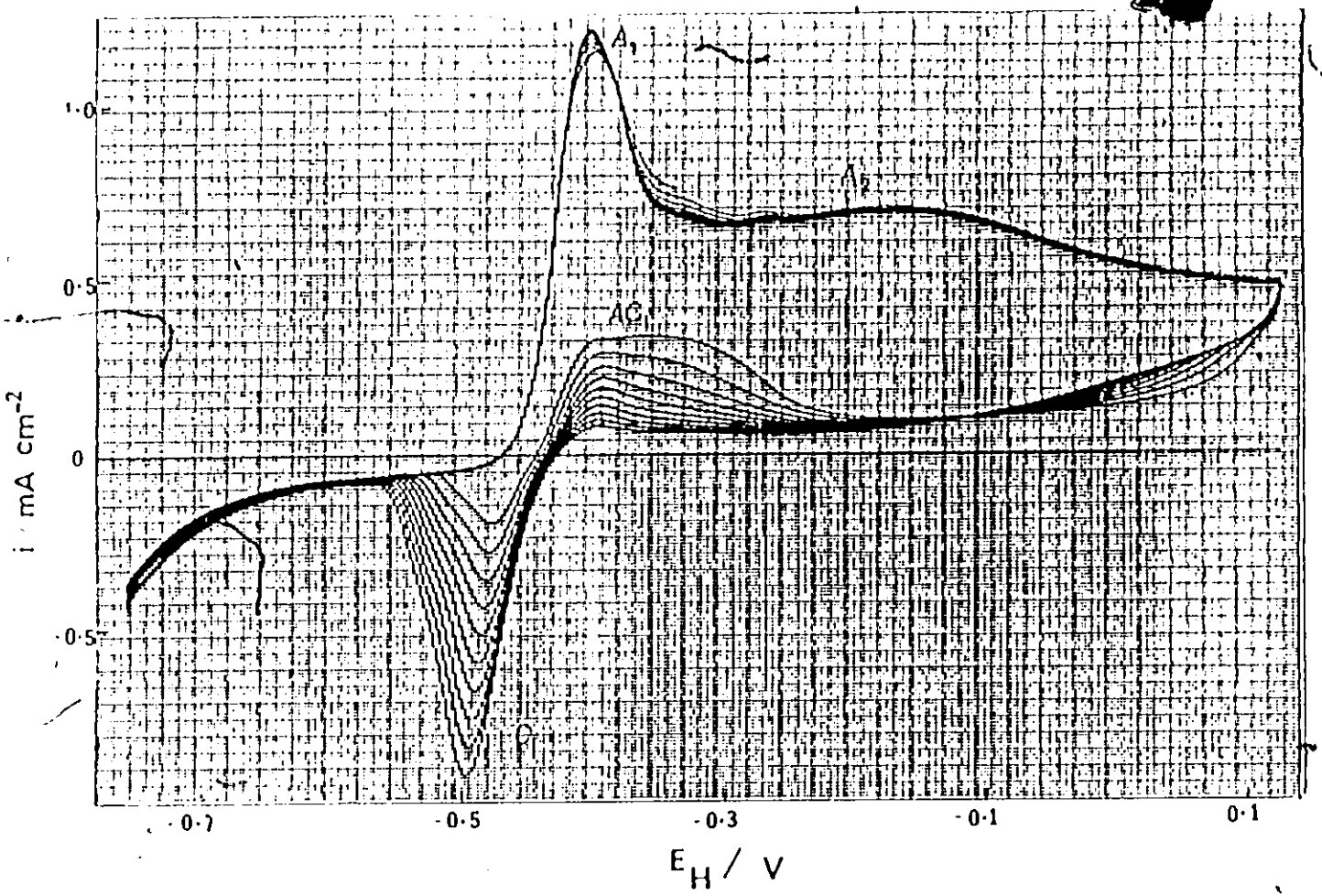

Fig. 3.32 (a) Series of cathodic CV profiles at various sweep-rates (for constant anodic sweep rates of 40 mV s^{-1}) showing variations of C_1 peak current at a rotation rate ω beyond which i_p at C_1 is independent of further increase of ω and plots of these i_p's are then linear in $\omega^{\frac{1}{2}}$ as shown in (b).

Solution: 1M Na_2SO_4 at pH 11.5 ; ω = 2500 rpm

s_{anodic} = 40 mV s^{-1} ; $s_{cathodic}$ = 40 mV s^{-1} to 4 mV s^{-1}

Electrode: RDE of apparent area 0.07 cm^2 and polished to 0.3

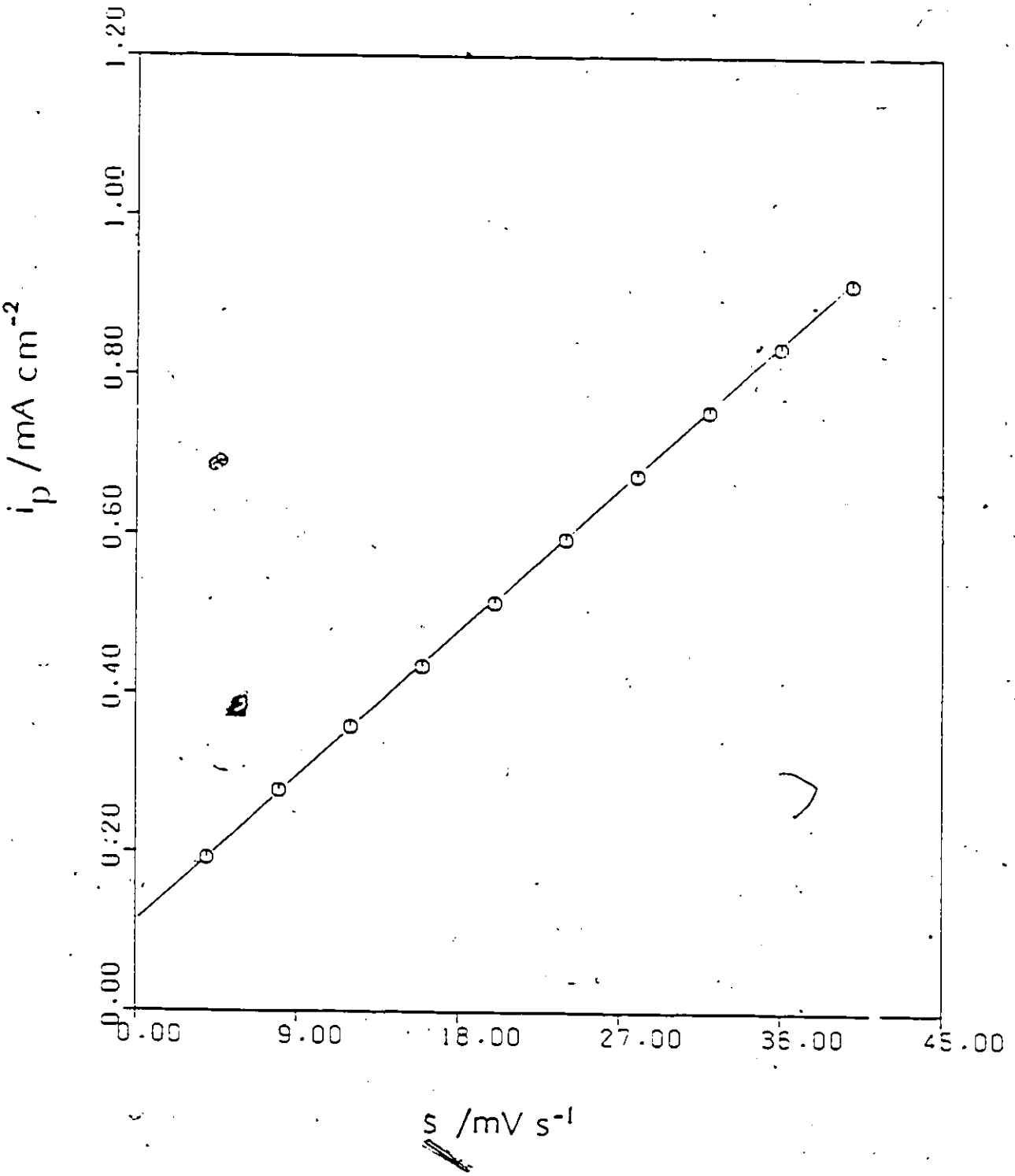
1.20
1.00
0.80
0.60
0.40
0.20
0.00
i_p /mA cm^{-2}
0.00
9.00
18.00
27.00
36.00
45.00
S /mV s^{-1}

Fig. 3.32 (b)

from Fig. 3.31b that at higher sweep-rates (100 mV s^{-1}) the current of peak C_1 depends much more on rotation-rate. Fig. 3.33 shows the series of CV's obtained when the cathodic sweep-rate is varied from 100 mV s^{-1} to 10 mV s^{-1}, keeping the anodic sweep-rate at 100 mV s^{-1} and maintaining the rotation rate at the limit beyond which there is little further dependence of i_p (C_1) on (i.e. similar conditions to those for Fig. 3.32a discussed above). Figs. 3.34a and 3.34b show the dependence of the currents of peak C_1 from Fig. 3.33 on s, $s^{1/2}$ and also the variation of $i_p s^{-1/2}$ with $s^{1/2}$: it is seen that $i_p s^{-1/2}$ is linear in $s^{1/2}$ (mixed process indicated). From the k_1 value, the thickness of the oxidized Zn film that is reduced is found to be only one monolayer. In this case there is no discontinuity in the $i_p s^{-1/2}$ vs $s^{1/2}$ plot (Fig. 3.34b) for peak C_1.

3.3.4 Behaviour of the Process Associated with Peak A_2

It can be seen from Fig. 3.35 that the effects of rotation on the current of peak A_1 and the broad region A_2 are the same, The slopes of $di_p/d\omega^{1/2} = 11.46$ $\mu A\ cm^{-2} rpm^{-\frac{1}{2}}$ (Fig. 3.31a). This means that diffusion of the same species controls the rate of the reaction at the peak A_1 and over the region A_2.

The broad peaked region A_2 (Fig. 3.31a) was observed only in the CO_3^{2-} solution. This situation, together with the wide range of potential over which the A_2 currents are rotation-dependent (beyond the A_1 peak), suggests that a residual current, dependent on mass-transfer of CO_3^{2-} ion, is passing through the film formed in A_1. Thus, in the carbonate solution, it seems that the

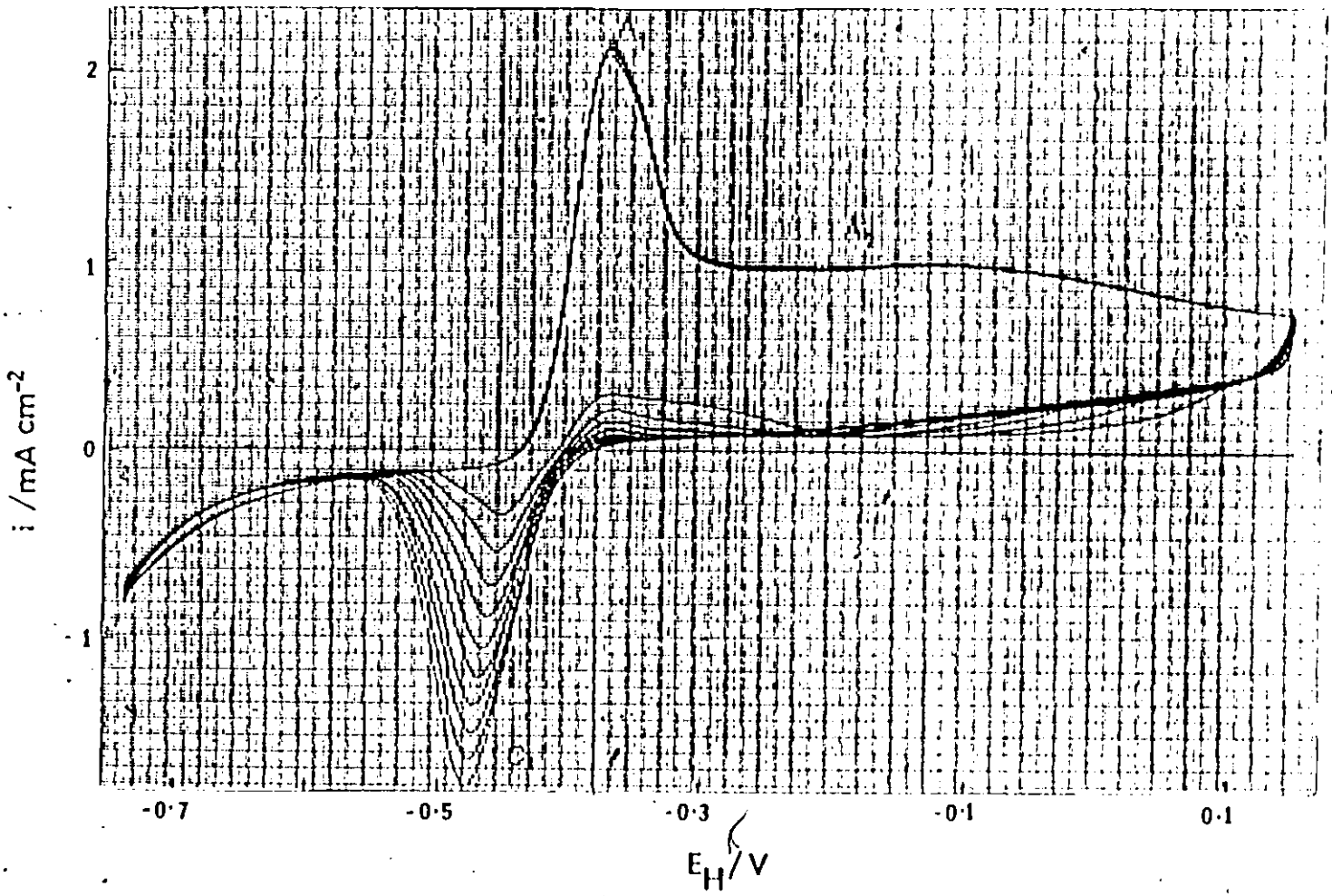

Fig. 3.33 Series of cathodic CV profiles at various sweep-rates (for constant anodic sweep-rate of 100 mV s^{-1}) showing variation of C_1 peak current at rotation rate 3600 rpm from 1M Na_2CO_3 solution at pH 11.5.

$s_{cathodic}$ - Sweep-rate varied from 100 mV s^{-1} to 10 mV s^{-1} with 10 mV s^{-1} sweep-rate decrease.

s_{anodic} - 100 mV s^{-1}.

Electrode - RDE, of apparent area of 0.07 cm^2 and etched in HBr.

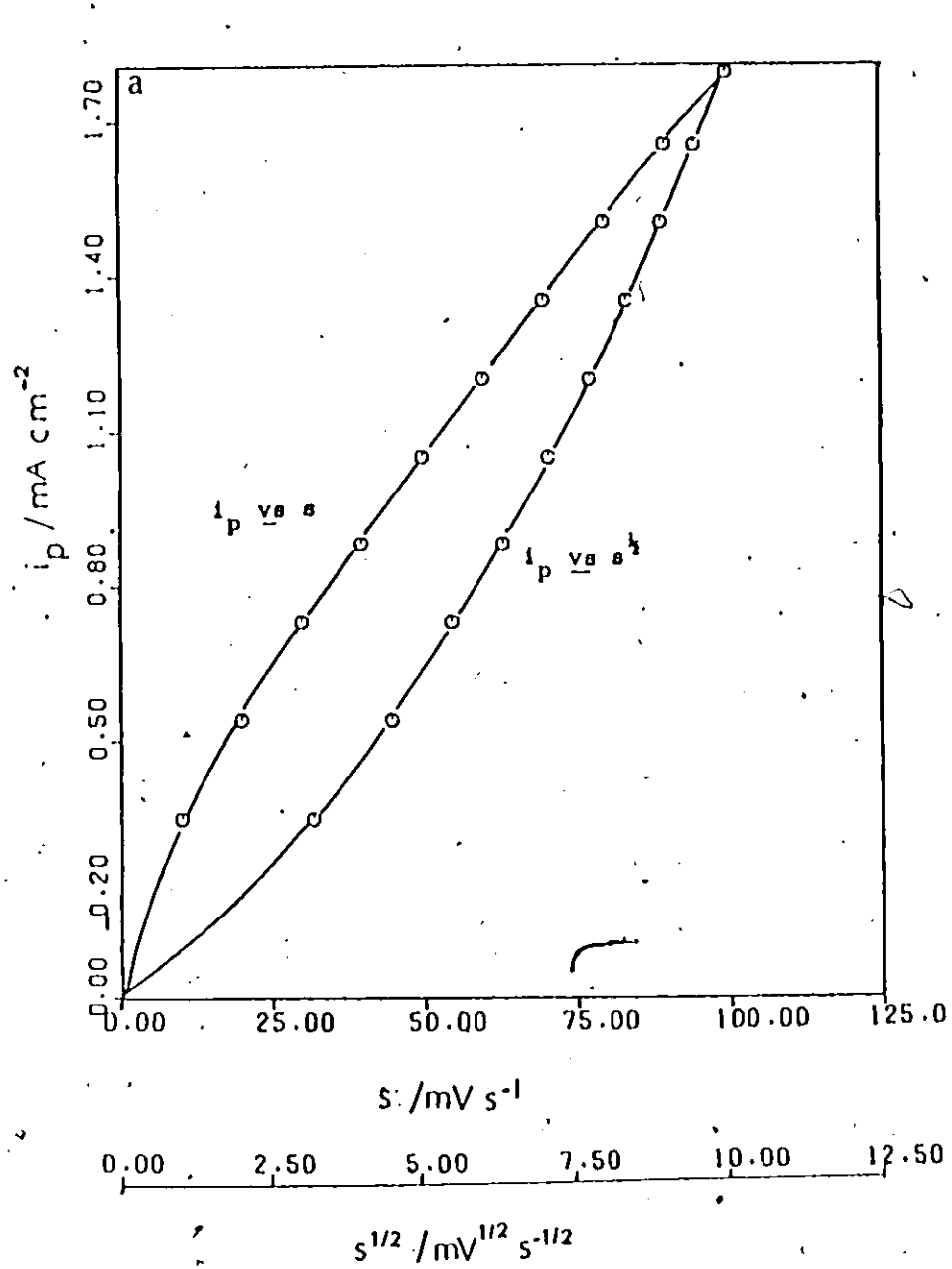

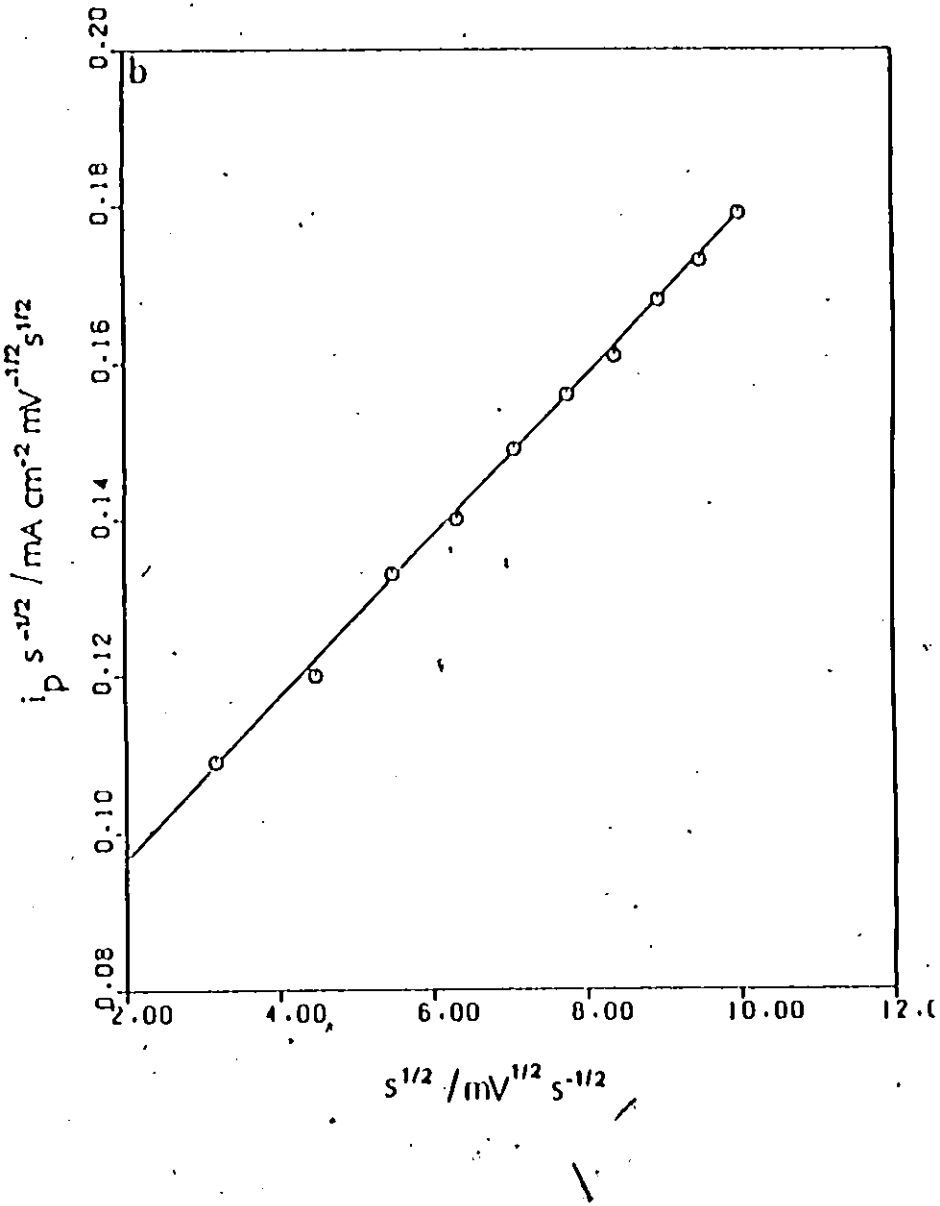

Fig. 3.34 Dependence of (a) i_p on s and $s^{\frac{1}{2}}$, and (b) $i_p s^{-\frac{1}{2}}$ on $s^{\frac{1}{2}}$ for C_1 peak in Fig. 3.33.

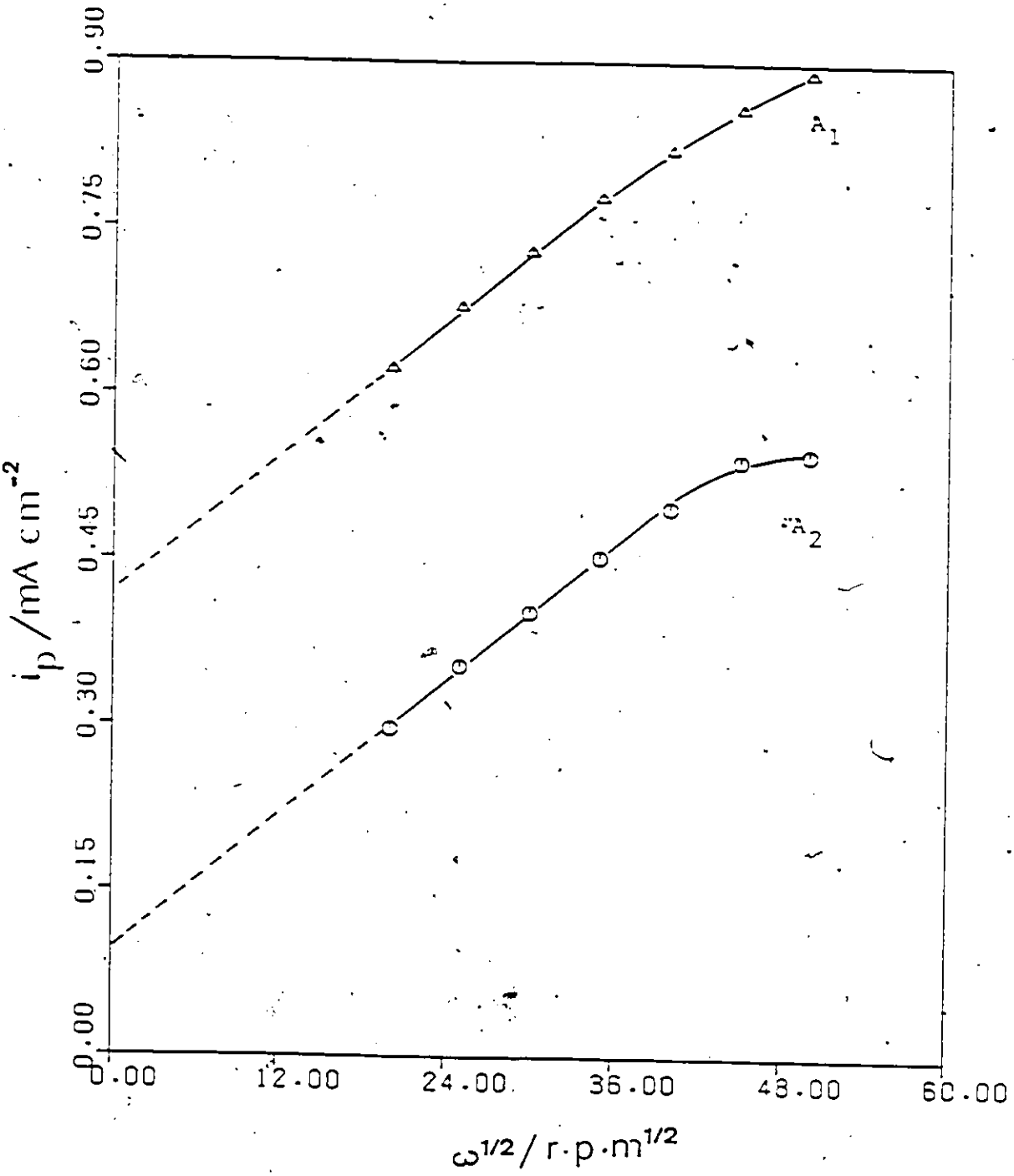

Fig. 3.35 Dependence of i_p on $\omega^{\frac{1}{2}}$ for peaks A_1 and A_2 in Fig. 3.31 a.

anodic film is less coherent and more porous than the films formed in the SO_4^{2-} or Cl^- solutions at same pH's. In fact CO_3^{2-} seems to help $ZnO/Zn(OH)_2$ to remain in a dissolved or colloidal state, unlike the behaviour in SO_4^{2-} or Cl^- solutions. This will be shown in the next section.

3.3.5 The Effect of Carbonate and Bicarbonate Ions

In this section are presented the results obtained in bicarbonate and carbonate solutions, and the behaviour observed is compared with that in sulphate and chloride solutions at the same pH.

It was clear already from Fig. 3.1 (Page 62) that the behaviour of Zn in Na_2CO_3 is different from that in 3M NaCl solutions at the same pH, viz. around 11.5 . On the other hand, the CV's obtained in 1M Na_2SO_4 at the same pH were similar to those for Zn in 3 M NaCl; thus Cl^- or SO_4^{2-} have no specific effects.

3.3.5 Current Peaks C_2, C_3 and C_4

In SO_4^{2-} and Cl^- solutions, a rapid rise in current occurs after peak A_1 and a corresponding cathodic peak (C_3) is seen just after reversing the direction of potential change after the sudden rise in current, whereas in 1M Na_2CO_3 the sudden rise in current occurs when the discharge voltage of oxygen is reached, i.e. for trivial reasons.

It was considered important to establish whether solution-soluble species are involved in the process occurring in peak C_3: Fig. 3.36a shows the behaviour of the currents at peak C_3 with

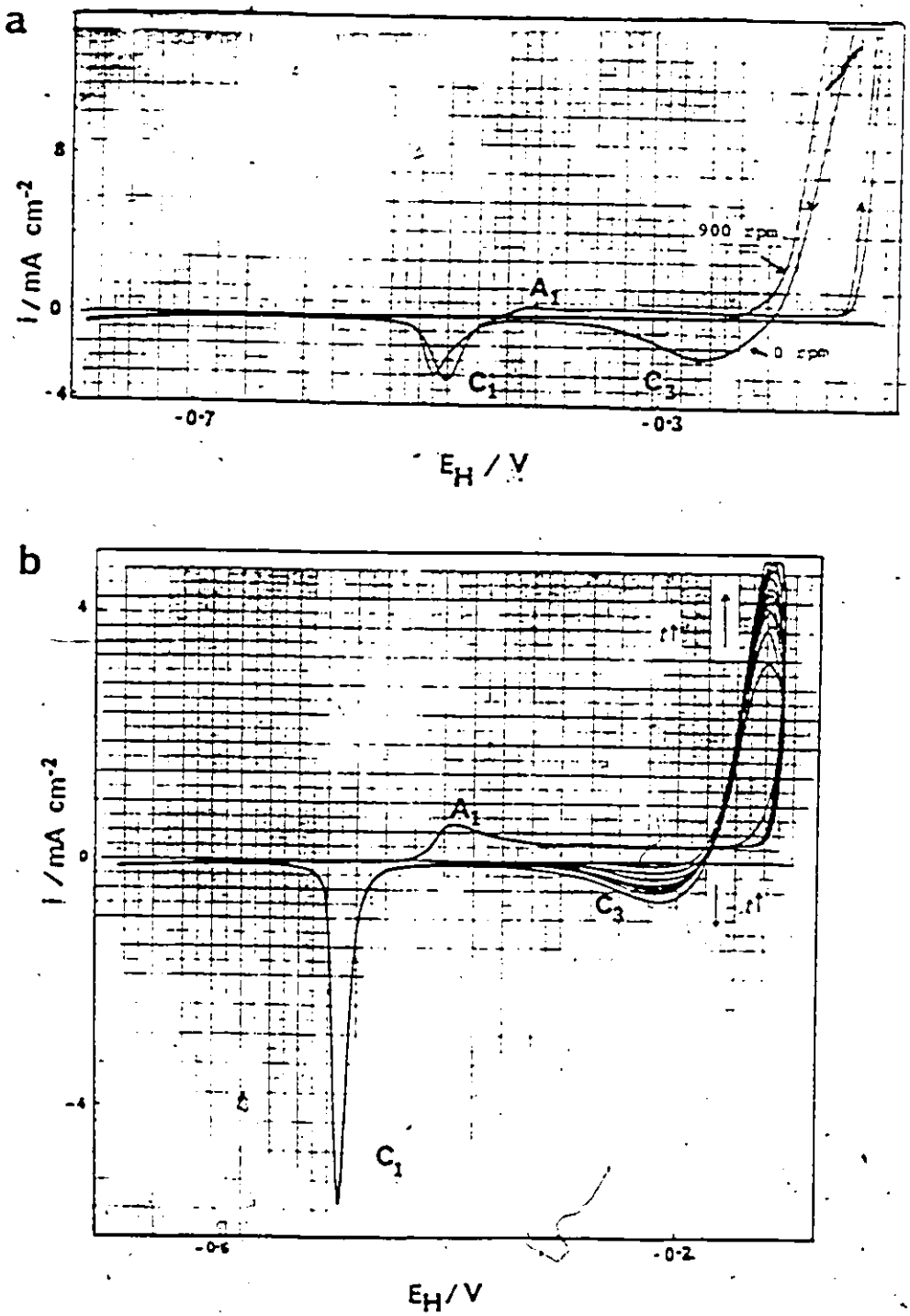

Fig. 3.36 (a) The effect of rotation on C_3 peak and (b) the change in C_3 peak with cycling for polycrystalline Zn RDE of apparent area 0.07 cm^2 in 3M NaCl solution at pH 11.5.

(a) s = 50 $mV\,s^{-1}$, ω = 0 and 900 rpm

(b) s = 50 $mV\,s^{-1}$, ω = 0 rpm.

and without rotation. It is seen that there is a significant effect of rotation on the peak C_3 and also that this peak gets larger with cycling (Fig. 3.36b) while peak A_1 remains unchanged with cycling.

The potential for film breakdown (indicated by the sudden increase of current on the anodic sweep and continuing substantial current on the reverse sweep) mainly depends on the mode of preparation of the electrode and it is almost constant for a particular electrode. Similar breakdown of the passive film occurs even at higher pH's. Fig. 3.37a shows such behaviour of the Zn electrode in 1M NaCl at pH 12.7. Dendrites or loosely adherent products were seen on the Zn electrode surface and also, simultaneously, darkening of colour of the coating can be observed after breakdown (see condition defined above) of the passive film. Fig. 3.37b shows a SEM picture of such a state.

The behaviour is clarified by the work of Huber et al. [9], where X-ray and electron-diffraction investigations showed that γ-$Zn(OH)_2$ and a small amount of a colourless oxide is formed on the surface of an active anode but ZnO is responsible for the passivation of the Zn electrode: the oxide formed on Zn in Na_2CO_3 solution is light in colour and scarcely conducts a current, whereas, in NaOH, the oxide formed is dark due to the presence of an excess of Zn. These workers attempted to measure the coating resistance; such measurements are, however, difficult to carry out since slight traces of moisture increase the conductance of the coating. In spite of this uncertainty, it was found that the resistance of the lighter coloured ZnO is several powers of ten greater than that of the dark one. This means that the behaviour

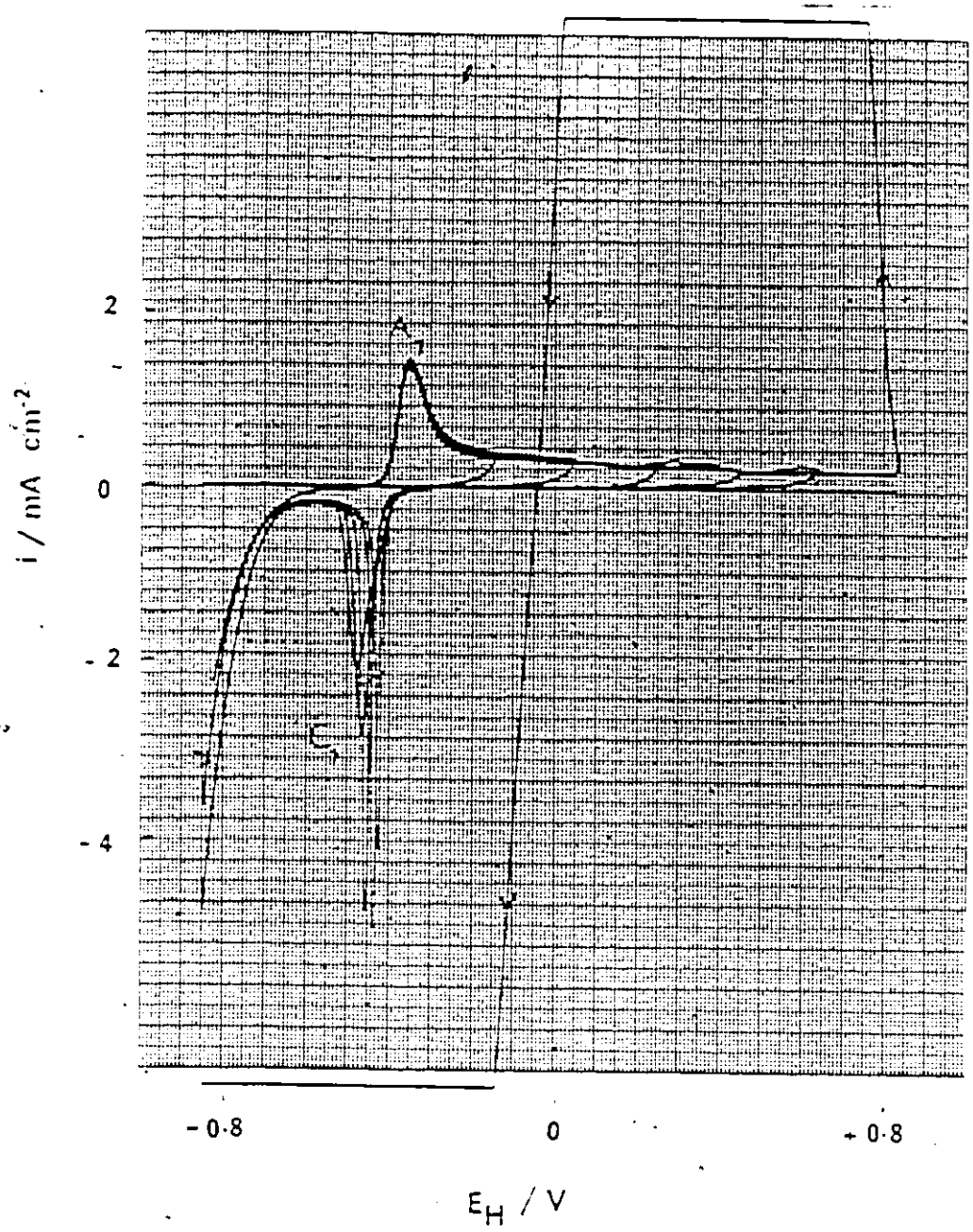

Fig. 3.2 a) Cyclic-voltammetry i vs E profiles for poly-crystalline Rh wire in 1M Na_2SO_4 at pH 6.7 with variable anodic end potentials and b) the state of the wire surface after breaking off the tip (SEM micrograph).

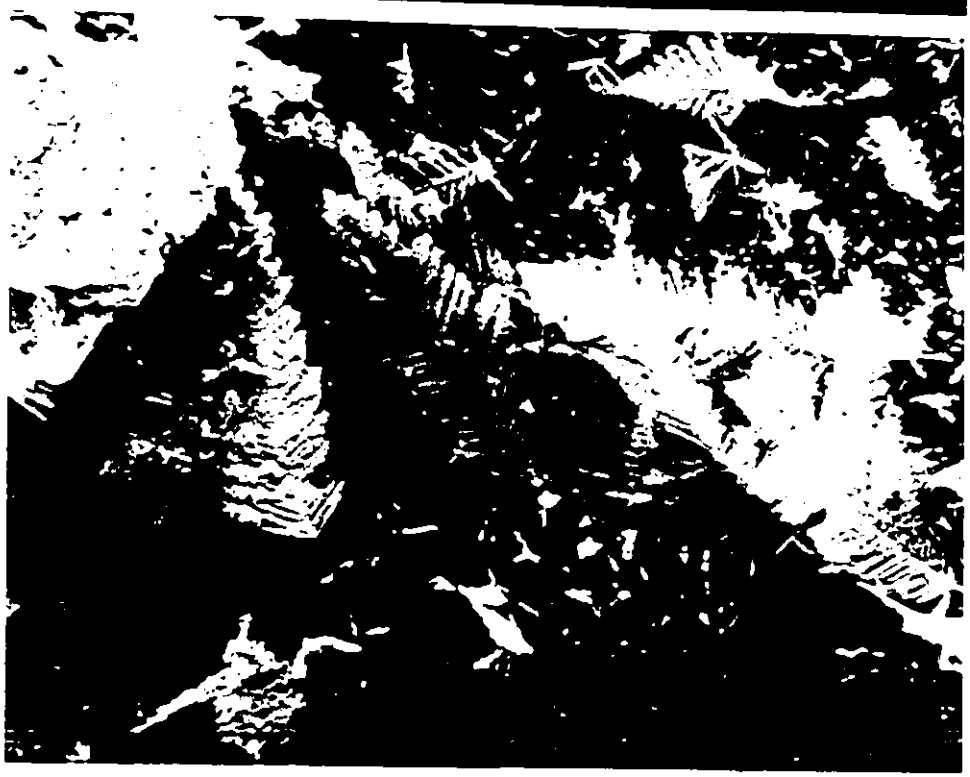

of Zn in various solutions, e.g. SO_4^{2-}, CO_3^{2-} and Cl^- appears to be a question of structure of the ZnO and does not, therefore, depend necessarily upon formation of films of different compounds.

It seems likely that breakdown of the film occurs from sites of ZnO containing excess Zn. The rapid increase in current is due to dissolution of Zn into the solution and a very high concentration of Zn ions near the electrode gives rise to dendritic growth (Fig. 3.37b) or loose deposits on the electrode surface when the current is reversed to a cathodic direction. The rotation effect shown in Fig. 3.36b is due to removal of Zn ions in solution near the electrode surface.

It is reasonable to assume that the lower reduction overvoltage associated with peak C_3 compared with peak C_1 arises because of good electrical contact between the cathodically deposited crystalline deposit of dendrites and the underlying film of oxide, which is reduced only at more cathodic potentials in peak C_1.

In 1M Na_2CO_3 solution at pH 11.5, as shown in Fig. 3.1, rapid rise in current occurs at high overvoltage. It seems likely that this is due to oxygen evolution; see Fig. 3.1a. The film is seen to be remarkably protective out to ca. −3.5 V. Another cathodic peak (C_2) can be distinguished in Fig. 3.1a. A more detailed study of the cathodic peaks was carried out by examining the behaviour of the Zn electrode in mixed solutions of CO_3^{2-} and Cl^-, and also holding the electrode potential constant for controlled periods of time, followed by recording the succeeding

CV upon applying a cathodic potential sweep at some controlled rate.

3.3.5.2 Potential Holding Effect

In 1M Na_2CO_3 + 2M NaCl solutions at pH 11.5 holding the potential for various periods of time at -0.192 V results in a slight increase in the reduction peak (C_1). A small cathodic peak (C_4) is also observed at a more positive potential than that of the C_1 peak after holding at 0.255 V. The charge under this peak depends, as may expected, very much on the anodic current passed during holding at the more positive end of the potential sweep. The currents in this peak are independent of rotation-rate, so C_4 probably corresponds to a film reduction process.

Increase of the range of potential in the CV to the range - 0.98V to + 1.0 V with holding at + 1 V gave rise to another cathodic peak between C_1 and C_4. The charge under this peak (C_2) depends very much on the holding time and is equivalent to the reduction of ca. six hundred layers of oxide/hydroxide of Zn, when the holding time was 80 s (Fig. 3.38). These "extra" cathodic peaks will be discussed further in chapter 4 where related results, obtained under galvanostatic conditions, are examined.

3.3.5.2 The Effect of Carbonate Ions on the Current Peak A_1

It was of interest to see whether there is any carbonate ion effect on dissolution of Zn. The data in Table 3.1 show that the potentials of peaks A_1 and C_1 in various electrolytes are independent of the electrolyte composition. Also it was assumed that these peaks are due to the formation and reduction of

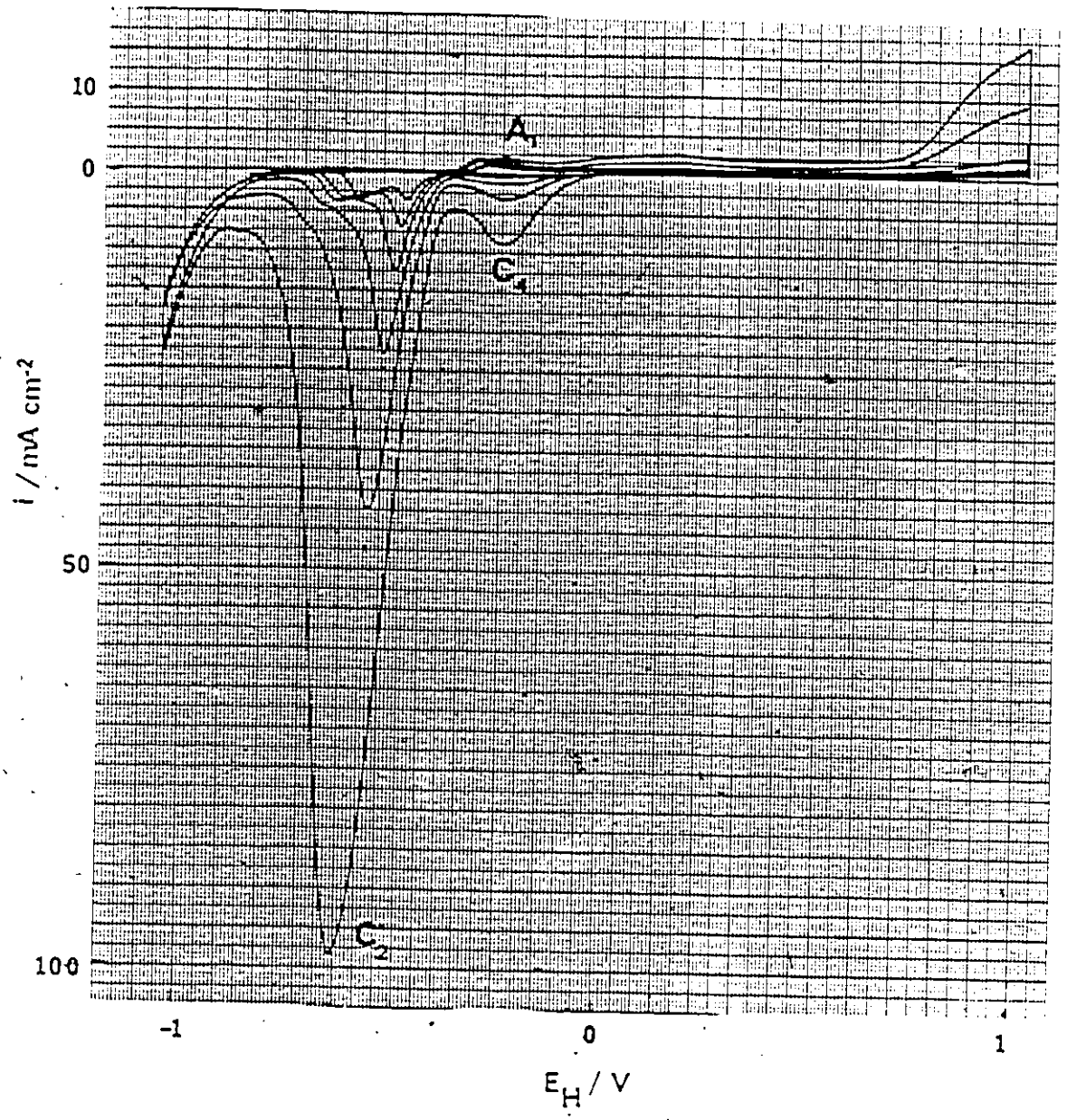

Fig. 3.38 Cyclic-voltammetry i vs E profiles for polycrystalline Zn electrode in 1M Na_2CO_3 - 2M NaCl solution at pH 11.5 for holding the potential for various periods of time at anodic end potential. s - 100 mV s^{-1}

holding times at 1.0 V - 0, 10, 20, 40, 60 and 80 s

$ZnO/Zn(OH)_2$ on the basis of comparison with the reversible potentials for these species. However, as was discussed on page 92 it is unclear why, in the pH range 12 to 11.5 (Fig. 3.13), there is an effect of rotation that is greater than can be attributed to the diffusion of OH^- ions. Therefore, a series of solutions were prepared containing varying concentrations of CO_3^{2-} ions but at a constant pH of 11.5. The ionic strength was kept constant by adding appropriate quantities of NaCl and Na_2SO_4.

Table 3.16 gives the slopes of i_p vs $\omega^{1/2}$ plots obtained with the rotating Zn disc electrode in the various solutions. Figs. 3.39a and 3.39b show the effect of carbonate concentration at constant ionic strength on the slopes of the i_p vs $\omega^{1/2}$ lines : the order with respect to carbonate seems to be near one from both graphs as also determined from the log-log plot of Fig. 3.40. "Mass-transport" of CO_3^{2-} ions evidently determines the current at peak A_1.

It seems likely therefore that CO_3^{2-} ions are involved indirectly in the anodic behaviour of the Zn electrode in carbonate solutions. This conclusion led to further work on the comparative effect of bicarbonate ion in order to understand the CO_3^{2-} effect better.

3.3.5.3 The Effect of Bicarbonate Ions

A series of experiments were carried out with solutions containing varying concentrations of HCO_3^- ions. The ionic strength was kept constant (1 mol dm^{-3}) by adding appropriate amounts of Na_2SO_4 and pH was maintained constant around 8.

Table 3.16

Carbonate Ion Effect on the Slopes of i_p vs $\omega^{\frac{1}{2}}$ Plots

a) Solution: xM Na_2CO_3 + yM NaCl, pH=11.6

Ionic strength: 4 mol dm^{-3}

Solution	Slope of i_p vs $\omega^{\frac{1}{2}}$ $\mu A\ cm^{-2}(rpm)^{-\frac{1}{2}}$
1.0M Na_2CO_3+1.0M NaCl	5.16
0.8M Na_2CO_3+1.6M NaCl	4.00
0.6M Na_2CO_3+2.2M NaCl	2.97
0.4M Na_2CO_3+2.8M NaCl	1.77
0.2M Na_2CO_3+3.2M NaCl	0

b) Solution: aM Na_2CO_3 + bM Na_2SO_4, pH=11.5

Ionic strength: 3 mol dm^{-3}

Solution	Slope of i_p vs $\omega^{\frac{1}{2}}$ $\mu A\ cm^{-2}(rpm)^{-\frac{1}{2}}$
1.0M Na_2CO_3+ 0 M Na_2SO_4	3.86
0.8M Na_2CO_3+0.2M Na_2SO_4	3.45
0.6M Na_2CO_3+0.4M Na_2SO_4	2.52
0.4M Na_2CO_3+0.6M Na_2SO_4	1.98
0.2M Na_2CO_3+0.8M Na_2SO_4	0.52

Notes:

1. Carbonate ion concentration varied keeping ionic strength constant in both cases (Cl^- or $SO_4^{=}$ ion solution).
2. All measurements made at $s = 5\ mV\ s^{-1}$ with Zn RDE etched in 48% HBr.
3. Rotation-rate (ω) was varied from 100 rpm to 2500 rpm.
4. Slopes of i_p vs $\omega^{\frac{1}{2}}$ values given are average of 5-10 runs. Results are reproducible.
5. The rotation effect on peak A_1 in 0.2M Na_2CO_3+ 3.2M NaCl is negligible.

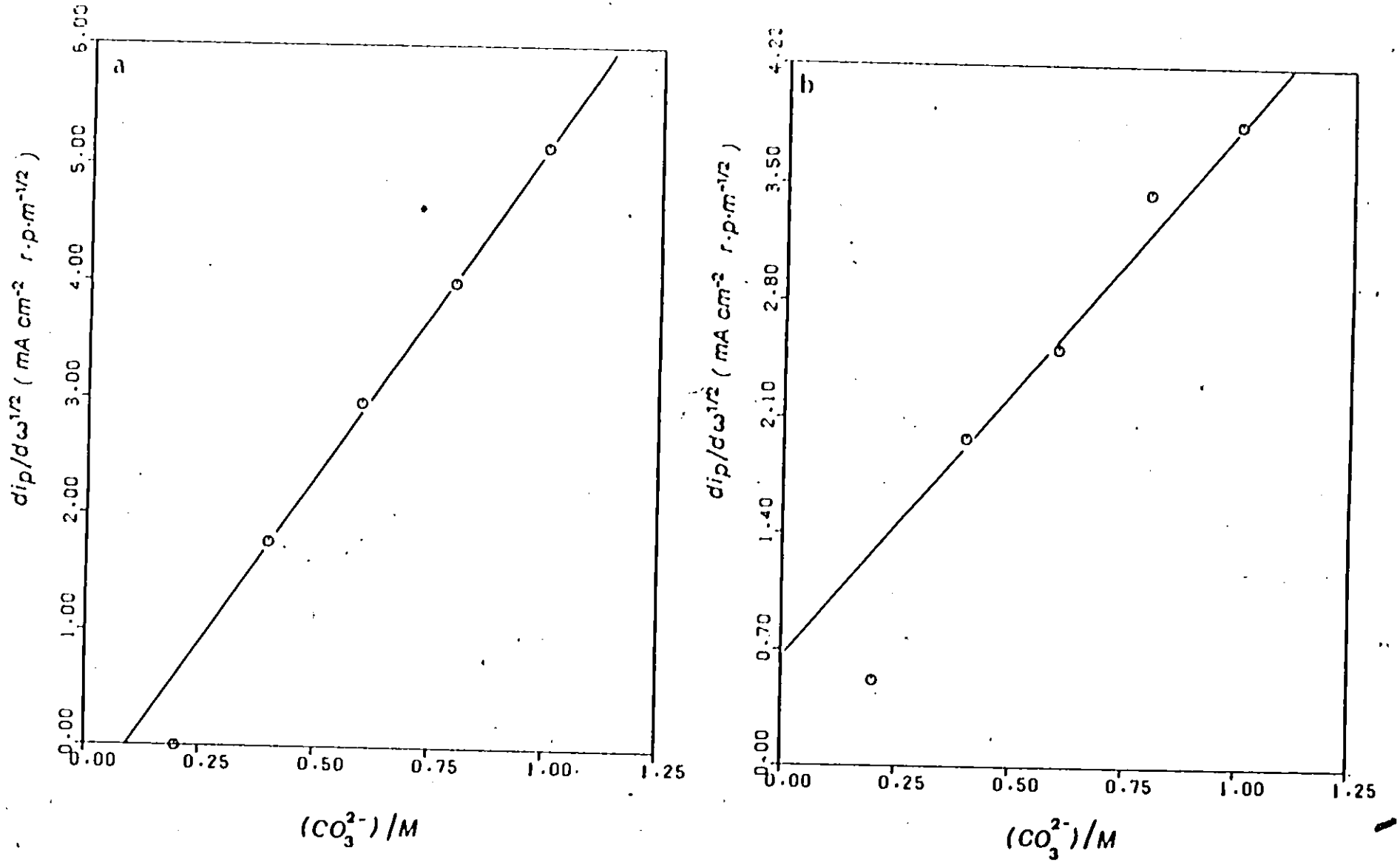

Fig. 3.39 The effect of carbonate ion concentration on the slope of the i_p *vs* $\omega^{\frac{1}{2}}$ at constant ionic strength of (a) 4 mol dm^{-3} in NaCl solution and (b) 3 mol dm^{-3} in Na_2SO_4 solution (see table 3.16).

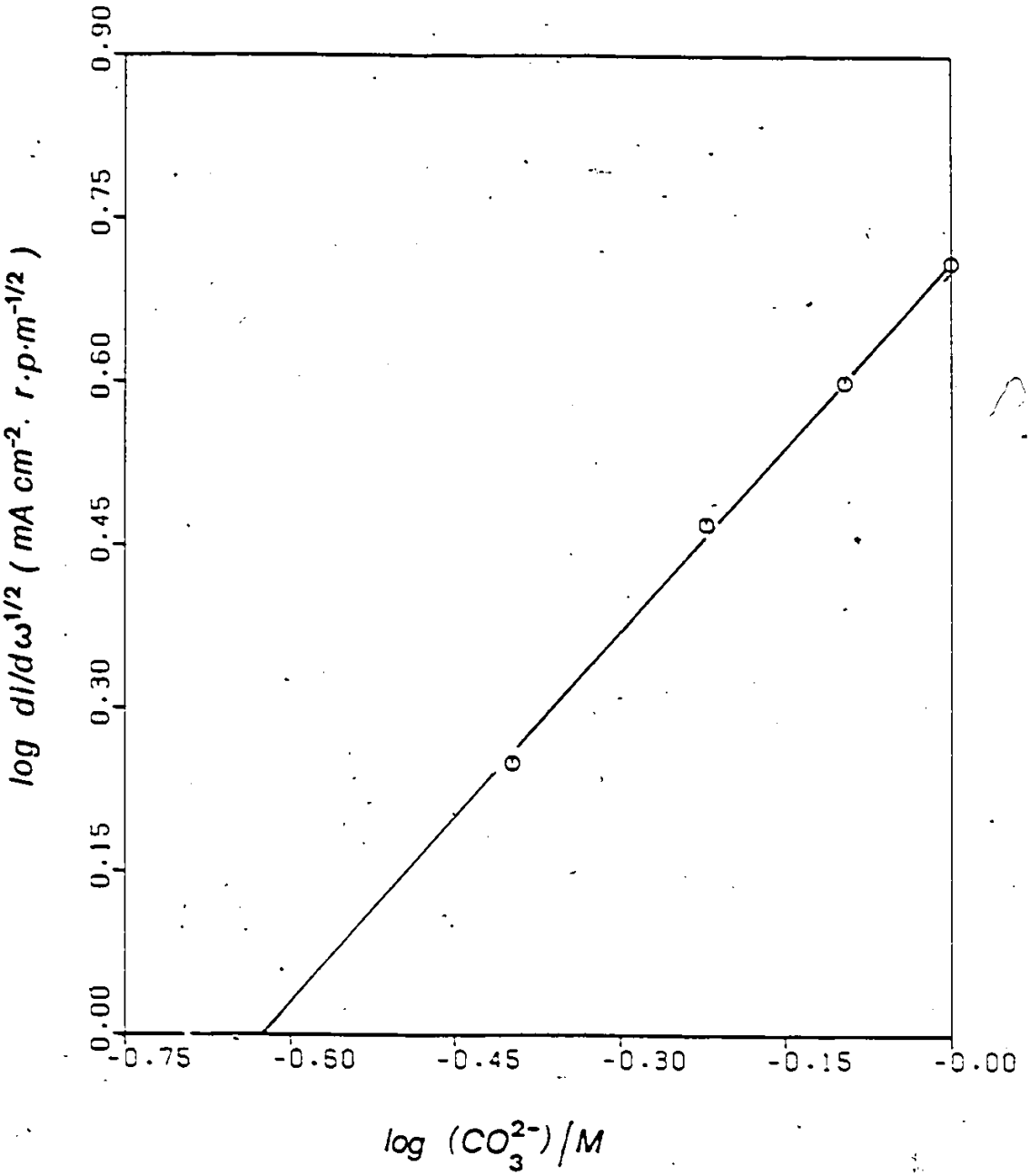

Fig. 3.40 Dependence of log ($d i_p / d \omega^{\frac{1}{2}}$) on log ($CO_3^{2-}$) from Table 3.16 a.

Fig. 3.41 shows a CV obtained for the Zn electrode in 0.33M Na_2SO_4 solution. It can be seen that Zn dissolves completely into solution and no passivation occurs at all. This is also clear from a RDE experiment in 1M Na_2SO_4 around pH 8, where the reduction peak C_5 (Fig. 3.41a) completely disappears with rotation. This behaviour is consistent with the Pourbaix diagram plotted for the $CO_3^{2-}/H_2O/Zn$ system as shown in Fig. 1.4; also Fig. 3.41b shows a SEM picture taken of a Zn electrode surface after electrochemical cycling under the conditions above (1M Na_2SO_4, pH around 8).

From CV's obtained with solutions containing varying concentrations of HCO_3^- ions it was found that HCO_3^- ions help to passivate the Zn electrode. This is consistent with the Pourbaix diagram, Fig. 1.4 and the extent of passivation evidently depends mainly on the concentration of bicarbonate ion.

It is interesting to see which species of the series: ZnO, $Zn(OH)_2$, $ZnCO_3$ or hydroxycarbonate ($Zn(OH)_{1.2}(CO_3)_{0.4}$) is likely to be responsible for the passivation. From the potentials of the A_1 and C_1 peaks in relation to Nernst potential (page 68) it seems likely that oxide/hydroxide should be responsible for the passivation even in the HCO_3^- solutions. However, the thickness of the film increases with HCO_3^- ion concentration at constant pH and ionic strength. Table 3.17 gives the q_a, q_c and q_a/q_c values. In 1M $NaHCO_3$, oxidation of the Zn anode becomes completely a diffusion-controlled process ($i_p \propto$ square root in s; see Table 3.4). In 1M $NaHCO_3$ a sudden rise in current takes place at lower sweep-rates (Fig. 3.42). This is not the case for the 0.2M $NaHCO_3$ + 0.27M Na_2SO_4 solution. The behaviour in 0.4M $NaHCO_3$ + 0.2M

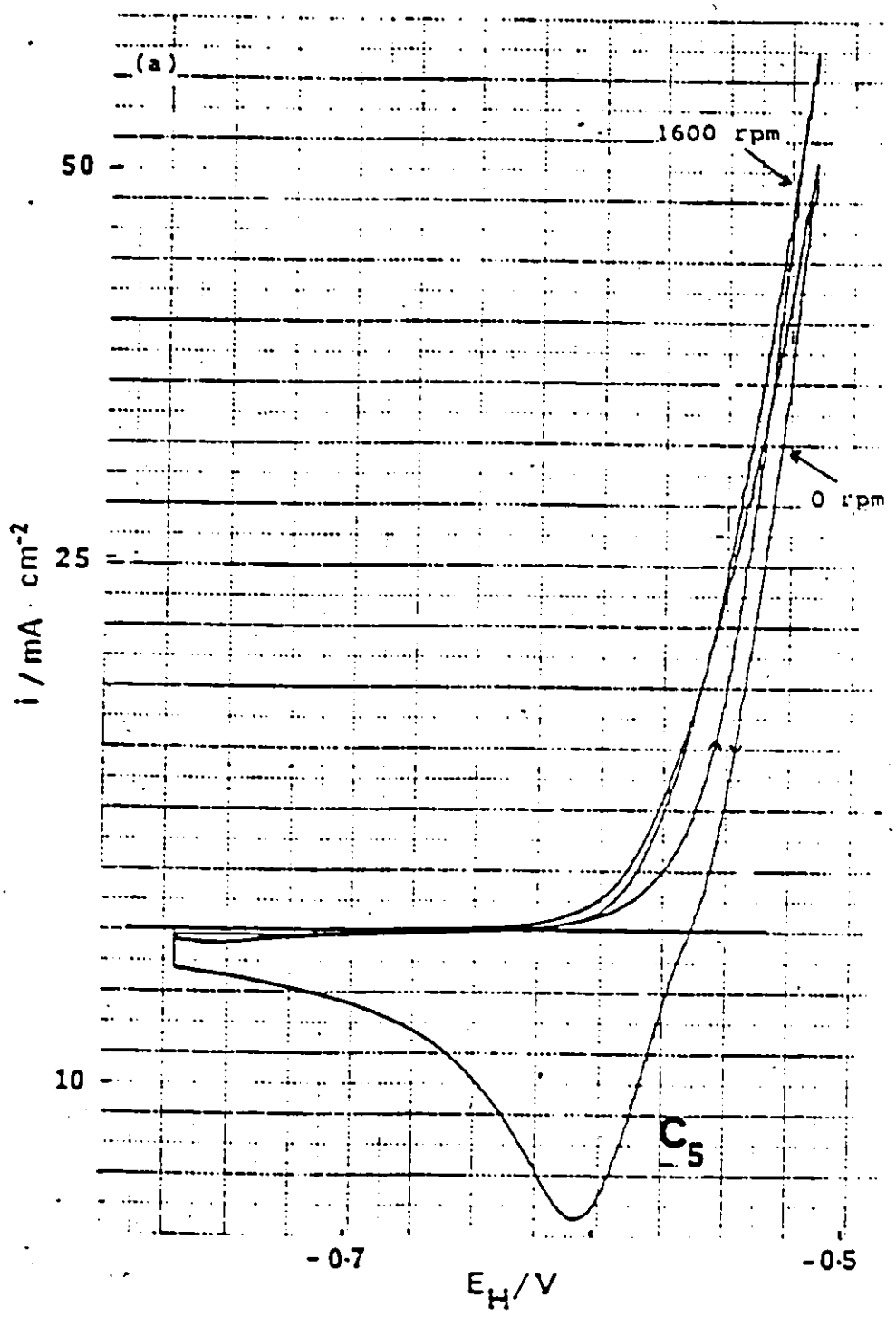

Fig. 3.41 (a) Cyclic-voltammetry i vs E profiles in 0.33M Na_2SO_4 solution at pH 8.1 for polycrystalline Zn RDE with rotation speeds 0 and 1600 rpm. (b) The state of the electrode surface after electrochemical cycling. (see following page)

ε - 50 mV s^{-1}

Table 3.17

Comparison of Charge Densities for A_1 and C_1 Peaks in the Presence of HCO_3^- Ions

Solution- 1M $NaHCO_3$

	Sweep-rates / mV s^{-1}			
	20	60	100	200
$q_a/\mu C\ cm^{-2}$	3629	1914	1508	1004
$q_c/\mu C\ cm^{-2}$	1169	877	693	542
q_a/q_c	3.1	2.2	2.2	1.9

Solution - 0.2M $NaHCO_3$ + 0.27M Na_2SO_4

	Sweep-rates / mV s^{-1}			
	20	60	100	200
$q_a/\mu C\ cm^{-2}$	1282	806	669	523
$q_c/\mu C\ cm^{-2}$	434	438	467	504
q_a/q_c	3.0	1.8	1.4	1.0

Notes

1. Both solutions have the same ionic strength (1 mol dm^{-3}) and the same pH (8.1).
2. All measured with Zn electrode etched in 48% HBr and roughness factor was assumed as 3 for charge density calculations.
3. All charges were calculated relative to the zero current baseline.
4. q_a, q_c and q_a/q_c values are higher for 1M $NaHCO_3$ than for 0.2M $NaHCO_3$ + 0.27M Na_2SO_4 solution.

Na_2SO_4 solution was intermediate between that in 1M and 0.2M $NaHCO_3$ solutions.

Fig. 3.43 shows the SEM pictures of a Zn electrode after electrochemical cycling at sweep-rates of 300-20 mV s^{-1} and 300-2 mV s^{-1} in 1M $NaHCO_3$ solution. It is seen that the surface has changed substantially. Similar surfaces were obtained after cycling in 0.4M $NaHCO_3$ + 0.2M Na_2SO_4 solution but not from 0.2M $NaHCO_3$ + 0.27M Na_2SO_4. The latter observation could be due to formation of insoluble compounds on the Zn electrode, e.g. either $ZnCO_3$ or the basic salt $Zn(OH)_{1.2}(CO_3)_{0.4}$.

It can be seen from Fig. 3.44 that the Zn electrodes which started to dissolve at lower sweep-rates in 1M $NaHCO_3$ were repassivated after many cycles due to formation of thick films; Fig. 3.45 shows SEM pictures taken of a repassivated electrode surface. It is difficult to identify the compounds that are deposited owing to the variety of compounds of zinc that may have been formed: oxide, hydroxide, carbonate and hydroxycarbonate.

3.3.5.4 Comparison of the Behaviour of Zn and Cd Electrodes in the $HCO_3^-/CO_3^{2-}/H_2O$ system

The behaviour of Zn and Cd electrodes in hydroxide and carbonate media is compared in this section. Table 3.18 gives the solubility products of cadmium and zinc oxides, hydroxides and carbonates, and also the possible chemical form of the coatings that can be produced in NaOH and Na_2CO_3 solutions. Fig 3.46 shows the solubility curves for Zn/H_2O, $Zn/H_2O/CO_3^{2-}$, Cd/H_2O and $Cd/H_2O/CO_3^{2-}$ systems.[140]

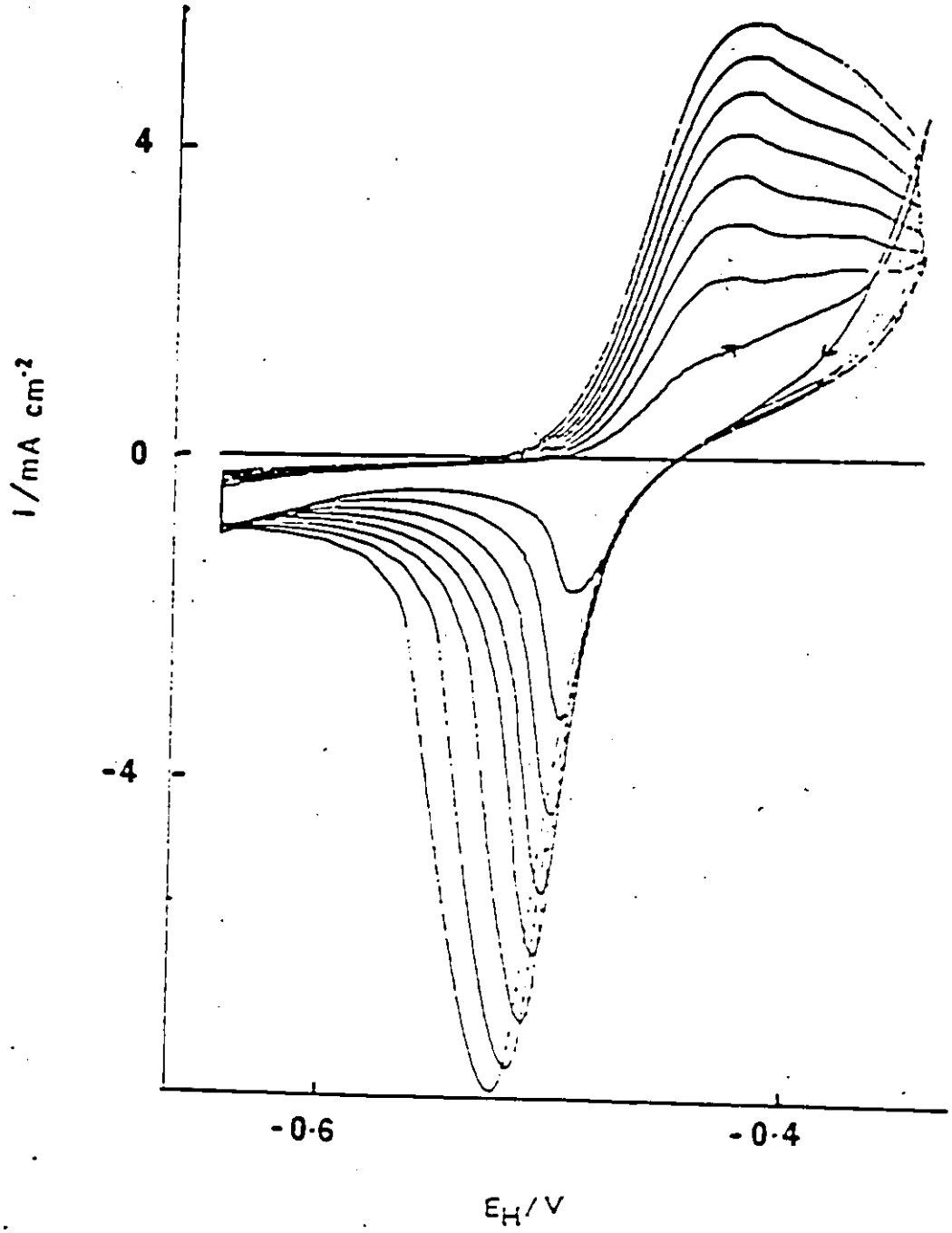

Fig. 3.42 Cyclic-voltammetry i vs E profiles in 1M $NaHCO_3$ solutions at pH 8.5 for polycrystalline Zn electrode with variable sweep-rate.

s = 300 mV s^{-1} --- 20 mV s^{-1}.
Electrode - polycrystalline, of apparent area of 0.07 cm^2 and etched in HBr.

Fig. 3.43 SEM pictures of the state of Zn electrode surface after electrochemical cycling over (A and C) 300 mV s^{-1} - 20 mV s^{-1} and (B and D) 300 mV s^{-1} - 2 mV s^{-1} sweep-rate ranges in 1M $NaHCO_3$ solution at pH ca. 8.5.

(see following page)

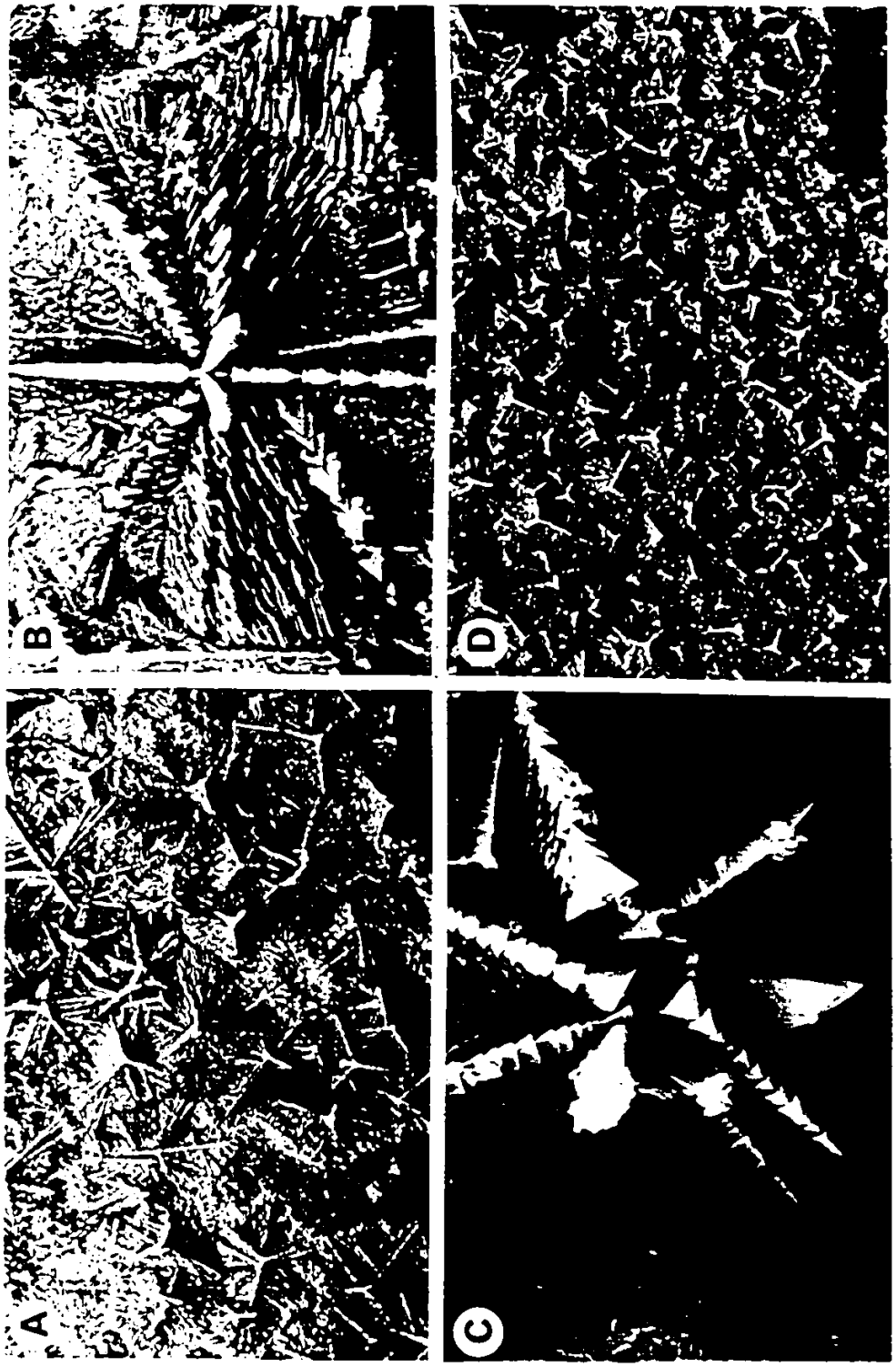
A
B
C
D

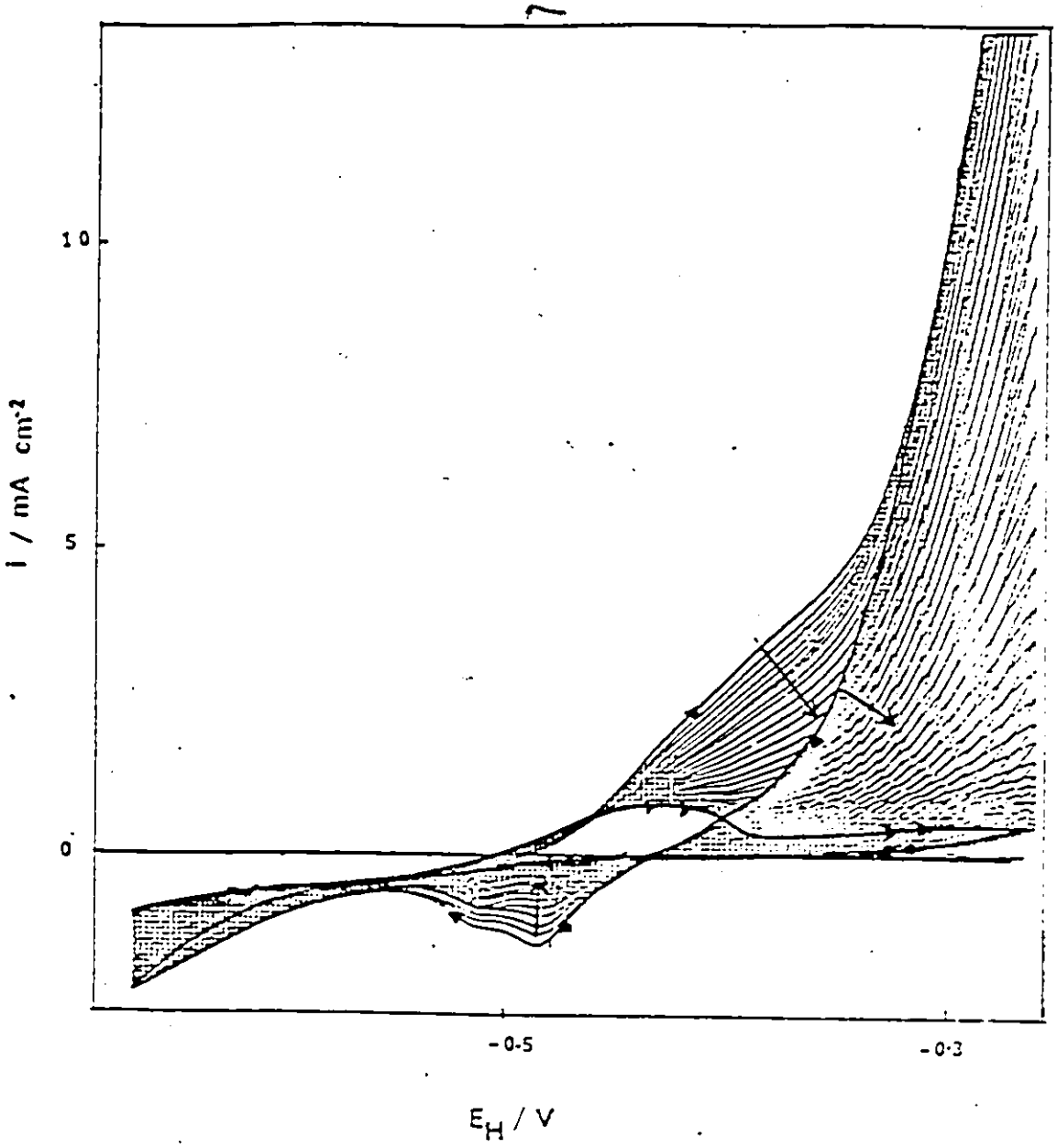

Fig. 3.44 Cyclic-voltammetry i vs E profiles showing the repassivation of Zn electrode which started to dissolve at lower sweep-rates in 1M $NaHCO_3$ solution at pH ca. 8.
σ - 50 mV s^{-1}, electrode - polycrystalline, of apparent area 0.07 cm^2, etched in HCl.

Fig. 3.45 The state of the repassivated Zn electrode surface in 1M $NaHCO_3$ at pH ca. 8.

(see following sheet)

Table 3.18

Solid Compounds Form in Cd and Zn Alkaline Systems and Their Solubility Products (Ref. 78)

Anode metal		Zn	Cd
Coating formed in	NaOH solution	ZnO	CdO → $Cd(OH)_2$
	Na_2CO_3 solution	ZnO	CdO → hydroxycarbonate → carbonate
Solubility Product	oxide	10^{-17}	10^{-13}
	hydroxide	10^{-17}	10^{-14}
	carbonate	10^{-12}	10^{-14}

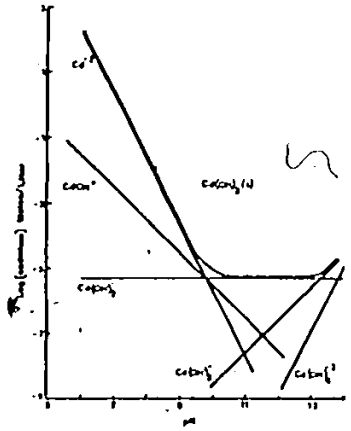

Figure A. Cadmium hydroxide solubility curve.

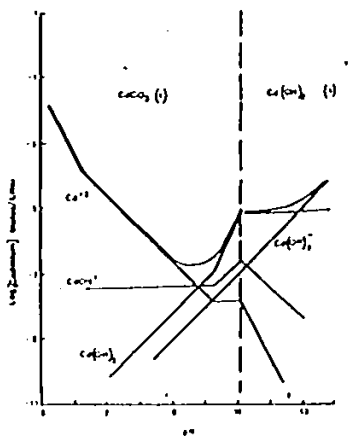

Figure B. Cadmium carbonate solubility diagram. $C_T = 10^{-3.3}$ mol/liter.

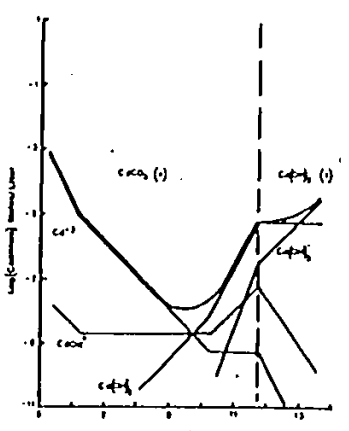

Figure C. Cadmium carbonate solubility diagram. $C_T = 10^{-1.0}$ mol/liter.

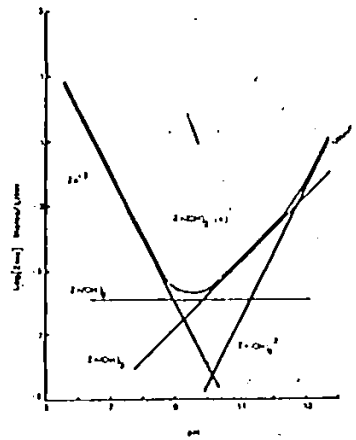

Figure D. Zinc hydroxide solubility curve.

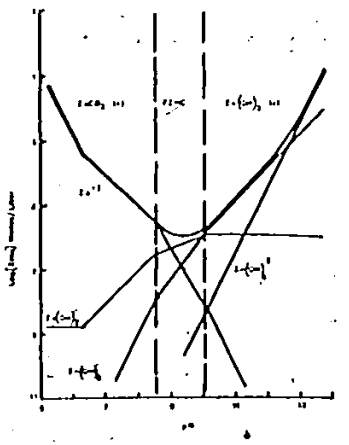

Figure E. Zinc carbonate solubility diagram. $C_T = 10^{-3.1}$ mol/liter.

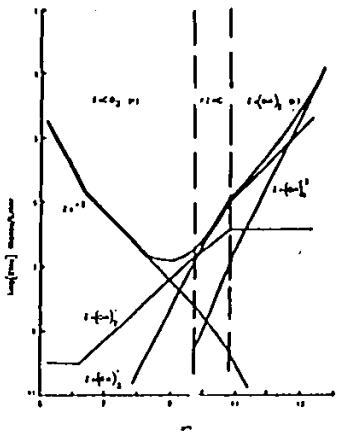

Figure F. Zinc carbonate solubility diagram. $C_T = 10^{-1.0}$ mol/liter.

Fig. 3.46 The solubility curves for Zn/H_2O, $Zn/H_2O/CO_3^{2-}$, Cd/H_2O and $Cd/H_2O/CO_3^{2-}$ systems. (Ref. 140)

The mechanism of the carbonate effect on oxidation of cadmium metal surfaces has been studied in the literature at a fundamental level[141-145]. In NaOH solutions, CdO is formed as the initial product but the solubility product of the CdO is about ten times higher than that of $Cd(OH)_2$. Therefore any oxide that forms on the Cd appears to be in an unstable condition and becomes converted to hydroxide or, when carbonate ions are present, to carbonate. This is not the case for Zn, since the solubility product of $ZnCO_3$ is much higher than that of the hydroxide or of the oxides which are approximately equally insoluble. Therefore the situation is quite different from that for Cd.

Huber[9], however, made an X-ray diffraction study of products of oxidation of Cd in Na_2CO_3 solution and found lines characteristic of $CdCO_3$ but no carbonate precipitation was observed for some time. Fig. 3.47 shows the $CdCO_3$ obtained in anodic dissolution of Cd in $NaHCO_3$ solution by Grauer[146]. It has a structure similar to that of the products of Zn dissolution in $NaHCO_3$. It seems likely that the reaction product formed in 1M $NaHCO_3$ and 0.4M $NaHCO_3$ + 0.2M Na_2SO_4 at lower sweep-rates is $ZnCO_3$ or more probably $Zn(OH)_{1.2}(CO_3)_{0.4}$.

The Cd electrodes used in carbonate electrolyte can "age" or develop a permanent decrease in reactivity[145]. This was explained in terms of carbonate being locked in the pores because of the difficulty in reduction or continuing oxidation of a non-conducting mass. Similar behaviour was observed in the course of the present work at Zn. Most results obtained with carbonate solutions were rather irreproducible, unlike the more satisfactory

Abb. 6. Sonatoides Cadmiumcarbonat, gebildet bei kathodischer Polarisation bei 80 °C. — 1μ.

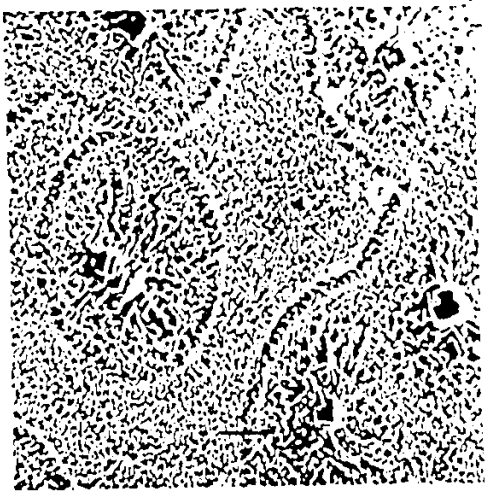

Abb. 8. Mit $CdCO_3$-Anhäufungen überdeckte Lokalanoden. Probe aus Kurzschlussversuch mit Kupfer bei 80°C. — 1μ.

Fig. 1.47 $CdCO_3$ obtained in anodic dissolution of Cd in $NaHCO_3$ solution. Bar = 4 μ

results in SO_4^{2-} and Cl^- solutions. For example, a series of experiments were carried out with increasing and decreasing rotation-rate to study the effect of rotation on the $i_p s^{-1/2}$ *vs* $s^{1/2}$ plots for Zn in 1M Na_2SO_4 solution (pH 11.5). Fig. 3.17 shows the results obtained with 1M Na_2SO_4 at pH 11.5 between 300 mV s^{-1} and 20 mV s^{-1} which may be compared with those of Fig. 3.48 1M Na_2CO_3 solution at pH 11.5. In these experiments, as mentioned earlier, the same electrode was used for a given set of measurements, i.e. for both increasing and decreasing rotation rates.

It is seen from Fig. 3.48 that, contrary to the behaviour in SO_4^{2-} solutions, the current decreases with ageing of the electrode, whether the rotation rate was being increased or decreased. It was also found difficult to compare the k_1 and k_2 values in Table 3.11 for Na_2CO_3 solution, unlike the situation for the data in Table 3.7 for Na_2SO_4 solution where the k_1 values of Table 3.7 for the lower sweep-rates are well reproducible.

Table 3.19 shows results obtained in several RDE experiments using a newly cut Zn electrode for each experiment. It is seen that the slopes of i_p *vs* $\omega^{1/2}$ plots are significantly different from one another. Therefore most of the RDE experiments in carbonate solutions in the present work had to be carried out with a freshly etched surface of the same Zn RDE in each experiment so that grain boundaries, the roughness factor and dislocations, etc, would be kept almost the same.

It is clear from these results that both carbonate and bicarbonate have an effect on Zn dissolution, passivation and the breakdown of films that is not determined directly by the pH.

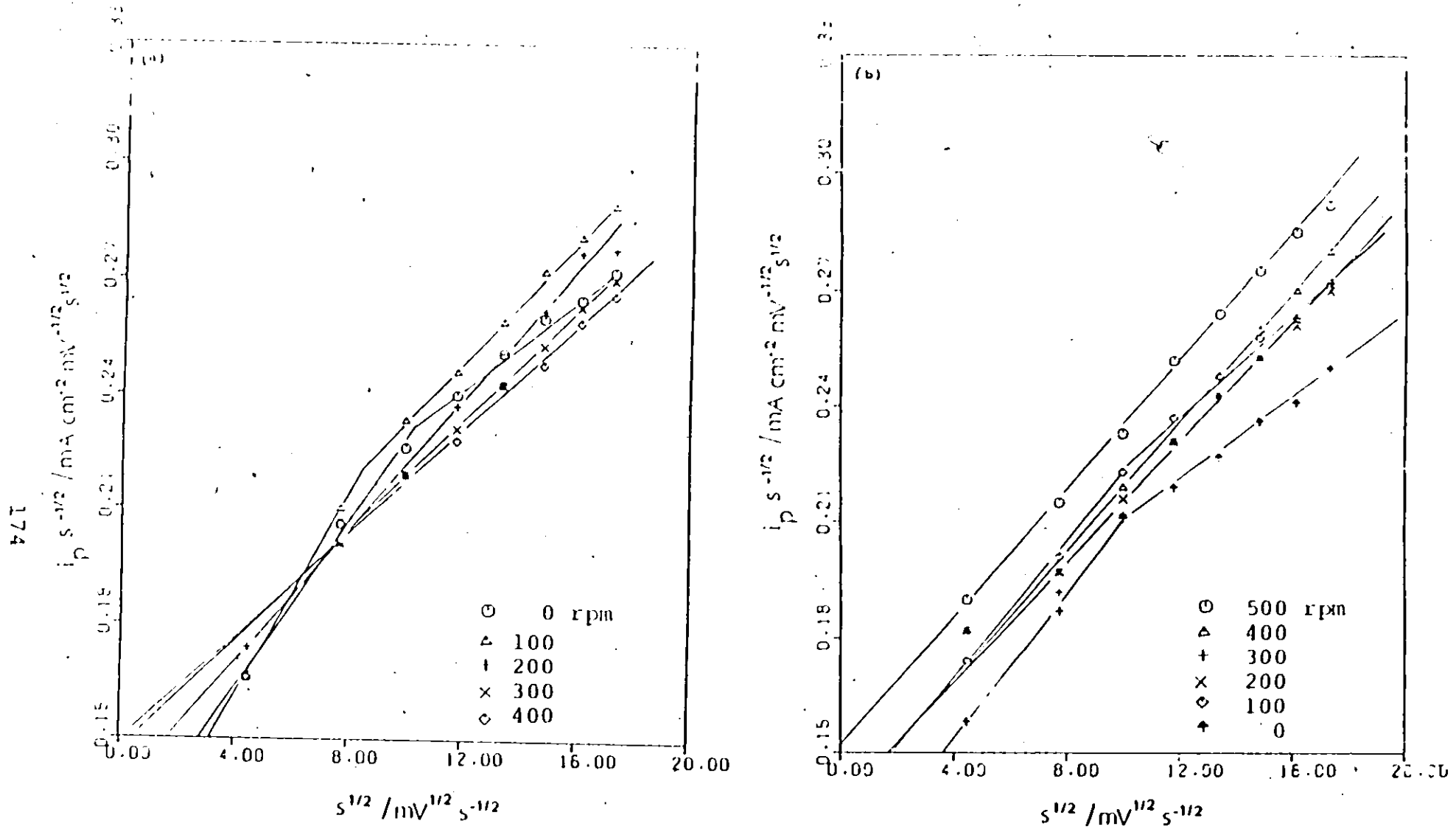

Fig. 3.48 The effect of (a) increasing and (b) decreasing rotation rates on $i_p s^{-\frac{1}{2}}$ vs $s^{\frac{1}{2}}$ dependence for A_1 peak in 1N Na_2CO_3 solution at pH 11.5 for polycrystalline Zn RDE.

ω - (a) 0, 100, 200, 300, 400 rpm

ω - (b) 500, 400, 300, 200, 100, 0 rpm

Table 3.19

Reproducibility of Slope of i_p vs $\omega^{\frac{1}{2}}$ Plots in the Presence of Carbonate Ion

Solution - 1.0M NaCl + 1.0M Na_2CO_3

pH	Slope of i_p vs $\omega^{\frac{1}{2}}$ $\mu A\ cm^{-2} rpm^{-\frac{1}{2}}$
11.44	7.78
11.48	6.36
11.46	10.23
11.59	5.23

Notes

1. All measurements were carried out in 1M Na_2CO_3 + 1.0M NaCl solution using a single Zn (RDE) etched in 48% HBr under reproducible conditions, but on different days.
2. All measurements were made at same sweep-rate (5 mV s^{-1}), and the slopes given are the average value of 2-11 runs.
3. There is poor reproducibility of results from one electrode to another.

However, Zn forms $ZnCO_3$ or hydroxy-carbonate indirectly in the presence of CO_3^{2-} and HCO_3^- ions, depending on the pH of the electrolyte and also on the nature of other ions present in solution.

3.4 Model

The results derived from the combination of studies on Zn oxidation by means of sweep-rate experiments in cyclic-voltammetry and rotation-rate experiments with the rotating disc electrode enable a model of the behaviour of the Zn electrode upon oxidation in alkaline solution, where film formation and passivation arise, to be proposed.

At the beginning of a CV peak profile, dissolution of Zn to form transiently soluble Zn(II) species in solution arises. Diminution of the initial rate of oxidation at the A_1 peak takes place because of film formation involving $Zn(OH)_2$, ZnO or hydroxy-carbonate species (in the presence of CO_3^{2-}, HCO_3^-, SO_4^{2-} or Cl^- ions). Formation of the film is dependent on pH due to the pH-dependent solubilities of zinc oxide or hydroxide, and the hydroxy-carbonate. At pH's above about 13, it was found that the oxidation process was purely diffusion-controlled for all solutions but at lower pH's (ca. 11.5) mixed-control was observed, involving a direct surface oxidation reaction.

By correlating the shapes of the peaks and their peak potentials for different Zn surface preparations, the passivation of Zn in the initial stages of its oxidation leads to the possibility of suggesting the following model for the oxidation process:

Two processes take place at lower pH's (ca. 11.5). Initially diffusion-controlled dissolution of the Zn occurs, most probably to give $Zn(OH)_2$. This is the nature of the process associated with the A_{1a} component of the A_1 peak. At this pH, $Zn(OH)_2$ is sparingly soluble, and some $Zn(OH)_2$ probably becomes precipitated to give a loosely adherent porous film on some parts of the electrode surface; such a film , if present, would not appreciably inhibit further electrode reaction at the Zn metal surface underneath. This dissolution, it is believed, takes place at active sites, e.g. at steps and kink sites, and/or grain boundaries.

The second component of the oxidation process (peak A_{1b}) is proposed to be formation of a passive film of ZnO or $Zn(OH)_2$, occurring by the surface process mechanism; growth continues until almost all the surface is covered and the oxidation reaction becomes passivated. If the concentration of active sites is constant, the dissolution processes will occur independently of the A_{1b} oxidation process, i.e. the currents of the two components are simply additive ($i_p = k_1 s + k_2 s^{1/2}$). This condition only arises, of course, if the deposited oxide species are porous or gelatinous and thus do not physically block the Zn surface for its oxidation, as indicated in the previous paragraph. Experimentally, the sweep-rate range can be divided into two regions, each obeying this relationship, but with different k_1 and k_2 values. The charge measurements from k_1 values obtained from $i_p s^{-1/2}$ *vs* $s^{1/2}$ plots for 1M Na_2SO_4 at pH 11.5 show that the thickness of the surface film corresponds closely to a monolayer at lower sweep-rate, ca. 20 mV s^{-1}. It has been seen from the

cyclic-voltammograms that passivation at a Zn (0001) single-crystal face arises because of direct film formation (peak A_{1b}) and no parallel direct dissolution takes place at all. q_a/q_c values are almost 1 for the Zn (0001) face in the sweep-rate range 2 mV s^{-1} - 300 mV s^{-1}, even though the sweep-rate dependence on i_p is unusual, i.e. at lower sweep-rates i_p is linear in s while i_p becomes linear in $s^{1/2}$ at higher sweep-rates. It seems likely that this unusual sweep-rate dependence on i_p of the A_{1b} process gives rise to the two regions in the $i_p s^{-1/2}$ *vs* $s^{1/2}$ plots for polycrystalline electrodes etched in HBr and the several regions for electrodes etched in TFMSA .

The diffusion process associated with the A_{1a} peak may be suggested to be the following:

(a) migration of Zn^{2+} species from the Zn metal surface; and

(b) diffusion of OH^- ions from the bulk of the solution towards and into the porous film.

In CO_3^{2-} containing solutions, the oxidation of Zn was found to be diffusion-controlled, i.e. first-order w.r.t CO_3^{2-} at pH's around 11.5 and was first-order w.r.t OH^- in the pH range 12 - 13.5.

In SO_4^{2-} solutions, unlike in CO_3^{2-} solutions, a plateau current region was seen just after the peak A_1 but in CO_3^{2-} solutions, the A_2 peak is observed before the plateau region begins. It is more likely that in SO_4^{2-} solutions a compact monolayer of ZnO forms at the A_{1b} peak and is responsible for the subsequent complete passivation while, and in the presence of

CO_3^{2-} ions, this film is not stable . Therefore, residual current is passing through the film formed at the peak A_1 which gives rise to A_2.

Studying the behavior of the C_1 peak obtained by reversing the potential after the A_2 peak and in experiments at high rotation-rates, it was found that the C_1 peak current is linear in sweep-rate; the corresponding thickness of the surface film is 2-3 layers of ZnO /or $Zn(OH)_2$, i.e. the amount of passive film of ZnO /or $Zn(OH)_2$ required for complete passivation of zinc in the presence of CO_3^{2-}, is generated only at higher potentials than in SO_4^{2-} solutions.

Liu et al.[72], using the galvanostatic technique, showed that at higher pH's (>14) passivation of the Zn electrode takes place through an initial dissolution of Zn with formation of zincate ions which accumulate near the Zn electrode surface; then, when a critical concentration of zincate is reached, the formation of a primary passivation film of ZnO is initiated ("dissolution and precipitation" mechanism). The mass-transfer of hydroxide ions at the electrode is diminished due to the presence of this (porous) ZnO layer. Finally, when the electrode potential reaches a value close to the Zn/ZnO standard potential, a compact layer of ZnO is formed which is responsible for the passivation of the electrode. Restricted rate of transfer of OH^- ions through a porous oxide film or formation of a compact film of ZnO has been proposed as the basis of passivation mechanisms for low and high current-densities, respectively . Results with the galvanostatic method show (Chapter 4) similar behaviour in passivation of the Zn electrode in pH ca. 11.5 where, at higher current-densities, a

pure "surface process" takes place while at lower current-densities, the oxidation reaction is under mixed-control with simultaneous diffusion and surface reactions taking place.

The processes discussed above, in relation to a possible model for Zn oxidation in alkaline solution, are illustrated in a schematic way in the figure below:

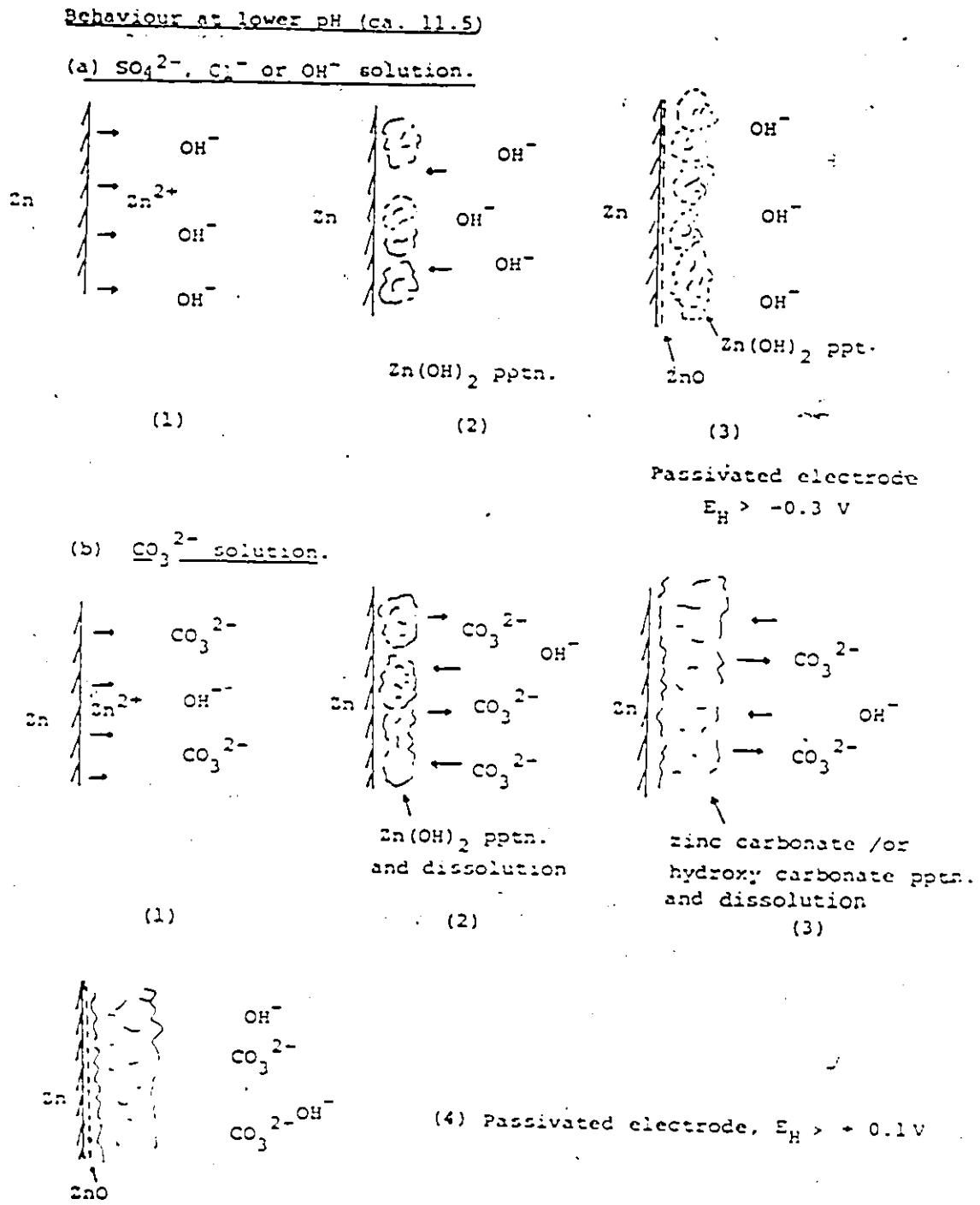

3.5 Summary

Cyclic-Voltammograms were performed in aq. Na_2CO_3 (1M, pH 11.5-13), Na_2SO_4 (1M, pH 8-13) and NaCl (3M, pH 8-13). Variously, one, two or three anodic (A_1, A_2 and A_3) and cathodic (C_1, C_2 and C_3) peaks, depending on surface preparation, electrolyte and pH, are observed. In 1M Na_2CO_3, pH 11.5, peaks designated as A_1, A_2, A_3, C_1, and C_2 peaks are all observed. In 3M NaCl, pH 11.5 and 1M Na_2SO_4, pH 11.5 breakdown of the film occurs just after peak A_1, and the species produced is reduced in the C_3 peak.

Peaks A_1 and C_1

1. Peaks A_1 and C_1 correspond to oxidation and reduction of ZnO or $Zn(OH)_2$, as deduced by comparison of the observed peak potentials with the calculated reversible potentials for formation of these species.

2. The shape of these peaks is dependent on surface preparation. At low sweep rates on Zn electrodes etched in $HClO_4$, two well-defined peaks, A_{1a} and A_{1b}, are observed, and a single cathodic peak. This cathodic peak could be resolved into two component peaks, C_{1a} and C_{1b}, at higher rotation rates. Under most other conditions, the component peaks were not well resolved. By correlating the shapes of the peaks for different surface preparations, it was determined that peak C_{1a} corresponded to peak A_{1a} and C_{1b} corresponded to peak A_{1b}.

3. On the (0001) face of single-crystal electrodes in 1M Na_2SO_4 at pH 11.5, only the A_{1b} and C_{1b} components are observed. q_a/q_c values are 1 for the Zn (0001) face in the sweep-rate range

2 mV s^{-1} - 300 mV s^{-1}, indicating a surface process. However, the widths of the peaks are narrower than is consistent with adsorption-controlled electrocrystallization.

4. On polycrystalline electrodes, formation of the films in the A_1 peak is dependent on pH, because of the pH-dependent solubilities of zinc oxide or hydroxide. At pH above about 13, pure diffusion control was found for all solutions but at lower pH, mixed control was observed.

Behaviour at High pH (>13)

(a) RDE measurements show that i_p is proportional to $\omega^{1/2}$ for the A_1 peak, indicative of diffusion control. The slope of these plots at different pH's is consistent with a reaction which is first order with respect to OH^- in the pH range 12-13.5. Since the solubility of zinc oxide or hydroxide depends on OH^- concentration, it is not clear whether the diffusing species is reactant OH^- or product Zn^{2+}.

(b) Diffusion control for the A_1 process is confirmed by the sweep-rate dependence, $i_p \propto s^{1/2}$.

Lower pH (ca. 11.5)

(a) RDE experiments on the A_1 peak yield $i_p = A + B\omega^{1/2}$, indicating both a diffusional and non-diffusional component. For carbonate-containing solutions, B was found to be proportional to CO_3^{2-} concentration, indicating a first-order reaction with respect to CO_3^{2-}.

(b) The sweep-rate dependence also shows mixed surface and diffusion control, according to the relation $i_p = k_1 s + k_2 s^{1/2}$. Plots of $i_p s^{-1/2}$ vs $s^{1/2}$ or $i_p s^{-1}$ vs $s^{-1/2}$ show two distinct

straight lines for polycrystalline electrodes etched in HBr and several regions for electrodes etched in TFMSA, indicating that this relationship is obeyed, but with different k-values in high and low sweep-rate regions.

(c) The breaks occurring in such plots arise at the same sweep-rate (ca. 20 mV s^{-1}) for the A_1 and C_1 peaks, indicating that the reactions of the component peaks are independent of each other.

(d) Plots of log i_p vs log s are linear with a slope of 0.75. This observed exponent, between 0.5 and 1, is due to the large degree of "compression" of the range of i_p vs s values which arises in a log-log plot.

(e) (i) The charge measurements from k_1 values obtained from $i_p s^{-1/2}$ vs $s^{1/2}$ plots for polycrystalline electrode etched in HBr from 1M Na_2SO_4 at pH 11.5 show that the thickness of the surface film corresponds closely to a monolayer at lower sweep-rate, ca. 20 mV s^{-1}.

(ii) In 1M Na_2CO_3 at pH 11.5 for polycrystalline electrodes etched in HBr, for sufficiently high rotation rates (>500 rpm), the $i_p s^{-1/2}$ vs $s^{1/2}$ plots show one straight line, rather than two distinct lines and it can be seen from q_a/q_c values that reation associated with the A_1 peak involves to a greater extent, a solution process than does that for 1M Na_2SO_4 solution.

(iii) In 1M Na_2SO_4 at pH 11.5 for Zn (0001) single-crystal face at lower sweep-rates, i_p was proportional to s and i_p was proportional to $s^{1/2}$ at higher sweep-rates, even though

the q_a/q_c values are almost 1 at lower and higher sweep-rates. It seems likely this unusual sweep-rate dependence on i_p of the A_{1b} process gives rise to the two regions in the $i_p s^{-1/2}$ vs $s^{1/2}$ plots for polycrystalline Zn electrodes etched in HBr and the several regions for electrodes etched in TFMSA.

HCO_3^- Solution, (pH 8)

The zinc electrode freely dissolves in SO_4^{2-} and Cl^- solutions in the absence of HCO_3^- but, in its presence, passivation occurs. The passivating species is thought to be ZnO or $Zn(OH)_2$. The thickness of the film is found to increase with increasing HCO_3^- concentration.

5. When sweep reversal was made at higher potentials in 1M Na_2CO_3 solution at pH 11.5 , i_p was proportional to s for C_1 peak, provided that the diffusional component was eliminated by electrode rotation. The thickness of the bound ZnO/ $Zn(OH)_2$ film then corresponded to 2-3 layers.

A_2 Peak

From RDE experiments, the diffusion of the same species controls the rate of the reaction at both peaks A_1 and A_2. The A_2 peak is observed only in CO_3^{2-} solutions. It is due to a residual current passing through the film formed in peak A_1. It is more likely that in SO_4^{2-} solutions a compact monolayer of ZnO forms at the A_{1b} peak and is responsible for the subsequent complete passivation while, in the presence of CO_3^{2-} ions, this compact film is not stable.

C_3 Peak

The C_3 peak becomes larger (greater charge) with successive cycling, while the A_1 and C_1 peaks remain unchanged. The C_3 currents decrease with increasing rotation rate. Both of these observations suggest that the breakdown of films occurs from a site of ZnO containing excess Zn. The rapid rise in current is due to to dissolution of Zn. The reduction of the soluble species at relatively positive potentials is due to the lower reduction overvoltage which arises because of the good electrical conductivity of the film.

Peaks C_2 and C_4

Peak C_4 could be observed after holding the potential at 0.255 V in 1M Na_2CO_3 + 2M NaCl solutions at pH 11.5. The currents in this peak are independent of rotation-rate indicating that C_4 probably corresponds to a film reduction process. Holding at +1V gave rise to another cathodic peak, between C_1 and C_4. The charge under this peak (C_2) is a strong function of the holding time.

Chapter 4

Galvanostatic Experiments with the Zn Electrode

4.1 Introduction

The behaviour of the Zn electrode in alkaline solutions was further studied using the galvanostatic (controlled current) technique (see section 2.2.4). This is complementary to the cyclic-voltammetry method. The procedure generates potential vs time relations in response to a pulse of constant current, in the non-steady state approach to an eventual steady state.

In the galvanostatic method the slope of an arrest region (see Fig. 4.1) of changing potential ΔE with time, Δt, is equivalent to the reciprocal of a capacitance $\frac{1}{C} = \Delta E / i\Delta t$, since $i\Delta t$ is charge, ΔQ, passed over the potential interval, ΔE, in the non-steady state. This capacitance is the same as that arising in a CV experiment and is equal to the double layer capacitance C_{dl} plus any Faradaic reaction capacitance associated with deposition of some electro-active species requiring passage of charge ΔQ, e.g., for formation of a monolayer of ZnO, over a potential range ΔE. Usually the Faradaic reaction C_F is much greater than C_{dl} at potentials where a surface process can take place.

Typical anodic and cathodic potential/time curves for passivation and reduction of the anodic film on Zn in 1M Na_2CO_3 solution at pH 11.5, at a constant anodic or cathodic current are shown in Fig. 4.1, together with the notation to be used for

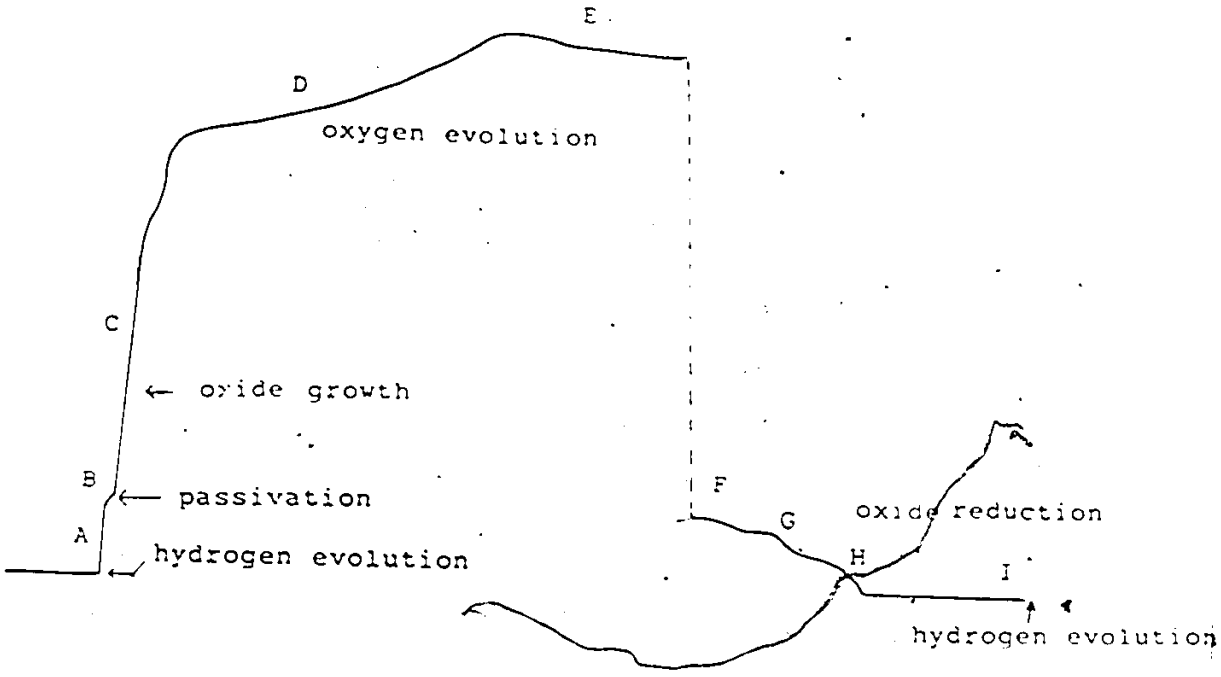

Fig. 4.5 Typical potential/time curve for Zn in 1M Na_2CO_3 at pH 11.5 during galvanostatic anodic charging and cathodic discharging.

designation of the various regions.

When a current step is applied to the system, initially at the hydrogen evolution region (left hand side of Fig. 4.1), the potential first rises rapidly while the double-layer capacitance is being charged (region A) and at the same time the Faradaic reaction begins to take place. The double-layer capacitance obtained from the slope of the initial region of the potential/time curve for a cleaved Zn electrode surface (Zn(0001)-face) is 20 $\mu F\ cm^{-2}$ in good agreement with that for a Hg electrode in the absence of specific adsorption of ions[124]. The first potential plateau (region B) seen after the double-layer charging process is due to passivation of the electrode, with following oxide growth (region C) and eventual simultaneous oxygen evolution beyond region C, in regions D and E. If the current is made cathodic, then the oxide formed in the previous anodic current pulse is reduced before the potential returns to that for hydrogen evolution at I.

4.2 Region B

In order to understand further the early stages of passivation of Zn in alkaline solutions, it was considered interesting to examine Zn passivation which arised in region B under galvanostatic conditions. Fig. 4.2 shows a typical potential/time curve obtained in an experiment carried out to study the behaviour in region B; in this figure, τ_B is the "transition" or passivation time during which current flows to form passivating film at an almost constant potential (hence

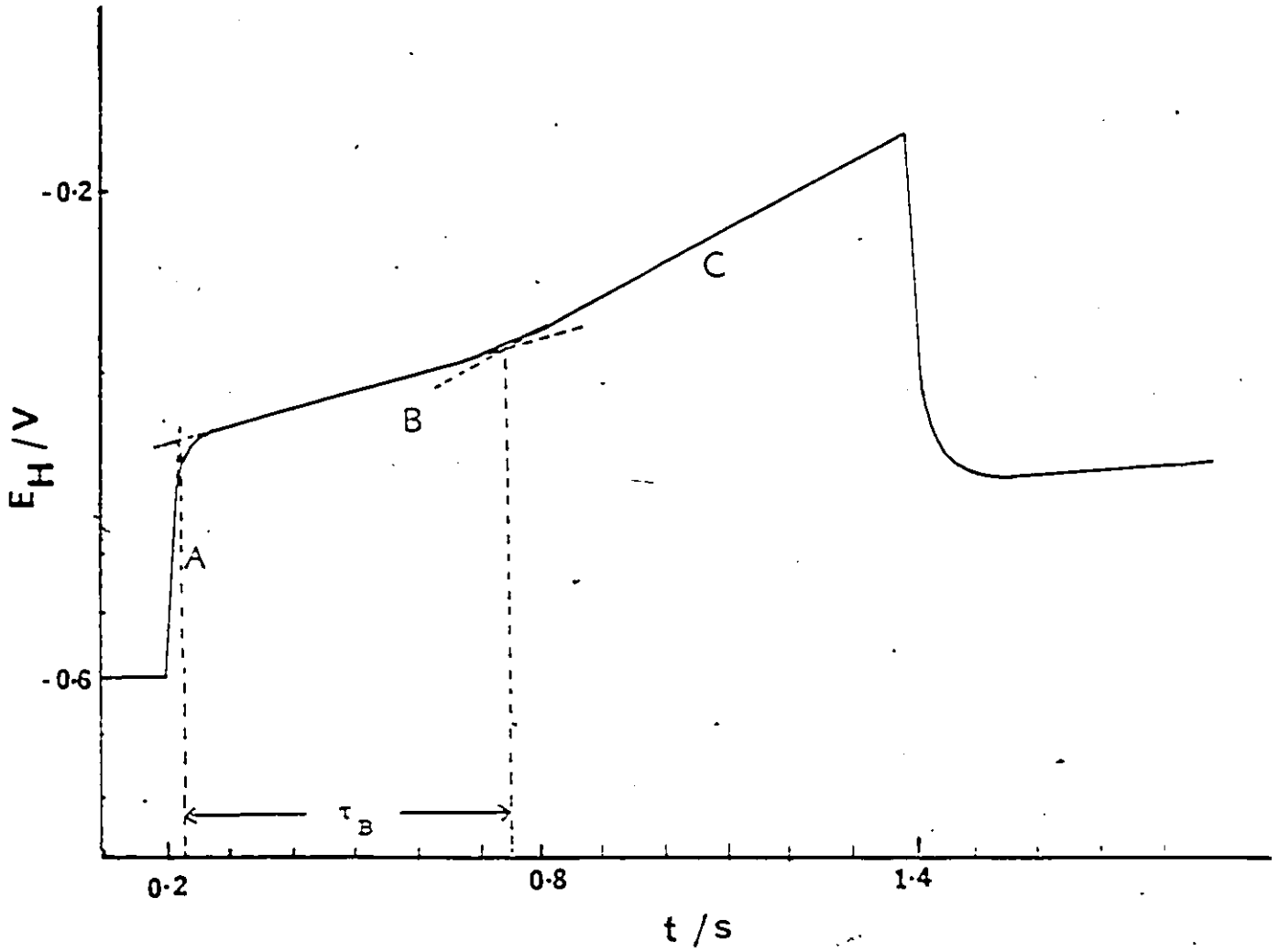

Fig. 4.2 Galvanostatic polarization E_H-t curve for polycrystalline etched Zn electrode in 1M Na_2SO_4 solution of pH 11.5 at 0.7 mA cm^{-2} current density.

"plateau" behaviour in region B).

The region B and the corresponding reduction plateau in the cathodic trace is likely to be due to formation of Zn hydroxide /or oxide, because the reversible potentials for ZnO, $Zn(OH)_2$ am. and ε-$Zn(OH)_2$ are -0.429 V, -0.394 V and -0.422 V, respectively (page 68) and those values lie between the potentials of the oxidation and reduction plateau.

The transition time (τ) multiplied by the constant current I applied gives the charge required to passivate the electrode surface. Ideally the quantity of charge required for passivation is independent of the applied current,* but this is not always the case.

Sand [147] derived the equation relating transition time to current for a diffusion-controlled electrochemical process. For this case $I\tau^{1/2}$ rather than I is a constant:

$$I\tau^{1/2} = \frac{\pi^{1/2} z F A D^{1/2} C}{2} \qquad (54)$$

where I is the electrolysis current, z the number of electrons involved in the electrolytic reaction, D is the diffusion coefficient of the of the electroactive species and C the concentration of the electroactive species.

A diffusion-controlled process has a slope -2 for a log τ vs log I plot, while the slope is -1 for a surface process (cf. the peak current vs sweep-rate relation in cyclic-voltammetry in chapter 3).

---

* This corresponds to i/s being constant in a cyclic voltammetry peak for a surface process (see chapter 3).

The transition time was measured as a function of the charging current I for a Zn single-crystal (0001) face and for polycrystalline (unetched and etched) zinc electrodes in 1M Na_2CO_3 and 1M Na_2SO_4 solution at pH 11.5. Fig. 4.3a shows logτ vs log i plot for the Zn single-crystal (0001) face in SO_4^{2-} solution while in Fig. 4.3b shows results obtained for the unetched polycrystalline surface in 1M Na_2SO_4 solution are shown. Plots (1) and (2) correspond to data from the first and the second run.

Table 4.1 summarizes the charges required for passivation in region B and the slopes of the log τ vs log i plots. It is seen that the charge required for passivation of the Zn (0001) face in Na_2SO_4 solution in region B is almost constant and corresponds to a monolayer (compare the CV results, Fig. 3.28 for these conditions). This result is to be compared with that for the Zn (0001) face in CO_3^{2-} solution where the oxidation charge density is higher at lower current-densities than at higher. It is also found that, in the first run, for unetched, the electrode surface is not completely covered with ZnO/ or $Zn(OH)_2$ (refer to Table 4.2). Both the (1) and (2) plots (Fig. 4.5) recorded for the unetched surface have a slope of -1.5* at low current densities and a slope of -1 at higher current-densities. This means that under the latter conditions the oxidation process is completely controlled by a surface reaction whereas at the lower current densities interpretation of the behaviour is unclear.

---

* This value corresponds to the slope of 0.75 ± 0.02 found in plots of log i_p vs log s in the CV experiments (Chapter 3).

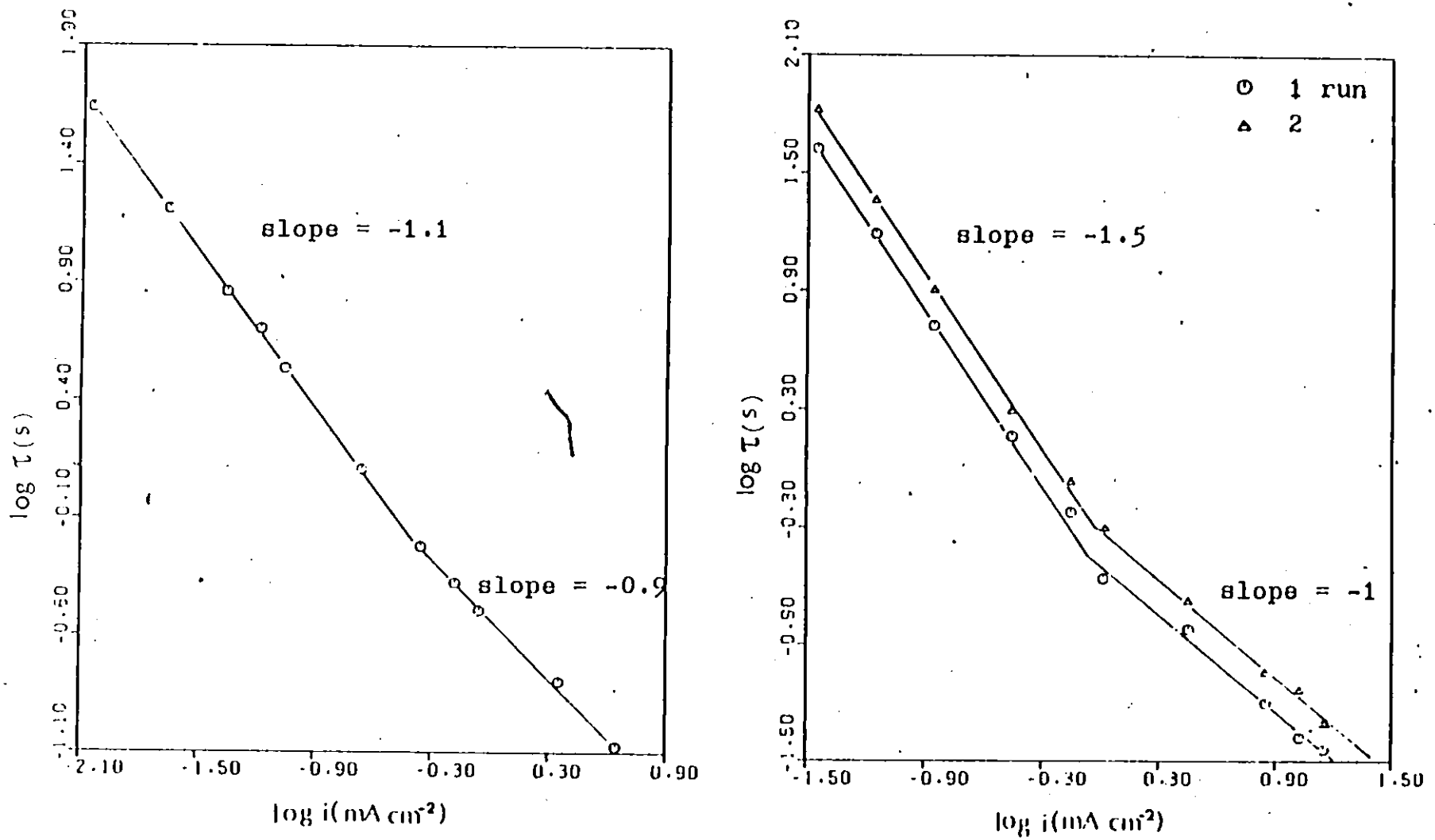

Fig. 4.3 Log τ vs log i relationship for (a) Zn (0001) (b) unetched polycrystalline Zn electrode in 1M Na_2SO_4 solution at pH 11.5.

Table 4.1

q_B and Slopes of log τ vs log i Plots for Single-Crystal (0001) Face and Unetched Polycrystalline Zn Electrodes

1.) Single crystal (0001) Face of Zn

	1M Na_2CO_3 solution, pH 11.5		1M Na_2SO_4 solution, pH 11.5	
Current Density i_2 /μA cm^{-2}	q_B/μC cm^{-2}	slope of log T vs log i	q_B/μC cm^{-2}	Slope of log T vs log i
9	---		387	
22	2746		361	
44	1557		320	1.1
66	——		335	
88	——		304	
221	1000	1.2	283	
443	920		268	
661	923		281	
885	——		286	
2213	——		358	0.9
4425	615		——	

Notes

1. Measurements were carried out in 1M Na_2CO_3 and 1M Na_2SO_4 at pH 11.5 for the Zn (0001) single-crystal electrode under galvanostatic conditions over a 9 μA cm^{-2} to 4425 μA cm^{-2} current density range and in 1M Na_2SO_4 solution at pH 11.5 for polycrystalline unetched and etched electrodes in the 10 μA cm^{-2} to 3x10^3 μA cm^{-2} current density range.
2. The polycrystalline electrode shows two regions in the log E vs log T plots and the results are reproducible, whereas for the single-crystal, only one region in both Na_2CO_3 and Na_2SO_4 media could be seen.

2.) Unetched Polycrystalline Electrode

	1M Na_2SO_4 solution, pH 11.5			
	Run I		Run II	
Current Density i_2 /μA cm^{-2}	q_B/μC cm^{-2}	slope of log T vs log i	q_B/μC cm^{-2}	slope of log T vs log i
10	---		632	
19	300		442	
39	204		308	
96	142	1.5	198	1.5
192	115		163	
289	112		142	
385	108		139	
962	——		162	0.9
1923	123		177	
2885	123		215	
3846	142		192	

3. Thicker films are obtained in CO_3^{2-} (2-8 layers) than in SO_4^{2-} solution (monolayer) for the Zn (0001) single-crystal while for the unetched polycrystalline Zn electrode the charge increased successively in the series of runs.

It is interesting to see whether there is any effect of rotation on the slope value of -1.5. Fig. 4.4 shows the effect of electrode rotation-rate on the log τ vs log i plot. It is seen from the results at 0 rpm rotation-rate that there is an effect of rotation on log τ vs log t plots other than that associated with roughening of the electrode . Fig. 4.5 shows the effect of current on the capacitance (the slope dq/dE) in the passivation region B at rotation-rates of 0 and 900 rpm. It is seen that the capacitance decreases rapidly with current and becomes independent of current at current-densities greater than 220 $\mu A\ cm^{-2}$. Similar experiments were carried out on the Zn (0001) face but, from a cyclic-voltammogram that was recorded after the series of galvanostatic experiments, it was evident that surface roughening had taken place.

Kausche[73] observed constancy of the product $i\tau^{3/2}$ with varying i for a Zn electrode in 1M Na_2CO_3. Frank et al.[74] obtained similar results with various other systems as summarized in Fig. 1.7. This unusual behaviour was explained in terms of diffusion-controlled supersaturation. Kausche believed that an adherent layer of solution, ca. 10^{-3}cm in thickness, near the electrode would become supersaturated after charging with several $\mu C\ cm^{-2}$ and considered that transport of zincate ions into the bulk of the solution, "other than by diffusion" could be suppressed. He also thought that the assumption made by Frank that "the thickness of the oxide nuclei decreases with increasing current density, due to increasing supersaturation," is not applicable to this case because oxide is formed at an early stage in the charging curve.

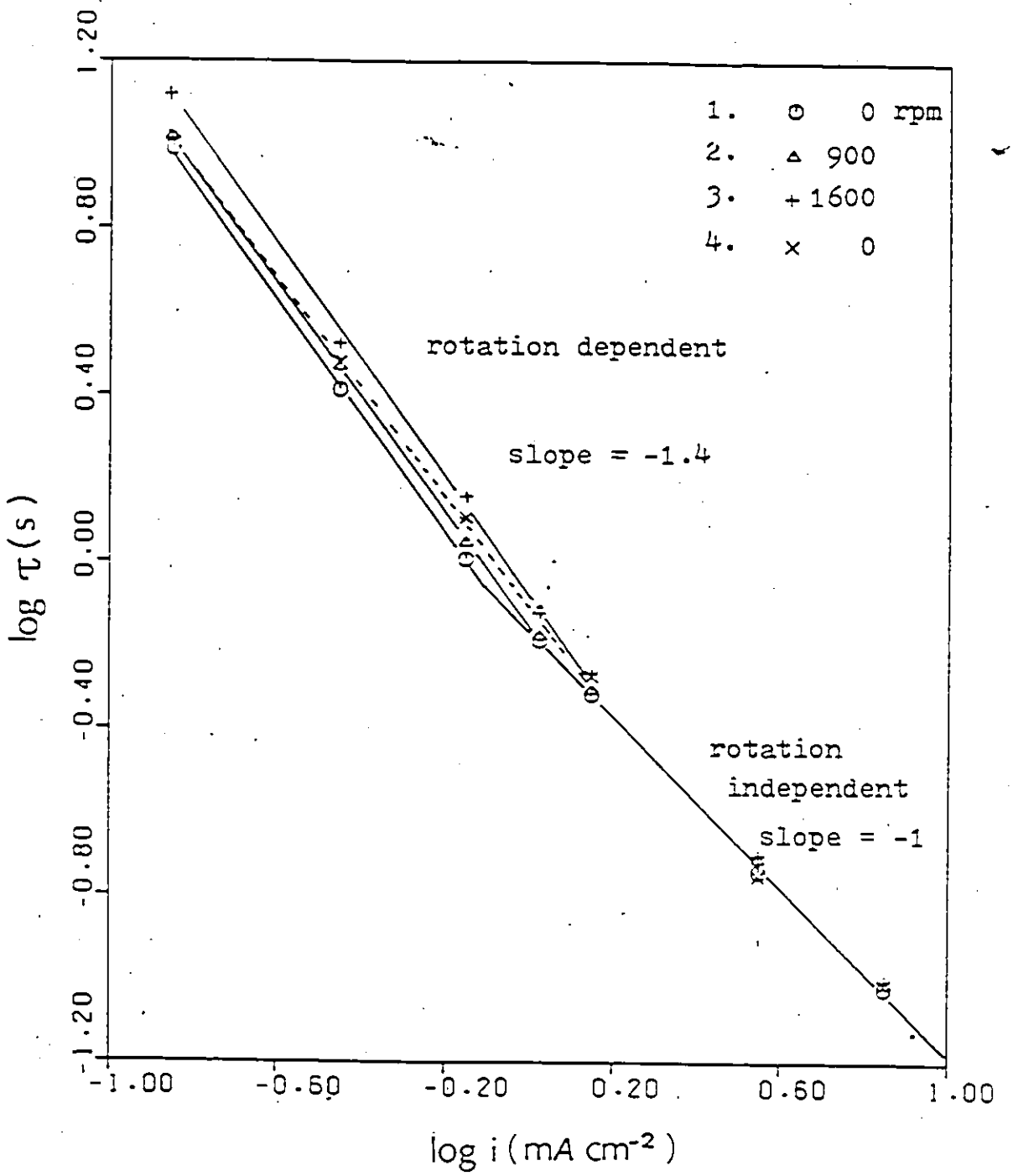

Fig. 4.4 The effect of rotation on the dependence of log τ on log i in 1M Na_2SO_4 solution at pH 11.5.

Electrode - RDE, of apparent area of 0.07 cm^2 and etched in HBr.

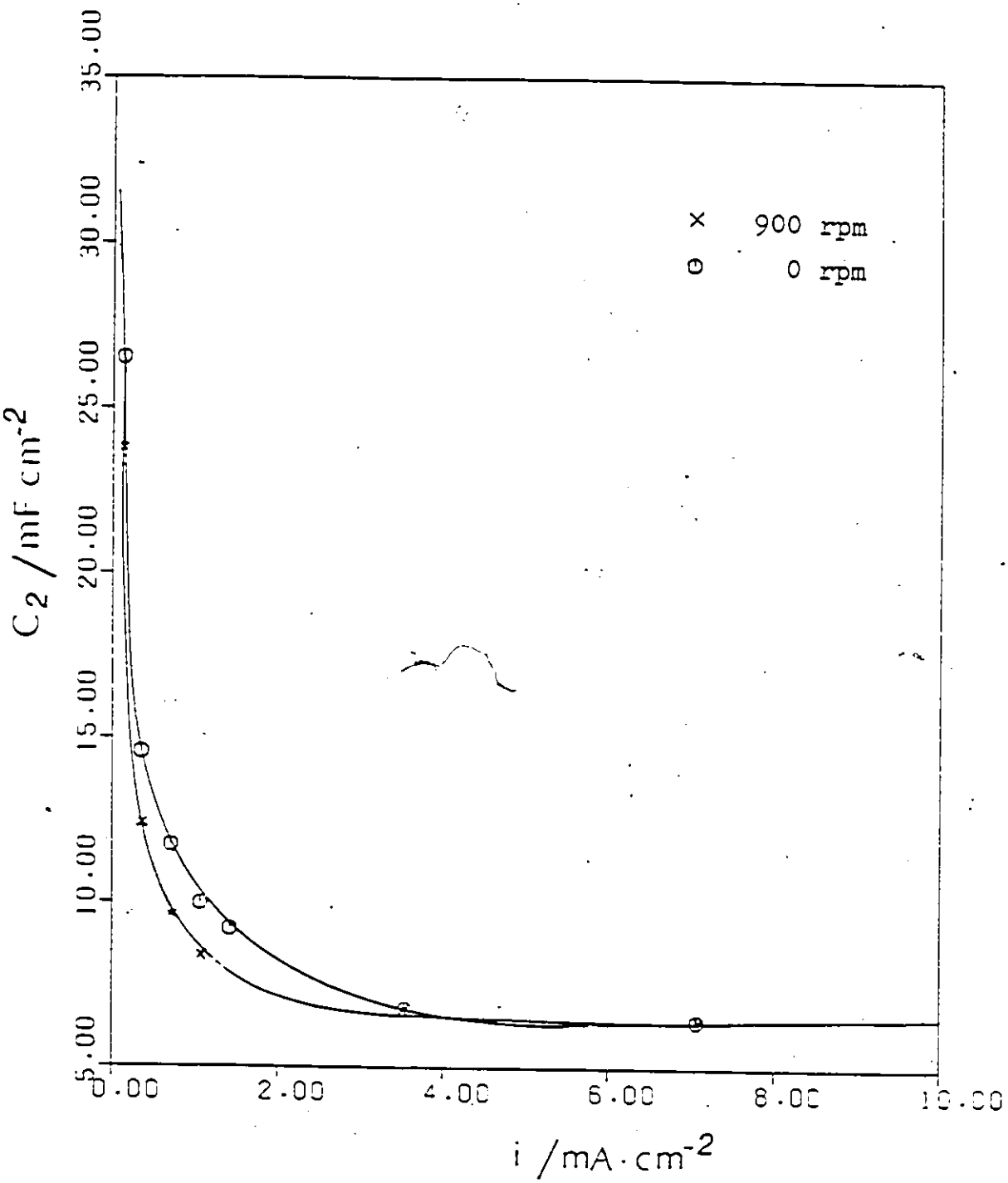

Fig. 4.5 Dependence of C_2 on i for polycrystalline etched electrode in 1M Na_2SO_4 solution at pH 11.5; ω=0 and 900 rpm.

This situation is exactly the same as that for the cyclic-voltammetry experiments, the slope of the log i_p vs log s relation (e.g. see Table 3.4) was 0.75 for 1M Na_2CO_3 at pH 11.5, i.e. between the limiting values of 1 and 0.5 expected for a surface process and a diffusion controlled process, respectively.

Now the question arises whether the slope of -1.5 for the log τ vs log i plots means that the transition time behaviour for these cases corresponds to two parallel processes, i.e. diffusion-control and surface reaction, as treated in eqns. (52) and (53).

If in this case

$$I = \frac{k_3}{\tau} + \frac{k_4}{\tau^{\frac{1}{2}}} \qquad (55)$$

where k's are some arbitrary proportionality constants having the correct dimensions, as in equations (52) and (53). Equation (55) can also be expressed either as

$$i\tau = k_3 + k_4\tau^{1/2} \qquad (56)$$

or

$$i\tau^{1/2} = k_3\tau^{-1/2} + k_4 \qquad (57)$$

Fig. 4.6 shows $i\tau$ vs $\tau^{1/2}$ and $i\tau^{1/2}$ vs $\tau^{-1/2}$ plots obtained for an etched polycrystalline Zn surface with rotation at ω = 900 rpm.

It is clear from these results that the slope value of -1.5 for the log τ vs log i plot is likely to be due to a process under mixed-control, which is consistent with the deduction from

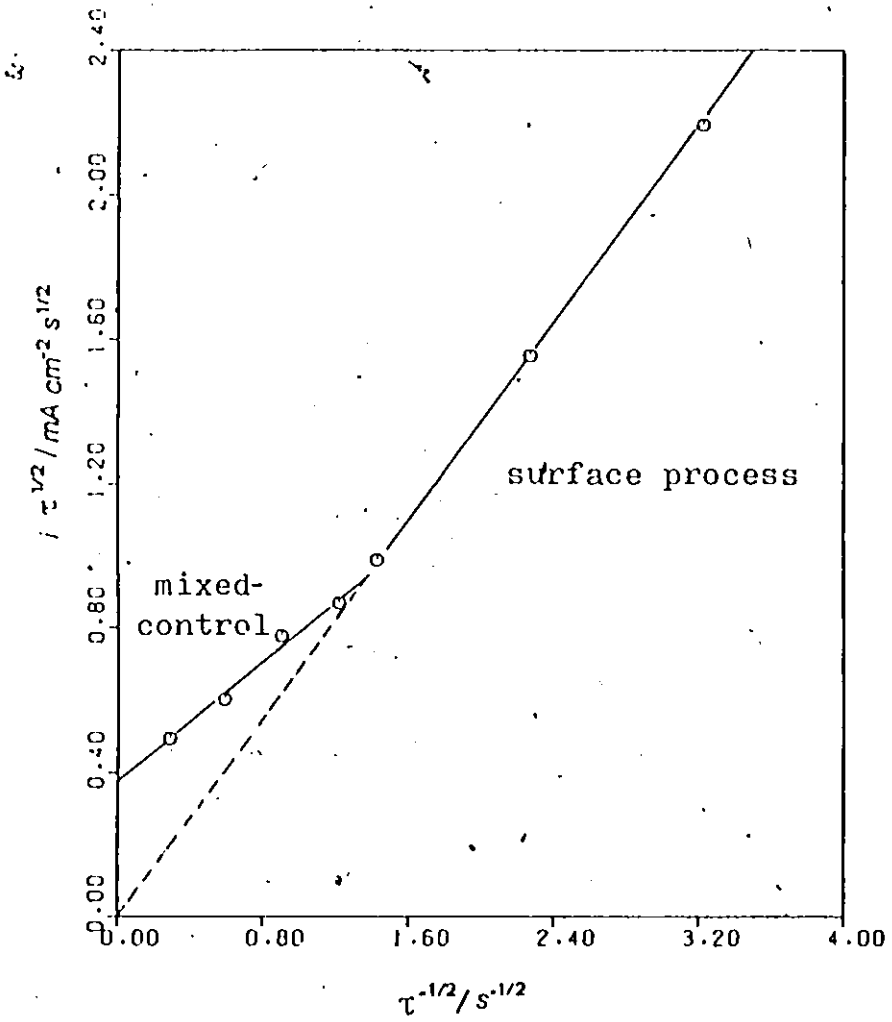

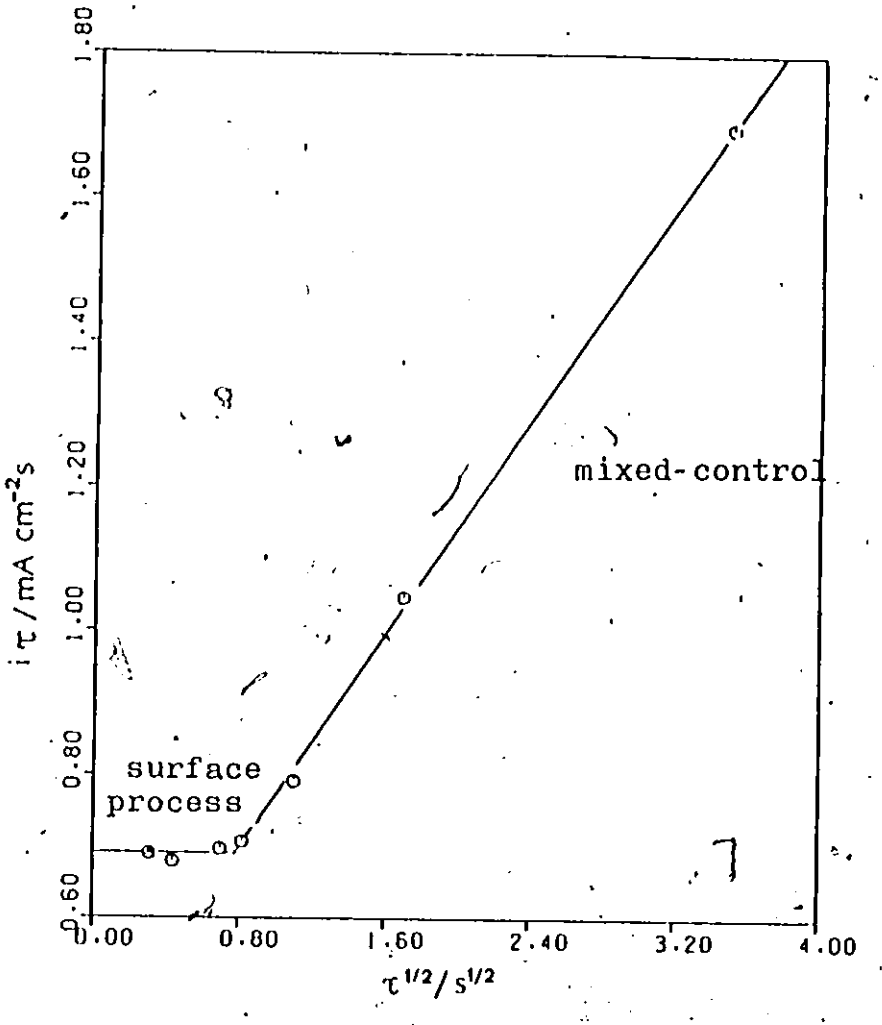

Fig. 4.6 Plots of (a) $i\tau^{\frac{1}{2}}$ vs $\tau^{-\frac{1}{2}}$ and (b) $i\tau$ vs $\tau^{\frac{1}{2}}$ for an etched Zn electrode in 1M Na_2SO_4 solution at pH 11.5 and 900 rpm.

the cyclic-voltammetric experimental results, page 97. Table 4.2 summarizes the slopes of the log τ vs log i relations and the derived thicknesses of oxide/ hydroxide films formed in region B.

It is clearly seen that more roughening occurs in the galvanostatic experiment than in the CV method, and a complete oxide monolayer is formed on the etched surface while at the unetched surface, only a fraction of the electrode area is covered and the apparent extent of coverage becomes increased with the number of runs (micro-roughening effect).

It seems likely that, at lower current-densities, dissolution of Zn oxide/hydroxide leads to the slope of -1.5 whereas at higher current densities there is no time for ZnO/or $Zn(OH)_2$ to dissolve. This is also clear from the measurements of capacitances of region B (Fig. 4.5) at $\omega = 0$ and $\omega = 900$ rpm which show that the capacitance decreases with increase in current-density.

4.3 Other Regions of the Galvanostatic E vs t Profile

When the current is reversed from the oxide forming anodic direction to a cathodic direction the deposited Zn oxide/ hydroxide (and some dissolved zinc) is reduced and the potential finally returns to that for hydrogen evolution. One way of studying the various regions observed in E vs t curves during charging is to change the upper limit of potential that is allowed to be attained in the E vs t plot before a reverse cathodic current pulse is applied. Fig. 4.7 shows such E vs t

Table 4.2

Comparison of the log i vs log i and $it^{\frac{1}{2}}$ vs $t^{\frac{1}{2}}$ Plots and Thickness of the Passivated Layer for Single-Crystal and Polycrystalline Electrodes

1M Na_2CO_3 pH 11.5	1M Na_2SO_4 pH 11.5			
Single-crystal (0001) face Area of the electrode = 1.13 cm^2 i = 22 - 4400 $\mu A\ cm^{-2}$	Single-crystal (0001) face Area of the electrode = 1.13 cm^2 i = 88 - 9000 $\mu A\ cm^{-2}$	Polycrystalline - unetched electrode Roughness factor - 3.5 Apparent area - 0.07 cm^2		Polycrystalline - etched electrode Roughness factor - 2 Apparent area - 0.07 cm^2
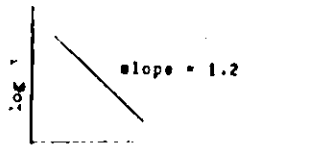		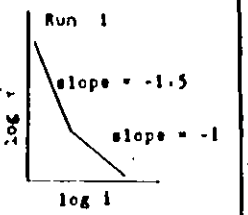	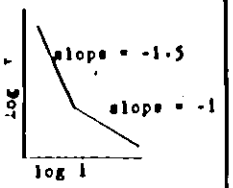	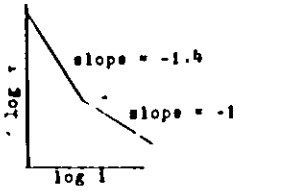
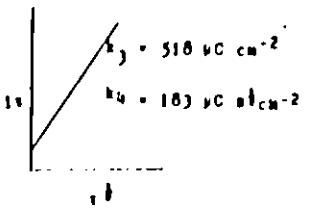	k_1 = 312 $\mu C\ cm^{-2}$	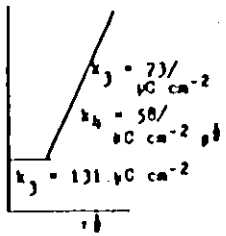	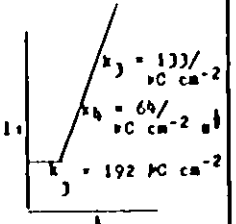	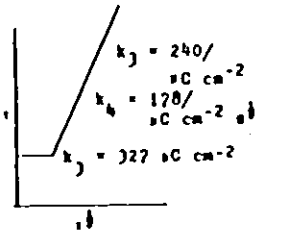
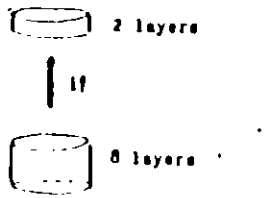	 100% surface process	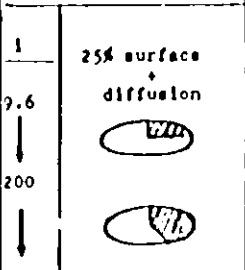	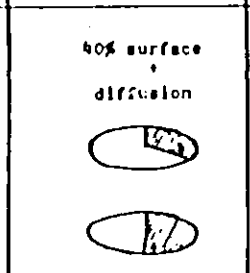	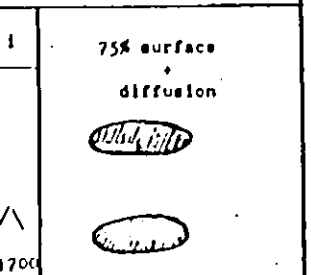

plots obtained for Zn in 3M K_2CO_3 solution with a progressively increasing potential limit in the anodic E vs t profile. Reversal of current in the region C gives only one potential arrest in the cathodic transient but for reversal following region C, two stages of reduction are observed (Fig. 4.7). Another region (G), in between regions F and H, can be identified if the current is reversed in region E.

It seems likely that the first process (region H) is due to reductin of ZnO/ $Zn(OH)_2$ formed in regions B and C of the anodic transient. It was seen that region C consists of two straight lines with various slopes. These two linear parts observed in region C probably correspond to peak A_2 and the plateau region observed in the cyclic-voltammogram for 1M Na_2CO_3 solution at pH (Fig. 3.1).

The arrest following region C, and the second reduction process (F) arising at lower overpotential, may be due to the reduction in region F of ZnO/ $Zn(OH)_2$ that had been formed with presence of excess Zn.

It can be seen that after passing through the region C, the Q_C/Q_A charge ratio is much less than 100% and also, in the region E, a steady-state is reached. The third reduction stage (G) observed in reversing the current in the region E increased (in charge) with time that the constant current had been applied with the potential being in the O_2 evolution region. This is due to growth of a non-conducting zinc-oxide film. This situation is similar to the case observed in Fig. 3.38 where the CV peak C_2 was increased with increased anodic holding time. It seems likely that the regions F, G and E correspond to the peaks C_4,

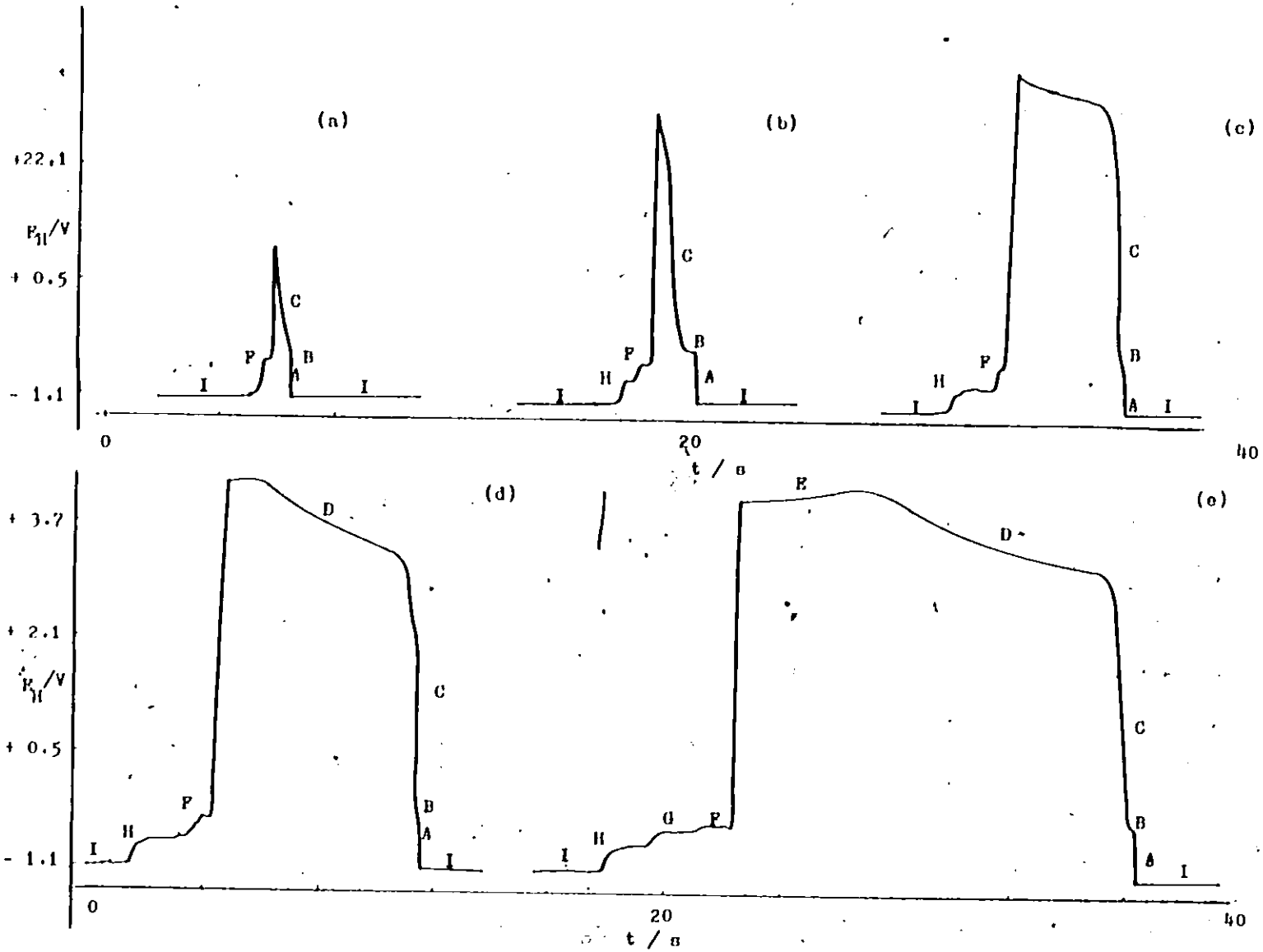

Fig. 4.7 Series of charging curves obtained at a current density of 14 mA cm^{-2} for an etched Zn electrode in 3M K_2CO_3 at pH 13.3 with progressively increasing potential limit in the anodic direction.

(see following page for charging curve 4.7 f)

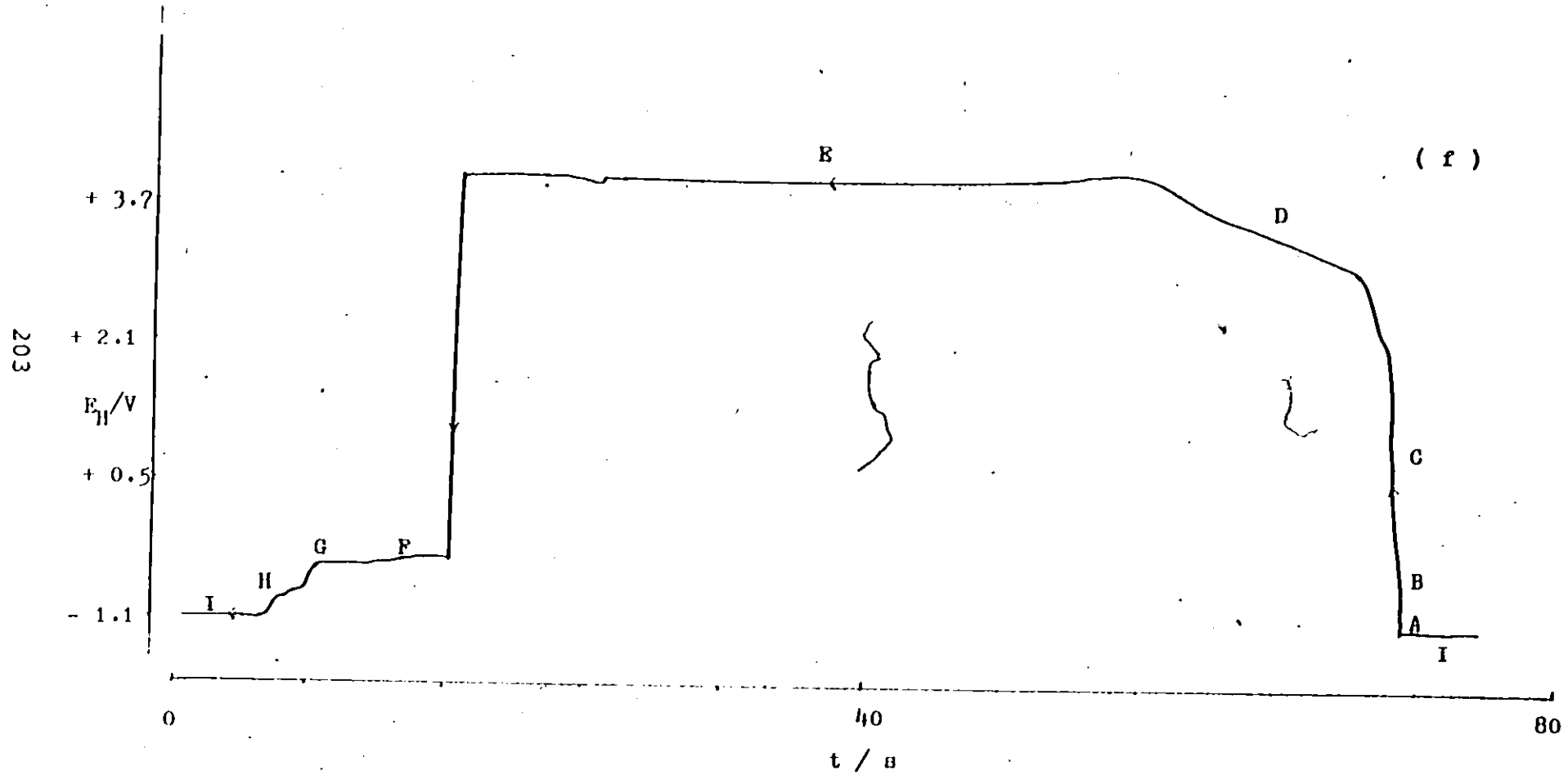

Fig. 4.7 (f) .

C_2, and C_1 observed in the cyclic-voltammetric experiments in 1M Na_2CO_3 + 2M NaCl solution at pH 11.5.

Fig. 4.8 shows the state of the Zn electrode after a series of galvanostatic anodic charging and cathodic discharging current pulse. The surface is evidently covered with a thick porous film which may be non-conducting; the darker regions that are seen may be due to redeposited Zn, with excess Zn in the oxide film.

Kaesche[73] had observed three cathodic regions for reduction of oxidized Zn in 1M Na_2CO_3 solution at pH 11.5. It was assumed that these regions were due to reduction of ZnO, observed molecular oxygen and zinc peroxide. However, Kaesche states that the assumption of the presence of zinc peroxide is open to question because Huber et al.[78] have shown that ZnO is the only species formed in a prolonged experiment on oxide film development studied by means of X-ray and electron diffraction, and electron microscopy methods.

Fig. 4.8 The state of a polycrystalline etched Zn electrode after series of galvanostatic charging and discharging in 3 M K_2CO_3 solution at a current density of 14 mA cm^{-2}. (Fig. 4.7 shows the E vs t curves obtained.)

4.5 Summary

A typical potential/time curve for Zn oxidation/reduction has four anodic regions (A, B, C, D and E) and four cathodic regions (F, G, H and I). A corresponds to double-layer charging. B is a plateau-region due to passivation of the electrode, which is followed by oxide growth (region C). Simultaneous O_2 evolution occurs beyond region C, in regions D and E. Region I is due to the H_2 evolution reaction region. B corresponds to the A_1 peak in cyclic-voltammetry, and region C corresponds to oxide growth in the A_1 and A_3 peaks. Regions F, G and H correspond to C_4, C_2 and C_1 respectively in the CV experiments in 1M Na_2CO_3.

Region B

1. The region B and the corresponding reduction plateau (region H) in the cathodic trace is likely to be due to formation of $Zn(OH)_2$ or ZnO, as shown by correspondence with the calculated reversible potentials for ZnO, $Zn(OH)_2$ am. and ε-$Zn(OH)_2$.

2. The charge required for passivation of the Zn(0001) face in 1M Na_2SO_4 at pH 11.5 in region B corresponds to a monolayer. In CO_3^{2-} solution the charge corresponds to more than a monolayer.

3. The slope of log τ vs logi plots is -1.5 at lower current densities and -1 at higher current densities for an unetched or etched polycrystalline electrode in 1M Na_2SO_4 at pH 11.5. There is some dependence of the value of the slope of -1.5 on rotation rate.

4. The slope of - 1.5 for log τ vs. log i plots does not correspond to pure diffusion control (-2) or pure surface control (-1), and is thus likely to be due to a process under mixed-control. Plots of $i\tau^{1/2}$ vs $\tau^{-1/2}$ are linear, suggesting the relationship $i = \frac{k_3}{\tau} + \frac{k_4}{\tau^{\frac{1}{2}}}$, analogous to the relationship $i_p = k_1 s + k_2 s^{1/2}$ found in cyclic-voltammetry. At lower current densities there is more time for $Zn(OH)_2$ or ZnO formed at the electrode to be dissolved, but at higher current densities diffusion is relatively less important and the oxidation is mainly a surface process.

CHAPTER 5

Steady-State Experiments With the Zn Electrode

5.1 Introduction

The purpose of this section of the work was to provide some complementary information on the nature of the zinc dissolution reaction in NaCl, Na_2SO_4, NaOH and Na_2CO_3 solutions at various pH's and at various Zn surfaces by means of the steady-state method.

In the steady-state method, the potential is progressivly raised (or lowered) by a potentiostatic circuit, or the current density is increased (or diminished) by a galvanostatic one, and the rate of reaction is measured directly in terms of current, I, as a function of potential, E, or overpotential, η, (or E as a function of I). In certain favourable cases, the reaction mechanism can be elucidated by determining the values of the Tafel slope b (= dE/d log I), because it depends on parameters which are determined by the reaction mechanism.

In the present work, the Tafel slopes have been determined in an exploratory way from log i vs E curves obtained by the potentiostatic method for the anodic direction of potential change for the Zn electrode. However, owing to the complexity of the process involved, as demonstrated by the nonsteady-state experiments described in earlier sections of this thesis, interpretation of steady-state results can be anticipated to be difficult, if only for the reason that partial diffusion-control is antici-

pated.

5.2 The Effect of pH

Fig. 5.1 shows an anodic polarization curve obtained for Zn in 1M Na_2CO_3 solution at pH 11.5. It can be seen that there is no straight line section in the whole of the polarization curve from which to recognise or evaluate a Tafel slope. IR-drop effects leads to a distortion of steady-state polarization curves, but this effect can be neglected in the present results, as discussed in section (2.2.5).

The reason for the complex behaviour is that there is no simple activation-controlled dissolution process, where an anodically dissolved cation readily moves away from the metal/ solution interface. This movement is in fact a diffusion-controlled process and, under the present conditions, the electrode can also become passivated so that $ZnO/Zn(OH)_2$ forms on the electrode and only partly dissolves, depending on the pH. A further increase in anodic dissolution rate therefore becomes more difficult and requires a disproportionate rise in anodic overpotential, giving rise to the so-called passivation phenomenon.

As was shown in Fig. 1.5, the lowest corrosion rate arises within the pH range 9 to 11; it was therefore considered interesting to carry out steady-state measurements at pH's higher or lower than 11.5.

Figs. 5.2 and 5.3 show the log i vs E curves obtained for ascending and descending directions of potential change in 3M NaCl and 1M Na_2CO_3 solution at pH 13.5 using an etched electrode.

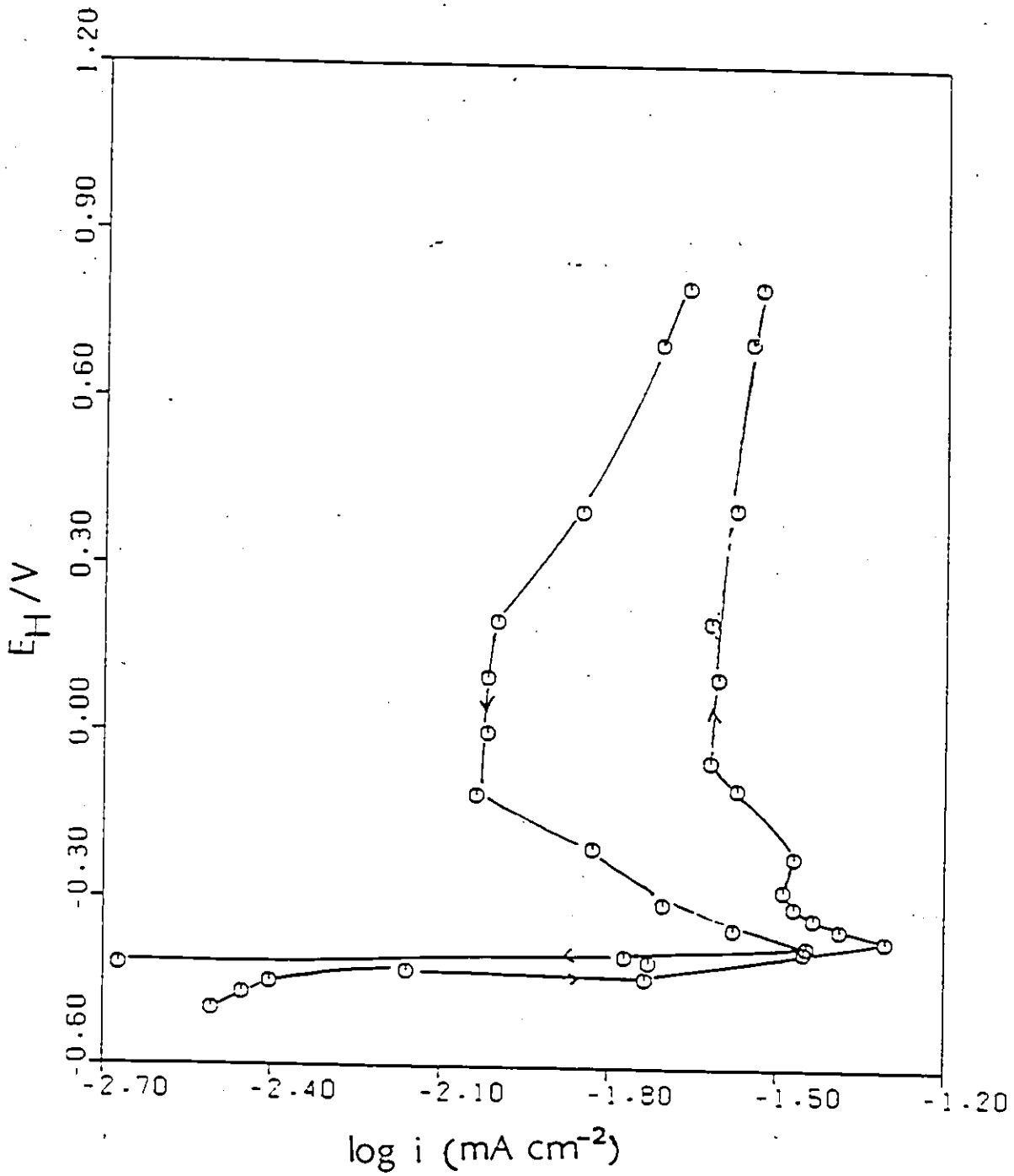

Fig. 5.1 Steady-state anodic (ascending/descending) polarization curve for an etched Zn electrode from 1M Na_2CO_3 solution at pH 11.5.

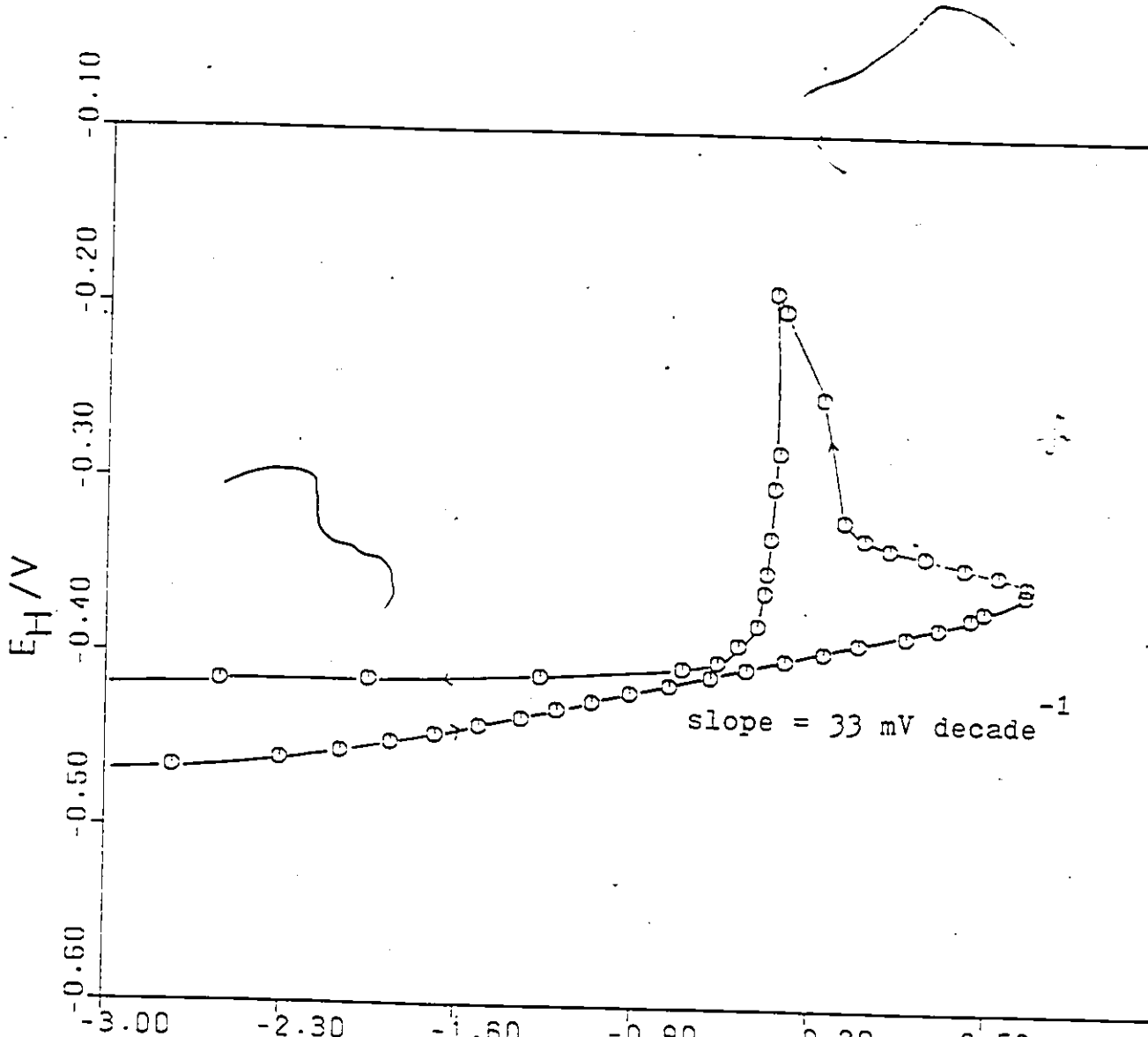

Fig. 5.2 Steady-state anodic polarization curve for an etched Zn electrode in 3M NaCl at pH 13.5.

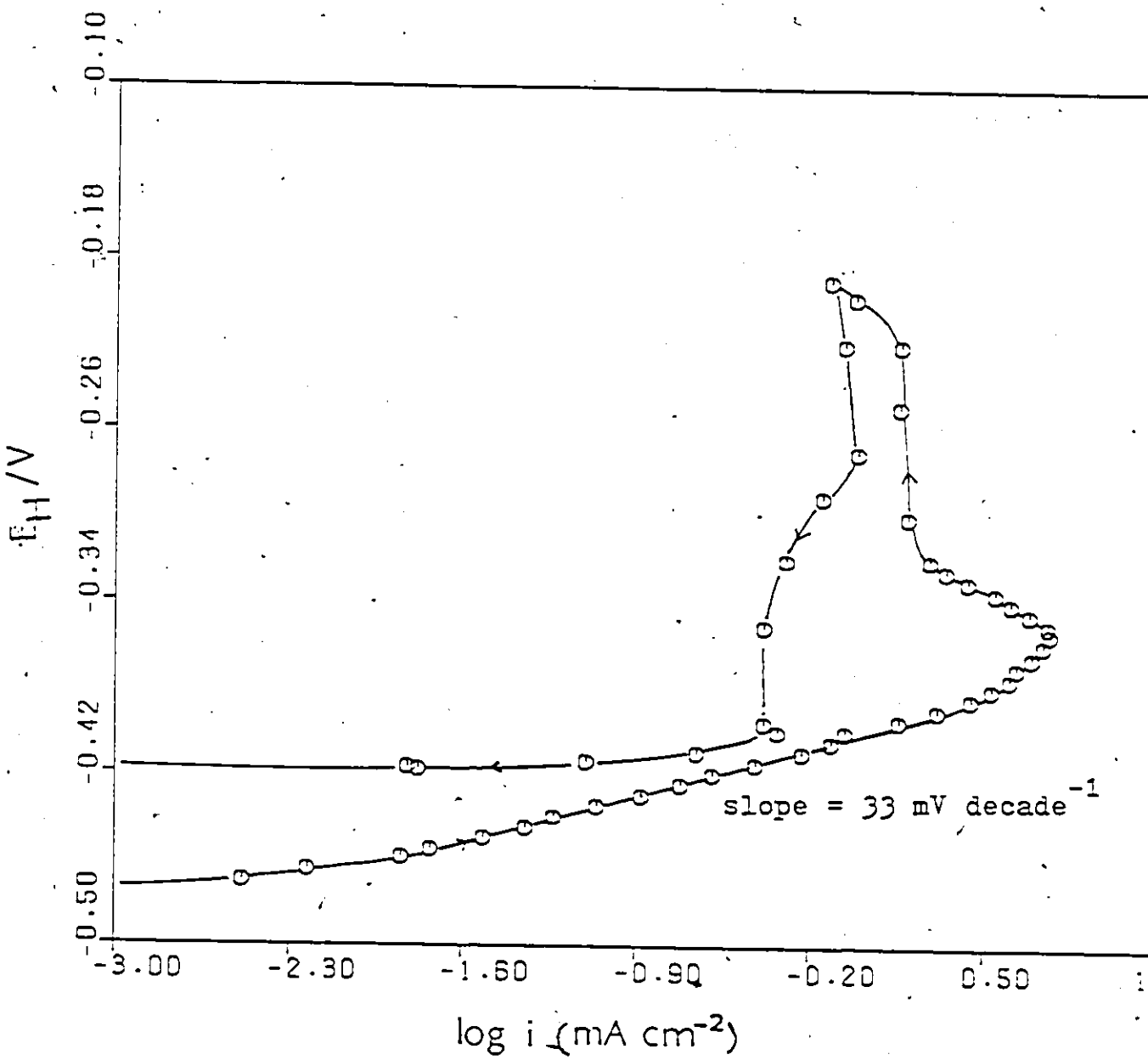

Fig. 5.3 Steady-state anodic polarization curve for an etched Zn electrode in 1M Na_2CO_3 at pH 13.5.

Such curves obtained in 1M Na_2SO_4 at the same pH were similar to that for 3M NaCl. The main difference between the curves obtained with CO_3^{2-}, in relation to SO_4^{2-} or Cl^- electrolytes, was the sudden breakdown of the passive film in the latter two solutions, a phenomenon also seen in the cyclic-voltammetry experiments (Fig.3.1). Also the transition charge required for onset of passivation is higher in CO_3^{2-} solution than in SO_4^{2-} or Cl^- solutions.

Fig. 5.4 shows the log i vs E curves obtained for Zn in 1M Na_2CO_3 solution at pH 13.5, where the anodic current was reversed before the passivation started. It is seen that the ascending and descending curves were virtually superimposible so that the surface had not changed. Fig. 5.5 shows log i vs E curves obtained in 1M Na_2SO_4 solution at pH 13.5 for etched electrodes after many runs: the current evidently does not change very much. From these results it can be seen that ZnO /or $Zn(OH)_2$ formed during passivation does not dissolve into solution rapidly but stays, rather, on the electrode surface as was concluded from the CV experiments.

Fig. 5.6 shows the log i vs E curves obtained in 1M Na_2SO_4 solution at pH 8.1 for etched, unetched surfaces and cleaved Zn (0001) face. Under these conditions, the log i vs E curves are linear over two decades, unlike the behaviour at other pH's >11.5. The currents were more than 1.5 mA for a polycrystalline electrode with an area 0.071 cm^2; therefore polarization studies at pH 8.1 were carried out with an electrode having a smaller surface area of about 0.018 cm^2, as discussed in section (2.2.5). It can be seen from the SEM pictures (Figs. 5.8a, b and c) of

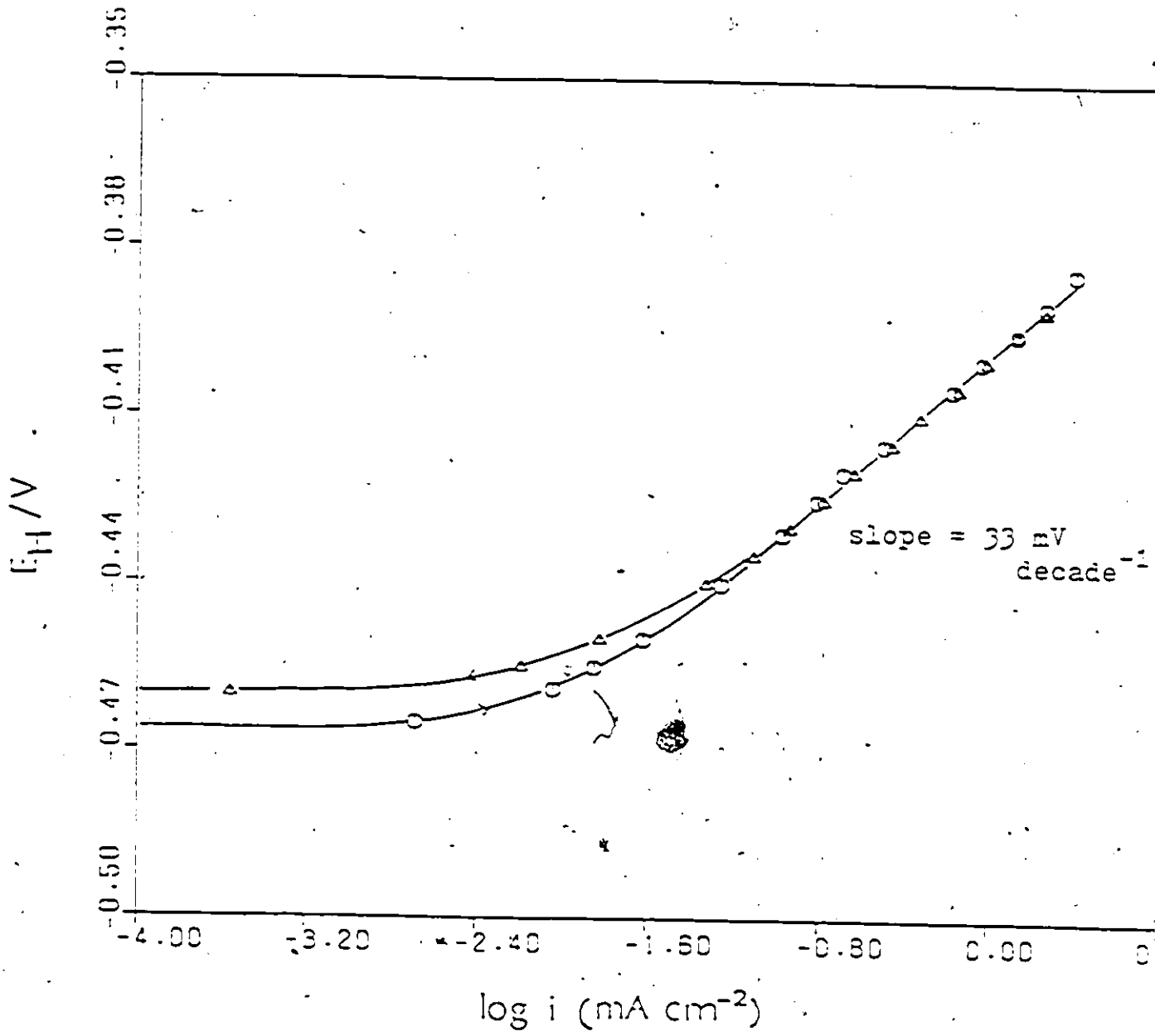

Fig. 5.4 Steady-state polarization curve (ascending/descending) for an etched Zn electrode in 1M Na_2CO_3 at pH 13.5.

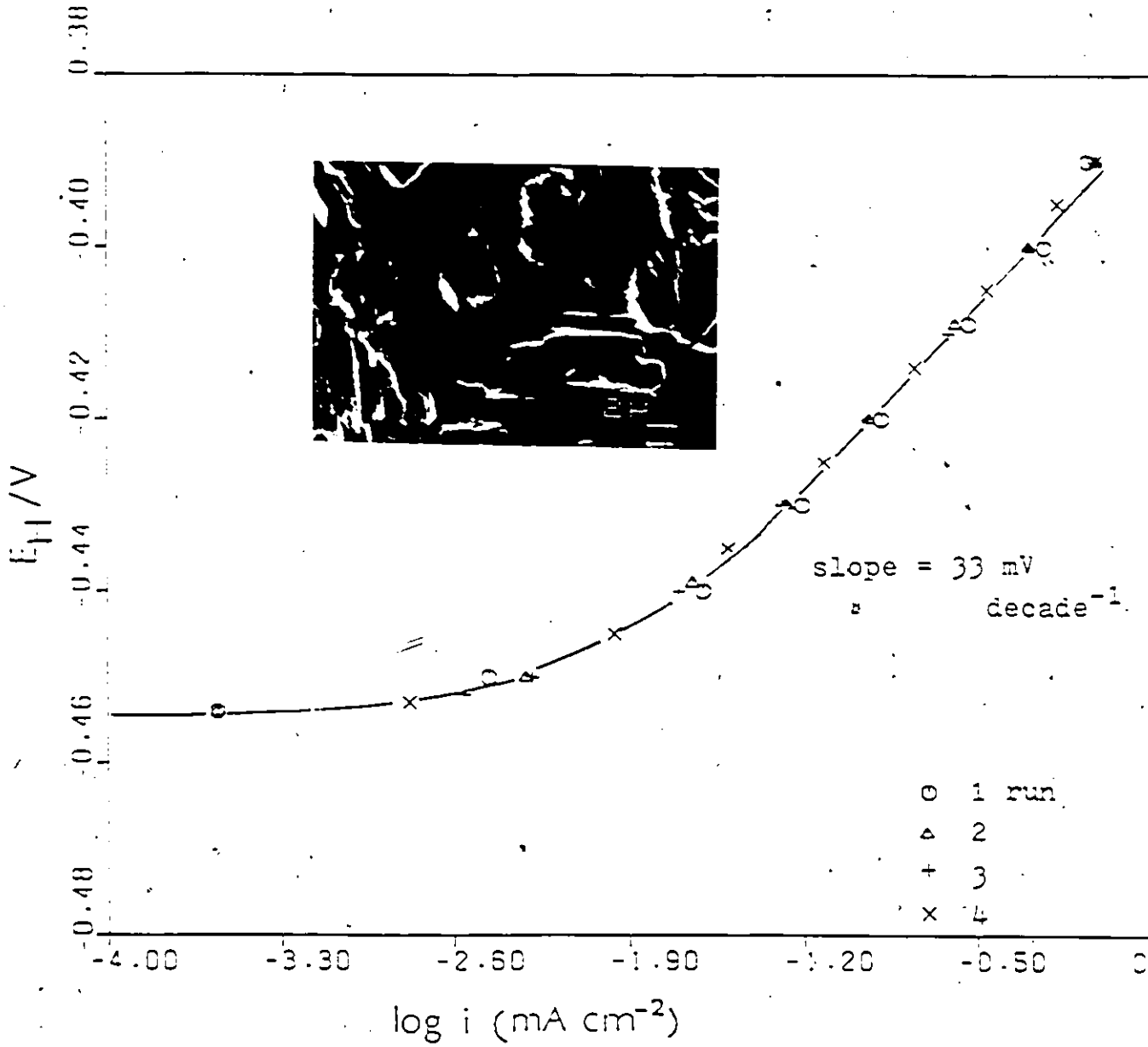

Fig. 5.5 Steady-state anodic polarization curves for an etched Zn electrode in Na_2SO_4 at pH 13.5 and the state of the electrode after four runs (SEM picture.)

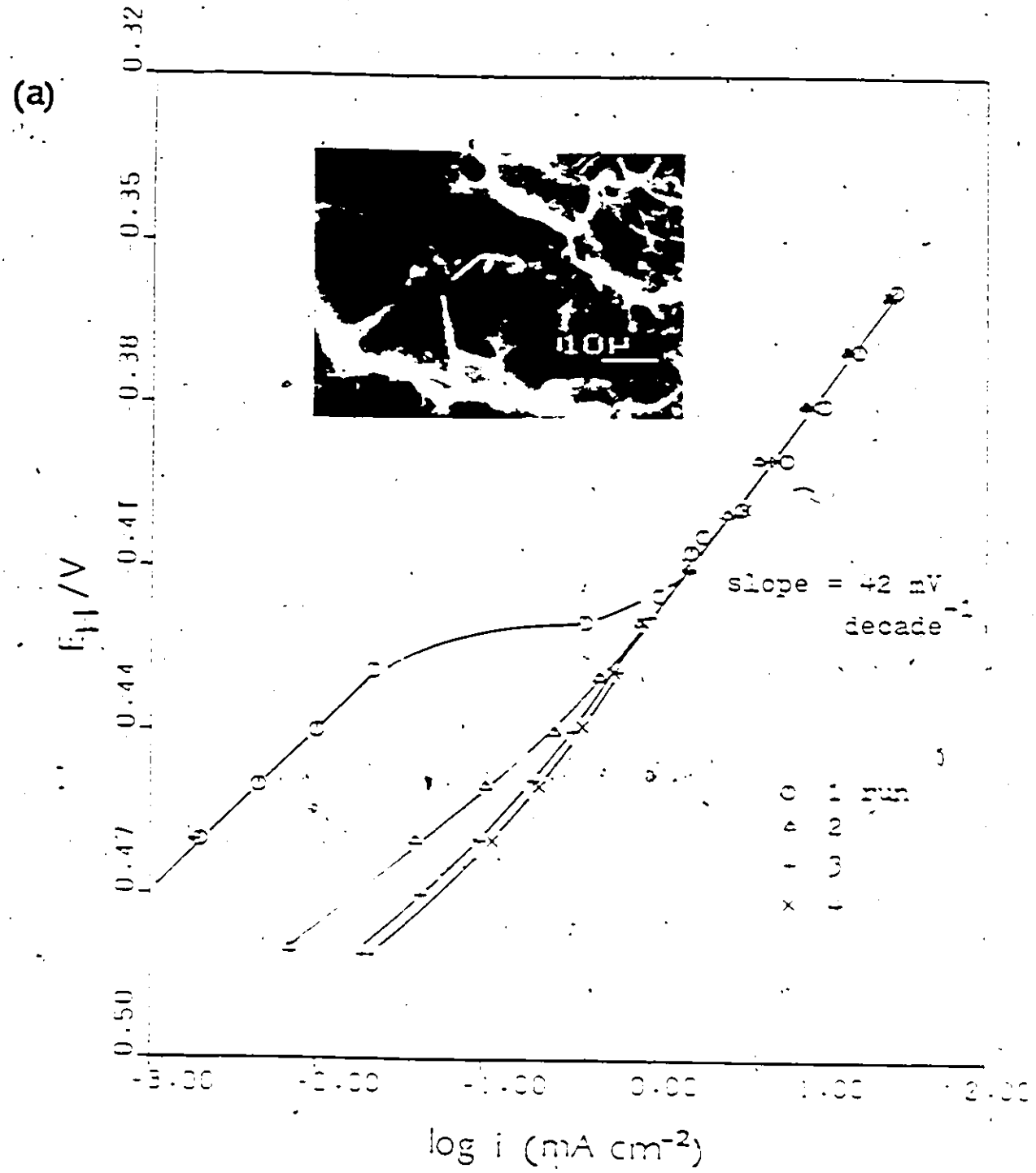

Fig. 5.6 Steady-state anodic polarization curve for Zn electrode in 1M Na_2SO_4 solution at pH 8.2 and the state of the electrode after four runs (SEM picture). (a) An etched electrode

(b) Unetched electrode,

(c) Zn (0001) face.

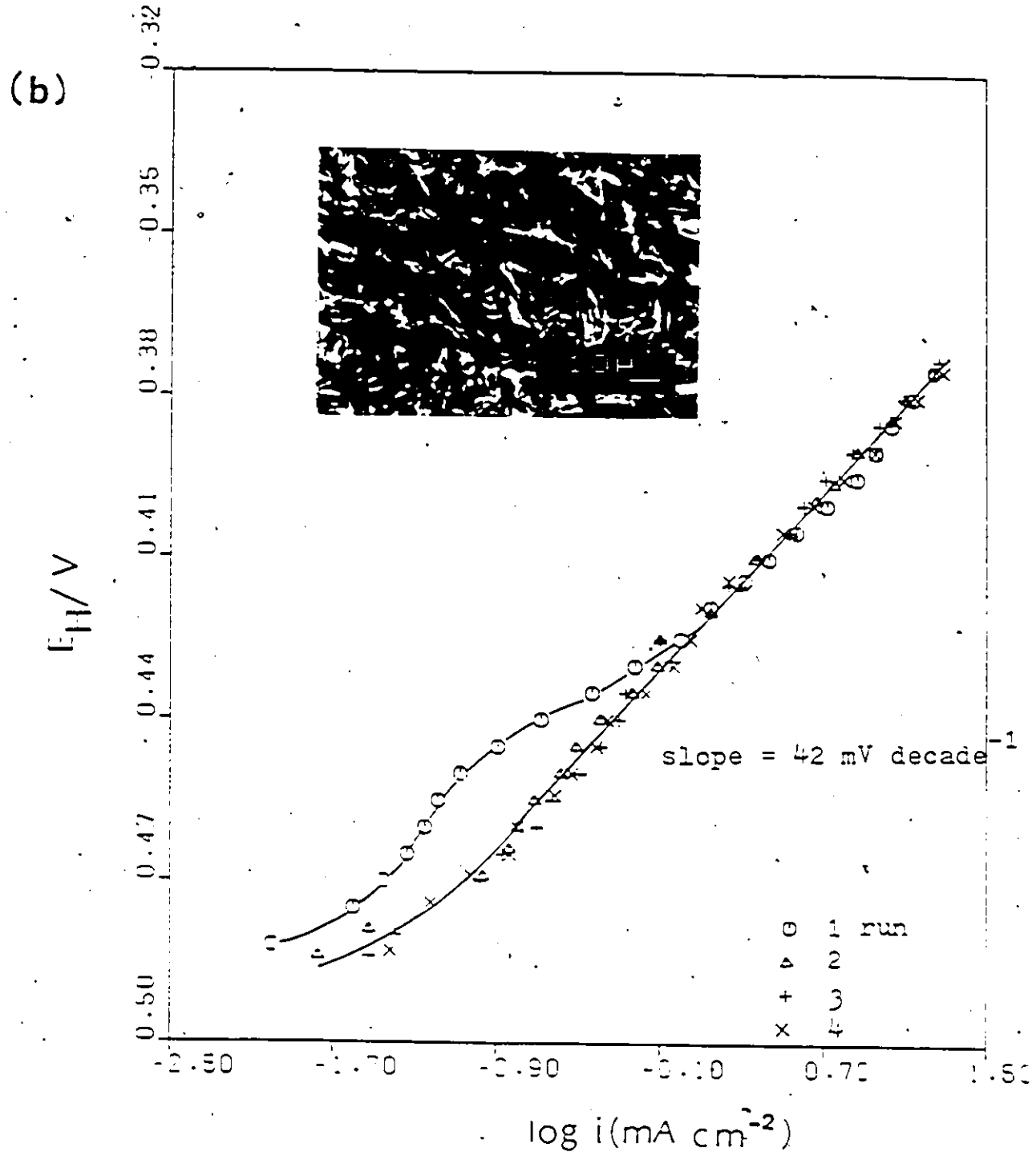
(b)
0.32
0.35
0.38
0.41
0.44
0.47
0.50
E_{H}/ V
slope = 42 mV decade^{-1}
1 run
2
3
4
log i(mA cm^{-2})

Fig. 5.6 (b).

(c)

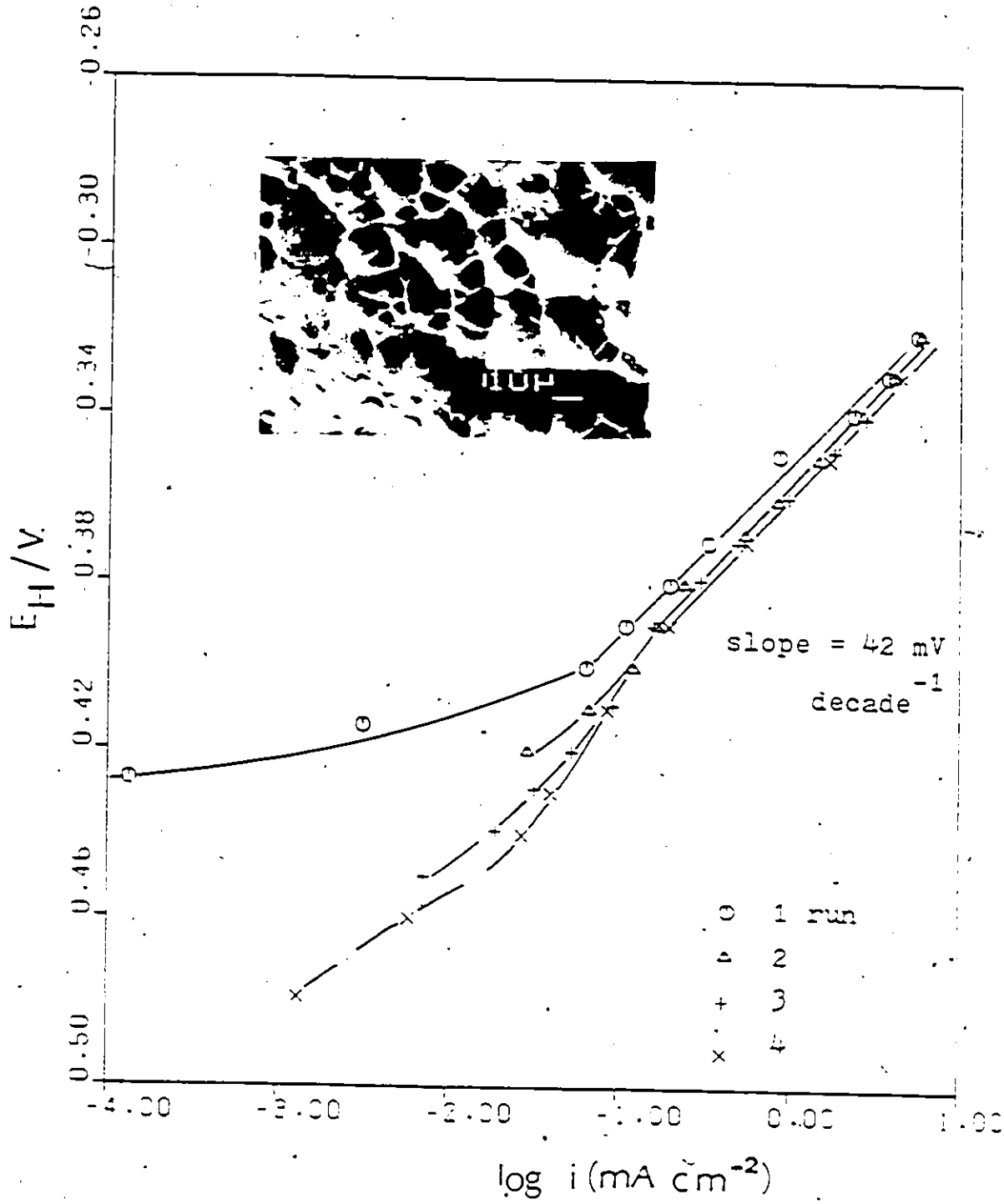
-0.26
-0.30
-0.34
-0.38
-0.42
-0.46
-0.50
E_H / V.
1 µm
slope = 42 mV decade^{-1}
○ 1 run
△ 2
+ 3
× 4
-4.00
-3.00
-2.00
-1.00
0.00
1.00
log i (mA cm^{-2})

Fig. 5.6 (c)

electrodes taken after their use in several steady-state measurements, that the surfaces have changed considerably; also it is clear from the polarization curves that the overpotential required for passage of given currents is higher for the Zn (0001) face than for polycrytalline electrodes (first run, Fig. 5.6c). Similar results were obtained by Ashton and Hepworth[43], i.e with regard to the effect of crystal orientation on the anodic dissolution of Zn single-crystals in NaOH solution (using steady-state measurements) and the dissolution overvoltages for Zn increase in the order (0001) > (1010) > (1120). Their polycrystalline electrode showed behaviour similar to that for the (1010) single-crystal plane.

5.3 The Tafel Slopes

Table 5.1 summarizes the Tafel slopes (in so far as linear regions can be distinguished under some conditions) obtained for polycrystalline and Zn (0001) face electrodes from CO_3^{2-}, SO_4^{2-}, Cl^- and OH^- solutions at various pH's. It can be seen that an anodic Tafel slope of 40 mV/decade is obtained in solutions at pH 8.1 and about 34-29 mV decade^{-1} at pH's 13.5.

Figs. 3.25c and 3.36 showed the effect of rotation on the dissolution currents for unetched Zn electrodes in 0.8M Na_2CO_3 + 0.2M Na_2SO_4 at pH 11.5 and 1M Na_2SO_4 at pH 8.1. It can be seen that the products of Zn oxidation that form during anodic polarization are soluble and dissolve into solution more at pH 8.1, where non-adherent $Zn(OH)_2$ is formed, than at pH 13.5, where a passivating oxide film is generated. It can also be seen that the Tafel slopes obtained for an etched surface are lower than

Table 5.1

Comparison of Tafel Slopes for Various Solutions and Electrodes

Solution	pH	Tafel slope mV decade^{-1}	α	Preparation of electrode
1M Na_2SO_4	8.1	42	1.4	etched
		42	1.4	unetched
		42	1.4	(0001)face
	11.5	—	—	etched
	12.1	—	—	etched
	12.5	32	1.8	etched
	13.5	30	2.0	etched
		34	1.7	unetched
3M NaCl	11.5	—	—	etched
	13.5	33	1.7	etched
1M Na_2CO_3	11.5	—	—	etched
	13.5	33	1.8	etched
1M NaOH	14	29	2.0	etched
		35	1.7	unetched

Notes

1. These Tafel slopes were obtained in the ascending direction of potential change.
2. The slopes given are an average of data for 4-6 runs.
3. Tafel slopes could not be obtained for any of the solutions above pH of 11.5
4. There is no effect of CO_3^{2-} on the Tafel slopes but the latter do depend on the state of the electrode and pH of the solution.

those for an unetched one, probably due to exposure of different distribution of crystal faces.

The mechanism of Zn dissolution has been studied by many workers. As discussed in chapter 1, active dissolution of Zn in ($3x10^{-2}$ - 2)M NaOH, made up to constant ionic strenth of 3M with NaCl, was studied by Armstrong et al.[40] using a RDE. An anodic Tafel slope of 42 ± 5 mV/decade was observed in that work and was explained in terms of a dissolution mechanism involving two consecutive one-electron charge transfer steps with monovalent zinc ions as the supposed adsorbed intermediate and the second electron transfer step being rate-determining.

The effects of anions on the active dissolution of Zn have also been examined by many workers. Bough[41-42] studied Zn dissolution in $NaClO_4$, NaCl and Na_2SO_4 in the pH range 3.8-5.8. A Tafel slope of 40 mV/decade was again obtained in both Na_2SO_4 and $NaClO_4$, and this is in agreement with the results obtained by other workers in both quiescent and stirred solutions of $NaClO_4$[80] and Na_2SO_4.[148] In NaCl, the anodic slope has a value close to 30 mV/decade in agreement with the results of Hurlen[104] in 1M KCl solution at a stationary electrode. A Tafel slope of 40 mV/decade instead of 30 was obtained when the galvanostatic-pulse method was used instead of steady-state measurements where an anodic film may have had more time to develop.

Fig. 5.7 shows the effect of rotation in SO_4^{2-}, ClO_4^- and Cl^- solutions. The diffusion-controlled nature of the currents arising in 1M NaCl solution is indicated by the effect of rotation in the Cl^- solution. This behaviour in the Cl^- solution was

explained in terms diffusion of Cl^- species from the electrode/solution interface as the rate-determining step. Such an effect was also seen by Armstrong [40] for the dissolution of Zn in 1M KOH solution, where diffusion of $[Zn(OH)_4]^{2-}$ species was considered to be the rate-limiting step.

It can be seen from the steady-state measurements for etched and unetched Zn surfaces that dissolution/oxidation at the etched electrode is more diffusion-controlled than at the unetched one, possibly because the etched electrode is more active. This is in agreement with conclusions from the cyclic-voltammetric experiments and galvanostatic experiments discussed in a previous section. Also CO_3^{2-} ions not have much effect on the mechanism of dissolution of Zn, unlike in passivation, i.e the Tafel slopes obtained from experiments in CO_3^{2-}, Cl^- and SO_4^{2-} ion solutions were almost the same. It seems likely that the Tafel slopes depend very much on the state of the electrode and pH of the solution.

It is seen from the results discussed in this chapter that information from steady-state experiments is often difficult to interpret. Such measurements have to be complemented by non-steady state investigations as have been made in the present work.

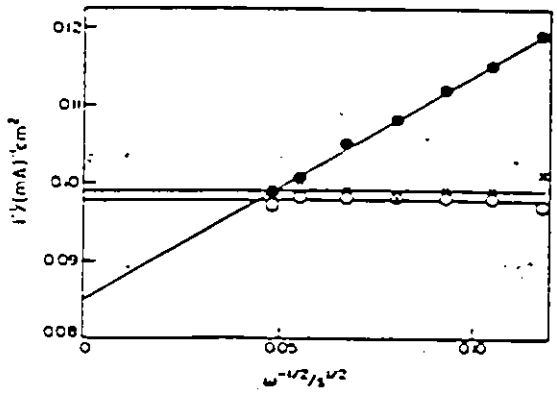

Fig. 5.7 Rotation speed dependence of the anodic dissolution c for zinc in molar solutions at pH 3.0. (O) $NaClO_4$, (×) Na_2SO_4, (●) NaCl

(Ref. 41)

5.4 Summary

1. The slopes of steady-state Tafel relations for Zn oxidation depend on the state of the electrode and pH of the solution.

2. From the Tafel slopes it can be seen that initially the products of electrochemical oxidation of Zn are soluble i.e. prior to onset of passivation. Their solubility is higher at pH 8.1, where non-adherent $Zn(OH)_2$ is formed, than at pH > 11.5, where an adherent passivating film of ZnO or $Zn(OH)_2$ is formed.

3. The oxidation processes of dissolution or film formation on an etched electrode are more diffusion-controlled than on an unetched one.

4. CO_3^{2-} ions do not have much effect on dissolution of Zn at higher pH.

CHAPTER 6

Electrodeposition of Zn and Morphology of Electrodeposits

6.1 Introduction

In this chapter are presented the details of the experimental arrangements, techniques used and results obtained in studies on electrodeposition of Zn from zinc ion solutions containing various anions over the pH range 5.8 to 2.8 . This aspect of the work was mainly concerned with establishing the morphologies of Zn electrodeposits generated from various electrolytes under cathodic galvanostatic conditions. Scanning electron microscopy was the procedure principally used.

6.2 Objective of this Part of the Work

While the results of morphological studies on Zn electrodeposits from various Zn ion solutions [Zn(II) in various states of complexation] are reported in this last chapter of this thesis, chronologically they were the first experiments conducted in the programme of work. Thus, the initial aims of the work were to establish Zn crystal morphologies developed under various conditions, in relation to dendrite formation in the charging direction of Zn battery operation and its control through variation of complexation or presence of additives. This aspect of work in the "cathodic direction" of the Zn electrode

process is complementary to that conducted in the "anodic direction" as described in earlier chapters. It was also intended to be complementary to other on-going parallel work by another researcher on the electrochemical calorimetry of Zn electrodeposition and dissolution[149].

6.3 Experimental

The electrical circuitry, cell and electrodes used in this part of the work are described below.

6.3.1 Electrical-Circuitry

A potentiostat can be used as a galvanostat by modifying the connection to the electrochemical cell. Instead of controlling the potential difference between the working and reference electrodes, the voltage drop across an external ohmic resistance in series with the cell, is controlled. Fig. 6.1 shows the basic electrical circuit used for these experiments. The resulting potential-time curves at constant current, thus obtained, were recorded by means of a Houston (type 2000) recorder.

6.3.2 Cell, Electrodes and Solutions

The two-compartment glass electrochemical cell used in the electrodeposition studies is shown in Fig. 6.2a; the reference electrode was contained in one compartment, and the counter and working electrode in the other.

A coil made of Zn wire 0.3 cm diameter was used as the

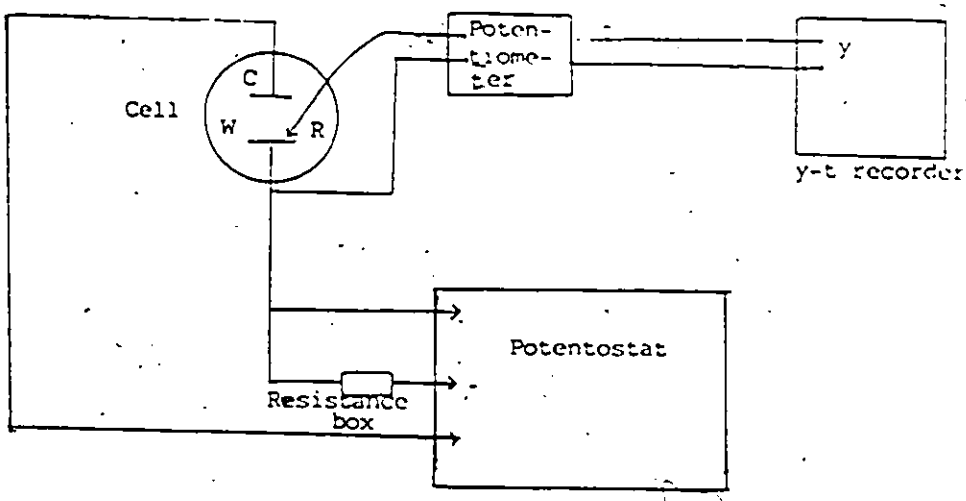

Fig. 6.1 Electrical circuitry employed in galvanostatic studies

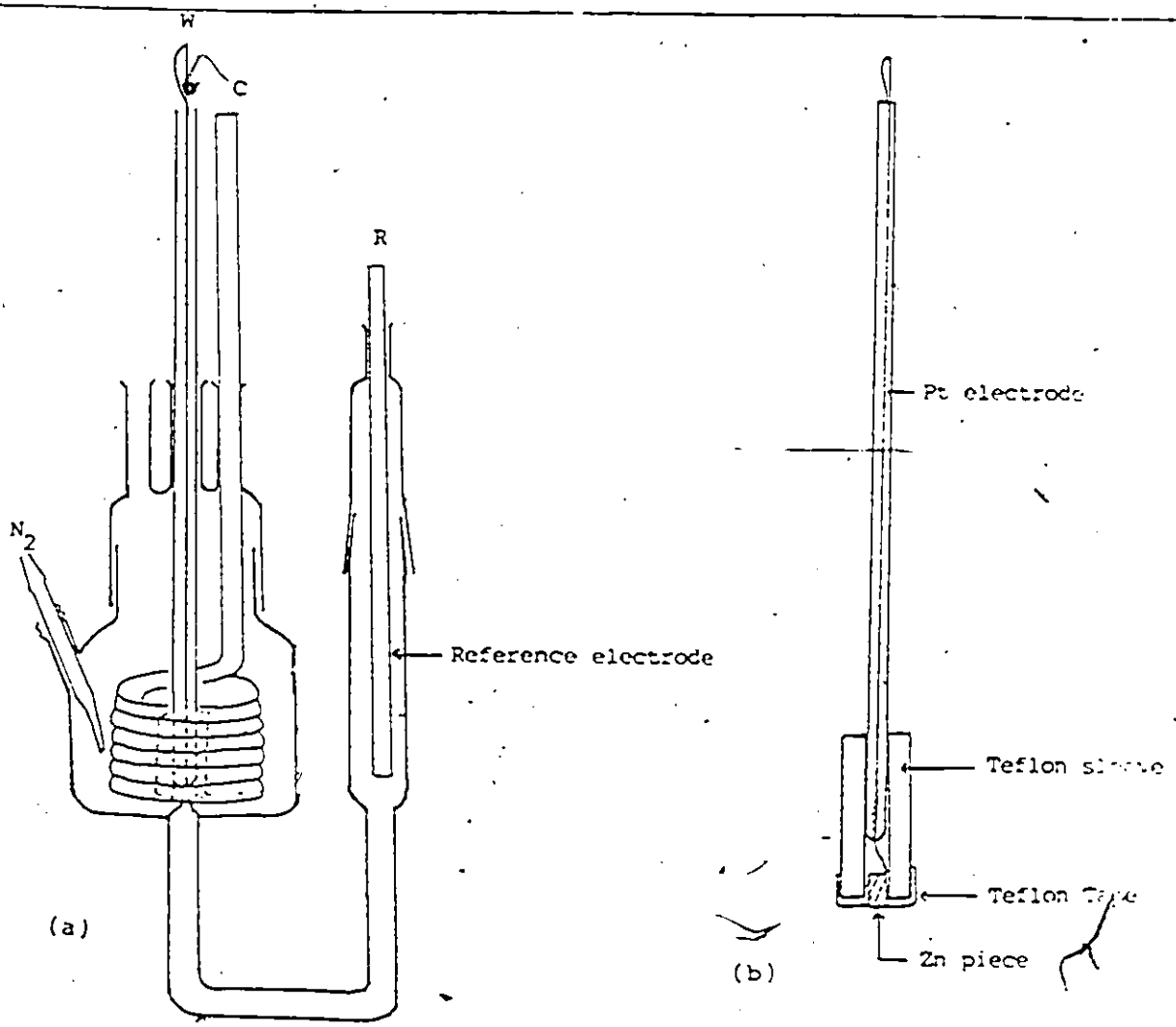

Fig. 6.2 (a) Two compartment cell and (b) Zn electrode used in electrodeposition studies.

counter electrode to provide a uniform field around the working electrode. The reference electrode was just a 0.3 cm diameter zinc wire immersed in the experimental Zn (II) ion solution. Both counter and reference electrodes were cleaned by etching in HBr (48%) solution, followed by thorough rinsing with doubly-distilled water.

The working electrode used is shown in Fig. 6.2b. Pieces of zinc 1 cm in length were cut from the 0.3 cm diameter polycrystalline wire and either etched in acid or mechanically polished successively with 300 and 600 grit sand paper, 3 μ and 1 μ diamond paste, followed by degreasing overnight in refluxing acetone in a Soxhlet extractor. These Zn pieces were rinsed thoroughly with water and pressed into the Teflon holder (Fig. 6.2b). The electrical connections were made by means of Pt wire. Teflon tape was used to cover the surface allowing only the cross-section of the Zn piece, 0.07 cm^2 in area, to be exposed to the test solution.

After each electrodeposition at a chosen current density and for a controlled time, the Zn working electrode was removed from the solution before switching off the current. The specimen was then washed thoroughly with distilled water first and then with methanol. The dried sample was then transferred to the SEM for morphological examination.

All solutions were prepared from "AnalaR" grade chemicals and were freed from oxygen by bubbling nitrogen gas through the solution in the cell prior to, and during, the electrochemical measurments. $Zn(SCN)_2$ used in this work was prepared by mixing solutions of $ZnSO_4$ and $Ba(SCN)_2$, filtering off the precipitated

$BaSO_4$ and evaporating the resulting solution to dryness [150]

The temperature of the test solutions used was controlled to ± 0.5 K by immersing the cell in a Polytem (model 80) thermostat adjusted to the required temperature. All depositions were carried out at 298 K, from unstirred solutions.

6.3.3 Current-Densities and Extents of Electrodeposition

The morphology of electrodeposits is normally determined not only by the chemical constitution (e.g. state of complexation) from which the metal is being deposited, but also by the substrate surface, the current-density and the extent of electrodeposition that is allowed to take place. Hence, in the following material, the SEM pictures to be shown will be specified with respect to the solution composition, pH, current-density and extent of deposition. The latter is conveniently described in a quantitative way in terms of the deposition charge passed in coulombs per square centimetre (C cm^{-2}). 1 C cm^{-2} is equivalent to deposition of ca. 2500 atomic layers of Zn per cm^2 if the Zn were deposited in flat layers.

6.4 Results and Discussion

6.4.1 The Behaviour of Etched and Mechanically Polished Surfaces

Zinc was electrodeposited on mechanically polished zinc surfaces that had been etched in HBr solutions of various concentrations for different lengths of time. Fig. 6.3 shows SEM pictures obtained before and after electrodeposition on surfaces etched in 1M aq. HBr solution for 30 s and 10 mins, with deposition being carried out from 0.5m $ZnBr_2$ solution at pH 5.5 at 141

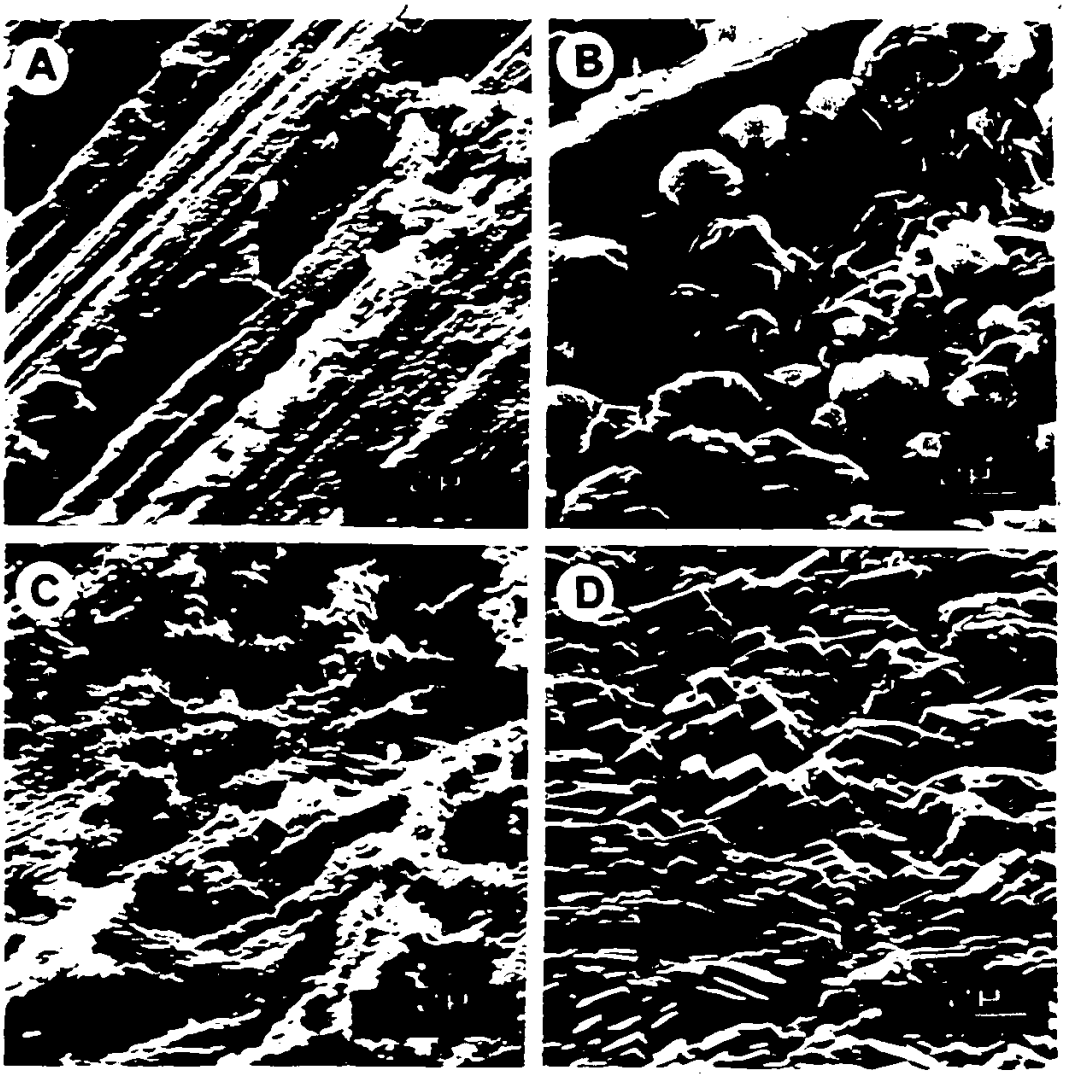

Fig. 6.3 The state of the surface before and after electrodeposition on Zn surfaces etched in 1M aq. HBr solution for 30 s [A,B] and 10 min [C,D]. Deposition is from 0.5 M $ZnBr_2$ solution at pH 5.5 at 141 mA cm^{-2} to a total extent of deposition of 2 C cm^{-2}.

mA cm^{-2} to an extent of 2 C cm^{-2} (equivalent approximately to $5x10^3$ equivalent atomic layers of Zn). Most of the deposits obtained on mechanically polished surfaces were similar to those obtained on a surface etched for 10 s; the electrodeposits obtained on surfaces etched in HBr (48%) for 8 s, (Fig. 2.4), were similar to those shown in Fig. 6.3D, but were smoother. Therefore most of the experiments were carried out on surfaces that had been etched in HBr (48%) for 8 s.

A typical overpotential*-time curve obtained for Zn deposition from 0.5M $ZnBr_2$ solution at pH 5.5 is shown in Fig. 6.4 together with the corresponding SEM picture obtained after Zn electrodeposition with 20 C cm^{-2} of charge (ca. $5x10^4$ equivalent atomic layers).

After an initial rapid rise in overpotential, the growth process continues with a declining overpotential. It was found that much larger overpotentials were required (50-100 mV) to initiate the electrodeposition on mechanically polished surfaces than on etched Zn surfaces; this is no doubt due to the greater density of nuclei for crystal growth present on the latter surfaces.

Similar overpotential-time curves have been observed by other workers. The form of such curves was attributed to the low rate of crystallization of ad-atoms formed initially by neutralization of the metal ions. In electrodeposition, the total overpotential is the sum of components due to diffusion and to irreversibility in the charge-transfer and crystallization

*Note: the kinetic significance of the overpotential behaviour recorded here (e.g. role of nucleation and growth processes, and coupled diffusion) will not be discussed.

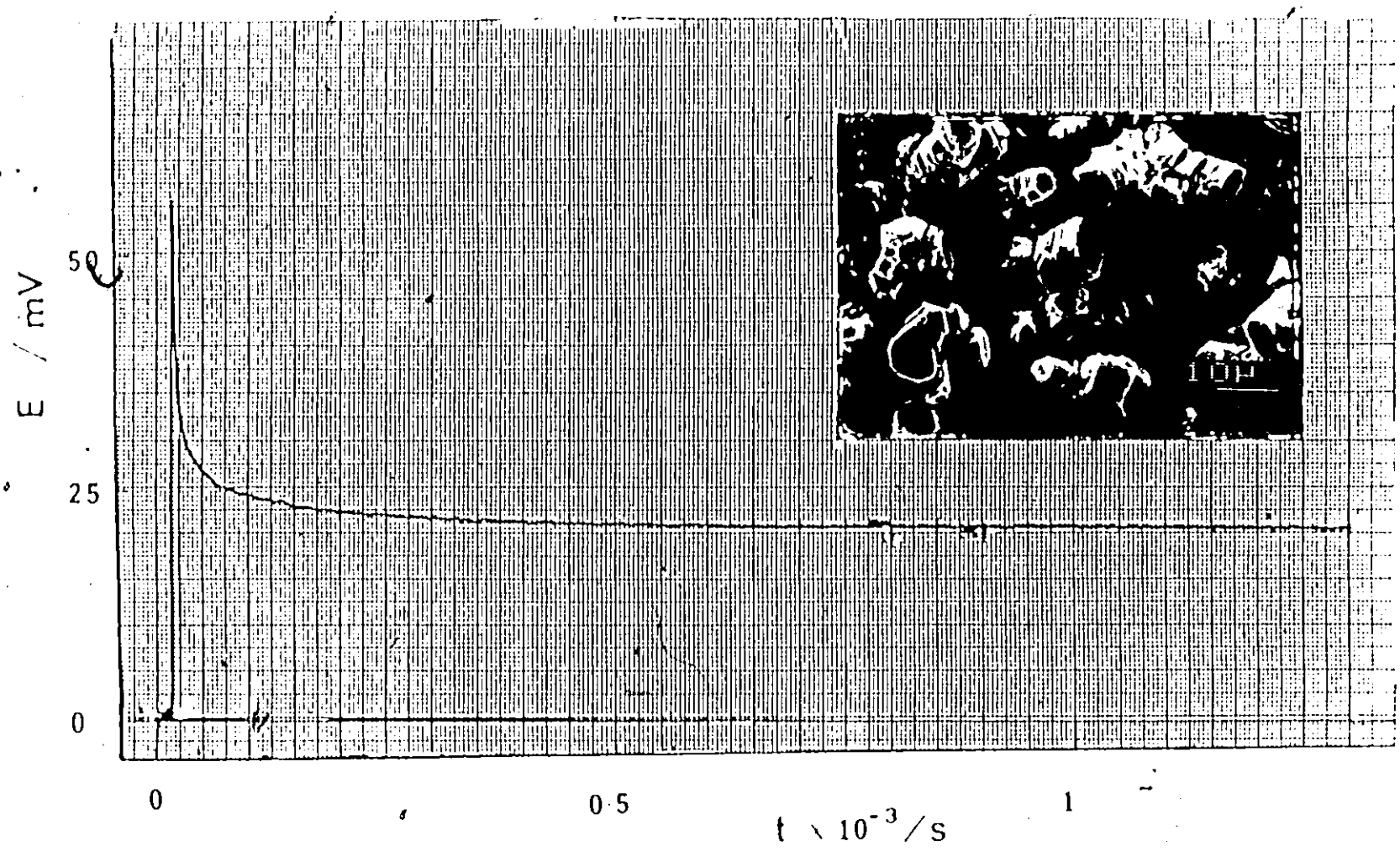

Fig 6.4 A typical overpotential-time curve and the corresponding SEM picture obtained for Zn electrodeposition on a mechanically polished surface from 0.5 M $ZnBr_2$ solution at pH 5.5 at a current density of 14 mA cm^{-2} with an extent of deposition of 20 C cm^{-2}.

processes. Crystallization overpotential arises when the process of building of ad-atoms into the crystal-lattice hinders the electrode process; an initial overpotential arises when nuclei for crystal growth have to be established but, in some cases, these may already be present, e.g. on disordered or stepped and kinked surfaces.

The crystallization process no longer hinders the rate of the overall electrodeposition process if the exchange rates of crystallization steps:

ad-atom (on metal phase) $\rightleftharpoons$ atom in the lattice

are high enough; the greater is the concentration of surface kinks (which provide crystal growth centers), the larger is the exchange current density for the crystallization process.

The overpotential required for electrodeposition on mechanically polished surfaces is similar to that required for formation of new nuclei on a foreign cathodic substrate, because the mechanically polished surfaces are, for unavoidable reasons, usually not clean, as mentioned in section (2.4.3). Also residues of the polishing material can become embedded, and remain, in the Zn surface. Therefore electrodeposition on a mechanically polished surface is generally more difficult (initially) compared to that on an etched surface because, on the latter, there are a large number of growth centers for crystal development. Similar behaviour was observed when Zn was electrodeposited on a Zn surface chemically polished in Cr_2O_3/ Na_2SO_4 /HNO_3 solution. It has been shown by other workers [33]

that the bright surface obtained after chemical polishing in this solution is due to a chromium oxide film formed on the Zn surface. Fig. 6.5 shows the SEM pictures obtained at chemically polished Zn surfaces before and after electrodeposition of Zn.

6.4.2 The Effect of pH

Figs. 6.6 and 6.7 show SEM pictures of Zn electrodeposited on an etched Zn surface under galvanostatic conditions from 0.5M $ZnBr_2$ solutions at pH 2.8 and 5.7, respectively. It can be seen that the electrodeposits obtained from the more acidic solution were smoother than from the other. It is seen that dendritic growth commences above a current-density of, ca. 354 mA cm^{-2} in the solution at pH 2.8 and above 70 mA cm^{-2} in the other solution. Fig. 6.8 shows the overpotential-time curves obtained for Zn deposition from 0.5M $ZnBr_2$ at pH 2.8 at current-densities of 70 mA cm^{-2} and 566 mA cm^{-2}. No initial nucleation transient of potential is seen here since the surfaces were etched, with resulting generation of growth centers. It is also seen that instability of overpotential during electrolysis occurs at higher current densities, corresponding to dendritic deposition.

Fig. 6.9 shows SEM pictures obtained after electrodeposition of Zn on an etched Zn surface from 0.5 $ZnBr_2$ solution at pH 2.8 at 71 mA cm^{-2} current-density with extents of deposition of 2 C cm^{-2} and 51 C cm^{-2}. It can be seen that the Zn is initially deposited in "layer" structures; at grain boundaries, a clear distinction exists between the orientation of the "layer" structures. As the deposits become thicker, their surfaces

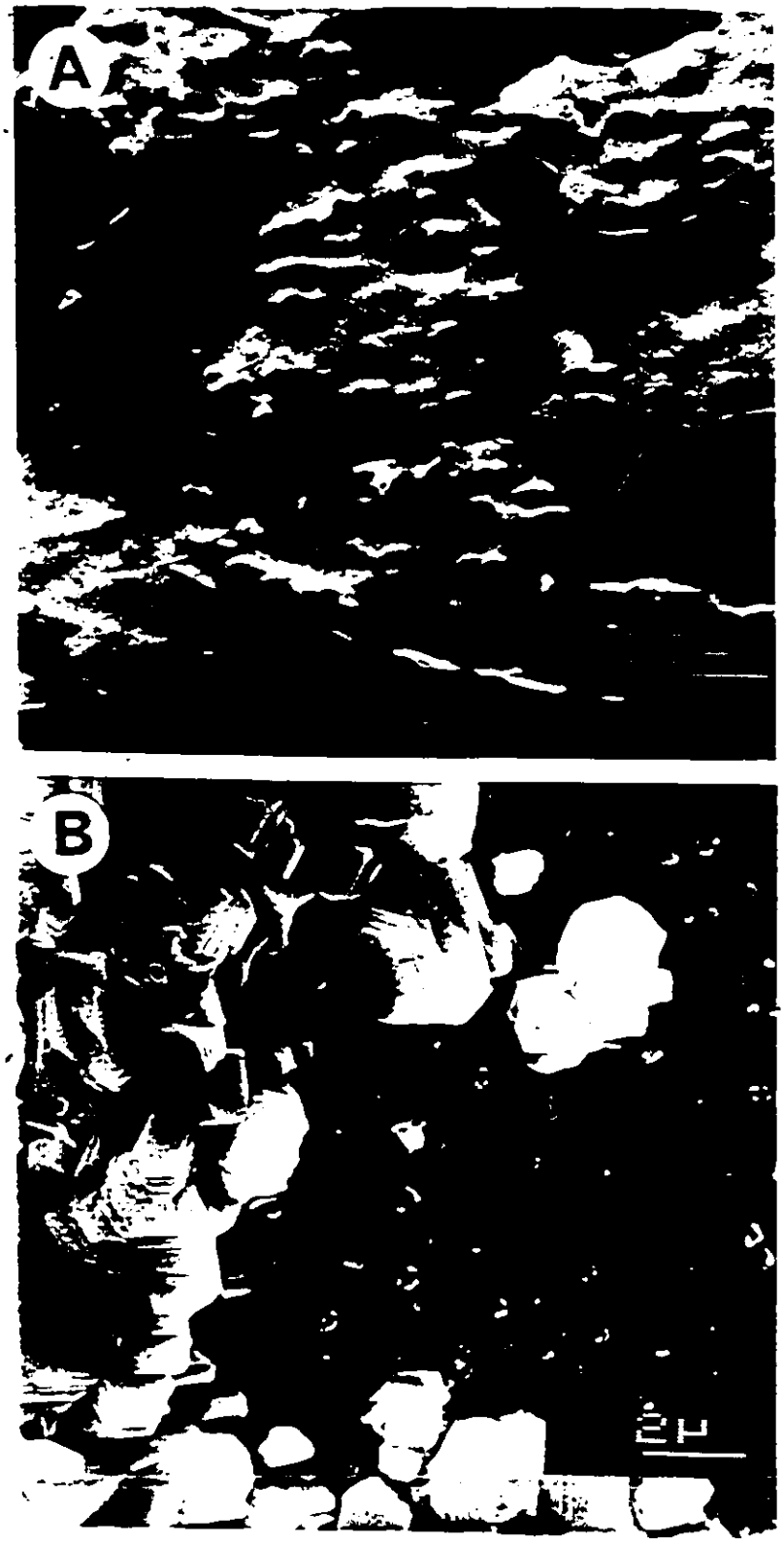

Fig. 6.5 The state of the surface (A) before and (B) after electrodeposited Zn on a surface, chemically polished in $Cr_2O_3/HNO_3/Na_2SO_4$ solution, from 0.5M $ZnBr_2$ solution at pH 2.8 at 70 mV cm^{-2} to an extent of deposition of 2 C cm^{-2}.

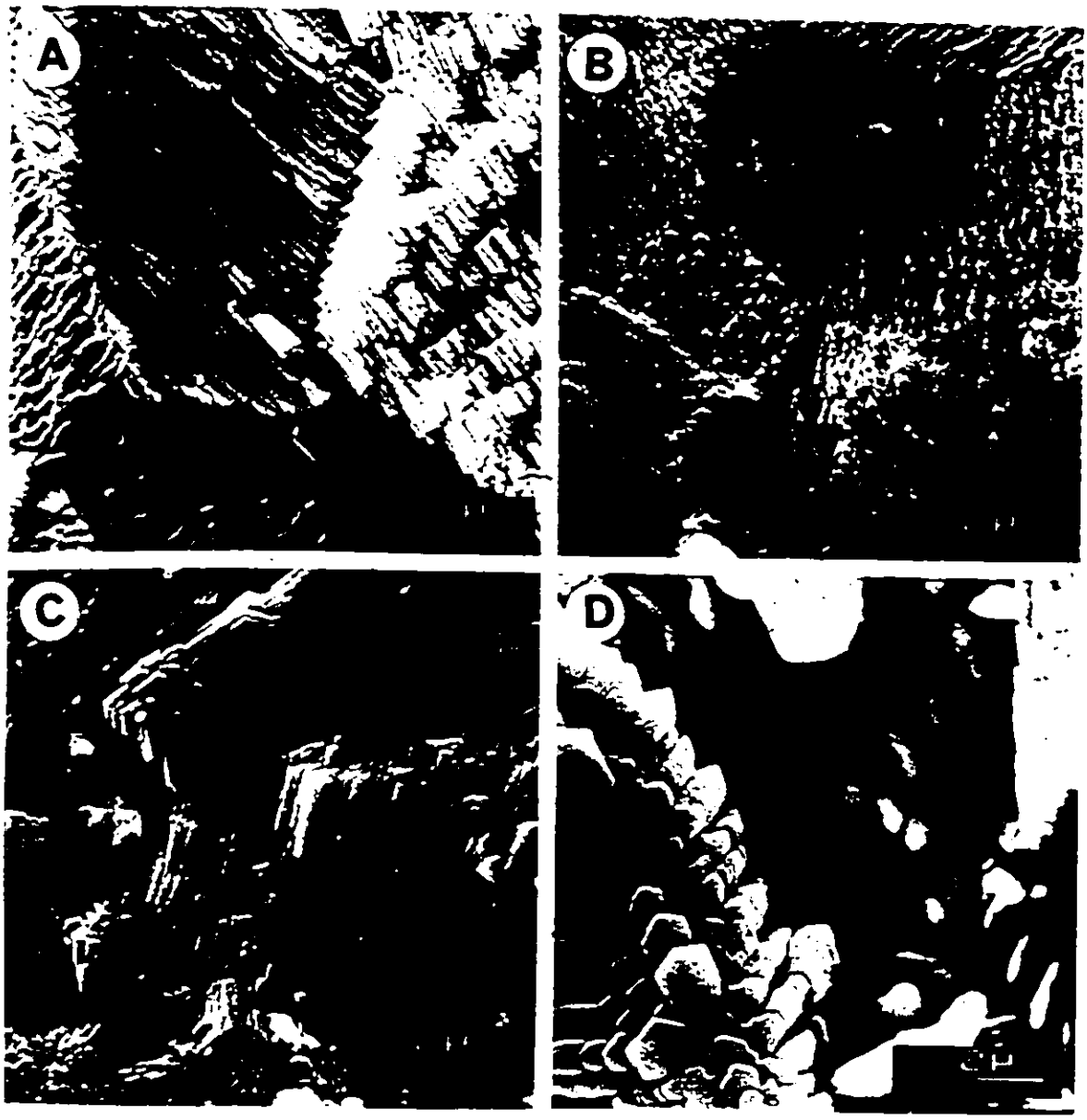

Fig. 6.6 Zn electrodeposits from 0.5M $ZnBr_2$ solution at pH 2.8 on Zn surface etched in 48% HBr. Extents of deposition of 2 C cm^{-2} at (A) 141 mA cm^{-2}; (B) 282 mA cm^{-2} (C) 354 mA cm^{-2}; (D) 566 mA cm^{-2}.

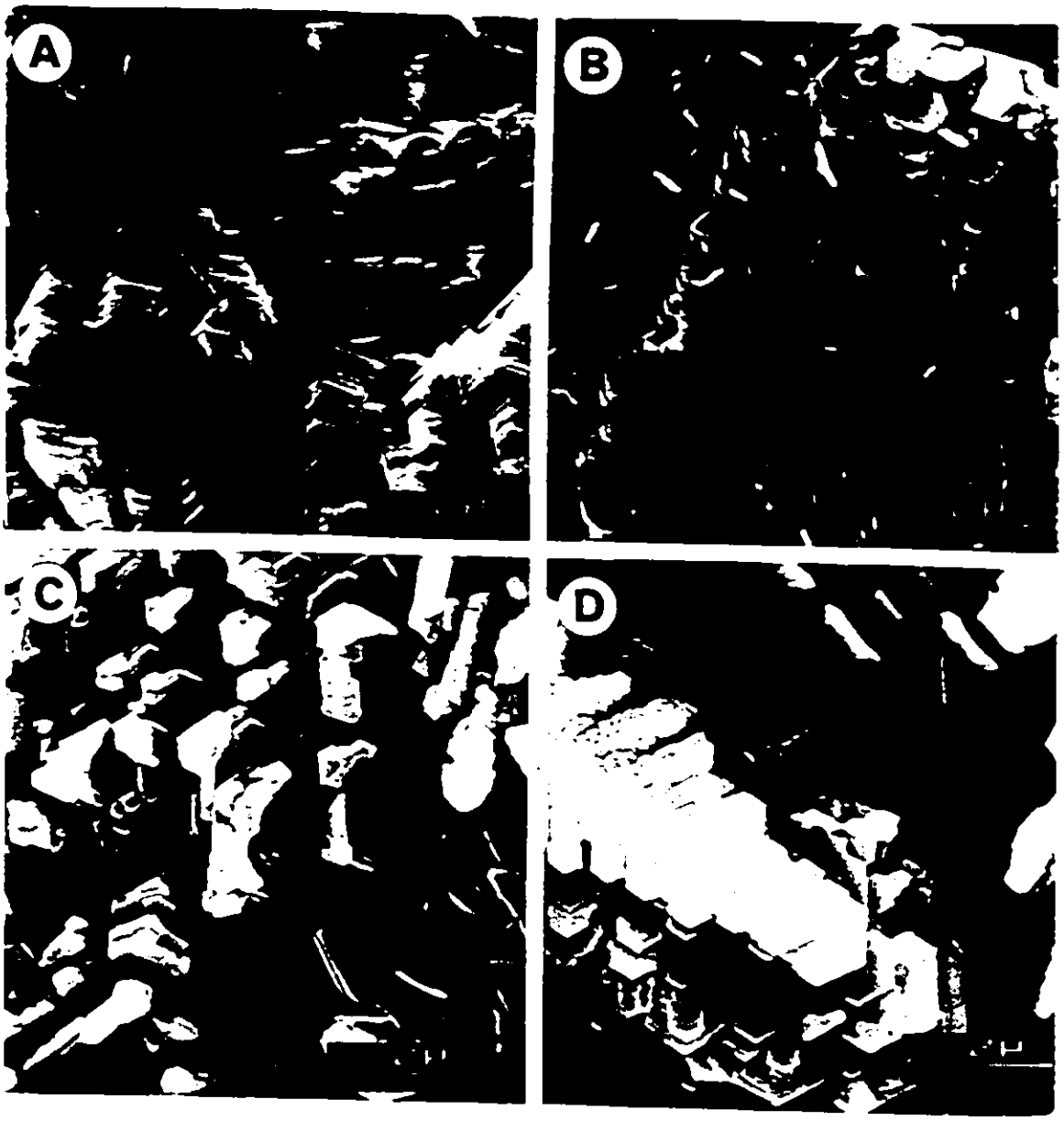

Fig. 6.7 Zn electrodeposits from 0.5M $ZnBr_2$ solution at oH 5.8 on a Zn surface in etched 48% HBr. Extents of deposition of 2 C cm^{-2} at
(A) 14 mA cm^{-2}; (B) 70 mA cm^{-2};
(C) 282 mA cm^{-2}; (D) 352 mA cm^{-2}.

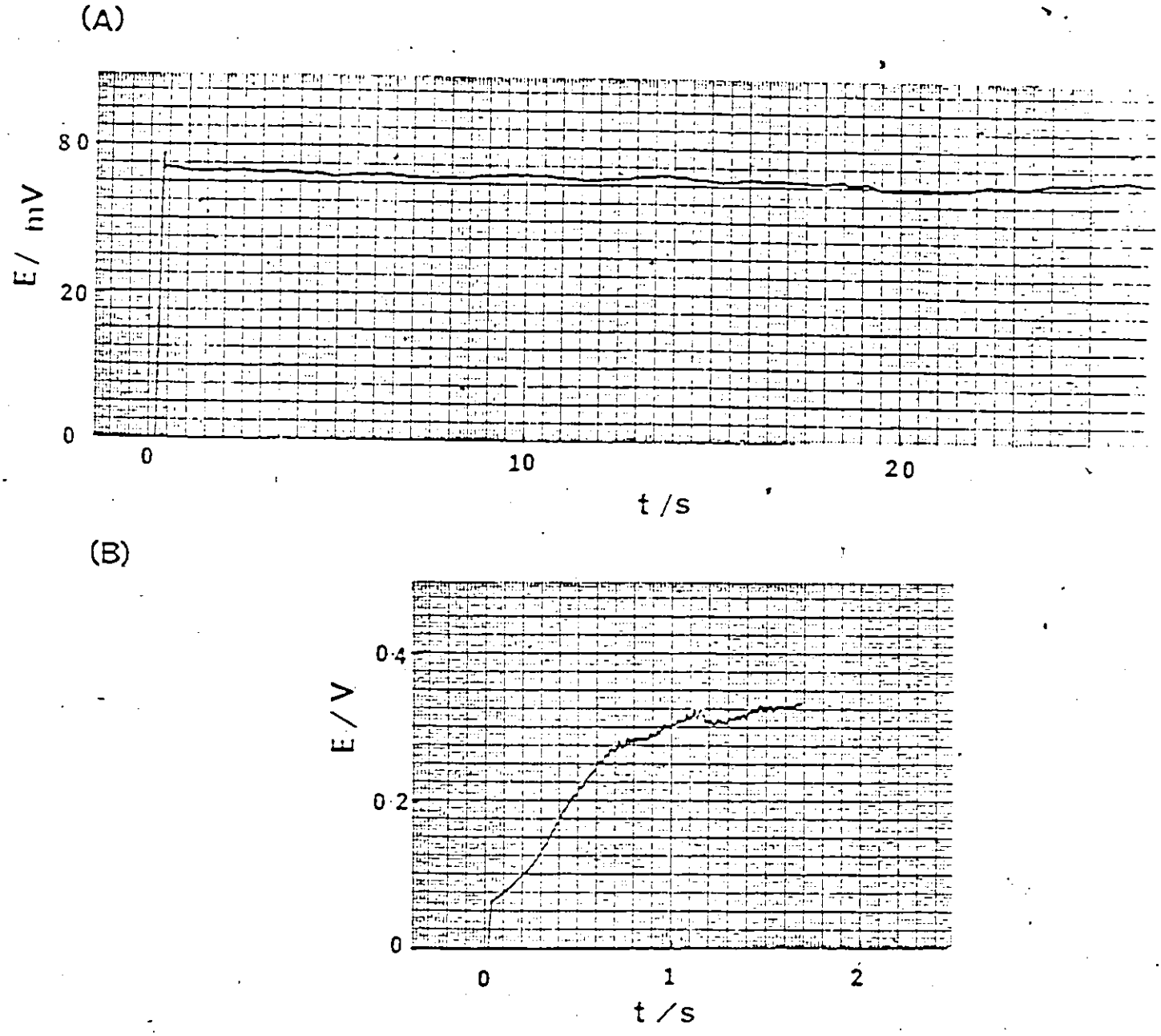

Fig. 6.8 Overpotential-time curves for Zn deposition at an etched Zn electrode from a 0.5M $ZnBr_2$ solution at pH 2.8 at current densities (A) 70 mA cm^{-2} and (B) 566 mA cm^{-2}.

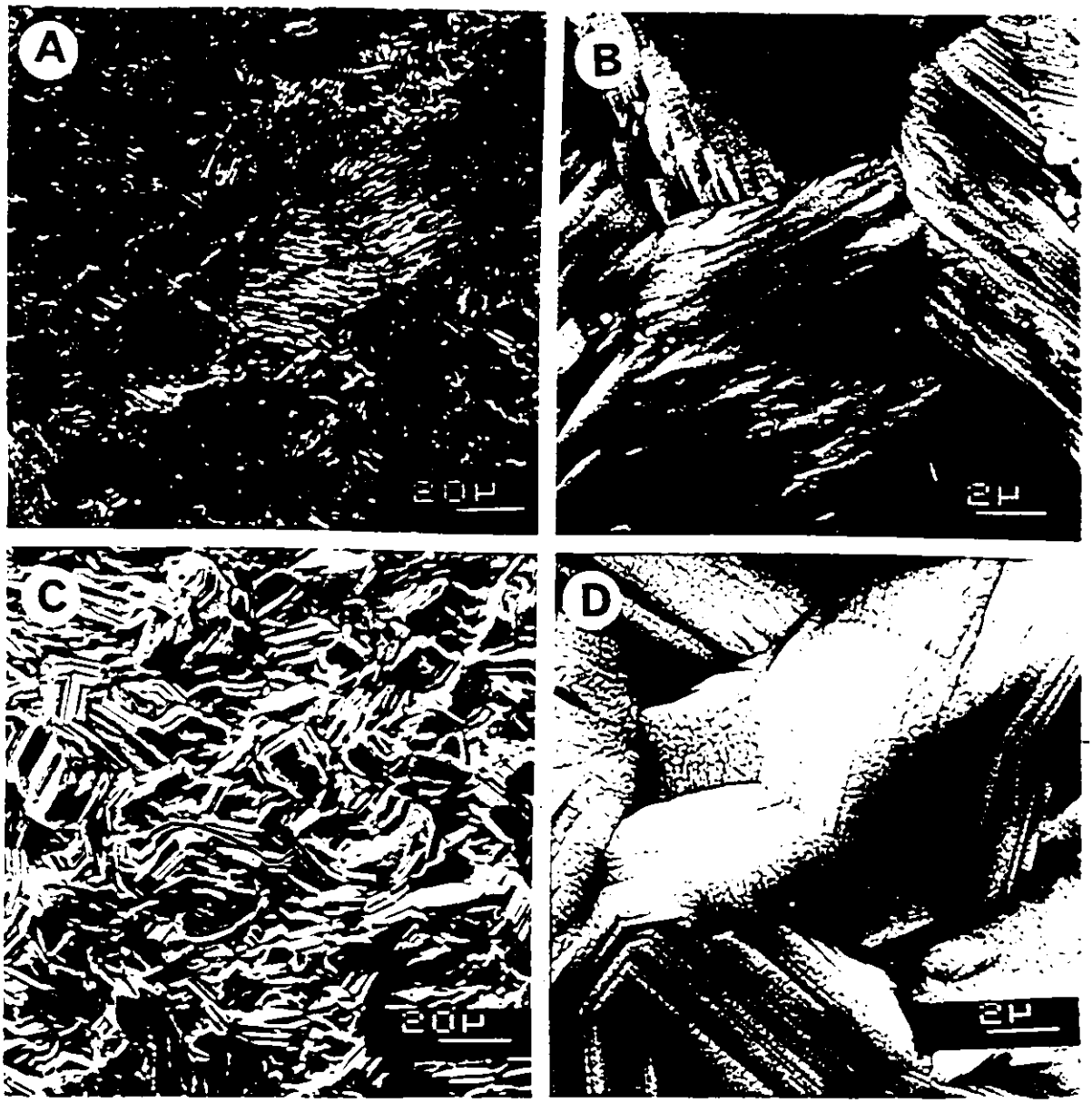

Fig. 6.9 Zn electrodeposits from 0.5M $ZnBr_2$ solution at pH 2.8 on an etched Zn surface in 48% HBr at a current density of 71 mA cm^{-2} with extents of deposition of (A,B) 2 C cm^{-2}; (C,D) 51 C cm^{-2}.

consist of randomly oriented blocks of parallel platelets packed together (see Fig. 6.9A).

Fig. 6.10 shows the SEM pictures of Zn surfaces after electrodeposition from a 0.5M $ZnBr_2$ solution at pH 5.7 using a current-density of 141 mA cm^{-2} for various deposition times. Under these conditions, the Zn is deposited in the form of "boulder" crystallites, the sizes of which continually increase during the course of the deposition. It seems likely that this behaviour is due to the Zn crystallites being oriented parallel to the basal plane and these are the "active" surfaces for further outward growth.

Fig. 6.11 shows the overpotential-time curves obtained for Zn electrodeposition to an extent of 80 C cm^{-2} at 140 mA cm^{-2}. It is seen that this curve is quite different from that obtained under conditions where the Zn deposition is dendritic, (Fig. 6.8). It seems likely that the overvoltage required for crystallization in such boulder-like morphologies is smaller and in fact negligible compared to that for dendritic growth.[83]

As seen in Fig. 6.12, these deposits finally develop well-oriented crystalline faces during the deposition. The difference between the overpotential-time curves in Figs. 6.12 and 6.11 is that both dendrites and boulder-like structures arise in the electrodeposition at a current density of 352 mA cm^{-2} for an extent of deposition of 40 C cm^{-2} from 0.5M $ZnBr_2$ solution at pH 5.7.

The deposition of Zn from zincate solutions at high pH was investigated by McBreen at el.[86-88] on several substrates using cyclic-voltammetry, potential pulse-methods, X-ray diffraction

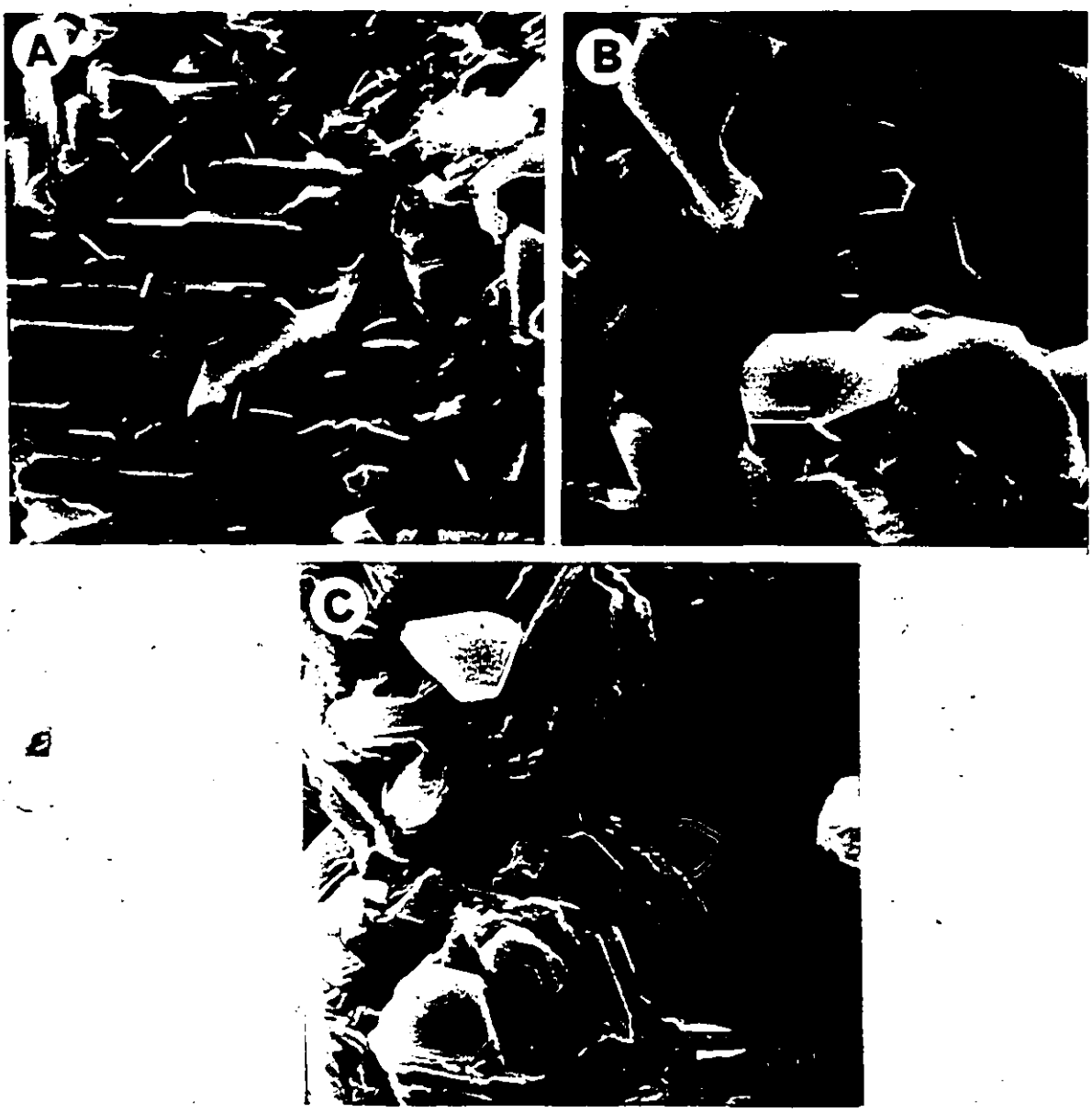

Fig. 6.10 Zn electrodeposits from $ZnBr_2$ solution at pH 5.8 on an etched Zn surface in 48% HBr at a current density of 141 mA cm^{-2} for extents of deposition

(A) 2 C cm^{-2}; (B) 10 C cm^{-2}; (C) 80 C cm^{-2}.

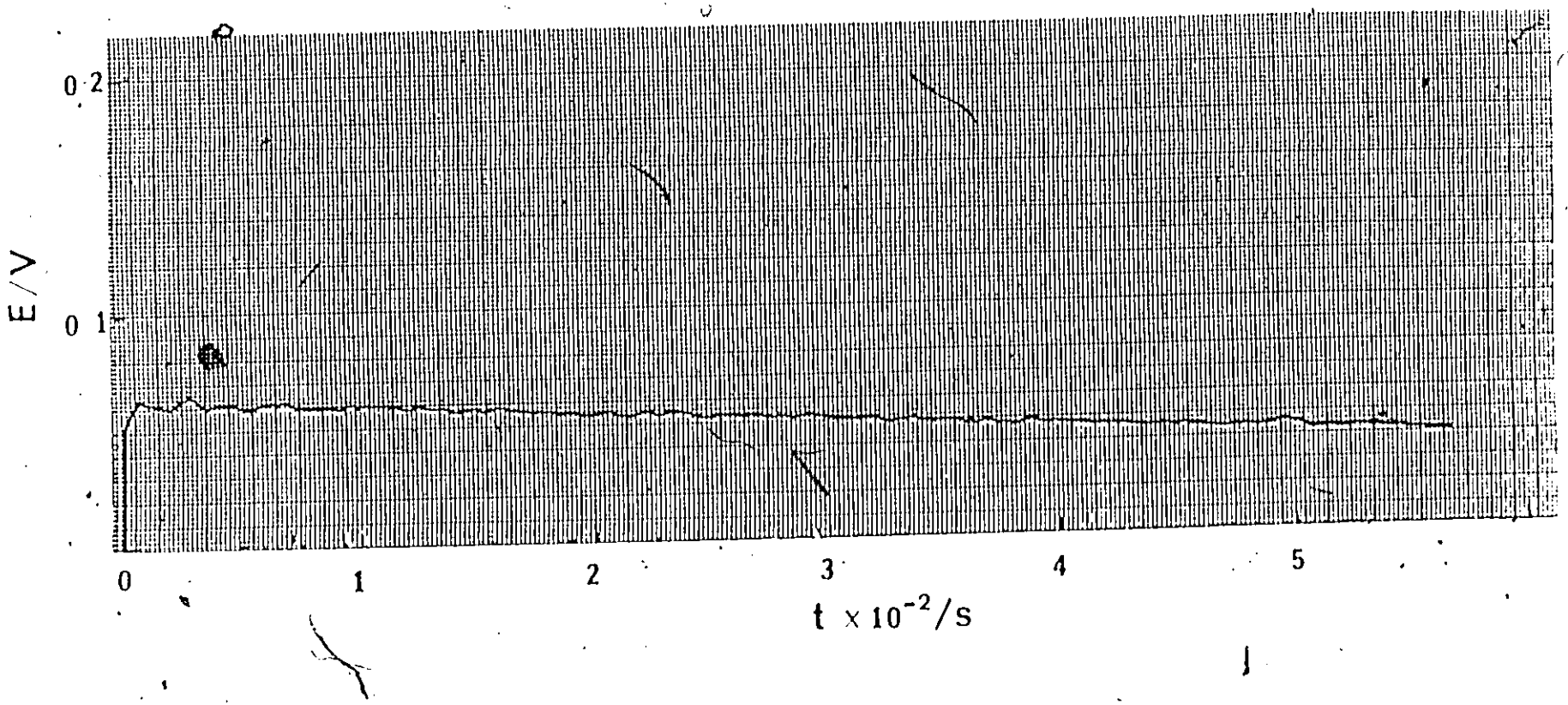

Fig. 6.11 Overpotential-time curves for Zn deposition on an etched Zn electrode from 0.5M $ZnBr_2$ solution at pH 5.7 at 140 mA cm^{-2} for an extent of deposition of 80 C cm^{-2}.

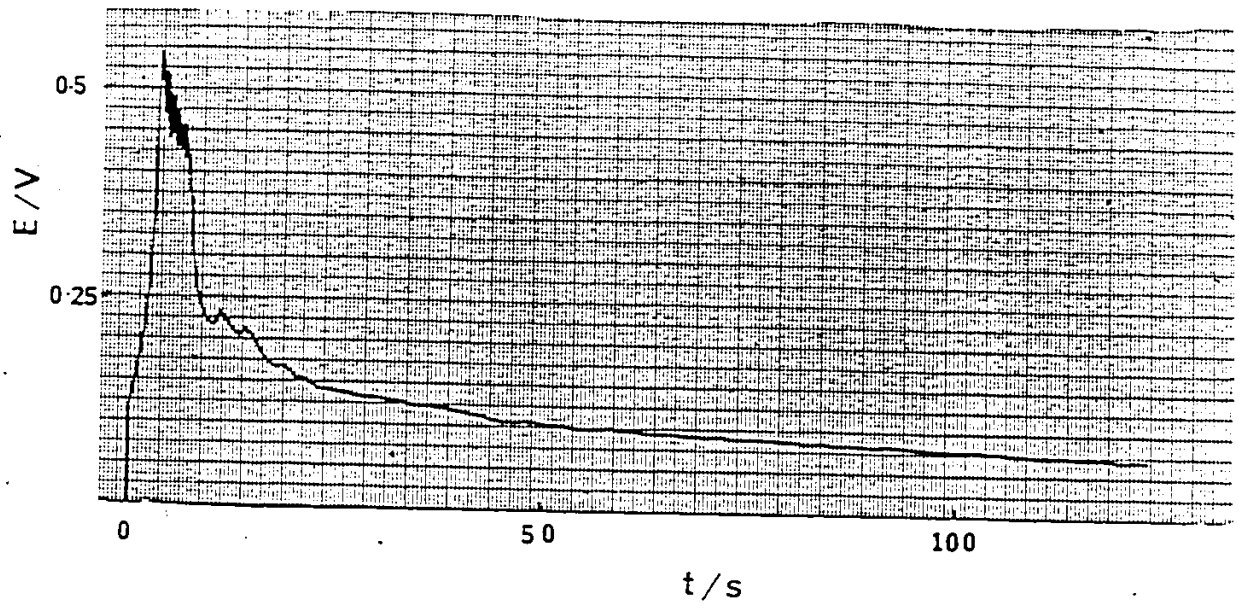

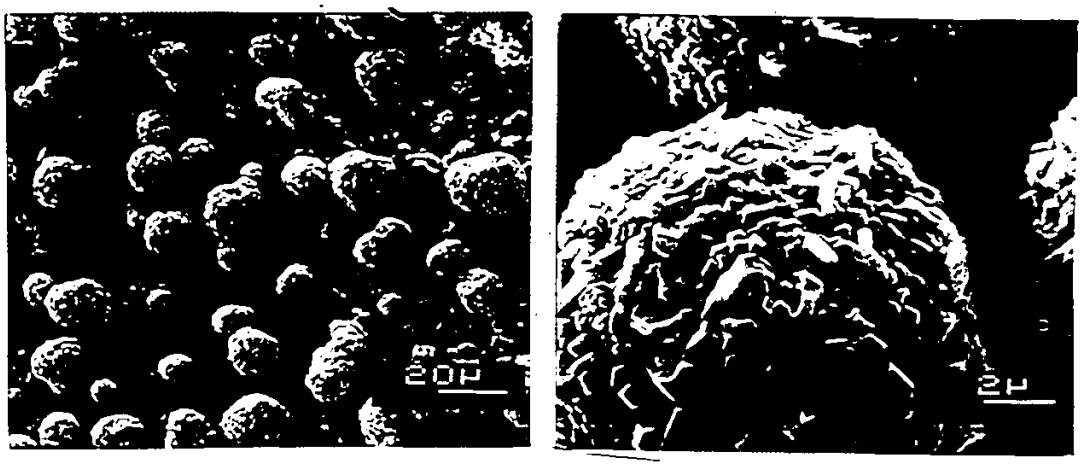

Fig. 6.12 Zn electrodeposits and E vs t curve obtained from a 0.5 M $ZnBr_2$ solution at pH 5.8 on an etched Zn surface at 352 mA cm^{-2} for an extent of deposition of 40 C cm^{-2}.

and SEM . Zn deposits on Ag, Cu, Au, Zn and Cd substrates were found "active" in McBreen's terminology and the Zn deposits were oriented parallel to the basal plane. On the other hand, Sn and In were less "active" and the deposits were oriented perpendicular to the basal plane.

From these results it was concluded that substrates with atomic radii that were 15% greater than that of Zn led to deposition in an orientation perpendicular to the basal plane and the surface morphology would not undergo change with thickening, whereas for substrates with atomic radii that were close to that of the radius of Zn, the electrodeposits were oriented parallel and the surface area increased with thickness.

The only difference between the two 0.5M $ZnBr_2$ solutions used in the present work was that one was at pH 2.8 and the other 5.7. It seems likely that at higher pH's $ZnBr_2$ becomes hydrolysed. This helps to form deposits oriented parallel to the exposed surface (polycrystalline Zn substrate).

Similar behaviour was also observed in 0.5M $ZnCl_2$ and 0.5M ZnI_2 solutions. Fig. 6.13 shows SEM pictures of deposits obtained from 0.5M $ZnCl_2$ solutions at pH's 1.9 and 4.9 under otherwise similar conditions.

6.4.3 The Effect of State of Complexation of Zinc Ions

6.4.3.1 Halide Ions

Electrodeposition of Zn was carried out from 0.5M $ZnCl_2$, $ZnBr_2$ and ZnI_2 solutions with varing concentrations of halide

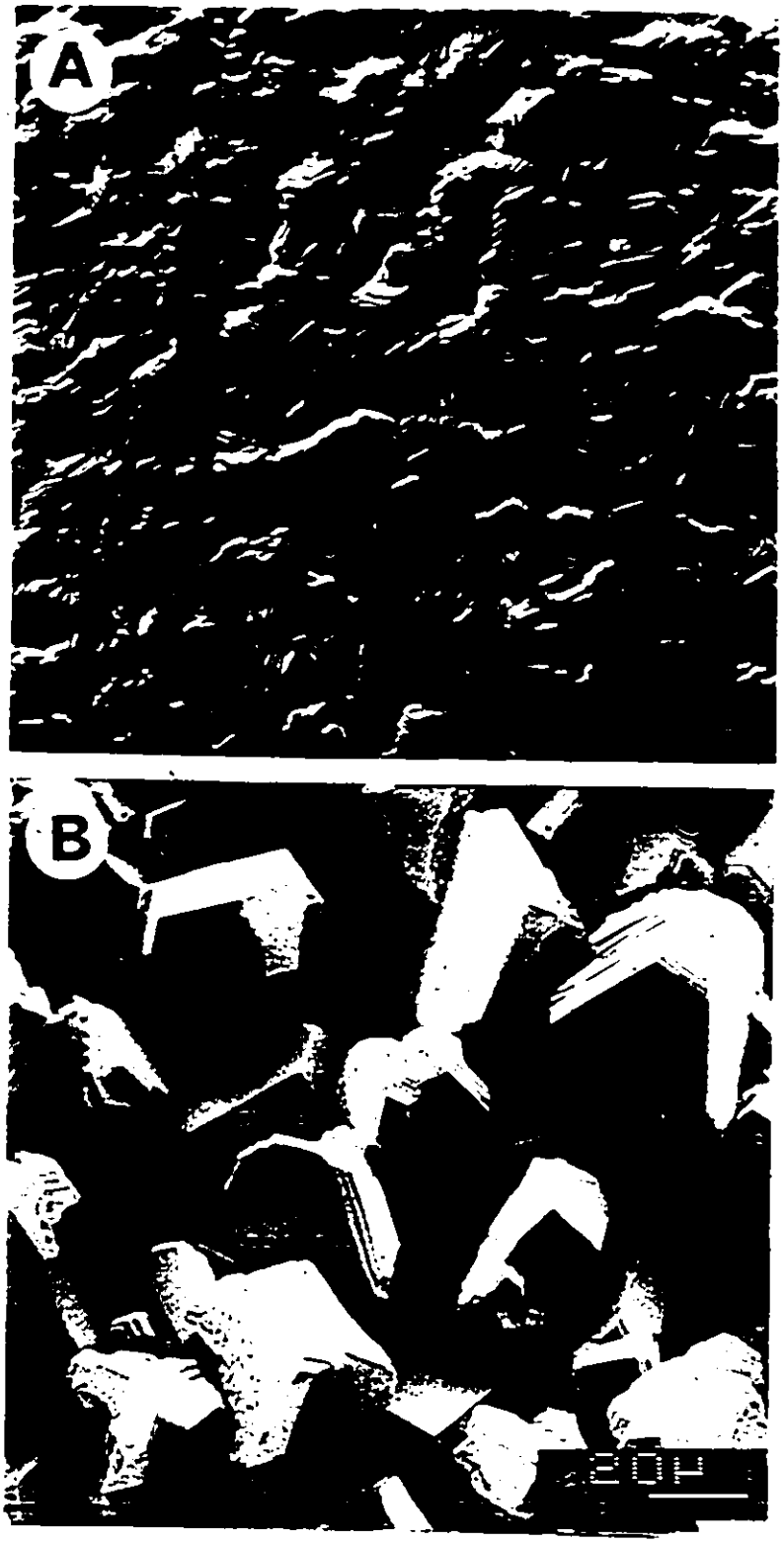

Fig. 6.13 Zn electrodeposits obtained from 0.5M $ZnCl_2$ solution at pH (A) 1.9 and (B) 4.9 at ca. 161 mA cm^{-2} for an extent of deposition of ca. 50 C cm^{-2}.

ions. The ionic strengths were in the range of 1.5 to 4.5 mol dm^{-3}. In the presence of halide ions, the dissolved zinc is present in the form of a range of halide (X) complexes, depending on the Zn^{++}/X^{-} concentration ratios. The distribution diagrams for complexation in zinc-chloride and zinc-bromide systems are shown in Fig. 1.2. It is clear that $[ZnCl_4]^{2-}$ is more stable than $[ZnBr_4]^{2-}$.

Fig. 6.14 shows SEM pictures of Zn deposits obtained from 0.5M $ZnBr_2$ + 4M NaBr solution at pH 3 at various current densities and Fig. 6.15 shows the corresponding overpotential-time curves obtained at 14 mA cm^{-2} and 92 mA cm^{-2}. It can be seen that the overpotential-time curves obtained for these solutions are quite different from those for 0.5M $ZnBr_2$ solutions at the same pH.

After the initial overpotential jump, corresponding to nucleation, a diffusion overpotential arises due to decrease in concentration of ions near the electrode. This behaviour can be explained as follows.

The simple salts form aquo-cations in aqueous solution. For deposition from hydrated metal ions the dehydration must be taken into account as a preliminary or coupled reaction step. This removal of the water molecules normally occurs in several steps. The energy for this transition depends on the nature of the metal ion.

Even though the deposition mechanism from solutions of simple salts is complex, additional problems arise in the case of deposition from complexes because, in such electrolytes, the metal to be deposited is often bound to negatively charged ions

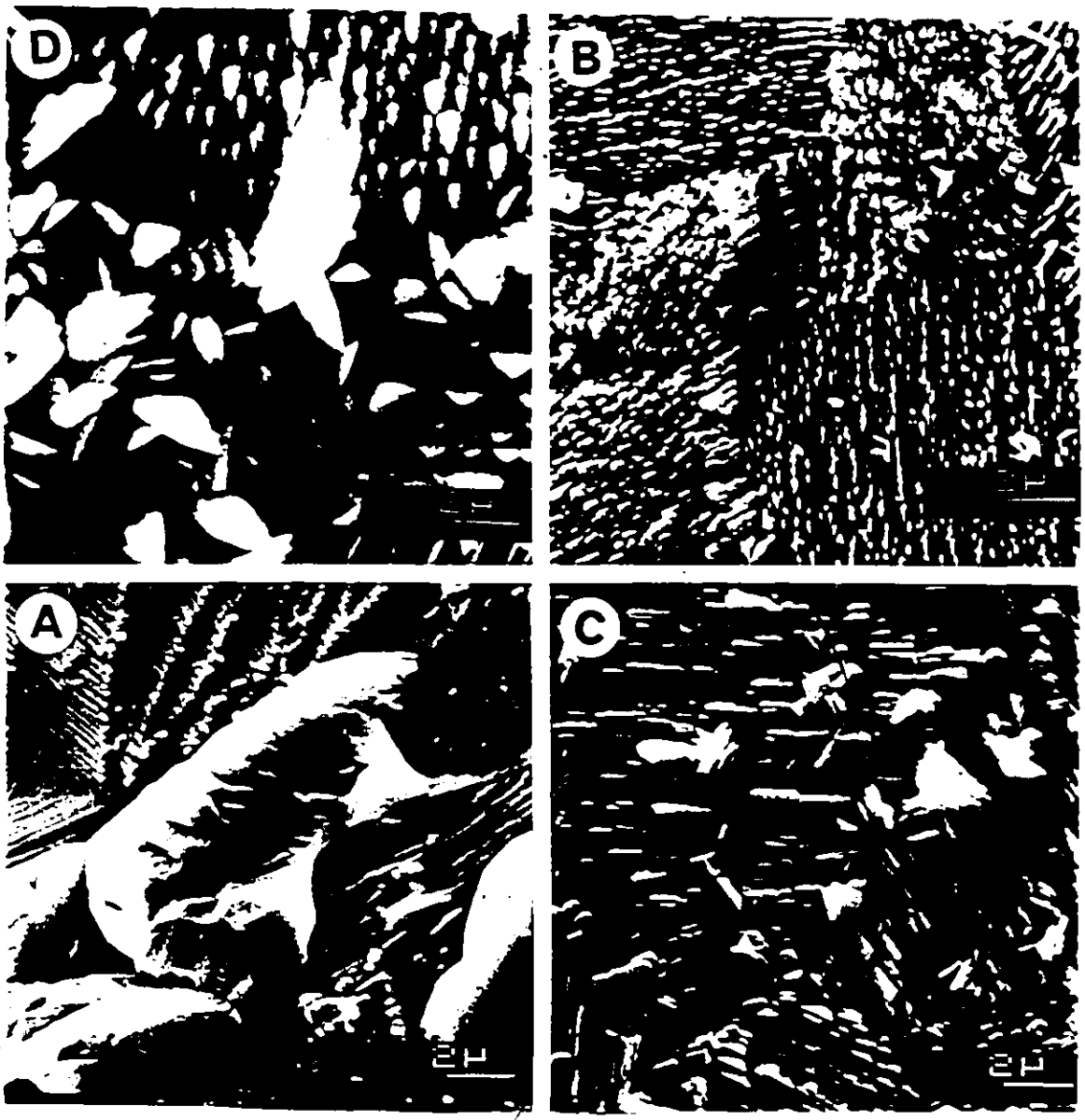

Fig. 6.14 Zn electrodeposits from 0.5M $ZnBr_2$ + 4M NaBr solution at pH 3 at current densities (A) 14 mA cm^{-2} (B) 92 mA cm^{-2} (C) 113 mA cm^{-2} (D) 142 mA cm^{-2} for an extent of deposition of 2 C cm^{-2}.

Note - Letters A ⟶ D not in an order.

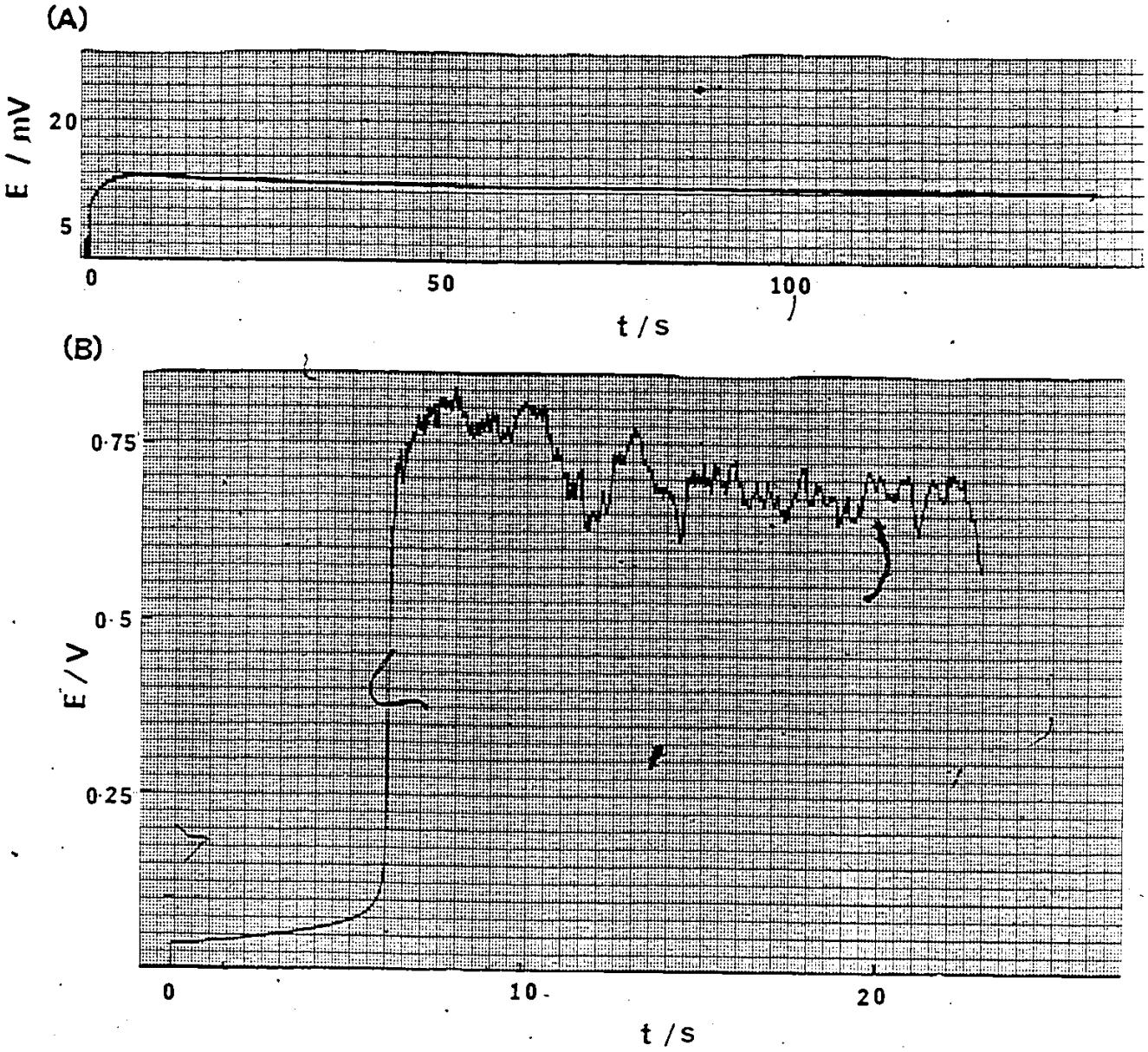

Fig. 6.15 Overpotential-time curve for Zn deposition at an etched Zn electrode from 0.5M $ZnBr_2$ + 4M NaBr solution at pH 3.04 at current desities (A) 14 mA cm^{-2} (B) 92 mA cm^{-2} for an extent of deposition of 2 C cm^{-2}.

as a complex anion. Although a dissociation equilibrium exists between the simple metal ion and the complex ion, the concentration of simple ion is low due to the normally high stability of the complex ions. Therefore the maximum rate of deposition is limited because of the slow supply of free metal ions to be deposited or to the higher activation energy for ion neutralization and atom transfer directly from the complex ion[25]. This leads to morphological changes of the electrodeposits from "smooth" to "dendritic", accompanied by an increase of overpotential.

Similar behaviour can also be seen with ZnI_2 and $ZnCl_2$ solutions (Fig 6.16). It is clear from previous work [95] that dendritic growth arises when the deposition current approaches the diffusion-limited value and the rate of growth, rather than the rate of nucleation, becomes the rate-controlling factor.

6.4.3.2 Thiocyanate Ion

Fig. 6.17 shows SEM pictures obtained after electrodeposition of Zn from 0.5M $Zn(SCN)_2$ solutions at pH 4.8 for an extent of electrodeposition of 2 C cm^{-2}, at various current densities. It can be seen that elongated crystallites start to deposit at lower current-densities and dendrites at higher current-densities.

It is clear that the deposits obtained from 0.5M $ZnBr_2$ solution under otherwise similar conditions are quite different. The electrodeposition evidently occurs mainly at the edges of the electrode with hardly any at its centre, especially at low current densities.

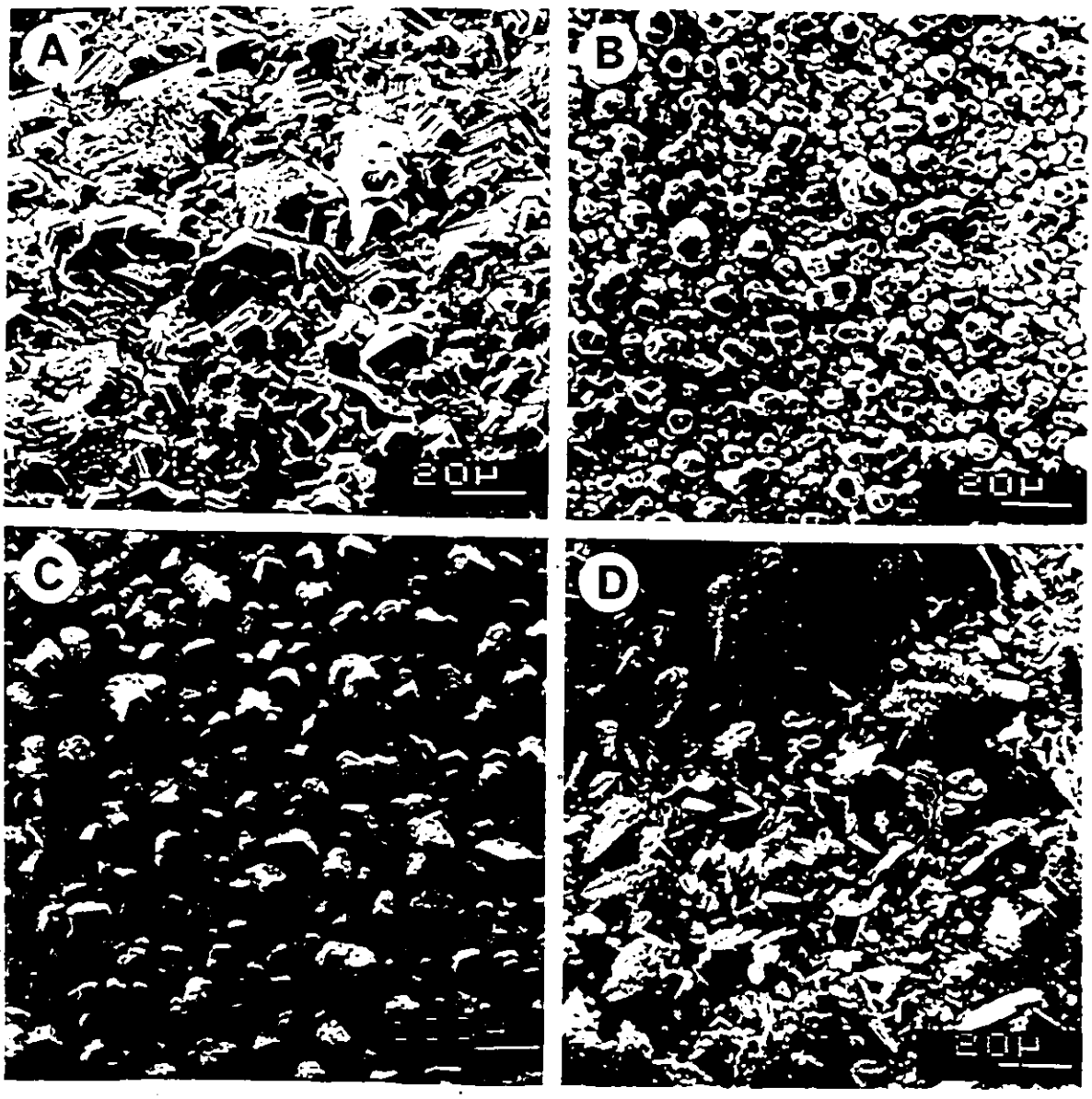

Fig. 6.16 Zn electrodeposits from (A) 0.5 M $ZnBr_2$ and (B) 0.5 M $ZnBr_2$ + 1M NaBr solutions at pH 2.8 at ca. 212 mA cm^{-2} for an extent of depositon of ca. 50 C cm^{-2}; (C) 0.5 M $ZnCl_2$ and (D) 0.5 M $ZnCl_2$ + 1M NaCl solutions at pH 4.8 at ca. 160 mA cm^{-2} for an extent of deposition of ca. 60 C cm^{-2}; (E) 0.5 M ZnI_2, (F) 0.5 M ZnI_2 + 1M NaI and (G) 0.5 M ZnI_2 + 2M NaI solutions at pH 2.6 ca. 90 mA cm^{-2} for an extent of deposition of ca. 50 C cm^{-2}.

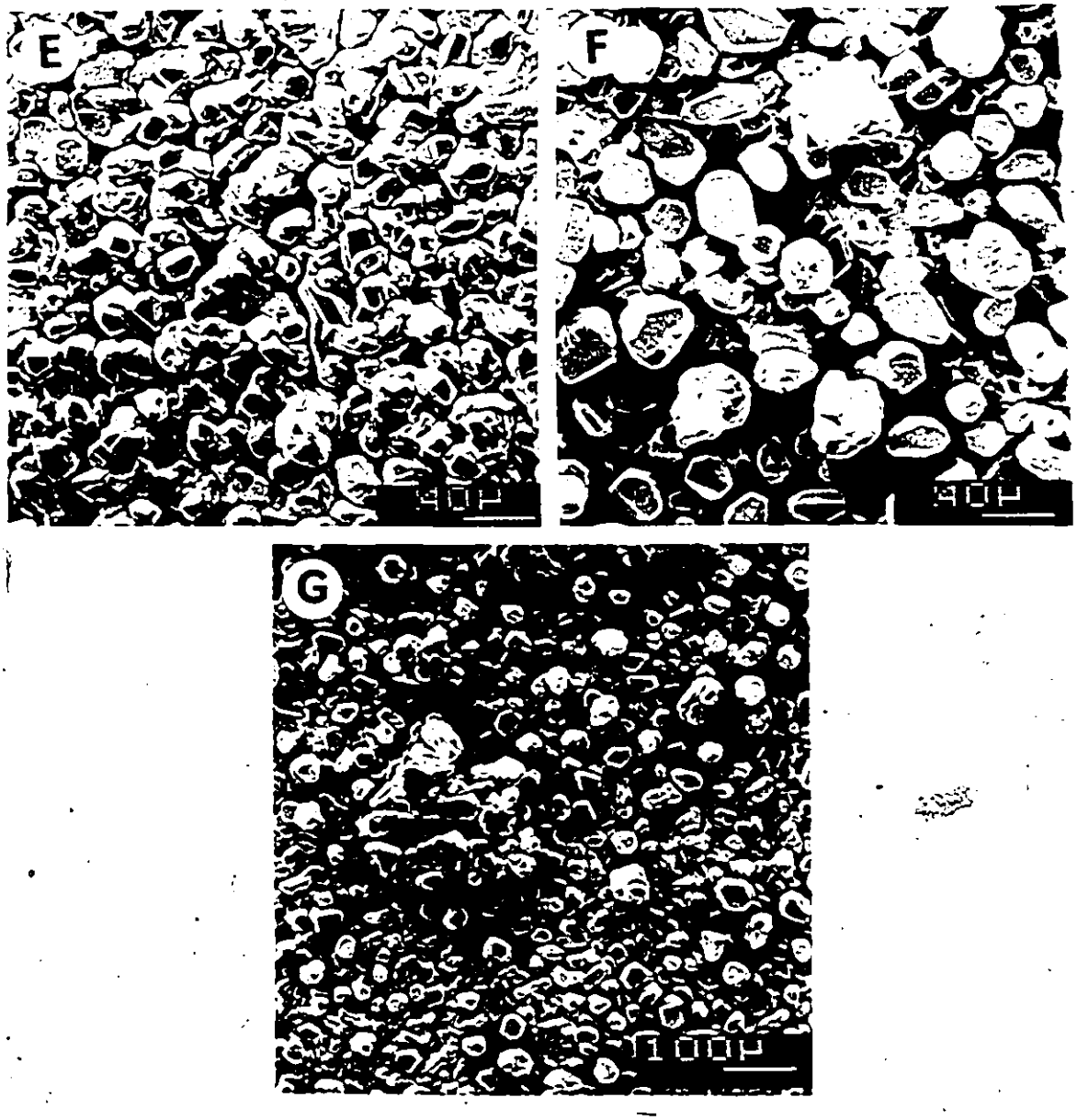
E
F
G

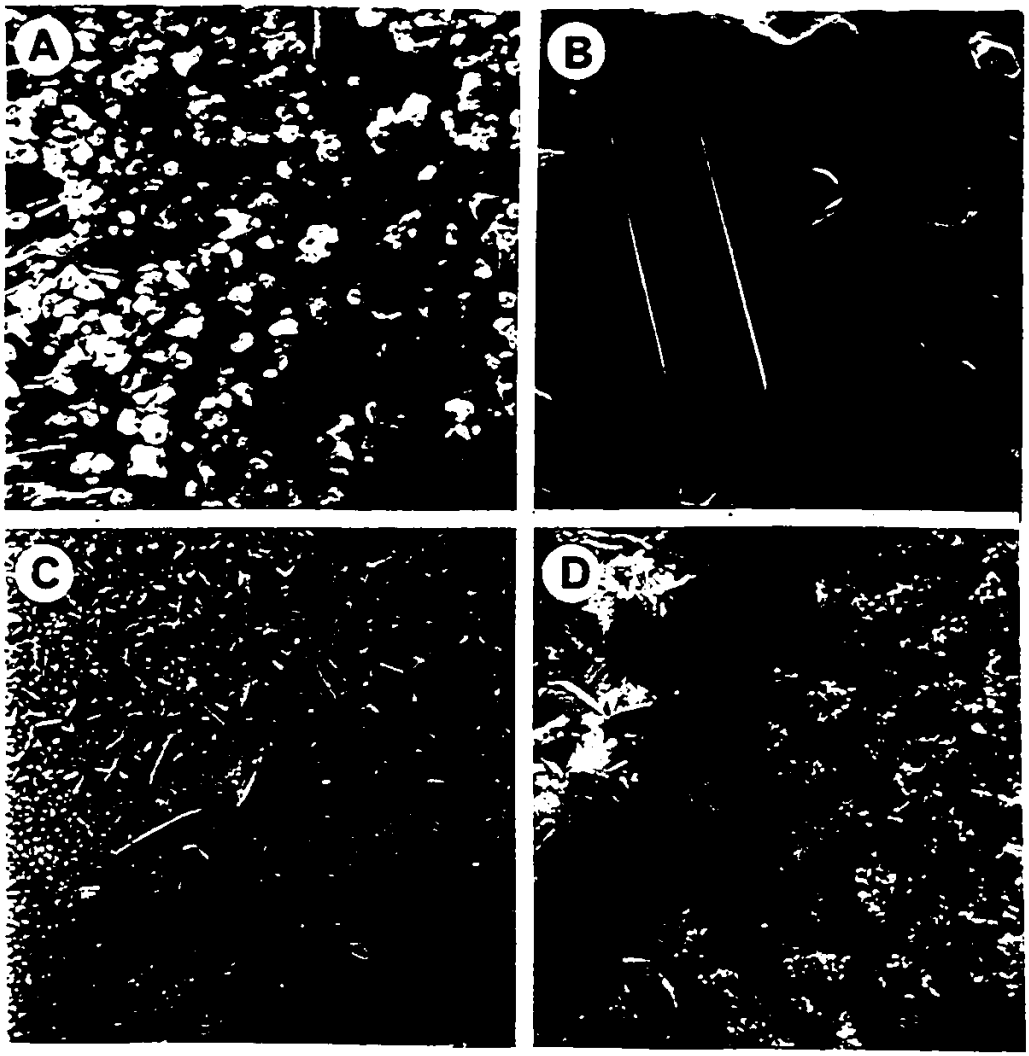

Fig. 6.17 Zn electrodeposits from 0.5M $Zn(SCN)_2$ solution at pH 4.8 on a Zn surface in etched 48% HBr. Extents of deposition of 2 C cm^{-2} at (A) 13 mA cm^{-2} (B) 71 mA cm^{-2} (C) 141 mA cm^{-2} (D) 566 mA cm^{-2}

Fig. 6.18a shows the overpotential-time curve obtained for Zn deposition at 354 mA cm^{-2} from 0.5M $Zn(SCN)_2$ solution. This curve is quite different from such curves obtained with zinc halide solutions (Fig. 6.12) at the same pH, i.e. the overpotential rises rapidly to high values. It seems likly that this behaviour may correspond to a nucleation overpotential required for small crystallite formation.

This behaviour was further studied using 0.5M $ZnCl_2$ + 1M NaSCN solution at pH 5.2; the overpotential-time curve obtained at 354 mA cm^{-2} is shown in Fig. 6.18B. There is a quite a large difference between the behaviour in Figs. 6.18A and 6.18B, that is the plot in Fig. 6.18B is similar to that obtained with zinc halide solutions containing excess halide ions; appreciable dendritic growth occurs due to rise of diffusion overpotential. The difference between the behaviour observed in these two solutions is clearly seen in Figs. 6.19a and 6.19b for conditions where electrodeposition of Zn was carried out for longer times.

It is clear that deposition from $Zn(SCN)_2$ leads to formtion of elongated Zn crystals during electrodeposition and the rate of nucleation is probably the controlling factor in determining the morphology . Once these crystals are formed, dendrites start to grow from nuclei on them due to approach to a diffusion-limited current situation. The SEM pictures in Fig. 6.20 show that these dendrites are quite different from those developed in deposition from 0.5M $ZnBr_2$ solutions (Fig. 6.7).

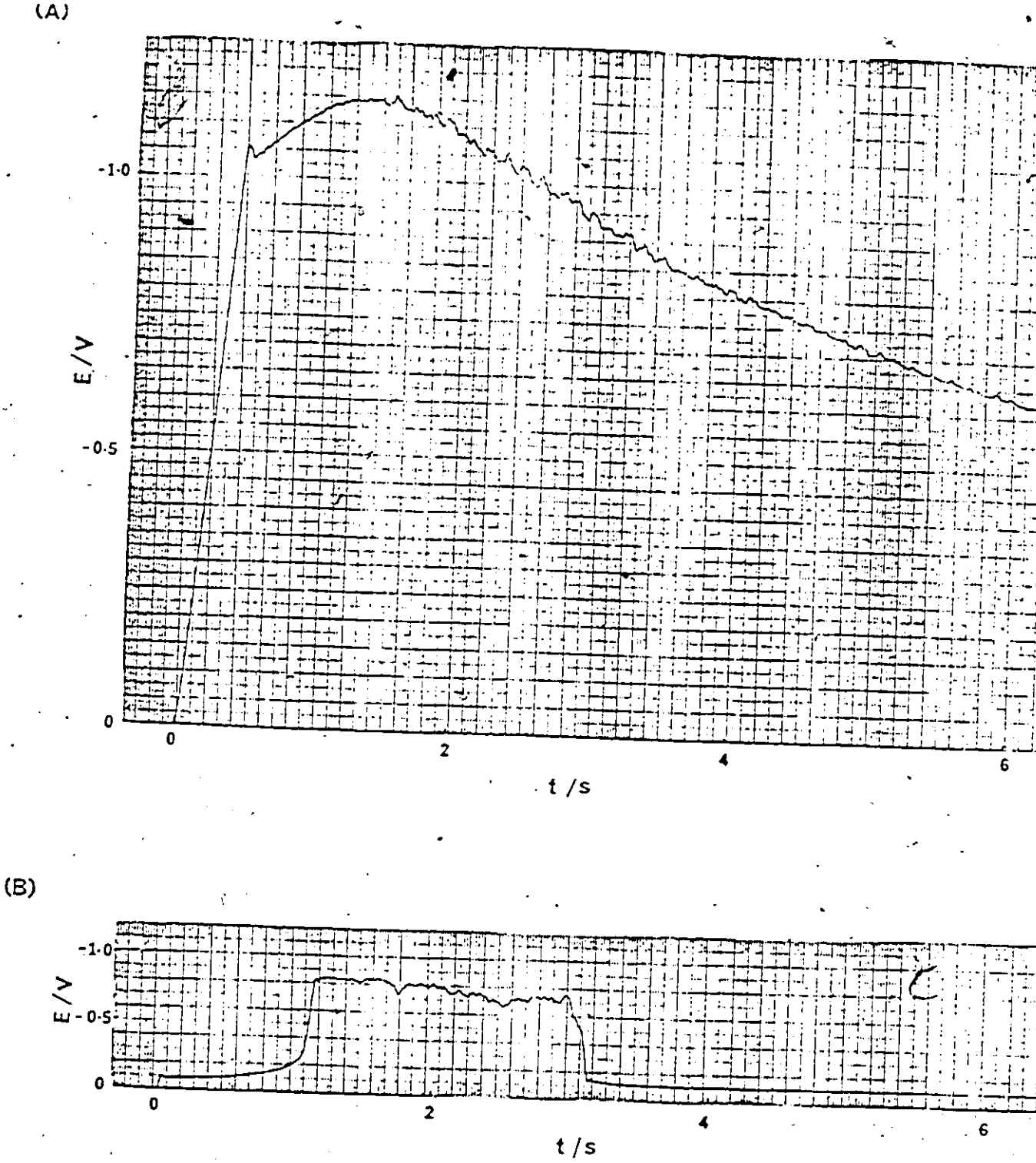

Fig. 6.18 Overpotential-time curves for Zn deposition at an etched Zn electrode from (A) 0.5M $Zn(SCN)_2$ at pH 4.8 and (B) 0.5M $ZnCl_2$ + 1.0M NaSCN at pH 5.2 at current density 354 mA cm^{-2} for an extent of deposition of ca. 2.0 cm^{-2}

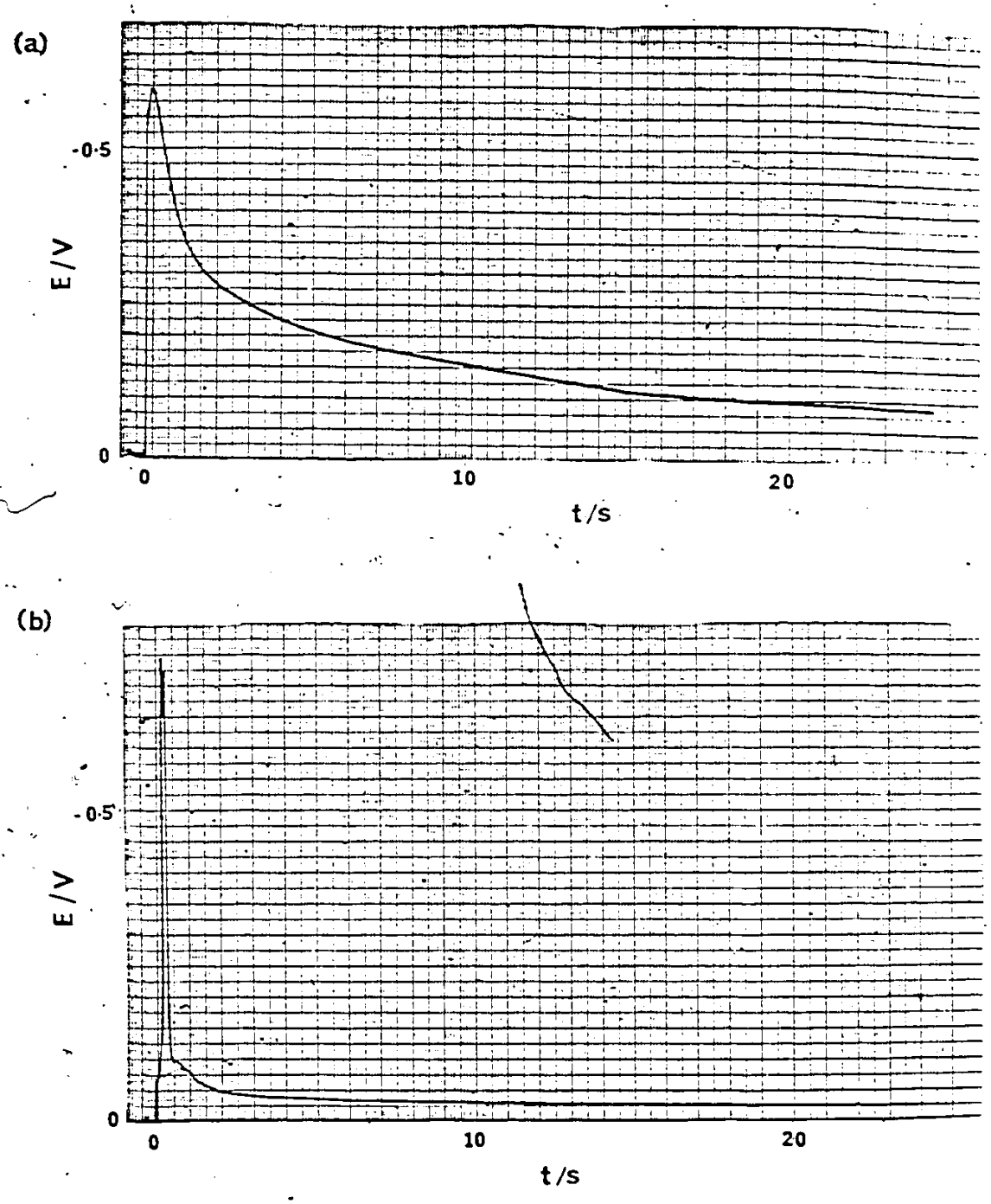

Fig. 6.19 Over-potential-time curves and Zn electrodeposits from (a) 0.5M $Zn(SCN)_2$ at pH 4.8 and (b) 0.5M $ZnCl_2$ + 1M NaSCN at pH 5.2 at current density 212 mA cm^{-2} for an extent of deposition of ca. 50 C cm^{-2}. SEM pictures - see following pages

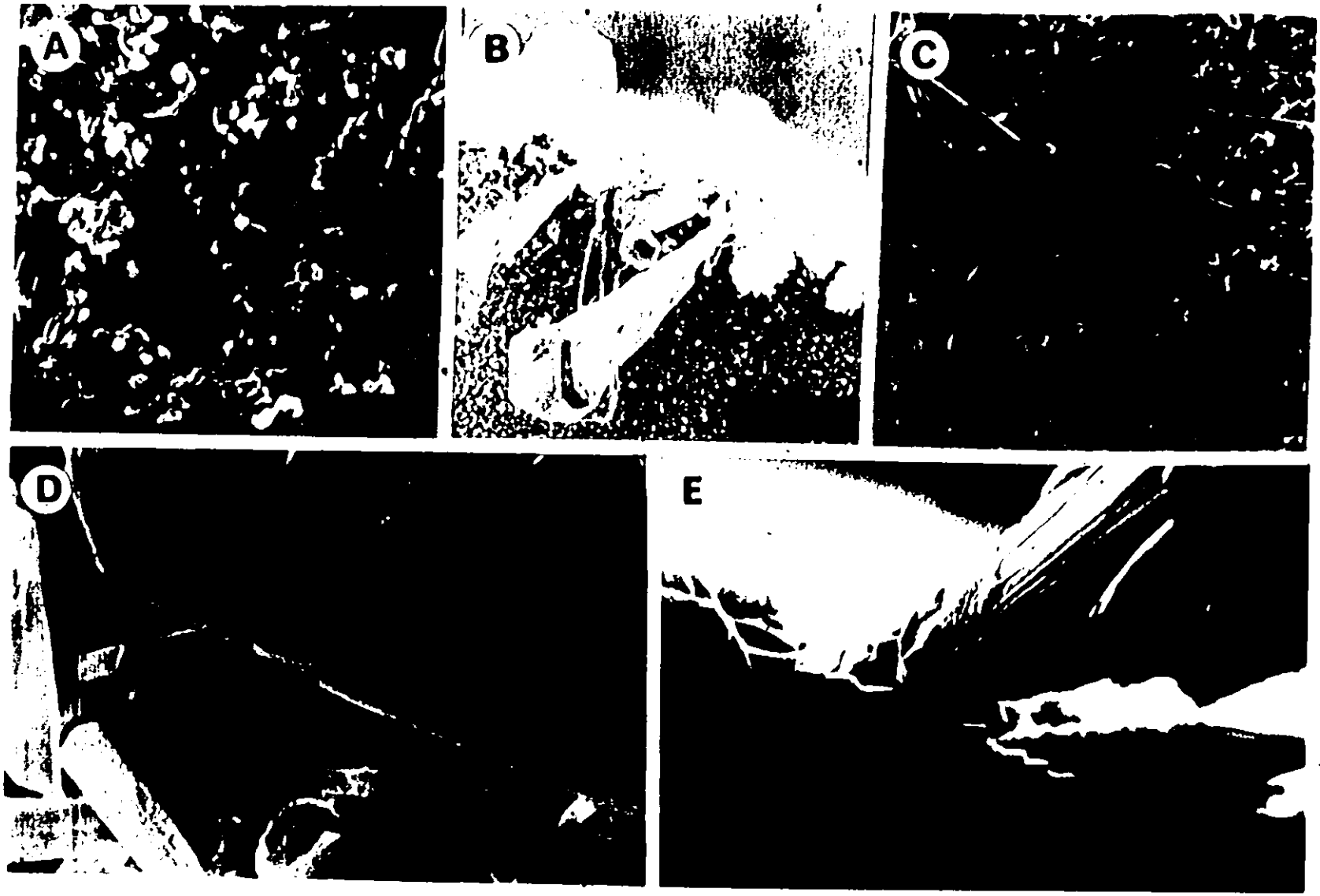

Fig. 6.19 (a) Solution - 0.5 M $Zn(SCN)_2$ (A) at the edge of the electrode and (B-E) at the center

Fig. 6.19 (b) solution - 0.5M $ZnCl_2$ + 1M NaSCN solution.

(A) at the edge of the electrode and (B) at the center.

Fig. 6:20 Zn electrodeposits from 0.5M $Zn(SCN)_2$ at pH 4.8 on a Zn surface etched in 48% HBr at 283 mA cm^{-2} for an extent of deposition of 2 C cm^{-2}.

Claims to Original Research

The mechanism and phenomenology of electrochemical passive film formation, dissolution and breakdown on Zn in aqueous solutions containing bicarbonate, carbonate, sulphate and chloride ions over the pH range 8 to 14 have been studied where, under such conditions, the nature of the anodic film and the extent of solubility of Zn as ZnO_2^{2-} ion can be varied. Previously, little or no work has been done under these conditions and most of early work has been carried out in strongly alkaline solutions. The following original contributions connected with these investigations have been made.

(1) Special attention was given to understanding the early stages of oxidation of Zn in the pH range where its dissolution rate is small (pH ca. 11.5), i.e. dissolution of Zn as ZnO_2^{2-} is diminished. Unusual peak current dependence on sweep-rate was observed at the A_1 peak at lower pH's, whereas at higher pH's (ca. 14) the reaction is purely diffusion-controlled. This behaviour at lower pH's is explained in terms of a mixed-control process by correlating the shapes of peaks and peak potentials for different Zn surface preparations, and the relation of the peak current to sweep-rate and to the effect of electrode rotation, i.e RDE experiments yield $i_p = A + B\,\omega^{1/2}$ and sweep-rate experiments showed $i_p = k_1 s + k_2 s^{1/2}$ relations for the A_1 peak,

(2) The two processes that take place at lower pH's are diffusion-controlled dissolution and direct film formation. It is

shown that only the latter kind of film formation takes place at the single-crystal Zn (0001) face. This compact film is responsible for passivation.

(3) The diffusion component for reaction at the A_1 peak in CO_3^{2-} solutions was found to be first-order w.r.t CO_3^{2-} ions in the pH range 11.5 - 12 and first-order w.r.t OH^- ions in the range 12.0 - 13.5. This behaviour is explained in terms of formation of hydroxy-carbonate films at lower pH's rather than ZnO which arises at higher pH's. A second peak A_2 is only observed in CO_3^{2-} solution, and the diffusing species for peaks A_1 and A_2 was found to be the same, as indicated by identical slopes of i_p vs $\omega^{1/2}$ plots in RDE experiments. This is explained in terms of residual current passing through the porous film that is already formed in the A_1 process .

(4) The breakdown of the passive films in Cl^- or SO_4^{2-} solutions and resistivity of passive films formed in CO_3^{2-}, solution has been examined and explained.

(5) Galvanostatic experiments provided additional evidence for the mixed-control process indicated at polycrystalline Zn electrodes and the direct film formation at the Zn (0001) face as observed in CV experiments.

(6) The effect of surface preparation and pH on the Tafel slopes for Zn oxidation in the pH range 8 to 13.5 has been explained.

(7) Morphologies of Zn crystals, electrodeposited from various Zn(II) complex-ion solutions, have been characterized by means of scanning electron microscopy.

References

1 C.H. Mathewson, ed., Zinc, Reinhold, New York, (1959).

2 Gmelin's Handbuch der Anorganischen Chemie, System-Number 32. Zinc, Verlag Chemie Weinheim (1924, 1956).

3 M. Farnsworth and C.H. Kline, Zinc Chemicals, Their properties and applications, International Lead, Zinc Research Organization Inc., New York (1968).

4 G. Bianci, G. Mazza and S. Trasatti, Intern. Congr. Metal, Corrosion, second, New York City 1963, 905-915 (Pub. 1966) CA 65,11755.

5 E.R. Jette and F. Foote, T. Chem.Phys., 3, 605 (1935).

6 J.R. Brown, J. Inst. Metals, 83, 49 (1954).

7 k. Huber, Z. Elektrochem, 48, 26 (1942).

8 K. Huber. Helv. Chim. Acta., 26, 1037 (1943).

9 K. Huber, J. Electrochem. Soc., 100, 376 (1953).

10 W. Feitknecht, Helv.Chim. Acta, 13, 314 (1930).

11 T.P. Dirkse, J. Electrochem. Soc., 101, 328 (1954).

12 J.S. Fordyce and R.L. Baum, J. Chem. Phys., 43, 2744 (1965).

13 G.H. Newman and G.E. Blomgren, J. Chem. Phys., 43, 2744 (1965).

E.R. Lippincott, J.A. Psell and M.C. Zobin, J. Chem. Phys., 20, 536 (1962).

14 R.J. Brodd and V.E. Leger, in Encyclopedia of Electrochemistry of the Elements, Vol. 5, A.J. Bard, ed., Dekker, New York, 1976.

15 D.E. Irish, B. McCarroll, and T.F. Young, J. Chem. Phys., 37, 3436 (1963).

16 M.C. Delwaulle, Compt. Rend. 240, 2132 (1955).

17 W. Yellin and R.A. Plane, J. Am. Chem. Soc., 83, 2448 (1961).

18 J.S. Silver, Thesis, University of Connectcut, 1953.

19 J. McBreen and E.J. Cairns, "The Zinc Electrode," Advances in Electrochemistry and Electrochemical Engineering, Vol. 11, H. Gerischer and C.W. Tobias, Editors, Interscience, New York (1978).

20 R. Grauer and W. Feitknecht, Corrosion Science, 7, 629 (1967).

21 W. Feitknecht, Principes chimique et thermotechniques de la corrosion des métaux dans une solution aqueuse, démontrés par l'example du zinc, métaux et corrosion, 23, 192 (1947).

22 W.S. Stumm and J.J. Morgan, Aquatic Chemistry, An introduction Emphesizing Chemical Equilibrium in Natural Waters, John Wiley (1981).

23 R.D. Armstrong and M.F. Bell, Electrochemistry, Volume 4. The chemical soc. Alden, Oxford (1972).

24 A. Fleischer and J.L. Lander, eds., Zinc-Silver Oxide Batteries, Wiley, New York, 1971.

25 H. Gerischer, Z. Phys. Chem. (Leipzig), 202, 302 (1953).

26 J.P.G. Farr and N.A. Hampson, Trans Faraday. Soc., 62, 3493, 1966.

27 J.P.G. Farr and N.A. Hampson, J. Electroanalyt. Chem., 13, 433 (1967).

28 J.P.G. Farr and N.A. Hampson, and M.E. Williamson, J. Electroanalyt. Chem., 13, 462 (1962).

29 N.A. Hampson, G.A. Herdman, and R.Taylor, J. Electroanalyt. Chem. Interfacial Electrochem., 25, 9 (1970).

30 J.O'M. Bockris, Z.Nagy and A. Damjanovic, J. Electrochem. Soc., 119, 285 (1972).

31 T.P. Dirkse, J. Electrochem. Soc., 126, 541 (1979).

32 T.P. Hoar, The Anodic Behaviour of Metals, in Modern Aspects of Electrochemistry. Vol. 2, J.O'M Bockris, (ed.). Academic Press, New York, (1959).

33 U.R. Evans, The Corrosion and Oxidation of Metals, St. Martin's, New York, (1960).

34 L.Young, Anodic Oxide Films, Academic Press, New York, (1961).

35 D.A. Vermilyea, Anodic Films in Advances in Electrochemistry and Electrochemical Engineering, Vol 3,, P. Delahay and C.W. Tobias (eds.) Interscience, New York, (1963).

36 C.J. Dell'oca, D.J. Pulfrey and L. Young, Anodic Oxide Films in Physics of Thin Films, Vol. 6, Academic Press, London,(1971).

37 A.K. Vijh, Electrochemistry of Metals and Semiconductors, Marcel Dekker, New York, (1973).

38 B. Roethelì, G. Cox and W. Litreal, Metal and Alloys, 3, 73. (1932).

39 Z. Zembura and L. Burzynska, Corrosion Science, 17, 871 (1977).

40 R.D. Armstrong and G.M. Bulman, J. Electroanalyt. Chem. Interfacial Electrochem., 25, 121 (1970).

41 L.M. Baugh, Electrochemica Acta, 24, 657 (1979).

42 L.M.Baugh, Electrochemica Acta, 24, 669 (1979).

43 R.F. Ashton and M. Hepworth, Corrosion, 24, 50 (1968).

44 B.N. Kabanov, R. Burnstein, and A.N. Frumkin, Discuss. Faraday Soc., No.1, 259 (1947).

45 B.N. Kabanov and D.I. Leikis, Acta Physiochemica URSS, 21, 769, (1946).

46 T.I. Popova, V.S. Boyotskii, and B.N. Kabanov, Doklady Akad. Nauk SSSR, 132, 639 (1960).

47 B.N. Kabanov, Electrochem. Acta, 6, 253 (1962).

48 R.W. Powers, and M.W. Breiter, J. Electrochem. Soc., 116, 719 (1969)

49 R.W. Powers, J. Electrochem. Soc., 116, 1652 (1969).

50 T.P. Dirkse, J. Electrochem. Soc., 102, 9 (1955).

51 T.P. Dirkse, D.Dewit and R. Shoemaker, J. Electrochem. Soc., 115, 422 (1968).

52 Z. Ya. Nikitina, J. Appl. Chem. (USSR), 31, 209 (1958).

53 M.N. Hull and J.E. Toni, Trans. Faraday Soc., 67,1128 (1971)

54 M.N. Hull and J.E. Ellison, Electrochem. Soc. Abstracts New York Meeting (1969), p.596.

55 M.N. Hull , J.E. Ellison and J.E. Toni, J. Electrochem. Soc., 117, 192, (1970).

56 M.N. Hull and J.E. Toni, Electrochem. Soc. Abstracts (Detroit Meeting, 1969), p.39.

57 N.A. Hampson and M.J. Tarbox, J. Electrochem. Soc., 110, 95 (1963).

58 N.A.Hampson, M.J. Tarbox, J.T. Lilley, and J.P.G. Farr, Electrochem. Tecnol., 2, 307 (1964).

59 T.P.Dirkse and N.A. Hampson, Electrochim. Acta, 16, 2049 (1971).

60 M. Eisenberg, H.F. Bauman and D.M. Brettner, J. Electrochem. Soc., 108, 909 (1961).

61 R.D. Armstrong, Corrosion Sci., 11, 693 (1971).

62 T. Popova, N.A. Simonova, and B.N. Kabanov, Electrokhimiya, 3, 1419, (1967)

63 T. Popova, T.C. Vidovich, N.I. Simonova, and B.N. Kabanov, Electrokhimiya, 3, 970 (1967).

64 E. Ivanov, T. Popova, and B. Kabanov, Elecktrokhimiya, 5, 353, (1969).

65 A. Oshe and B. Kabanov, Zaschita Metallov, 4, 260 (1968).

66 S. Szpak, C.J. Gabriel, J. Electrochem. Soc., 126, 1914 (1979).

67 R.D. Armstrong, G.M. Bulman, H.Q.Thirsk, J. Electroanal. Chem., 22, 55 (1969).

68 Z. Nagy, J.O'M. Bockris, J. Electrochem. Soc., 119, 285 (1972).

69 T. Katan, J.R. Savory, J. Perkins, J. Electrochem. Soc. 126, 1835 (1979).

70 J.R. Selman, J. Tavakoli- Attar, J. Electrochem. Soc., 127, 1049, (1980).

71 A.R. Despic, Proc Electrochem. Soc.,(1980) 80 III Symposium on Electrode processes, Boston 1979.

72 Ming-Biann Liu, G.M. Cook and N.P. Yao, J. Electrochem. Soc., 128, 1663 (1981).

73 H. Kaesche, Electrochim. Acta, 9, 383, (1964).

74 U.F. Frank, Techn. Hochschule Aachen Get., Werkstoffe Korrosion, 14, 367 (1963).

75 M. Yamashita, T. Yoshimura, P.C. Jones and A.N. Strochan, J. Appl. Electrochem., 1, 213 (1971).

76 Y. Sato, H. Niki and T. Takamuru, J. Electrochem. Soc., 118, 1269, (1971).

77 J.C. Buchholz , Surface Science, 101, 146 (1980).

78 K. Huber, Helv. Chim. Acta, 26, 1253, (1943).

79 J.P. Elder, J. Electrochem. Soc., 116, 1757 (1969).

80 L. Gaiser and K.E. Heusler Electrochim. Acta., 15, 161 (1970)

81 H.B. Alcazar and J.A. Harrison, Electrochim. Acta, 22, 627, (1977).

32 J.W. Diggle, A.R. Despic, and J.O'M. Bockris, J. Electrochem. Soc., 116, 1503 (1969).

83 J.W. Diggle, A.R. Despic and J.O'M. Bockris, J. Electrochem. Soc., 115, 507, (1968).

84 F. Mansfeld and S.Gilman, J.Electrochem. Soc., 117, 1521 (1970).

85 I. Epelboin, M. Ksouri, R. Wiart, Faraday Sym. Chem. Soc., 12, 115, (1977).

86 J. Bressan and R. Wiart, J. Applied Electrochem., 9, 43, (1979).

87 J.E. Oxely and C.W. Fleischman; improvement of Zn electrodes for electrochemical cells, first, second and third quarterly reports, N66-13568, N66-19656, and N66-26870 (1965-1966). 'The growth of dendrites from alkaline Zn solutions,' Extended Abstracts, The Electrochemical Society, Battery Division, 10, 3 (1965).

88 R.Yu. Bek. and N.T Kudryavtsev, Zhur, Priklad, Khim, 34 (1961), 2613, 2620; (chem. Abs., 56, 1284d, 1284j (1962))

89 F. Mansfeld and S. Gilman, J.Electrochem. Soc. 117, 588, (1970).

90 F. Mansfeld and S. Gilman, J.Electrochem. Soc. 117, 1154, (1970).

91 F. Mansfeld and S. Gilman, J.Electrochem. Soc. 117, 1328, (1970).

92 J.O'M. Bockris and J.W. Diggle and A. Damjanovic, first quarterly report to NASA, Contract NO. NAS 5-9591, March 1966.

93 J.W. Diggle, A. Damjanovic, and J. O;M. Bockris, Paper 18, Presented at Electrochemical Society Meeting, Detroit, October 1969.

94 N.T. Kudryvtsev, Zhur. fiz. Khim. 26, 270 (1952).

95 R.D. Naybour, Electrochim. Acta, 13, 763 (1968).

96 R.D. Naybour, J. Electrochem. Soc., 116, 520 (1969).

97 O. Kardas, Plating 61, 129, 229, 316 (1974).

98 J. McBreen, E. Gannon, Electrochim. Acta, 26, 1439 (1981).

99 M.G. Chu, J.McBreen, G. Adzic, J. Electrochem. Soc., 128, 2281 (1981).

100 J. McBreen, M.G. Chu and G. Adzic, J. Electrochem. Soc., 128, 2287 (1981)

101 K. Boto, Electrodeposition and Surface Treatment, 3, 77 (1975).

102 J. Barton and J.O'M. Bockris, Proc. Roy. Soc., A 268, 485 (1962).

103 T. Hurlen and E. Eriksard, J. Electroanal. Chem., 45, 205 (1973).

104 T. Hurlen and K.P. Fischer, J. Electroanal. Chem. 61, 165 (1975).

105 E. Eriksurd, J. Electroanal. Chem., 76, 27 (1977).

106 H.B. Sierra Alcazar and J.A. Harrison, Electro. Chim. Acta, 22, 627 (1977).

107 I. Epelboin, M. Ksouri and R. Wiart, Electroc. Chim. Acta, 20, 603 (1975).

108 J.T. Kim and J. Jorne, J. Electrochem. Soc., 127, 8 (1980).

109 I. Epelboin, M. Ksouri and R. Wiart, J. Electrochem. Soc., 122, 1206 (1975).

110 D-T. Chin and S. Venkatesh, J. Electrochem. Soc., 128, 1439 (1981).

111 D.J. McKinnon, J.M. Brannen and V.I. Lakshmann, J. Appl. Electrochem. 9, ,603 (1979).

112 Y. Oren and V. Landau, Electrochim. Acta, 27, 73 (1982).

113 J. McBreen and E. Gannon, J. Electrochem. Soc., 130, 1667 (1983).

114 V.V. Romanov, Zhur. Prikland. Khim., 34, 2692 (1961).

115 V.I. Chernenko, A.A. Risakov and Z.I. Pristinskaya, Electrokhimiya, 5, 519 (1968).

116 K.I. Popov, M.D. Maksimovic and M.S. Simic, Surf. Technol., 16, 209 (1982).

117 N. Ibi, Surf. Technol., 10, 81 (1980).

118 K.I. Popov, M.D. Maksimovic, B.M. Ocokoljic and B.J. Lazarevic, Surf. Technol., 11, 99 (1980).

119 J Newman, J. Electrochem. Soc., 113, 501 (1966).

120 B.E. Conway, Proc. Royal Soc. (London), A 256, 128 (1960).

121 A.M. Feltham and M. Spiro, Chem. Revs. 71, 177 (1971).

122 W.J. MacNeil-Tegart, The electrolytic and chemical polishing of metals in research and industry, Permagon, London, (1959).

123 F.P. Bowden and E.K. Rideal, Proc. Royal. Soc. (London) 120A, 80, (1928).

124 D.C. Grahame, Chem. Rev., 41, 441, (1947).

125 R.S. Nicholson and I.Shain, Anal. Chem., 36, 706 (1964).

126 P. Delahay and G. Perkins, J. Phys. Coll. Chem., 55,586 1146 (1951).

127 W.M. Schwarz and I. Shain, J. Phys. Chem., 69, 30 (1965).

128 A. Sevick, Coll. Czech. Chem. Comm. 13 349 (1948).

129 S. Srinivasan and E. Gileadi, Electrochemica Acta, 11 321 (1966).

130 H. Angerstein-Kozlowska, J. Klinger and B.E. Conway, J. Electroanal. Chem., 75, 61 (1977).

131 E. Laviron, Bull. Soc. Chim. France, 2256 (1968).

132 P. Delahay, "New Instrumental Method in Electrochemistry, Chapter 6., Wiley, New York, 1954.

133 A.J. Calander, N.R. de Tacconi, R. Pereiro and A.J. Arvia, Electrochim. Acta, 19 901 1974.

134 G.I. Finch and A.G. Quarrell, Proc. Roy. Soc. A141, 398 (1933), Proc. Phys. Soc. 46, 148 (1934).

135 L.N.D. Lucas, Proc. Roy. Soc (London) A125, 126 (1952).

136 G. Heiland, E. Mollow and F. Stöckman, Solid State Phys. 8 193, (1959).

137 S.C. Abrahams and J.L. Bernstein, Acta cryst., B25 1233, (1968).

138 V.G. Levich, "Physiochemical Hydrodynamics," Prentice-Hall, Englewood Cliffs, N.J., 1962.

139 D.A. Harrington, "The Electrochemistry of Bismuth in Alkaline sulphide Solution," Ph.D Thesis, University of Auckland, 1981.

140 J.W. Patterson, Proceedings of The Industrial Waste Water Conference, 36th, 579 (1982).

141 P.E. Lake and E.J. Casey, "Sintered Plates of Nickel Cadmium Batteries. II. Extent of Effects of Carbonate Contamination on Electrical Output," DRCL Report No. 186, April, 1955.

142 P.E. Lake and E.J. Casey, J. Electrochem . Soc., 105, 52 (1958); 106, 913 (1959).

143 P.E. Lake and E.J. Casey, J.Electrochem . Soc., 106, 532 (1960).

144 P.E. Lake and J.M. Goodings, Can. J. Chem., 36, 1089 (1958).

145 E.J. Casey, A.R. Dubois, P.E. Lake and W.J. Moroz, J. Electrochem. Soc., 112, 371 (1965).

146 R. Grauer and U.Gut, Corros. Sci. 10, 503 (1970).

147 H.J.S. Sand, Phil. Mag., 1, 45 (1901).

148 D.M. Drazic, S. Hadzi Jordanov and Z. Nagy, Croat. Chem. Acta, 45, 199 (1973).

149 V.S. Donepudi and B.E. Conway, J. Electrochem. Soc., 131, 1477 (1984).

150 J.C. Bailar, H.J. Emeléus, R. Nyholm and A.F. Trotman-Dickenson, ed., Comprehensive Inorganic Chemistry, vol.3 Pergamon, New York, (1973).

151 B.E. Conway and J.O'M Bockris, Plating, 46, 371 (1959).